Macropore flow and transport dynamics in partially saturated low permeability soils

by

Edwin E. Cey

A thesis
presented to the University of Waterloo
in fulfillment of the
thesis requirement for the degree of
Doctor of Philosophy
in
Earth Sciences

Waterloo, Ontario, Canada, 2007

Author's Declaration

I hereby declare that I am the sole author of this thesis. This is a true copy of the thesis, including any required final revisions, as accepted by my examiners.

I understand that my thesis may be made electronically available to the public.

Edwin Cey

Abstract

Near-surface sediments play an important role in governing the movement of water and contaminants from the land surface through the vadose zone to groundwater. Generally, low permeability surficial soils restrict water flow through the vadose zone and form a natural protective barrier to migration of surface applied contaminants. These types of fine-grained soils commonly contain macropores, such as fractures, animal burrows, and root holes, that have been identified as preferential flow pathways in the subsurface. Accordingly, macropores have the potential to influence groundwater recharge rates and compromise the protective capacity of surficial soils, particularly where the overburden is thin and aquifers are close to the surface. Partially saturated flow and transport in these environments is inherently complex and not well understood. The objective of this thesis was to examine preferential flow processes and the associated movement of contaminants in macroporous, low permeability soils. This was accomplished by conducting numerical and field experiments to investigate and describe the dynamics of macropore flow during episodic infiltration through the vadose zone and evaluate the corresponding influence of macropores on vertical water flow and contaminant transport.

Numerical simulations were conducted to identify the important physical factors controlling flow and transport behaviour in partially saturated, fractured soils. A three-dimensional discrete fracture model, HydroGeoSphere, was used to simulate infiltration into homogeneous soil blocks containing a single vertical rough-walled fracture. Relatively large rainfall events with return periods ranging from 5 to 100 years were used, since they are more likely to generate significant preferential flow. Initial results showed that flow system dynamics were considerably more sensitive to matrix properties, namely permeability and antecedent moisture content, than fracture properties. Capillary forces, combined with the larger water storage capacity in the soil matrix, resulted in significant fracture-matrix interaction which effectively limited preferential flow down the fracture. It is also believed that fracture-matrix interaction reduced the influence of fracture roughness and other related small-scale fracture properties. The results imply that aperture variability within individual fractures may be neglected when modeling water flow through unsaturated soils. Nevertheless, fracture flow was still an important process since the fracture carried the majority of the water flow and virtually all of the mass of a surface applied tracer to depth in the soil profile.

Model runs designed to assess transport variability under a variety of different physical settings, including a wider range of soil types, were also completed. Vertical contaminant fluxes were examined at several depths in the soil profile. The results showed that the presence of macropores (in the form of fractures) was more important than matrix permeability in controlling the rate of contaminant migration through soils. The depth of contaminant migration was strongly dependent on

the antecedent moisture content and the presence of vertically connected fractures. Soil moisture content played a pivotal role in determining the onset and extent of preferential flow, with initially wet soils much more prone to macropore flow and deep contaminant migration. Simulations showed that surface applied tracers were able to reach the base of 2 m thick fractured soil profiles under wetter soil conditions (i.e., shallow water table). Likewise, long-duration, low-intensity rainfall events that caused the soil to wet up more resulted in proportionately more contaminant flux at depth. Fractured soils were particularly susceptible to rapid colloid movement with particle travel times to depths of 2 m on the order of minutes. The main implication is that the vulnerability of shallow groundwater is related more to vertical macropore continuity and moisture conditions in the soil profile, rather than traditional factors such as soil thickness and permeability.

Macropore flow and transport processes under field conditions were investigated using small-scale infiltration experiments at sites in Elora and Walkerton, Ontario. A series of equal-volume infiltration experiments were conducted at both sites using a tension infiltrometer (TI) to control the (negative) infiltration pressures and hence the potential for macropore flow. A simulated rainfall experiment was also conducted on a small plot at Walkerton for comparison with the TI tests. Brilliant Blue FCF dye and fluorescent microsphere tracers were applied in all tests as surrogates for dissolved and colloidal contaminant species, respectively. Upon completion of infiltration, excavations were completed to examine and photograph the dye-stained flow patterns, map soil and macropore features, and collect soil samples for analysis of microspheres. Cylindrical macropores, in the form of earthworm burrows, were the most prevalent macropore type at both sites. In the TI tests, there was a clear relationship between the vertical extent of infiltration and the maximum pressure head applied to the TI disc. Larger infiltration pressures resulted in increased infiltration rates, more spatial and temporal variability in soil water content, and increased depths of dye penetration, all of which were attributed to preferential flow along macropores. Preferential flow was limited to tests with applied pressure heads greater than -3 cm. Under the largest applied pressures (greater than -1.0 cm), dye staining was observed between 0.7 and 1.0 m depth, which is near the seasonal maximum water table depth at both field sites. The tension infiltrometer was also used to infiltrate dye along an exposed vertical soil face, thereby providing a rare opportunity to directly observe transient macropore flow processes. The resulting vertical flow velocities within the macropores were on the order of tens of meters per day, illustrating the potential for rapid subsurface flow in macropores, even under partially saturated conditions. The results suggest that significant flow occurred in partially saturated macropores and this was supported by simple calculations using recent liquid configuration models for describing flow in idealized macropores.

On all excavated sections, microspheres were preferentially retained (relative to the dye) in the top five centimeters of the soil profile. Below this zone, dye patterns correlated well with the presence of microspheres in the soil samples. There was evidence for increased retention of microspheres at lower water contents as well as a slightly greater extent of transport for smaller microspheres. In general, the microsphere and dye distributions were clearly dictated by vadose zone flow processes.

As in the numerical experiments, water storage in the soil matrix and related macropore-matrix interaction were important factors. Mass transfer of water through the macropore walls promoted flow initiation in the macropores near surface. Deeper in the soil, water drawn away from the macropores into the matrix significantly retarded the downward movement of water along the macropores. Imbibition of dye from the macropores into the matrix was repeatedly observed on excavated soil sections and during the transient dye test. Microspheres were also transported laterally into the soil matrix indicating that conceptual models for colloid transport in the vadose zone need to account for this mass transfer process.

Overall, the tension infiltrometer performed extremely well as a tool for controlling macropore flow under field conditions and, together with the dye and microsphere tracers, provided unique and valuable insights into small-scale flow and transport behavior. The field experiments raise concerns about the vulnerability of shallow groundwater in regions with thin, macroporous soils. Only a fraction of the visible macropores contributed to flow and transport at depths greater than 40 cm. However, with dye and microsphere transport observed to more than 1.0 m depth, rapid macropore flow velocities, and the sheer number of macropores present, there was clearly potential for significant flow and transport to depth via macropores. Under the right conditions, it is reasonable to speculate that macropores may represent a significant pathway for migration of surface applied contaminants to groundwater over the course of a single rainfall event.

Acknowledgements

Funding for this research was provided by the Natural Sciences and Engineering Research Council of Canada (NSERC), Ontario Ministry of the Environment, the Canadian Water Network, and the Canada Foundation for Innovation. Additional financial support was also provided by NSERC, Golder Associates Ltd., University of Waterloo, and the Canadian Water Resources Association in the form of scholarships and bursaries.

Many, many people have helped me throughout the course of my PhD adventure. First, I must express my sincere gratitude to my thesis advisor, Dr. Dave Rudolph. In addition to being a great mentor, Dave has provided wisdom, encouragement, guidance, and unwavering support - academically, professionally, financially and personally - throughout my studies. I have truly enjoyed working with Dave and simply cannot thank him enough for all that he has done for me and my family throughout our many years in Waterloo.

I would also like to thank Dr. Bob Gillham, Dr. Gary Parkin, and Dr. René Therrien for their time and efforts in serving on my thesis committee. Each of them has provided valuable contributions to the thesis in the form of review comments, helpful suggestions, and sound advice. Gary Parkin and his soil research group at the University of Guelph also deserve special credit for providing much needed equipment, technical support and laboratory services. Thanks also to my external reviewers, Dr. Jonathan Price and Dr. Anderson Ward, for generously offering their time.

To Rob McLaren, a big thank you for your invaluable assistance with all things computer related. Whether it was one of my numerous inane questions about HydroGeoSphere code, assistance with numerical simulations that never seemed to converge, or problems with computer hardware, Rob was always willing to help. I would also like to acknowledge and thank Markus Weiler for lending IDL programming code that formed the basis for several of my image analysis routines.

Joanna Passmore deserves special recognition for all of her contributions to this work. Jo provided technical expertise for the microspheres and the rainfall simulator, spent countless hours in the field and laboratory, and was a great springboard for my crazy thoughts and ideas. In short, without her assistance this research would not have come anywhere near as far (and I might still be out-standing in my field). Kate Critchley and Andrew Wiebe also worked tirelessly in the field under less than ideal conditions, and made many long days much more manageable and memorable. Many other people contributed to the field investigations, including Peter von Bertoldi, Dave Kells, Colby Steelman, Scott Piggott, Odum Idika, Steve Frey, Brewster Conant, Paul Johnson, and Bob Ingleton. Your efforts were much appreciated. Thanks must also go to Colby Steelman and Zsolt Molnar for conducting laboratory soils testing and Ryan Snider for spending many hours in front of a microscope counting fluorescent dots.

This research would not have been possible without the cooperation of the Biesenthal family who graciously allowed me to conduct my field experiments on their farm near Walkerton. Allowing me access to their land, knowing I would be filling it with holes, was generous indeed. But, their willingness to welcome strangers into their home and share their time and experiences, after all they had been through themselves, was truly inspiring.

Thanks to all my fellow students and friends at the University of Waterloo. There are simply too many names to mention, but I am truly grateful to all those who I've had the privilege to meet and share time (and beers) with along the way. Thank you for making my time at Waterloo a special experience that I will always remember.

Finally, special thanks must go to my beautiful wife, Christine, and my adorable children, Jason, Taylor and Emma. You were all forced to sacrifice so that I could chase my dream, yet you were behind me all the way. Without your love, support and smiling faces to come home to, none of this would have been possible. And yes, now Daddy can get a real job!

Dedication

In loving memory of my mother, who I knew all too briefly.

Table of Contents

List of Tables

List of Figures

Chapter 1
Thesis Introduction

1.1 Background

Surficial geologic deposits form a vital link between meteoric waters and subsurface aquifers. In many regions of Canada, surficial soils are derived from low to moderate permeability sediments, often of glacial origin. Given their relatively low permeability, these types of soils are generally considered to limit the vertical flux of water and contaminants from surface to groundwater. This effectively reduces groundwater recharge rates while at the same time protects underlying sand, gravel or bedrock aquifers from contamination by surface sources [*Robertson et al.*, 1996; *Robins*, 1998].

Macropores are one important feature that can potentially increase fluxes through low permeability sediments. Macropores of different sizes and types have long been recognized as important preferential pathways for water flow and the associated movement of contaminants [*see Beven and Germann*, 1982]. There are other forms of preferential flow, such as funnel flow and unstable finger flow, but they are not the focus of this research. The term macropore simply refers to a large soil pore. There is no well-defined size criterion for macropores, although they typically have some arbitrary minimum size on the order of 0.1-5 mm [*Beven and Germann*, 1982]. For the purposes of this study, a macropore will be defined as any relatively large soil pore that is distinct from the soil matrix and functions as a preferential flow pathway in the subsurface. They can be broadly classified into two types: (1) linear, cylindrical macropores that are the result of plant root holes and burrowing animals (i.e., earthworms, ants, moles, etc.), and (2) planar fractures formed by desiccation, freeze/thaw, cultivation, or geologic processes.

Flow in macropores can have significant hydrologic implications. Water can move quickly through macropores and bypass a large portion of the soil matrix. During a rainfall event, infiltrating water can penetrate much deeper along macropores than would occur under uniform piston-type flow conditions in the soil matrix. If the water penetrates deeper than the zone of active evapotranspiration, it can result in enhanced groundwater recharge. This is particularly important in arid and semi-arid regions where potential evapotranspiration exceeds precipitation on an annual basis. Studies have shown that a significant component of groundwater recharge can be attributed to preferential flow along shallow macropores in semi-arid regions [*Wood et al.*, 1997; *Scanlon and Goldsmith*, 1997]. The increased infiltration that can occur in macroporous soils will also affect

rainfall-runoff relationships. Obviously, an increase in the infiltration rate will lower the amount of runoff that occurs for a given rainfall event. The area of influence can extend from infiltration in micro-scale basins around individual macropores [*Weiler and Naef*, 2003a] up to the response at hill-slope or watershed scales [*Buttle and Turcotte*, 1999; *Zhang et al.*, 2007].

Perhaps the most significant influence of macropore flow is the potential it creates for rapid downward transport of surface-applied contaminants, particularly those that are hazardous at low levels. In regions where aquifers are overlain by structured soils, it is critically important to understand the influence of macropores on the flux of both water and contaminants through the vadose zone. High flow rates within macropores reduce the time required for solutes or colloids to migrate through a low permeability unit, as well as decrease the contact area available for contaminant attenuation processes, such as adsorption, degradation or colloid attachment. Numerical models have been used to demonstrate that macroporosity can significantly reduce the degree of protection afforded by low-permeability sediments [*Harrison et al.*, 1992]. A large number of field studies have also shown preferential transport of solutes in a wide range of macroporous sediments [*Coles and Trudgill*, 1985; *Flury et al.*, 1994; *Kelly and Pomes*, 1998; *McKay et al.*, 1998; *Perillo et al.*, 1999; *Jorgensen et al.*, 2002; *Weiler and Naef*, 2003b]. Recently, there has been a renewed emphasis in Canada on evaluating groundwater that is susceptible to surface contamination, particularly by pathogens, in the wake of the Walkerton groundwater tragedy. This has led to GUDI assessments, or Groundwater Under the Direct Influence of surface water. The aim is to establish if there is a hydraulic connection between surface water and groundwater, and determine if contaminants (primarily pathogens) can reach the groundwater source. In these types of evaluations, the presence of macropores and their ability to transport colloids (i.e., particles the size of bacteria or viruses) to groundwater is a major concern. Studies in saturated porous media have shown that colloids are not only transported through macropores, but the transport velocities of colloidal species can be orders of magnitude greater than dissolved species [*McKay et al.*, 1993c; *McKay et al.*, 2000]. It is evident that flow through low-permeability, macroporous soils could have serious consequences for groundwater quality and aquifer vulnerability assessments. Unfortunately, studies of colloid transport in natural unsaturated field soils are sorely lacking.

In the vadose zone, one might expect macropore flow to be particularly important because macropores are very common. There tends to be an abundance of macropores in the vadose zone because of the significant geological, biological, chemical and hydrological activity that occurs. These macropores can also extend to considerable depth. For example, studies of the Lambton Clay Plain in southwestern Ontario have shown that fractures and root holes can extend to depths in excess of 6 m below ground surface [*McKay and Fredericia*, 1995; *Fidler*, 1997]. Despite the increasing

evidence that macropore flow and transport is widespread in shallow hydrologic systems [*see for example Flury et al.*, 1994], macropore flow behaviour in the vadose zone remains poorly understood. This stems partly from the fact that macropore flow processes are more complex and difficult to investigate in partially saturated systems than in comparable saturated systems. In partially saturated soils, the flow system becomes increasingly complicated by the interrelationship between capillary pressure, soil water content, and hydraulic conductivity [*see Hendrickx and Flury*, 2001 *and references therein*]. In other words, fluxes and flow pathways become dependent on soil moisture conditions, which can be markedly different for the matrix and macropores. Under very dry conditions, capillary theory dictates that macropores will be predominantly air-filled and can possibly serve as barriers to water movement. As the soil approaches saturation, larger and larger pores become water-filled. Once the macropores become water-filled, they have the capacity to transmit large volumes of water at relatively high velocities. Macropore flow is traditionally considered to be initiated when a portion of the soil matrix reaches saturation (or close to saturation) such that the soil matric potential exceeds the water entry potential of the macropore [*Hendrickx and Flury*, 2001]. Consequently, macropore flow is most often associated with long-duration or high-intensity rainfall events when near-surface soil moisture is elevated. However, it is becoming increasingly recognized that flow in macropores will occur under partially saturated conditions. Water flow along the walls of macropores can occur via capillary flow, film flow, or thin rivulets, but the relative importance of each of these mechanisms under different field conditions is not yet clear [*Tokunaga and Wan*, 1997; *National Research Council*, 2001; *Dragila and Wheatcraft*, 2001]. As a result of these complexities, flow conditions within an individual macropore or network of macropores are expected to vary considerably in both space and time throughout the course of a single infiltration event. Field observations in fractured rock experiments support the notion of highly dynamic flow under partially saturated conditions, even for relatively constant boundary conditions [*Dahan et al.*, 1999; *Su et al.*, 2000; *Podgorney et al.*, 2000].

Additional flow complexity arises due to water exchange between the matrix and macropore domains. During infiltration, macropore flow may be initiated by near saturated conditions within the matrix and subsequent flow into macropores. On the other hand, water flowing downward through a macropore can be imbibed back into drier soil matrix materials deeper in the soil profile. The imbibition of water from the macropore into the matrix can have a major influence on flow and effectively retard the migration of flow along the macropore. This process is analogous to matrix diffusion in solute transport theory, whereby solute transport velocity is attenuated within a macropore because of molecular diffusion into the porous matrix [*Foster*, 1975]. Macropore-matrix transfer of water (and contaminants) is one of the key differences between saturated and partially saturated systems. Capillary forces in the vadose zone that drive water transfer between the

macropore and matrix domains are essentially absent from saturated systems. Mass transfer has been identified as an important mechanism in partially saturated flow systems [*National Research Council*, 2001], but it has not been extensively studied and thus its affect on overall flow and transport behaviour remains unknown. A better understanding of the small-scale flow processes described above is required in order to ultimately determine the influence of macropore flow on groundwater recharge rates and vertical contaminant fluxes.

Many challenges still exist in characterizing and quantifying macropore flow and transport in natural soils. The spatial and temporal variability of macropore flow phenomena make it difficult to monitor flow processes in situ. In order to capture this variability, field techniques generally consist of either detailed temporal or spatial monitoring systems. The first type relies on monitoring transient flow, pressure, or water content responses at one or more discrete locations in the subsurface. This provides a description of the transient system response, but without a very dense network of monitoring points, flow and transport within individual macropores may be missed altogether. Studying water or tracer breakthrough using tile-drains, lysimeters or large soil columns [*Kelly and Pomes*, 1998; *Laegdsmand et al.*, 1999; *e.g., Kung et al.*, 2000] can alleviate some of these concerns by integrating a larger volume of soil. The tradeoff is the loss of small-scale detail that may be crucial to understanding flow dynamics. Conversely, high spatial resolution data sets can be obtained using tracers, most notably dye tracers [*Flury et al.*, 1994], but much of the information regarding transient behaviour is lost. The best monitoring approach appears to be a combination of detailed spatial and temporal measurements [*e.g., Weiler and Naef*, 2003b].

Most field experiments also suffer from an inability to control the onset of macropore flow. The initiation of macropore flow is controlled by capillary pressure head in the macropore and surrounding matrix. An instrument called a tension infiltrometer has long been used to estimate soil macroporosity and unsaturated hydraulic conductivity by applying a constant negative infiltration pressure (i.e., tension) to a porous disc situated on the soil surface and subsequently measuring infiltration rates [*Watson and Luxmoore*, 1986]. The applicability of using any device to measure a single hydraulic conductivity curve in macroporous soils is tenuous at best. Yet, the ability to control infiltration pressures, and by association macropore flow, is a major benefit. Tension infiltrometers have the potential to be combined with other investigation methods, such as dissolved or colloidal tracers, to control and characterize macropore flow and transport behaviour in the field.

As an alternative to field experiments, numerical models are another tool that can provide unique and valuable insights into macropore flow and transport processes. Given the complex flow behaviour, existing models cannot yet accurately predict flow and transport in anything but the simplest macroporous systems. Modelling is hampered by a lack of information on the geometry of

macropore networks along with the inability to accurately describe flow within macropores and between the macropores and matrix [*Simunek et al.*, 2003]. Nevertheless, numerical simulations can address topics that would be difficult or impossible to investigate in the field. This includes the influence of small-scale features such as macropore roughness, continuity, and hydraulic characteristics as well as plot-scale properties such as antecedent water content and matrix hydraulic properties.

1.2 Research Objectives

The primary objective of this thesis is to develop an improved understanding of macropore flow and transport processes in the vadose zone of structured, low permeability soils. The majority of the research deals with investigating and describing the dynamics of flow along macropores during episodic infiltration events through the vadose zone. This involves basic research on the mechanisms of flow and the relevant physical parameters that control macropore flow at a relatively small-scale. At the same time, an examination of the migration of solute and colloid species through macroporous soils is superimposed on the problem. In the end, it is hoped that the understanding gained can be used to evaluate the affect of macropores on groundwater resources in terms of recharge and the associated migration of contaminants.

The specific goals of this research are summarized below.

- Using numerical and field methods, identify the key physical parameters and processes that control macropore flow and transport during infiltration through the vadose zone.
- Incorporate salient pore-scale features, such as fracture roughness and macropore hydraulic characteristics, into an existing numerical model and subsequently demonstrate the relative importance of these and other features on water and contaminant fluxes.
- Improve our understanding of macropore-matrix interaction in partially saturated systems and assess its importance for bulk vertical flow and transport.
- Apply a combination of research instruments and techniques in order to control and adequately monitor macropore infiltration processes in natural field soils.
- Provide a quantitative, or at least semi-quantitative, approach to characterizing the potential for vertical transport of solutes and colloids in a field setting.

1.3 Thesis Organization

This thesis contains six chapters with the core chapters (Chapters 2-5) written in manuscript format. That is, each of the core chapters was written as a stand-alone document intended for either submission as a peer-reviewed manuscript or technical report. By necessity, this resulted in some repetition of introductory material, background information, and methodology. As mentioned earlier, the main objective was to improve the understanding of macropore flow and transport processes in partially saturated, low permeability soils. This was achieved using two main investigation methods: (1) numerical simulations as described in Chapters 2 and 3, and (2) field experimentation described in Chapters 4 and 5. Chapter 2 presents fracture flow and transport simulations designed to identify the parameters controlling vertical water fluxes and evaluate the role of fracture-matrix interaction during infiltration into a partially saturated fractured soil block. Additional numerical simulations are used in Chapter 3 to investigate the importance of macropores on vertical contaminant migration through thin overburden deposits with a wider range of soil hydraulic properties. Readers will note that Chapter 3 is a departure in style from the other core chapters because it was written as a technical report for the Ontario Ministry of the Environment. The results of tension infiltration and simulated rainfall experiments from two field sites are presented in Chapters 4 and 5. Chapter 4 describes macropore flow processes using the results of the tension infiltration experiments. Chapter 5 examines dye and microsphere tracer patterns from all infiltration experiments to better understand contaminant transport processes, particularly those for colloids, in the vadose zone. Finally, Chapter 6 provides a listing of the important conclusions presented in earlier chapters along with recommendations for future work.

1.4 References

Beven, K. and P. Germann (1982), Macropores and water flow in soils, *Water Resour. Res.*, *18*(5), 1311-1325.

Buttle, J.M. and D.S. Turcotte (1999), Runoff processes on a forested slope on the Canadian shield, *Nord. Hydrol.*, *30*(1), 1-20.

Coles, N. and S. Trudgill (1985), The movement of nitrate fertiliser from the soil surface to drainage waters by preferential flow in weakly structured soils, Slapton, S. Devon, *Agr. Ecosyst. Environ.*, *13*(3-4), 241-259.

Dahan, O., R. Nativ, E.M. Adar, B. Berkowitz, and Z. Ronen (1999), Field observation of flow in a fracture intersecting unsaturated chalk, *Water Resour. Res.*, *35*(11), 3315-3326.

Dragila, M.I. and S.W. Wheatcraft (2001), Free-surface films, in *Conceptual Models of Flow and Transport in the Fractured Vadose Zone*, pp. 217-241, National Academy Press, Washington, D.C.

Fidler, S.R. (1997), Spatial and temporal variability of hydraulic response in fractured low permeability sediments, PhD thesis, University of Waterloo, Waterloo, Ontario, Canada.

Flury, M., H. Fluhler, W.A. Jury, and J. Leuenberger (1994), Susceptibility of soils to preferential flow of water: a field study, *Water Resour. Res.*, *30*(7), 1945-1954.

Foster, S.S.D. (1975), Chalk groundwater tritium anomaly - possible explanation, *J. Hydrol.*, *25*(1-2), 159-165.

Harrison, B., E.A. Sudicky, and J.A. Cherry (1992), Numerical analysis of solute migration through fractured clayey deposits into underlying aquifers, *Water Resour. Res.*, *28*(2), 515-526.

Hendrickx, J.M.H. and M. Flury (2001), Uniform and preferential flow mechanisms in the vadose zone, in *Conceptual Models of Flow and Transport in the Fractured Vadose Zone*, edited by National Research Council, pp. 149-187, National Academy Press, Washington, D.C., USA.

Jorgensen, P.R., M. Hoffmann, J.P. Kistrup, C. Bryde, R. Bossi, and K.G. Villholth (2002), Preferential flow and pesticide transport in a clay-rich till: Field, laboratory, and modeling analysis, *Water Resour. Res.*, *38*(11), 1246, doi:10.1029/2001WR000494.

Kelly, B.P. and M.L. Pomes (1998), Preferential flow and transport of nitrate and bromide in claypan soil, *Ground Water*, *36*(3), 484-494.

Kung, K.-J.S., E.J. Kladivko, T.J. Gish, T.S. Steenhuis, G. Bubenzer, and C.S. Helling (2000), Quantifying preferential flow by breakthrough of sequentially applied tracers: silt loam soil, *Soil Sci. Soc. Am. J.*, *64*(4), 1296-1304.

Laegdsmand, M., K.G. Villholth, M. Ullum, and K.H. Jensen (1999), Processes of colloid mobilization and transport in macroporous soil monoliths, *Geoderma*, *93*(1-2), 33-59.

McKay, L.D., D.J. Balfour, and J.A. Cherry (1998), Lateral chloride migration from a landfill in a fractured clay-rich glacial deposit, *Ground Water*, *36*(6), 988-999.

McKay, L.D. and J. Fredericia (1995), Distribution, origin, and hydraulic influence of fractures in a clay-rich glacial deposit, *Can. Geotech. J.*, *32*(6), 957-975.

McKay, L.D., W.E. Sanford, and J.M. Strong (2000), Field-scale migration of colloidal tracers in a fractured shale saprolite, *Ground Water*, *388*(1), 139-147.

McKay, L.D., R.W. Gillham, and J.A. Cherry (1993), Field experiments in a fractured clay till; 2. Solute and colloid transport, *Water Resour. Res.*, *29*(12), 3879-3890.

National Research Council (2001), Conceptual models of flow and transport in the fractured vadose zone, in *Conceptual Models of Flow and Transport in the Fractured Vadose Zone*, pp. 9-44, National Academy Press, Washington, D.C.

Perillo, C.A., S.C. Gupta, E.A. Nater, and J.F. Moncrief (1999), Prevalence and initiation of preferential flow paths in a sandy loam with argillic horizon, *Geoderma*, *89*(3-4), 307-331.

Podgorney, R.K., T.R. Wood, B. Faybishenko, and T.M. Stoops (2000), Spatial and temporal instabilities in water flow through variably saturated fractured basalt on a one-meter scale, in *Dynamics of Fluids in Fractured Rock*, Geophysical Monograph 122, edited by B. Faybishenko, P.A. Witherspoon, and S.M. Benson, pp. 129-146, American Geophysical Union, Washington, D.C., USA.

Robertson, W.D., B.M. Russell, and J.A. Cherry (1996), Attenuation of nitrate in aquitard sediments of southern Ontario, *J. Hydrol.*, *180*(1-4), 267-281.

Robins, N.S. (1998), Recharge: the key to groundwater pollution and aquifer vulnerability, in *Groundwater Pollution, Aquifer Recharge and Vulnerability*, Vol. 130, edited by N.S. Robins, pp. 1-5, Geological Society, Special Publications, London, England.

Scanlon, B.R. and R.S. Goldsmith (1997), Field study of spatial variability in unsaturated flow beneath and adjacent to playas, *Water Resour. Res.*, *33*(10), 2239-2252.

Simunek, J., N.J. Jarvis, M.T. van Genuchten, and A. Gärdenäs (2003), Review and comparison of models for describing non-equilibrium and preferential flow and transport in the vadose zone, *J. Hydrol.*, *272*(1-4), 14-35.

Su, G.W., J.T. Geller, K. Pruess, and J. Hunt (2000), Overview of preferential flow in unsaturated fractures, in *Dynamics of Fluids in Fractured Rock*, Geophysical Monograph 122, edited by B. Faybishenko, P.A. Witherspoon, and S.M. Benson, pp. 147-155, American Geophysical Union, Washington, DC, USA.

Tokunaga, T.K. and J. Wan (1997), Water film flow along fracture surfaces of porous rock, *Water Resour. Res.*, *33*(6), 1287-1295.

Watson, K.W. and R.J. Luxmoore (1986), Estimating macroporosity in a forest watershed by use of a tension infiltrometer, *Soil Sci. Soc. Am. J.*, *50*(3), 578-582.

Weiler, M. and F. Naef (2003a), Simulating surface and subsurface initiation of macropore flow, *J. Hydrol.*, *273*(1-4), 139-154.

Weiler, M. and F. Naef (2003b), An experimental tracer study of the role of macropores in infiltration in grassland soils, *Hydrol. Process.*, *17*(2), 477-493.

Wood, W.W., K.A. Rainwater, and D.B. Thompson (1997), Quantifying macropore recharge: examples from a semi-arid area, *Ground Water*, *35*(6), 1097-1106.

Zhang, G.S., K.Y. Chan, A. Oates, D.P. Heenan, and G.B. Huang (2007), Relationship between soil structure and runoff/soil loss after 24 years of conservation tillage, *Soil & Tillage Research*, *92*(1-2), 122-128.

Chapter 2
Simulation of Groundwater Recharge Dynamics in Partially Saturated Fractured Soils Incorporating Spatially Variable Fracture Apertures

2.1 Introduction

Groundwater recharge is an important component of the hydrologic cycle, yet its estimation can be a difficult task [*Scanlon et al.*, 2002]. This is due in large part to the number and complexity of processes occurring in the near surface environment. Groundwater recharge is dependent upon a variety of factors, including climate, vegetation, topography, geology, and soil properties [*de Vries and Simmers*, 2002]. Of particular concern in regions with structured soils is the influence of macropores. Research has shown that macropores can have a major influence on groundwater flow velocities, recharge rates and contaminant transport rates [*McKay et al.*, 1993b; *Wood et al.*, 1997; *Kelly and Pomes*, 1998; *Gerber et al.*, 2001; *Jorgensen et al.*, 2002]. There is increasing evidence that macropore flow is widespread and can represent a significant portion of the total flow system [*Flury et al.*, 1994; *Kelly and Pomes*, 1998; *Weiler and Naef*, 2003b]. Realistic estimates of groundwater recharge in these systems are vital for groundwater resource management and evaluation of aquifer vulnerability [*Robins*, 1998].

Fine-grained or structured soils contain macropores generated by weathering, desiccation, biological activity, and other processes [*Beven and Germann*, 1982]. Macropores may be broadly classified into two groups: planar features, such as fractures, and linear features, such as many biopores. Considering the frequency of occurrence, significant depths of penetration in cohesive sediments, and the propensity for mass transfer between the fracture and the soil matrix, due to their larger area-to-volume ratio, this study focuses specifically on fractures. This mass transfer between planar fracture voids and the adjacent low permeability, high porosity matrix has been identified as a critical feature controlling water and contaminant movement in vadose zone soils [*Simunek et al.*, 2003; *Weiler and Naef*, 2003b].

The current understanding of flow processes in the fractured vadose zone is limited [*Hendrickx and Flury*, 2001]. The difficulty inherent in measuring hydraulic properties in an unsaturated fracture, for example, has resulted in a paucity of experimental data at the fracture scale. Detailed measurements of infiltration in unsaturated natural fracture systems [*Dahan et al.*, 1999; *Podgorney et al.*, 2000] and flow through unsaturated fracture replicas [*Su et al.*, 1999] consistently demonstrate

the highly variable nature of the flow system dynamics in both time and space. Small-scale physical processes result in complex flow phenomena that can be challenging to describe and interpret [*National Research Council*, 2001]. Under partially saturated conditions, there are complex relationships between pressure, saturation and hydraulic conductivity in both the matrix and the fracture network. As a result, fractures could serve as either preferential flow pathways or as capillary barriers in the vadose zone [*Wang and Narasimhan*, 1985], depending on saturation conditions. It is therefore difficult to distinguish whether the matrix or the fractures represent the predominant flow system for a given groundwater recharge event. In addition, natural fractures have rough walls that control the flow and distribution of water in the fracture plane, particularly during variably saturated conditions where capillary pressures are a function of pore (or aperture) size. Very little is known about the influence of fracture roughness on partially saturated flow. Finally, there is the potential for significant imbibition of water from the fractures into the matrix during a recharge event, given the relatively large porosity and small pore sizes in the matrix compared to the fracture. The temporally and spatially varying hydraulic properties of the matrix and fractures create a dynamic system with substantial fracture-matrix interaction.

Valuable insight into the hydraulic behavior of fractured porous media has been derived through the use of numerical modeling tools [*Kwicklis and Healy*, 1993; *Gerke and van Genuchten*, 1993; *Berkowitz et al.*, 2001; *Simunek et al.*, 2003]. Discrete fracture models [*e.g., Therrien and Sudicky*, 1996] are particularly well suited for examination of small-scale flow dynamics. Discrete fracture models describe flow in both the fracture and matrix, while allowing explicit representation of relevant physical features at the fracture scale, such as incorporation of fracture roughness. Further, a common node approach can be used, where continuity of hydraulic head is assumed at common fracture and matrix nodes, thereby fully coupling the matrix and fracture flow fields. This enables the critical mass exchange between the fracture and matrix to be handled as part of the numerical solution, rather than requiring input of mass transfer coefficients as in the case of dual continuum approaches.

In this study we use a discrete fracture model to examine the nature of water flow dynamics and matrix-fracture interactions in shallow, fractured soils during simulated precipitation events. The goals are to investigate (1) the main processes controlling water flow during infiltration of meteoric water through a fractured vadose zone, (2) the relative contributions of the matrix and especially the fracture to deeper infiltration, (3) the influence of physical parameters, such as fracture roughness and matrix storage, on bulk vertical water fluxes, and (4) the degree to which fracture-matrix interaction governs water flow and the onset of preferential flow. The contributions of the fracture and the matrix to deep percolation are compared for different physical scenarios to identify the most

important factors influencing flow system response. The results provide insights into fracture flow processes and small-scale flow system dynamics in partially saturated systems. Important implications for groundwater resources in terms of estimating recharge rates and evaluating preferential flow mechanisms as controls for contaminant transport are discussed within the context of the numerical results.

2.2 Problem Description

This study uses numerical simulations to evaluate the complexity of groundwater recharge mechanisms and the important parameters controlling flow through low permeability, fractured soils under partially saturated conditions. The model is designed to represent infiltration through a typical soil profile during a large rainfall event. The study focuses on infiltration through a range of weathered fine-grained soils that are common in many glaciated regions and prone to preferential flow along the highly conductive fractures. The physical parameters defining the nature of the porous medium and fracture features are drawn from values reported in the literature. The physical dimensions of the model are limited to represent a simple vertical flow unit containing a single fracture. The model depth is restricted to the upper two meters of the soil profile, where fracturing is extensive, soil is predominantly unsaturated, and the flow system is most active during a recharge event. The fracture network is reduced to a single vertical fracture that extends throughout the soil profile. Although this represents a major simplification of the fracture network, it is consistent with field evidence showing that active, first order fractures often extend to considerable depth [*McKay et al.*, 1993b; *Fidler*, 1997]. In addition, we focus on relatively long, high-intensity rainfall events because they are most likely to generate significant vertical fluxes and preferential flow.

By varying individual system parameters for a series of model runs, we assess the relative sensitivity of each parameter in shaping the flow system response. Specifically, we investigate the influence of matrix properties, fracture properties, antecedent moisture conditions, and rainfall characteristics. Matrix properties, such as hydraulic conductivity and the description of unsaturated constitutive relations, are likely to influence infiltration in the matrix as well as fracture-matrix water exchange. Similarly, antecedent moisture conditions, which represent the water storage capacity of the highly porous matrix, can impact macropore flow and recharge rates. Varying rainfall intensity and duration is examined for rainfall events of equal probability (i.e., similar return periods) because they are significant factors influencing the onset of preferential flow [*Beven and Germann*, 1982; *Coles and Trudgill*, 1985].

Using the model we are also able to evaluate the influence of fracture properties, such as mean fracture aperture, fracture roughness, and hydraulic properties, which would be an extremely difficult

task in a field or even a laboratory setting. An important contribution of this study is the assessment of the role of fracture roughness on preferential flow. It is hypothesized that fracture roughness can lead to channeling of water in the plane of a fracture, resulting in increased flow velocities and transport rates down the fracture. Existing models of vadose zone fracture flow generally do not incorporate fracture aperture variability and represent fractures as parallel plates [*e.g., Therrien and Sudicky*, 1996] or with an assumed simplified geometry [*e.g., Gerke and van Genuchten*, 1996]. Those models that do incorporate fracture aperture variability often assume that the matrix is impermeable [*Pruess and Tsang*, 1990; *Kwicklis and Healy*, 1993; *Pruess*, 1998]. Previous attempts at incorporating variable aperture fractures into multiphase flow models have been limited to coupled one- or two-dimensional flow systems [*Abdel-Salam and Chrysikopoulos*, 1996; *Roels et al.*, 2003]. To the author's knowledge, this is the first attempt at incorporating variable fracture apertures for simulating partially saturated infiltration in a fully three-dimensional system.

2.3 Numerical Methods

The numerical model employed in this study, designated HydroGeoSphere, is a three-dimensional fully integrated subsurface and overland flow and solute transport model [*Therrien et al.*, 2005]. HydroGeoSphere is commercially available and is built upon the original subsurface model of *Therrien and Sudicky* [1996], which is capable of simulating variably saturated discretely-fractured porous media. A modified form of Richards equation is used to describe transient subsurface flow in both the matrix and the fracture. The model uses a common node approach, where fractures are discretized on the face of matrix blocks and they share common nodes. This approach ensures the continuity of hydraulic head at the fracture-matrix interface and no fluid leakage terms are required to account for mass exchange between fracture and matrix.

Simulations are performed on a simple three-dimensional soil block measuring 2.0 m high by 0.5 m wide by 0.5 m deep. A single vertical fracture is located in the middle of the domain at y = 0.25 m as shown in Figure 2.1. The soil block is discretized into elements 0.02 m by 0.02 m by 0.02 m in size. The mesh is refined near the fracture plane, where a nodal spacing of 0.002 m is used adjacent to the fracture in the y-direction, and gradually increased to a maximum of 0.02 m further from the fracture. This results in a domain with a total of 91,910 nodes and 85,000 elements, including 2,500 fracture elements.

All lateral boundaries in the model are assigned a no-flow boundary condition. Infiltration along the upper boundary is simulated using a constant flux equivalent to the applied rainfall rate. Overland flow is incorporated into the simulations to enable ponding and possible overland flow of water applied in excess of the infiltration rate. Any infiltration excess is allowed to either pond on the

surface or flow toward the fracture. However, runoff out of the model domain is not permitted since a detailed analysis of rainfall-runoff relationships is beyond the scope of this study. This is considered representative of a physical system with flat to gently undulating topography where groundwater recharge is focused in micro-depressions. The bottom boundary is assigned a constant head to simulate the presence of a static water table either beneath or within the flow domain. Top and bottom boundary conditions for the simulations are provided in Table 2.1 and Table 2.2. Hydrostatic initial conditions were assigned for all simulations. Details of the model dimensions and boundary conditions for the simulations are provided in Appendix A.

2.3.1 Porous Matrix Properties

The constitutive relation between capillary pressure, saturation and relative hydraulic conductivity is required in order to simulate variably saturated flow in porous media. The *van Genuchten* [1980] model is often used to describe these constitutive relations. The capillary pressure-saturation relationship of *van Genuchten* [1980] is given by

$$S_e(h) = \begin{cases} \left(1 + \alpha|h|^n\right)^{-m}, & h < 0, \\ 1, & h \geq 0, \end{cases} \tag{1}$$

where h is the pressure head, and α, n and m are empirical fitting parameters. The effective saturation, S_e, is given by

$$S_e(h) = \frac{\theta(h) - \theta_r}{\theta_s - \theta_r} \tag{2}$$

where θ is volumetric water content and θ_s and θ_r are the saturated and residual volumetric water contents, respectively. Additionally, applying Mualem's model for predicting unsaturated hydraulic conductivity [*Mualem*, 1976] yields $m = 1 - 1/n$.

The hydraulic conductivity $K(h)$ for the combined van Genuchten-Mualem (VGM) model is given as

$$K(h) = \begin{cases} K_s \cdot S_e^{0.5}\left[1-\left(1-S_e^{1/m}\right)^m\right]^2, & h < 0, \\ K_s, & h \geq 0, \end{cases} \tag{3}$$

where K_s is the saturated hydraulic conductivity of the porous matrix and S_e is defined in equation (2) above.

The VGM relation for relative hydraulic conductivity can induce numerical instability for small values of the fitting parameter n (i.e., n < 1.5), which are typical of relatively fine-grained soils [*Vogel et al.*, 2001]. A modified form of the VGM model was adopted by *Vogel et al.* [2001] to correct the shape of the *K(h)* function near saturation for small values of n, and consequently improve numerical stability. The modified VGM model involves the introduction of a minimum capillary height parameter, h_{min}, as well as the introduction of the parameter θ_m to replace θ_s in a revised form of the effective saturation equation as follows:

$$S_e^*(h) = \frac{\theta(h) - \theta_r}{\theta_m - \theta_r}. \tag{4}$$

The modified equations then become

$$S_e^*(h) = \begin{cases} \left(1 + \alpha|h|^n\right)^{-m}, & h < h_{\min}, \\ 1, & h \geq h_{\min}, \end{cases} \tag{5}$$

$$K(h) = \begin{cases} K_s \cdot S_e^{0.5}\left[\dfrac{1 - F(S_e)}{1 - F(1)}\right]^2, & h < h_{\min}, \\ K_s, & h \geq h_{\min}, \end{cases} \tag{6}$$

$$F(S_e) = \left(1 - S_e^{*1/m}\right)^m. \tag{7}$$

The parameters h_{min} and θ_m have little or no physical meaning and can be considered curve fitting parameters used to modify the shape of the water retention and hydraulic conductivity curves near saturation. *Vogel et al.* [2001] recommend using a small h_{min} value when no measured data are available. A value of h_{min} = -2.0 cm is adopted for this study. Accordingly, θ_m is set slightly larger than θ_s using the approximation

$$\theta_m = \theta_r + (\theta_s - \theta_r) \cdot \left[1 + (2\alpha)^n\right]^m \tag{8}$$

presented by *Vogel et al.* [2001]. In this study, the modified VGM model is employed for soils with small values of *n* (i.e., $n \leq 1.5$). The original VGM model is employed for soils with *n* values greater than 1.5. Parameter values used for the simulations are listed in Table 2.1 and Table 2.2. The soil water constitutive relations (*h*-*S*-K_r) using the parameters for the Base Case (see below) are shown in Figure 2.2.

2.3.2 Fracture Properties

Natural fractures have rough walls that control the flow and distribution of water. This roughness is expected to be particularly important under variably saturated conditions where capillary pressures are a function of pore (or aperture) size. The original model was modified to incorporate fracture roughness by assigning spatially variable apertures within the fracture plane. Fracture apertures are generated stochastically using Fourier transform techniques developed by *Robin et al.* [1993]. The aperture distribution is assumed to follow a spatially correlated log-normal distribution with a correlation length of 0.1 m (Table 2.1). The use of spatially correlated apertures preserves the connectivity of apertures of a particular size at a local scale. A log-normal distribution is chosen because it matches reasonably well with measured aperture distributions on rock fractures [*Gale*, 1987; *Keller*, 1998] and is consistent with earlier modeling studies [*Kueper and McWhorter*, 1991; *Abdel-Salam and Chrysikopoulos*, 1996; *Vandersteen et al.*, 2003]. The aperture field is mapped onto the fracture plane, with each fracture element assigned an aperture that is assumed to be constant for that element (i.e., a local parallel-plate approximation). Figure 2.1 shows a single realization of the aperture field within the fracture domain.

Fracture saturation and hydraulic conductivity are assigned on an element-by-element basis as functions of the elemental aperture. The Brooks-Corey model [1964] is used to describe the constitutive relations for the fracture. The capillary pressure-saturation relationship is given by

$$S_e = \left(\frac{h_{ae}}{h} \right)^{\lambda}, \quad h \le h_{ae} \tag{9}$$

where h_{ae} is the air entry pressure head and λ is an empirical pore size distribution index. The air entry pressure head for each fracture element can be related to fracture aperture by a simplified form of the Young-Laplace equation

$$h_{ae} = -\frac{2\sigma \cos(\beta)}{b \rho_w g} \tag{10}$$

where σ is the interfacial tension between air and water, β is the contact angle measured through the wetting phase, b is the fracture aperture, ρ_w is water density, and g is acceleration due to gravity. For all simulations, the contact angle, β, is assumed to be zero (i.e., water is perfectly wetting).

The saturated hydraulic conductivity K_{fs} for a constant aperture fracture element is given by

$$K_{fs} = \frac{b^2 \rho_w g}{12 \mu_w} \tag{11}$$

where μ_w is the viscosity of water. Utilizing a modified form of the Brooks-Corey expression based on theory by *Mualem* [1976], the relative hydraulic conductivity K_r for the element can be written as

$$K_r = \left(\frac{h_{ae}}{h} \right)^{2.5\lambda+2}, \quad h \le h_{ae} \tag{12}$$

The use of the Brooks-Corey model to describe constitutive relations for the fracture appears to be a reasonable approximation if each fracture element is considered a local macroscopic continuum. For idealized parallel plates, once the pressure head has decreased below the critical air entry value h_{ae}, the fracture would theoretically drain instantly, effectively reducing the saturation and relative hydraulic conductivity to zero. Such a free drainage situation is unlikely for natural rough-walled fractures. In a natural fracture, water will remain held under capillary forces in micro-scale roughness or as thin films on the fracture surface [*Tokunaga and Wan*, 1997; *Tokunaga et al.*, 2000]. This has led many researchers to conceptualize unsaturated flow in a rough-walled fracture as analogous to unsaturated flow in a porous medium [*Pruess and Tsang*, 1990; *Kwicklis and Healy*, 1993; *Liu and Bodvarsson*, 2001]. Standard constitutive relations can thus be used to describe the relationship between capillary pressure, saturation and hydraulic conductivity in a natural fracture. *Liu* [2004] has shown that a Brooks-Corey type model could accurately represent data from film flow experiments on fractured rock [*Tokunaga and Wan*, 1997; *Tokunaga et al.*, 2000]. Using the Brooks-Corey model, the λ parameter is considered to represent the micro-scale roughness at a scale below the level of fracture discretization. This conceptualization is consistent with the work of *Kueper and McWhorter* [1991]. The resulting constitutive relations for the fracture are qualitatively very similar to the more physically rigorous liquid configuration model of *Or and Tuller* [2003]. Fracture parameter values used in the simulations are listed in Table 2.1 and Table 2.2.

2.3.3 Implementation of Numerical Tracers

A numerical tracer technique is implemented to monitor movement of both *in situ* and infiltrating water throughout the simulations. Two separate hypothetical conservative tracers are utilized. A precipitation (Precip) tracer with a specified concentration of 1.0 kg/m^3 is applied with the rainfall on the upper soil surface. An initial Precip tracer concentration of 0.0 kg/m^3 is assigned throughout the soil block. Conversely, a Matrix tracer with an initial concentration of 1.0 kg/m^3 throughout the soil (representing *in situ* porewater) is flushed from the system by the applied rainfall, which has a specified concentration of 0.0 kg/m^3. The intent is not to conduct a detailed study of solute transport, but rather to allow differentiation between infiltrating rainfall and antecedent soil moisture when examining vertical flow rates. The solute transport parameters used for the numerical tracers are listed in Table 2.1.

2.3.4 Simulated Cases for Sensitivity Analyses

A large number of infiltration simulations were performed to evaluate the sensitivity of various input parameters during hypothetical groundwater recharge events. All simulations are referenced to a standard Base Case with input parameters listed in Table 2.1. Simulation parameters for the Base Case are chosen to be representative of hydrologic and soil conditions encountered in southern Ontario, however, these same conditions may apply to a wide range of settings where structured soils are found. Whenever possible, realistic field measured values or "average" values published in the literature are selected from a range of typical values. Given that published information on fracture roughness (aperture variability statistics) for unconsolidated porous materials do not exist, these parameter values are selected from published fractured rock experiments. The simulated rainfall rates are chosen to represent relatively extreme rainfall events for southern Ontario and are consistent with a return period of approximately 100 years. The rainfall conditions are chosen because they are likely to generate preferential flow under a range of different soil types.

For the remaining simulated cases, selected model input parameters are systematically varied about the "average" values used in the Base Case, within a reasonable range, to investigate sensitivity. The results of twelve cases with varying fracture and matrix properties, water table depth (i.e., antecedent moisture conditions), and rainfall intensity are presented here. The model input values used for the analyses are shown in Table 2.2. A summary of model input parameters for all simulated cases is provided in Appendix A.

2.4 Simulation Results and Discussion

2.4.1 Base Case Response

Infiltration for the Base Case represents a 1-in-100 year storm with a rainfall rate of 0.05 m/d falling on soil with matrix K_s = 0.02 m/d. The soil is in initial equilibrium with the water table at 3.0 m depth. The resulting initial soil matrix saturations throughout the profile are determined from the soil water retention curve shown in Figure 2.2. Initially the top 2.0 m of the fracture is essentially at or near residual saturation. The geometric mean fracture aperture in the Base Case is 100 μm, which corresponds to an equivalent bulk K_{fs} of 628 m/d for the fracture.

The simulation results for the Base Case after 4.0 days of rainfall are shown in Figure 2.3. Preferential flow down the fracture is clearly indicated by the Precip tracer concentration profile (Figure 2.3a). The fracture roughness results in widely ranging saturation conditions within the fracture (Figure 2.3b). The highest saturation regions of the fracture correspond to the smallest aperture regions (refer to aperture distribution in Figure 2.1), as expected based on capillary theory.

This variability in fracture aperture and saturation introduces flow channeling within the plane of the fracture. The groundwater velocity vectors plotted in Figure 2.3c show that flow is channeled through the mid-range apertures (40 to 150 μm). Flow tends to bypass the largest aperture segments because these segments remain preferentially unsaturated, resulting in an associated reduction in the relative hydraulic conductivity of the fracture. The largest aperture regions, which would be the dominant flow pathway under saturated conditions, are contributing little to vertical water flux. Flow tends to bypass the smallest aperture segments of the fracture because, although fully saturated, they have a much smaller hydraulic conductivity. Since the hydraulic conductivity of a saturated fracture segment is proportional to the square of the aperture, a small reduction in aperture can significantly decrease the saturated hydraulic conductivity of the fracture.

In order to assess the dynamics of the groundwater recharge process and the associated potential for contaminant movement, the transient vertical flows of water and numerical tracers are estimated. At each model time step, the vertical volumetric water flow rate crossing a horizontal slice at a depth of 0.5 m below ground surface (bgs) is calculated (see slice in Figure 2.1). The vertical mass flow rate of the Precip and Matrix tracers is also calculated at each time step. The total vertical flow rates are separated into contributions from the porous matrix elements and the fracture elements. Examining water and tracer fluxes across a slice is a novel approach that provides a more useful understanding of groundwater recharge potential and fracture-matrix mass exchange than interpretation of hydraulic heads or saturation conditions alone. The vertical flow rate of water calculated at 0.5 m depth is not equal to the amount of groundwater recharge that would reach an underlying aquifer, due to processes such as lateral flow, redistribution, and evapotranspiration. However, given a limited rooting depth for vegetation (<0.5 m bgs) and a relatively shallow water table (<10 m bgs), the calculated vertical flow rate serves as a reasonable proxy for groundwater recharge. In the same manner, the tracer flow rates give a reasonable indication of the potential for vertical solute transport to underlying groundwater resources.

The transient variations in vertical water and tracer flow rates at 0.5 m depth for the Base Case are shown in Figure 2.4. Initially, there is virtually no flow at 0.5 m depth in either the matrix or the fracture. Vertical water flow via the matrix begins to increase sharply after 1.0 day (Figure 2.4a). This early matrix flow is comprised of antecedent soil water that has been displaced downward by infiltrating rainwater, as indicated by the lack of a corresponding increase in Precip tracer flow during the same time period (Figure 2.4b). Although not shown, water is beginning to pond at the surface and saturates the smallest aperture regions near the top of the fracture at approximately 1.0 day. Beginning at around 1.4 days, there is a sharp increase in fracture water flow and an associated decrease in matrix water flow (Figure 2.4a). After both the matrix and fracture wetting fronts pass the

0.5 m depth, the fracture and matrix flow rates asymptotically approach steady-state values, with fracture flow constituting over 70% of the total vertical water flow near the end of the event.

The Base Case simulation results demonstrate that fracture-matrix interaction is key in controlling water and contaminant movement through fractured porous materials. There are two major competing processes: (1) preferential flow along the fracture, and (2) imbibition of water from the fracture into the matrix. For the Base Case, fracture flow is the dominant vertical flow process for water and, in particular, the surface applied tracer. It can be seen from Figure 2.4b that nearly the entire Precip tracer flow occurs through the fracture. The total Precip tracer flow (Figure 2.4b) closely follows the water flow in the fracture (Figure 2.4a), with only a slight reduction likely resulting from tracer diffusion into the matrix. Integrating over the entire five day infiltration event, the fracture contributes 65% of the total volume of water passing 0.5 m depth and accounts for 95% of the total Precip tracer mass. This illustrates the importance of the fracture network with respect to the movement of surface water to depth and has major implications for the mobility of contaminants originating at ground surface. In field situations, early breakthrough of contaminants at depth could have significant negative impacts on the quality of water resources, such as underlying aquifers or water bodies receiving tile drainage from agricultural fields.

In contrast, matrix imbibition is a significant process that limits the depth of penetration of infiltrating water and migration of *in situ* contaminants. Under the conditions simulated, the porous matrix has a large capacity for imbibing and storing water that flows down the fracture. Due to capillary forces, there is a significant horizontal hydraulic gradient near the wetting front (see Figure 2.3c at a depth of 1.5 m) that continually draws water away from the fracture. In the Base Case, the matrix allows sufficient water exchange such that the fracture and matrix wetting fronts are roughly coincident throughout the infiltration event (Figure 2.3b). The wetting front has not reached 2 m depth (Figure 2.3b) despite four days of continuous rainfall at a rate (0.05 m/d) 2.5 times greater than the saturated hydraulic conductivity of the matrix (0.02 m/d). Matrix imbibition is clearly effective at retarding the advance of the wetting front in the fracture.

The capillary forces that control matrix imbibition also play an important role in the movement of *in situ* contaminants. Figure 2.4 demonstrates that the flow of the *in situ* Matrix tracer is controlled by flow through the porous matrix. The total Matrix tracer flow (Figure 2.4c) is a subdued replica of the water flow through the porous matrix (Figure 2.4a). This indicates that the vertical water flow through the matrix is comprised primarily of water contained in the system prior to the infiltration event. The portion of the total Matrix tracer flow contributed by the fracture is very small. The lower permeability and greater capillary forces in the matrix restrict the advective transfer of the *in situ* tracer to the fracture. The practical implication is that *in situ* subsurface contaminants are highly

unlikely to be remobilized to a fracture and preferentially flow down the fracture, even under recharge conditions when fracture flow is significant. In effect, this physical process effectively slows vertical contaminant migration and improves the possibility that kinetically controlled attenuation mechanisms (*e.g.*, biodegradation and nutrient uptake) can influence contaminant fate and persistence in the subsurface.

The results indicate that the opposing processes of fracture flow and matrix imbibition, among others, give rise to complicated flow systems in vadose zone soils. The dynamics of the fracture-matrix interactions will vary depending on soil type, fracture properties, and other parameters. Given the complexity of these systems, it is difficult to predict in advance what physical processes will be most significant and where water and contaminants will end up following a precipitation event. The coupling of fracture and matrix flow processes in the model is critical for quantifying the variability of fracture and matrix fluxes, given the significant and highly transient nature of the fracture-matrix mass exchange. The quantitative results are not intended to provide absolute estimates of vertical flow rates or *in-situ* saturation conditions, but rather provide insights into the relative importance of different flow processes. As such, the Base Case results can now serve as a useful starting point to examine the control that different physical parameters have on system behavior.

2.4.2 Parameter Sensitivities

In order to assess the response of the modeled flow system to variations in input parameters, the transient vertical water fluxes for a variety of different simulated cases are compared to the reference Base Case.

2.4.2.1 Influence of Matrix Properties

The influence of varying selected matrix properties is shown in Figure 2.5. From Figure 2.5a it can be seen that the saturated hydraulic conductivity K_s of the matrix has a significant influence on the flow system. As might be expected, decreasing K_s by one order of magnitude (Case 1a) compared to the Base Case causes the fracture flow system to dominate. With a reduction in K_s the matrix is less effective at imbibing fluid from the fracture, creating a greater disequilibrium between the fracture and the matrix. Conversely, increasing K_s by one order of magnitude (Case 1b) causes fracture flow rates to become negligible since the matrix K_s exceeds the applied rainfall rate. The bulk vertical flow rates are similar for both Cases 1a and 1b. Given that groundwater flow velocity is inversely proportional to the effective area over which flow actually occurs, the fracture dominated flow in Case 1a results in much higher groundwater velocities. As a result, there is much faster downward transport of contaminants from surface in the lower hydraulic conductivity material.

The primary vertical flow mechanism (i.e., fracture versus matrix) is heavily dependent on the K_s of the matrix material. In unsaturated soils, the flow regime may switch from fracture dominated to matrix dominated with relatively small variations in K_s. The changes in matrix K_s could arise from soil layering, fracture coatings, or other features that inherently produce heterogeneity. The variability in matrix hydraulic conductivity may partly explain the substantial spatial variability in fracture flow observations in the field [*Glass et al.*, 2002; *Weiler and Fluhler*, 2004], where apparently similar fractures or other macropores differ substantially in their ability to transmit fluids.

The influence of modifying the VGM model parameters that define the constitutive relations for the matrix is shown in Figure 2.5b. In this scenario the K_s of the matrix remains constant, but the α and n parameters used for the constitutive relations are modified. The α and n parameters used for Case 2 are within one standard deviation of the average values for silt or silt loam textured soils [*Schaap and Leij*, 1998]. The values are typical of initial model parameter estimates suggested by *Carsel and Parrish* [1988] for soils in the textural range from sandy loam to clay loam. It can be seen from Figure 2.5b that the selection of VGM parameters has a considerable influence on the flow system response. Using parameters representative of coarser-grained material (Case 2a) delays the arrival of both the fracture and matrix wetting fronts at 0.5 m depth. This is a consequence of the lower initial matrix saturations generated by the revised VGM parameters. The altered shape of the soil water characteristic curve results in drier initial conditions. The upper portion of the soil profile becomes more effective at imbibing water from the fracture and requires larger amounts of water to reach saturation, thus delaying the advance of the wetting fronts. For this same reason, the use of VGM parameters representative of finer-grained materials (Case 2b) causes an increase in apparent antecedent moisture. This reduces the available soil moisture storage capacity, decreasing the time required for advancement of the wetting fronts and causing vertical flow at depth to increase more quickly.

It is apparent that the rate of vertical water flow is sensitive to the selection of the VGM model parameters. In many numerical simulations that include the vadose zone, it is common practice to estimate unsaturated soil hydraulic properties because they are either too expensive or too difficult to measure directly. Generic soil hydraulic properties are often selected from a soils database or they may be generated from pedotransfer functions based on soil texture, bulk density, organic matter or other available data. Even in an ideal situation, where VGM parameters are measured on field samples, the spatial variability can be large [*e.g., Hills et al.*, 1992; *Mallants et al.*, 1996], making selection of effective parameters difficult at a field scale. The uncertainty in these parameter estimates can drastically affect the nature, magnitude and timing of potential groundwater recharge as demonstrated by the vertical flow rates plotted in Figure 2.5b. Selection of appropriate VGM

parameters is made increasingly difficult by complex flow processes that occur in unsaturated fractured porous media. In this instance, application of VGM parameters for finer-grained material results in much quicker arrival of water at depth than for coarser-grained materials. Remembering that this result is not due to a variation in K_s, since it remains constant for each of the three cases, the results seem counter to initial expectations.

The sensitivity of the flow system dynamics to matrix properties is a key observation, especially considering the fact that the majority of bulk vertical water flow occurs through the fracture. The sensitivity of flow to matrix parameters points to fracture-matrix mass exchange as an important controlling process in moderating fracture flow. The results imply that careful selection of matrix hydraulic parameters is required for reliable simulations of flow and transport at small scales. The accuracy of flow predictions for a given rainfall event will depend heavily on the accuracy of matrix parameters due to their increased sensitivity. Given the spatial heterogeneity of matrix parameters, the relative uncertainty of groundwater recharge estimates obtained from field-scale simulations may be quite large and any results should be viewed with caution. It is important to note that we did not examine the long-term response of the system. At longer temporal scales, *Jansson et al.* [2005] have shown that flow transients can be dampened out due to flow redistribution, subsurface storage, evapotranspiration and other mechanisms. Further investigation is required to determine the net effect of short-term preferential flow events on long-term groundwater recharge estimates. Nevertheless, definition of matrix properties is crucial for contaminant transport, which can be highly dependent on individual rainfall events.

2.4.2.2 Influence of Fracture Properties

Figure 2.6a illustrates the influence of mean fracture aperture on the fluid flow rates. Decreasing the mean aperture to 50 μm (Case 3a) does not alter the timing of the fluxes observed at 0.5 m depth, but it causes a reduction in the magnitude of the fracture flow relative to the Base Case. Since the hydraulic conductivity of a saturated fracture segment is related to the aperture according to equation (11), a small reduction in aperture can significantly decrease the hydraulic conductivity of the fracture.

An increase in mean fracture aperture to 200 μm (Case 3b) did not significantly change the flow system response compared to the Base Case. Figure 2.6a demonstrates that the timing and magnitude of the vertical flow rates for both the 100 μm and 200 μm mean apertures were very similar. In fact, the vertical fracture flow rates are slightly smaller for the 200 μm fracture than for the 100 μm fracture. This outcome is somewhat unexpected given the four-fold increase in the saturated hydraulic conductivity of the fracture that results from doubling the mean fracture aperture.

It is not entirely clear why the flow behavior is so similar for the 100 μm (Base Case) and 200 μm (Case 3b) fracture aperture cases. One possible explanation is that there is a particular aperture threshold size, which is primarily dependent on the rainfall rate, that determines whether fractures flow under saturated or partially saturated conditions. Fractures with most of their aperture segments below this threshold size would be almost entirely saturated under steady flow conditions and therefore have the potential to restrict flow in the fracture. In this instance, flow through the fracture serves as the rate limiting process, and the system responds by forcing more water flow through the matrix. Above the threshold size, flow in the fractures is limited by the applied rainfall rate. The larger fractures have sufficient permeability to transmit the water even though they are only partially saturated. Increasing the size of the fracture above the threshold does not induce increased flow in the fracture; instead the fracture will flow at nearly the same rate but at a lower overall saturation.

Based on this explanation, the 50 μm fracture in Case 3a is representative of a fracture with the majority of aperture segments slightly below the threshold size and hence it flows under nearly saturated conditions. At the end of the 5-day rainfall event, when the wetting front has reached the lower boundary of the model domain and flow is nearly steady, the average fracture saturation is 93%. Small portions of the fracture, coinciding with the largest aperture regions, remain unsaturated, but this has relatively little influence on the overall flow in the fracture. The 100 μm (Base Case) and 200 μm (Case 3b) fractures have average saturations of 70% and 44%, respectively, at the end of the 5-day rainfall event. At the same time, approximately 59% of the total fracture area has greater than 80% saturation in the Base Case, compared to 28% of the area in Case 3b. Both fractures have the majority of aperture segments above the threshold size and thus flow under partially saturated conditions. The vertical flow rate in both fractures is nearly the same, since it is limited by the applied rainfall rate. Consequently, the larger fracture maintains a lower saturation in order to transmit the same volume of water. If the rainfall rate were increased, the threshold fracture aperture size would be expected to increase accordingly.

Vertical water flow rates associated with changes in fracture aperture variability are shown in Figure 2.6b. An increase or decrease in the variance of fracture apertures had little influence on the simulated flow rates. A wider distribution of fracture apertures (Case 4a) caused a slight decrease in the fracture flow rate after 2.5 days, while use of a parallel plate fracture (i.e., no aperture variance), as in Case 4b, resulted in a slightly increased fracture flow rate compared to the Base Case. The timing of the flow system response was nearly identical in each of the three cases. Although further examination is required, these results suggest that aperture variability is not a significant control on vertical water flow rates. The results of other simulations not presented here also indicate that other

fracture parameters, namely the spatial correlation length for fracture aperture and the Brooks-Corey λ parameter, have little influence on flow system response.

The relative insensitivity of simulated vertical flow rates to fracture properties has important implications for fracture modeling strategies. Parallel plate approximations for fractures are commonly used when modeling groundwater flow processes. However, the suitability of this practice for modeling flow in the vadose zone has not been rigorously tested in previous studies. The results of this numerical experiment suggest that fracture roughness, along with other small-scale geometric and hydraulic fracture parameters, could potentially be neglected in larger scale simulations of groundwater flow. There is a major practical benefit in that gathering detailed information on fracture geometry and hydraulic properties may not be as critical for groundwater recharge simulations. Reliable field data on the location, size and extent of fractures is very difficult to obtain and verify, particularly for large-scale problems. Detailed information on aperture distributions and spatial correlation is even more difficult to collect and is usually limited to micro-scale investigations on individual fractures. Field measured mean fracture apertures and spacings [*e.g., McKay et al.*, 1993b; *Hinsby et al.*, 1996; *Fidler*, 1997] would appear to be suitable for most flow simulations. That stated, fracture aperture variability may indeed be important for transport of solutes and colloidal materials. Based on the degree of flow channeling and associated fingering of the numerical tracers observed within the fracture plane, it is possible that fracture roughness will be an important parameter for contaminant transport. This will be the subject of subsequent research.

Of the fracture parameters tested, mean aperture appears to be the most important in terms of influencing flow rates. This is consistent with earlier studies of multiphase flow in variable aperture fractures [*Mendoza*, 1992; *Steele and Lerner*, 2001; *Vandersteen et al.*, 2003]. It should be noted, however, that these other studies did not incorporate the influence of a porous matrix. Few other studies have investigated water flow in and exchange between a variable aperture fracture and an unsaturated porous matrix. The simulations of *Abdel-Salam and Chrysikopoulos* [1996], using a quasi-three-dimensional model for fractured rock, were similar in nature and offer the most reasonable comparison. They showed that the influence of fracture aperture variability was muted and there was less fingering within the fracture plane when there was moisture exchange between the fracture and the matrix. We observed similar results, although the degree of fracture-matrix water exchange was significantly greater in our study due to differences in porosity of the geologic material. The majority of modeling studies involving unsaturated fracture flow have dealt with fractured rocks, which generally have low primary porosity (e.g., $\theta_s = 0.005$ used in *Abdel-Salam and Chrysikopoulos* [1996]) compared to typical structured soils ($\theta_s = 0.40$ in this study). The higher matrix porosity increases the capacity for imbibition of water during infiltration, at least under partially saturated

conditions, thereby reducing the influence of aperture variability and other parameters related to fracture roughness (i.e., Brooks-Corey λ and aperture spatial correlation length).

Overall, the simulation results are considerably less sensitive to variations in fracture parameters than matrix parameters. The fracture controlled bulk water flow to depth in all but one of the simulated cases (Case 1b), yet the variability of the flow system response is most sensitive to matrix, not fracture, properties. This behaviour suggests that incorporation of matrix flow processes is necessary even in situations where fracture-dominated flow occurs. In the context of groundwater recharge, the interplay between fracture and matrix flow processes is key in determining how fast and how deep water will penetrate following a given precipitation event. Depending on the matrix-fracture interaction, meteoric waters infiltrating from ground surface will either rapidly bypass the root zone and maximum evaporative depth, or be held in the shallow soil environment and subjected to these removal mechanisms. There are obvious consequences related to the efficiency of a precipitation event at actually inducing groundwater recharge below the active zone of evapotranspiration. It is also apparent that coupling of matrix and fracture flow processes is vital for examining flow behaviour in systems with such a high degree of fracture-matrix interaction. In this study, the fracture and matrix flow processes are fully coupled with the model calculating the mass exchange as part of the solution. The resulting assessment of vertical fluxes is not biased by specification of fracture-matrix mass exchange terms, and we are able to openly evaluate which properties exhibit the strongest control on flow system dynamics.

2.4.2.3 Influence of Initial and Boundary Conditions

Figure 2.7 demonstrates the influence of varying initial and boundary conditions on the vertical flow rate characteristics. Varying water table depth, which influences antecedent moisture conditions, is shown to have a significant effect (Figure 2.7a). A shallower water table results in increased initial pressure heads throughout the model domain and consequently higher initial matrix and fracture saturations. When the water table elevation is raised to 1.0 m below ground surface (Case 5a), there is a decrease in the available water storage capacity in the system (relative to the Base Case) and both the fracture and matrix reach saturation more quickly following the onset of infiltration. The total vertical water flow rate is then dominated by the fracture because of its much greater hydraulic conductivity. Lowering the water table to 5.0 m below ground surface (Case 5b) decreases the initial saturations. The matrix then has a larger capacity to imbibe and store infiltrating water, whether from ground surface or the fracture. This produces a slight delay in the arrival of both the fracture and matrix wetting fronts at 0.5 m depth, although the magnitudes of the flow rates remain similar to the Base Case. The overall effect is similar to the influence of changing matrix storage properties by modifying the shape of the water retention curve discussed in section 2.4.2.1.

Antecedent moisture conditions play an important role in initiating and maintaining flow in the fracture. As matrix pressure heads increase and the soil approaches saturation, the role of imbibition is increasingly muted. Consequently, fracture flow is initiated more readily and water flows down the fracture almost unabated. The flow system response will become increasingly sensitive as soil moisture approaches saturation. The degree of sensitivity will obviously depend on the shape of the soil water retention curve (see Figure 2.2), soil layering, and the history of prior infiltration events. The end result is that structured soils in shallow water table environments or after recent rainfall events will be highly susceptible to preferential flow and potentially vulnerable to contaminant migration. Moreover, in areas with seasonally fluctuating water tables, groundwater recharge rates would be expected to vary considerably during the year.

To simulate the influence of rainfall rate, two infiltration simulations (Cases 6a and 6b) were performed with higher intensity rainfall events (Figure 2.7b). In order to remain consistent with the Base Case, the duration of these rainfall events was decreased to represent equivalent 1-in-100 year storm events (see Table 2.2). The resulting vertical flow rates for a rainfall event with an intensity of 0.125 m/d and duration of one day are shown in Figure 2.7b. As expected, the increased rainfall rate causes vertical flow to occur more quickly at 0.5 m depth. With a rainfall rate more than six times greater than the matrix K_s, vertical flow is predicted at 0.5 m depth in the fracture approximately 0.5 days after initiation of rainfall. The matrix and fracture wetting fronts arrive almost simultaneously. Following initiation of flow at depth, the fracture flow rate increases quickly and is the major component of total vertical flow for the duration of the rainfall event. The magnitude of the total flow rate near the end of the rainfall event is greater under the increased rainfall rate. The peak total flow rate for Case 6a reaches only 79% of the rainfall input since it is a much shorter duration event than the Base Case; one day compared to five days. Following cessation of rainfall, the fracture flow rate drops quickly as water redistributes and is imbibed into the porous matrix.

The results for Case 6b, a rainfall event with an intensity of 1.2 m/d and duration of one hour (0.042 d), show there is very little vertical flow at 0.5 m depth either during or following rainfall (Figure 2.7b). What little flow that does occur is primarily gravity drainage of water through the matrix following the rainfall event. The relatively low flow rate at depth is attributed to the short rainfall duration and the comparatively small volume of water that was applied. The lack of vertical flow for Case 6b is striking considering that it also represents a storm with a 100-year return period. It seems that large infiltration volumes are required to overcome matrix storage and initiate preferential flow at depth. Case 6b once more illustrates the governing influence that the matrix has in moderating fracture flow.

The influences of antecedent moisture and rainfall intensity were examined independently in this study and both had a considerable impact on vertical flow in the system. Other researchers suggest that a number of factors, primarily rainfall intensity and antecedent moisture content, combine to control the development of preferential flow in structured soils [*Coles and Trudgill*, 1985; *Heppell et al.*, 2002]. *Heppell et al.* [2002] used statistical analysis of field data to investigate antecedent and rainfall controls on macropore flow in clay soils. They distinguished between macropore flow controlled by antecedent moisture and that controlled by rainfall characteristics (intensity, duration, and total rainfall). While related, they conclude that rainfall intensity and amount are more important than antecedent conditions in generating macropore flow. It is difficult to compare our results to those of *Heppell et al.* [2002] since the various antecedent moisture cases simulated here had a rainfall duration that was long enough (i.e., 5 days) to not only initiate fracture flow, but to allow steady flow to develop at 0.5 m depth, regardless of antecedent moisture conditions. We can state, based on the results from Case 6, that rainfall duration appears to be more important than rainfall intensity in terms of controlling deep fracture flow for rainfall events of equal probability. It is important to remember that the model only represents local scale ponding and overland flow on a flat surface. That is, it does not account for surface runoff beyond the lateral boundaries of the model. Under field or watershed scale conditions, the influence of rainfall intensity would likely be increased due to overland flow processes, and the subsequent impact on groundwater recharge would depend on surface topography, slope position, vegetation, and other factors. The complex interrelationship between antecedent moisture, rainfall characteristics and the onset of preferential flow warrants further investigation.

2.5 Summary and Conclusions

The goal of this paper was to investigate the role of fracture-matrix interaction and different parameters in controlling transient infiltration through partially saturated fractured soils. A discrete fracture model with fully coupled fracture and matrix flow processes was used to simulate flow and transport through a variably saturated fractured porous medium containing a single variable aperture fracture. Infiltration simulations were performed using extreme rainfall events (100-year return period) on a relatively simple physical system designed to represent a low permeability fractured soil. Although the model results should be used with caution when predicting actual groundwater recharge rates, they provided valuable insights into flow processes and identified the key parameters that control episodic groundwater recharge in these environments.

Simulations showed complex flow dynamics in the fractured vadose zone with a high degree of fracture-matrix interaction. The matrix exhibits a strong influence on water flow through the system.

Imbibition of water from the fracture into the matrix, which has a much larger storage capacity, limits the advance of the wetting front in the fracture. Modifying initial matrix saturation conditions, whether by changing soil constitutive relations or water table depth, and other matrix properties (e.g., K_s) significantly alters the timing and magnitude of vertical water flow. Together, the results demonstrate the importance of vadose zone matrix properties in controlling the timing and pathway of water flow during groundwater recharge events. The larger storage capacity and greater capillary forces in the matrix also serve to slow the vertical migration of contaminants, most notably *in-situ* contaminants. Once a contaminant is contained within the matrix, whether by direct infiltration, matrix imbibition or diffusion, only a small fraction is likely to be mobilized back into the fracture. The imbibition of water and associated contaminants from the fracture into the matrix, combined with the unlikely remobilization of contaminants back into the fracture, effectively retards the vertical migration of contaminants through the vadose zone. In turn, this improves the chances for chemical and biological attenuation mechanisms to act in further reducing contaminant fluxes.

Varying fracture properties had a comparatively minor influence on flow system response. As in other studies, the mean fracture aperture had the greatest influence on fracture hydraulic properties. It is believed that water exchange between the fracture and the matrix during infiltration reduced the influence of aperture variability and other parameters related to small-scale fracture roughness. This result implies that fracture aperture variability can be neglected in larger-scale models of groundwater recharge, at least in terms of water movement. Since information on fracture geometry at field scales is extremely difficult to obtain or verify, this would be highly advantageous. There is limited evidence that tracer movement may be influenced by fracture roughness, but further simulations are required for confirmation.

In spite of the insensitivity of the flow system to fracture properties, the fracture still played an important role in both vertical water and tracer movement. For the Base Case, the fracture contributed the majority of the water flow and transported nearly the entire mass of surface applied tracer at 0.5 m depth. Evidently, determining the factors and mechanisms that control the onset of fracture flow in natural systems will be vitally important for predicting groundwater recharge and water quality impacts in fractured soil environments. Fracture flow has serious implications for migration of surface applied chemicals and is expected to be even more important for the transport of colloids, such as pathogens and colloid-bound radionuclides, that are less prone to matrix diffusion.

Additional simulations looking at a number of factors in combination would be beneficial for characterizing groundwater recharge. The influence of several key physical parameters was demonstrated in this study. However, the relationship between some parameters remains uncertain and is likely to be vitally important for flow and transport processes. For example, field evidence

suggests a strong interrelationship between rainfall intensity, rainfall duration, and antecedent soil moisture content in controlling flow system behavior. Further quantification of this and other relationships is necessary for improved understanding of groundwater recharge and preferential flow.

2.6 References

Abdel-Salam, A. and C.V. Chrysikopoulos (1996), Unsaturated flow in a quasi-three-dimensional fractured medium with spatially variable aperture, *Water Resour. Res.*, *32*(6), 1531-1540.

Berkowitz, B., R. Nativ, and E. Adar (2001), Evaluation of conceptual and quantitative models of fluid flow and chemical transport in fractured media, in *Conceptual Models of Flow and Transport in the Fractured Vadose Zone*, pp. 115-147, National Academy Press, Washington, D.C., USA.

Beven, K. and P. Germann (1982), Macropores and water flow in soils, *Water Resour. Res.*, *18*(5), 1311-1325.

Brooks, R.H. and A.T. Corey (1964), Hydraulic properties of porous media, Hydrology Papers No. 3, University of Colorado, Fort Collins, Colorado, USA.

Carsel, R.F. and R.S. Parrish (1988), Developing joint probability distributions of soil water retention characteristics, *Water Resour. Res.*, *24*(5), 755-769.

Coles, N. and S. Trudgill (1985), The movement of nitrate fertiliser from the soil surface to drainage waters by preferential flow in weakly structured soils, Slapton, S. Devon, *Agr. Ecosyst. Environ.*, *13*(3-4), 241-259.

Dahan, O., R. Nativ, E.M. Adar, B. Berkowitz, and Z. Ronen (1999), Field observation of flow in a fracture intersecting unsaturated chalk, *Water Resour. Res.*, *35*(11), 3315-3326.

de Vries, J.J. and I. Simmers (2002), Groundwater recharge: an overview of processes and challenges, *Hydrogeol. J.*, *10*(1), 5-17.

Fidler, S.R. (1997), Spatial and temporal variability of hydraulic response in fractured low permeability sediments, PhD thesis, University of Waterloo, Waterloo, Ontario, Canada.

Flury, M., H. Fluhler, W.A. Jury, and J. Leuenberger (1994), Susceptibility of soils to preferential flow of water: a field study, *Water Resour. Res.*, *30*(7), 1945-1954.

Gale, J.E. (1987), Comparison of coupled fracture deformation and fluid flow models with direct measurements of fracture pore structure and stress-flow properties, in *Proceedings of the 28th U.S. Symposium on Rock Mechanics*, edited by Farmer, Ian W., Daemen, Jaak J. K., Desai, C. S., Glass, C. E., and Neuman, Shlomo P., pp. 1213-1222, A.A. Balkema, Rotterdam, Netherlands, 29 June-1 July 1987.

Gerber, R.E., J.I. Boyce, and K.W. Howard (2001), Evaluation of heterogeneity and field-scale groundwater flow regime in a leaky till aquitard, *Hydrogeol. J.*, *99*(1), 60-78.

Gerke, H.H. and M.T. van Genuchten (1993), A dual-porosity model for simulating the preferential movement of water and solutes in structured porous media, *Water Resour. Res.*, *29*(2), 305-319.

Gerke, H.H. and M.T. van Genuchten (1996), Macroscopic representation of structural geometry for simulating water and solute movement in dual-porosity media, *Adv. Water Resour.*, *19*(6), 343-357.

Glass, R.J., M.J. Nicholl, A.L. Ramirez, and W.D. Daily (2002), Liquid phase structure within an unsaturated fracture network beneath a surface infiltration event: Field experiment, *Water Resour. Res.*, *38*(10), 1199, doi:10.1029/2000WR000167.

Hendrickx, J.M.H. and M. Flury (2001), Uniform and preferential flow mechanisms in the vadose zone, in *Conceptual Models of Flow and Transport in the Fractured Vadose Zone*, edited by National Research Council, pp. 149-187, National Academy Press, Washington, D.C., USA.

Heppell, C.M., F. Worrall, T.P. Burt, and R.J. Williams (2002), A classification of drainage and macropore flow in an agricultural catchment, *Hydrol. Process.*, *16*(1), 27-46.

Hills, R.G., D.B. Hudson, and P.J. Wierenga (1992), Spatial variability at the Las Cruces trench site, in *Proceedings of the International Workshop on Indirect Methods for Estimating the Hydraulic Properties of Unsaturated Soils*, edited by van Genuchten, M. T., Leij, F. J., and Lund, L. J., pp. 529-538, University of California, Riverside, California, USA, 11-13 October 1989.

Hinsby, K., L.D. McKay, P. Jorgensen, M. Lenczewski, and C.P. Gerba (1996), Fracture aperture measurements and migration of solutes, viruses, and immiscible creosote in a column of clay-rich till, *Ground Water*, *34*(6), 1065-1075.

Jansson, C., B. Espeby, and P.E. Jansson (2005), Preferential water flow in a glacial till soil, *Nord. Hydrol.*, *36*(1), 1-11.

Jorgensen, P.R., M. Hoffmann, J.P. Kistrup, C. Bryde, R. Bossi, and K.G. Villholth (2002), Preferential flow and pesticide transport in a clay-rich till: Field, laboratory, and modeling analysis, *Water Resour. Res.*, *38*(11), 1246, doi:10.1029/2001WR000494.

Keller, A. (1998), High resolution, non-destructive measurement and characterization of fracture apertures, *Int. J. Rock Mech. Min. Sci. & Geomech. Abstr.*, *35*(8), 1037-1050.

Kelly, B.P. and M.L. Pomes (1998), Preferential flow and transport of nitrate and bromide in claypan soil, *Ground Water*, *36*(3), 484-494.

Kueper, B.H. and D.B. McWhorter (1991), Behavior of dense, nonaqueous phase liquids in fractured clay and rock, *Ground Water*, *29*(5), 716-728.

Kwicklis, E.M. and R.W. Healy (1993), Numerical investigation of steady liquid water flow in a variably saturated fracture network, *Water Resour. Res.*, *29*(12), 4091-4102.

Liu, H.H. (2004), A constitutive-relationship model for film flow on rough fracture surfaces, *Hydrogeol. J.*, *12*, 237-240.

Liu, H.H. and G.S. Bodvarsson (2001), Constitutive relations for unsaturated flow in a fracture network, *J. Hydrol.*, *252*(1-4), 116-125.

Mallants, D., B.P. Mohanty, D. Jacques, and J. Feyen (1996), Spatial variability of hydraulic properties in a multi-layered soil profile, *Soil Sci.*, *161*(3), 167-181.

McKay, L.D., J.A. Cherry, and R.W. Gillham (1993), Field experiments in a fractured clay till: 1. Hydraulic conductivity and fracture aperture, *Water Resour. Res.*, *29*(4), 1149-1162.

Mendoza, C.A. (1992), Capillary pressure and relative transmissivity relationships describing two-phase flow through rough-walled fractures in geologic materials, PhD thesis, University of Waterloo, Waterloo, Ontario, Canada.

Mualem, Y. (1976), A new model for predicting the hydraulic conductivity of unsaturated soils, *Water Resour. Res.*, *12*(3), 513-522.

National Research Council (2001), Conceptual models of flow and transport in the fractured vadose zone, in *Conceptual Models of Flow and Transport in the Fractured Vadose Zone*, pp. 9-44, National Academy Press, Washington, D.C., USA.

Or, D. and M. Tuller (2003), Hydraulic conductivity of partially saturated fractured porous media: flow in a cross-section, *Adv. Water Resour.*, *26*(8), 883-898.

Podgorney, R.K., T.R. Wood, B. Faybishenko, and T.M. Stoops (2000), Spatial and temporal instabilities in water flow through variably saturated fractured basalt on a one-meter scale, in *Dynamics of Fluids in Fractured Rock*, Geophysical Monograph 122, edited by B. Faybishenko,

P.A. Witherspoon, and S.M. Benson, pp. 129-146, American Geophysical Union, Washington, D.C., USA.

Pruess, K. (1998), On water seepage and fast preferential flow in heterogeneous, unsaturated rock fractures, *J. Contam. Hydrol.*, *30*(3-4), 333-362.

Pruess, K. and Y.W. Tsang (1990), On two-phase relative permeability and capillary pressure of rough-walled rock fractures, *Water Resour. Res.*, *26*(9), 1915-1926.

Robin, M.J.L., A.L. Gutjahr, E.A. Sudicky, and J.L. Wilson (1993), Cross-correlated random field generation with the direct fourier transform method, *Water Resour. Res.*, *29*(7), 2385-2397.

Robins, N.S. (1998), Recharge: the key to groundwater pollution and aquifer vulnerability, in *Groundwater Pollution, Aquifer Recharge and Vulnerability*, Vol. 130, edited by N.S. Robins, pp. 1-5, Geological Society, Special Publications, London, England.

Roels, S., K. Vandersteen, and J. Carmeliet (2003), Measuring and simulating moisture uptake in a fractured porous medium, *Adv. Water Resour.*, *26*(3), 237-246.

Scanlon, B.R., R.W. Healy, and P.G. Cook (2002), Choosing appropriate techniques for quantifying groundwater recharge, *Hydrogeol. J.*, *10*(1), 18-39.

Schaap, M.G. and F.J. Leij (1998), Database-related accuracy and uncertainty of pedotransfer functions, *Soil Sci.*, *163*(10), 765-779.

Simunek, J., N.J. Jarvis, M.T. van Genuchten, and A. Gärdenäs (2003), Review and comparison of models for describing non-equilibrium and preferential flow and transport in the vadose zone, *J. Hydrol.*, *272*(1-4), 14-35.

Steele, A. and D.N. Lerner (2001), Predictive modelling of NAPL injection tests in variable aperture spatially correlated fractures, *J. Contam. Hydrol.*, *49*(3-4), 287-310.

Su, G.W., J.T. Geller, K. Pruess, and F. Wen (1999), Experimental studies of water seepage and intermittent flow in unsaturated, rough-walled fractures, *Water Resour. Res.*, *35*(4), 1019-1037.

Therrien, R., R.G. McLaren, E.A. Sudicky, and S.M. Panday (2005), HydroGeoSphere: A three-dimensional numerical model describing fully-integrated subsurface and surface flow and solute transport, Groundwater Simulations Group, Waterloo, Ontario, Canada.

Therrien, R. and E.A. Sudicky (1996), Three-dimensional analysis of variably-saturated flow and solute transport in discretely-fractured porous media, *J. Contam. Hydrol.*, *23*(1-2), 1-44.

Tokunaga, T.K., J. Wan, and S.R. Sutton (2000), Transient film flow on rough fracture surfaces, *Water Resour. Res.*, *36*(7), 1737-1746.

Tokunaga, T.K. and J. Wan (1997), Water film flow along fracture surfaces of porous rock, *Water Resour. Res.*, *33*(6), 1287-1295.

van Genuchten, M.T. (1980), A closed-form equation for predicting the hydraulic conductivity of unsaturated soils, *Soil Sci. Soc. Am. J.*, *44*, 892-898.

Vandersteen, K., J. Carmeliet, and J. Feyen (2003), A network modeling approach to derive unsaturated hydraulic properties of a rough-walled fracture, *Transport Porous Med.*, *50*(3), 197-221.

Vogel, T., M.T. van Genuchten, and M. Cislerova (2001), Effect of the shape of the soil hydraulic functions near saturation on variably-saturated flow predictions, *Adv. Water Resour.*, *24*(2), 133-144.

Wang, J.S.Y. and T.N. Narasimhan (1985), Hydrologic mechanisms governing fluid flow in a partially saturated fractured porous medium, *Water Resour. Res.*, *21*(12), 1861-1874.

Weiler, M. and H. Fluhler (2004), Inferring flow types from dye patterns in macroporous soils, *Geoderma*, *120*(1-2), 137-153.

Weiler, M. and F. Naef (2003), An experimental tracer study of the role of macropores in infiltration in grassland soils, *Hydrol. Process.*, *17*(2), 477-493.

Wood, W.W., K.A. Rainwater, and D.B. Thompson (1997), Quantifying macropore recharge: examples from a semi-arid area, *Ground Water*, *35*(6), 1097-1106.

2.7 Figures and Tables

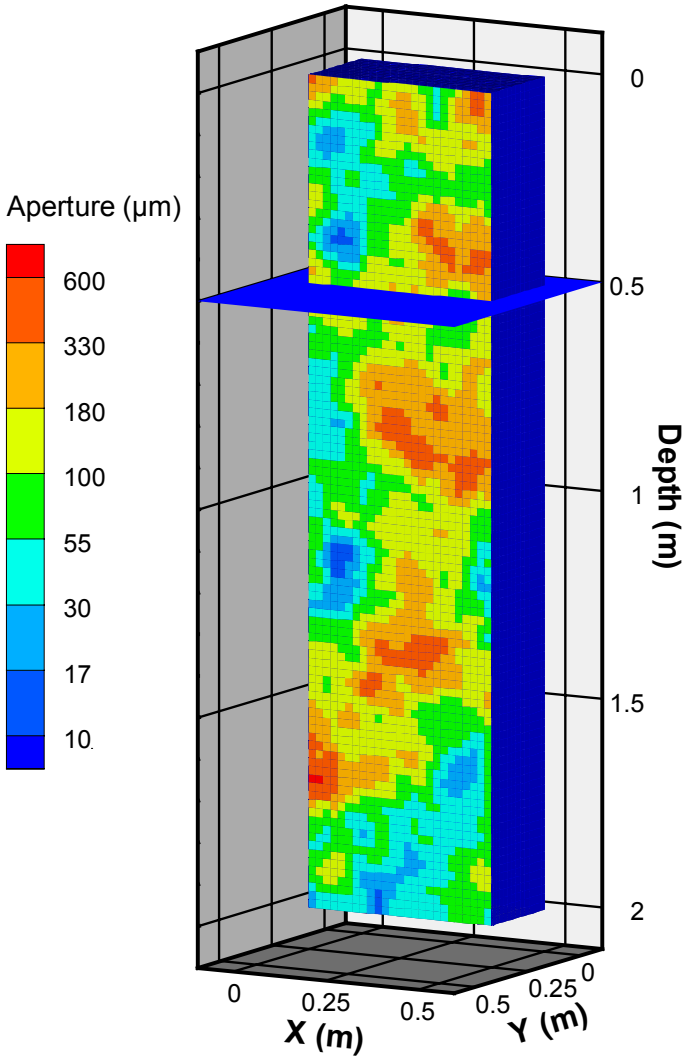

Figure 2.1. Model half-domain showing the spatial aperture distribution within the fracture plane, located at Y = 0.25 m, for the Base Case (refer to Table 2.1 for statistical properties of the fracture aperture distribution). Vertical water flow rates are calculated at the location of the horizontal slice (Depth = 0.5 m).

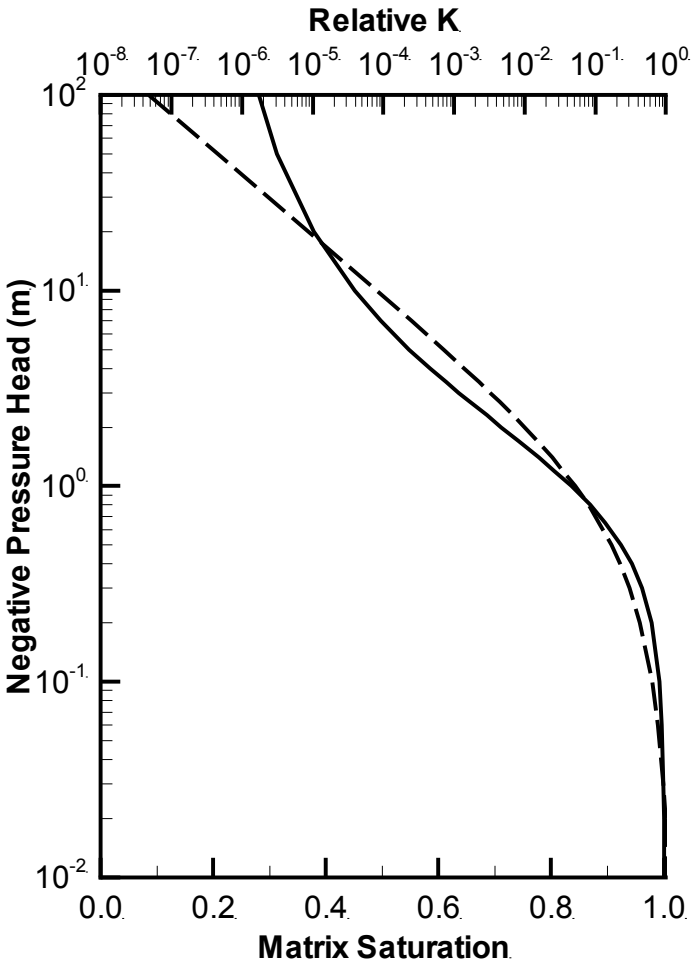

Figure 2.2. Graph of the constitutive relations for the Base Case soil matrix showing saturation (solid line) and relative hydraulic conductivity (dashed line) versus capillary pressure head.

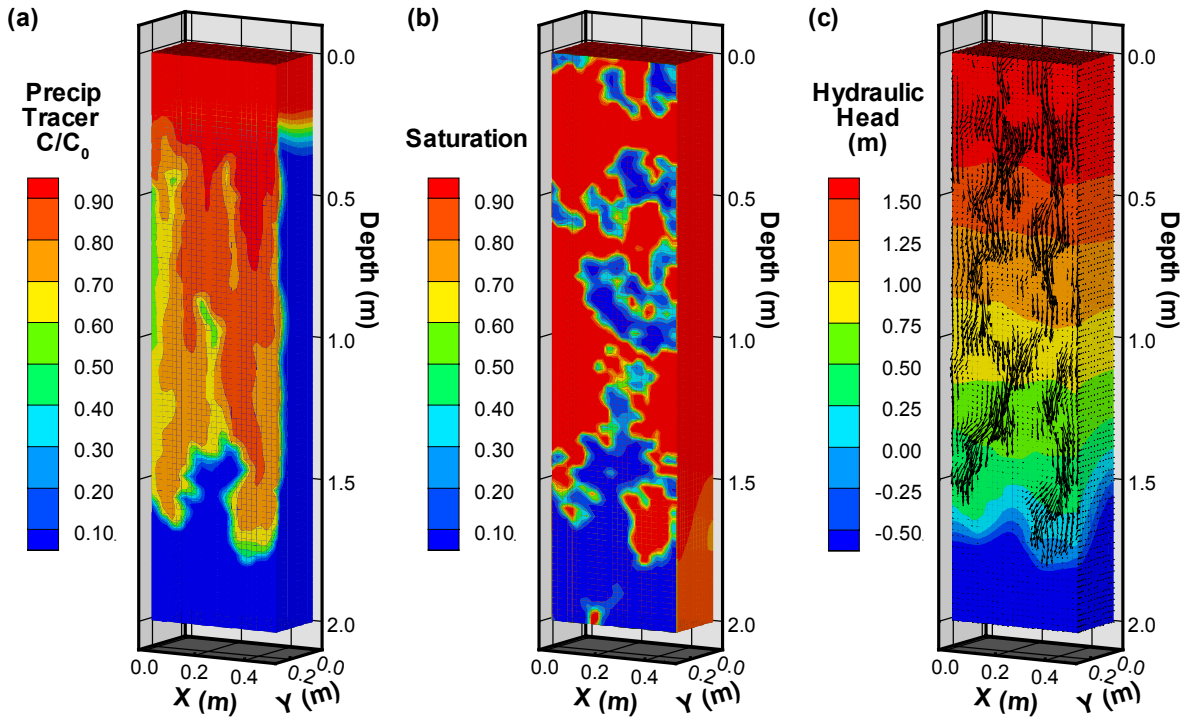

Figure 2.3. Simulation results showing (a) Precip tracer concentration, (b) saturation and (c) hydraulic head for the model half-domain after 4.0 days of continuous rainfall. The fracture plane is shown at Y = 0.25 m. Arrows representing groundwater velocity vectors within the fracture plane are included in the hydraulic head diagram (c).

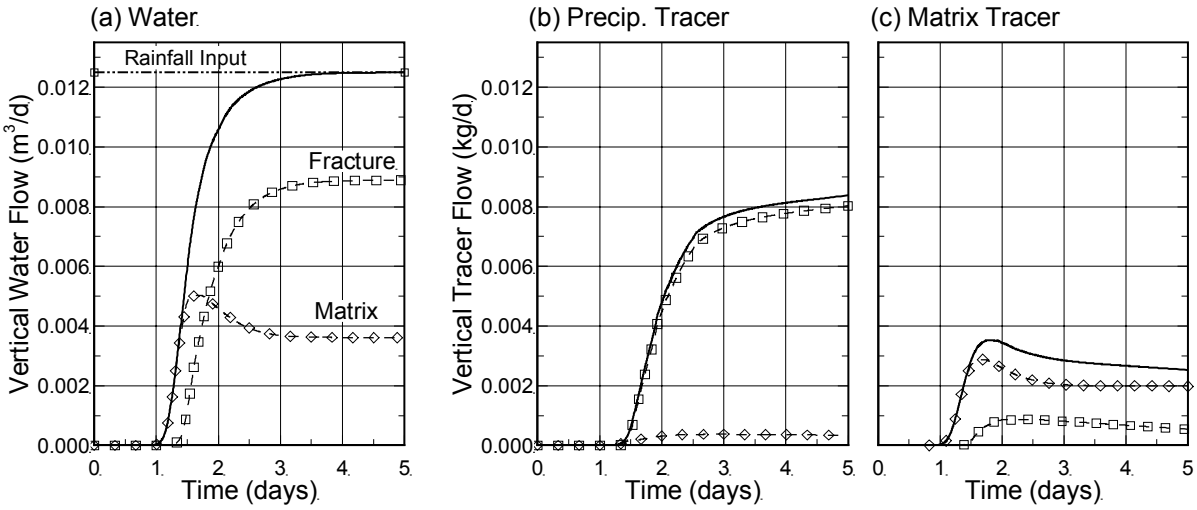

Figure 2.4. Comparison of vertical flow rates for (a) water, (b) Precip tracer, and (c) Matrix tracer crossing a horizontal slice at 0.5 m depth for the Base Case. The total vertical flow rate (solid line) is separated into contributions from the fracture (□) and matrix (◊). The applied rainfall rate (dash-dot-dot line) is shown in the water flow diagram.

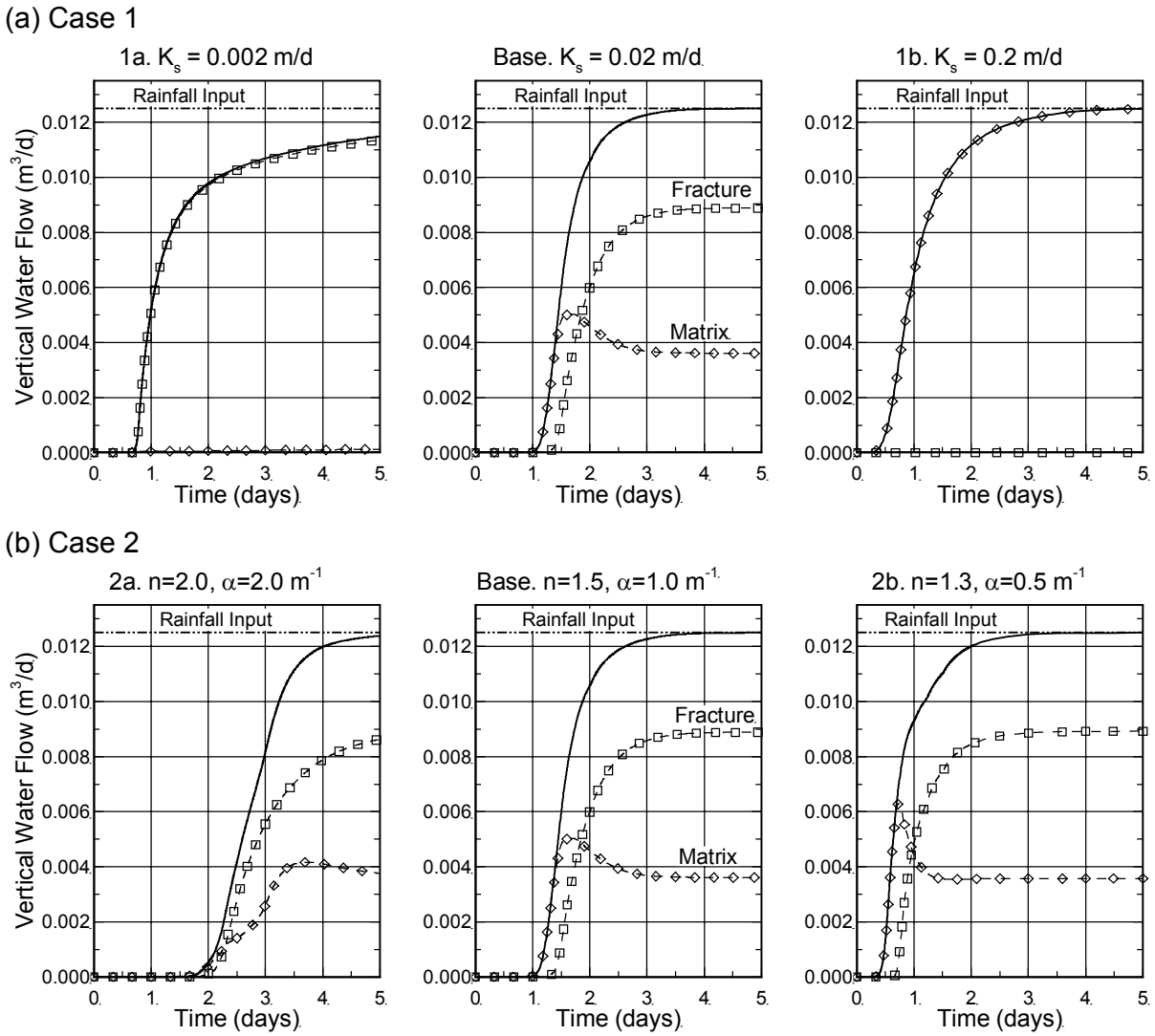

Figure 2.5. Transient vertical water flow rates at 0.5 m depth for varying values of (a) matrix saturated hydraulic conductivity and (b) van Genuchten parameters. The total vertical flow rate (solid line) is separated into contributions from the fracture (□) and matrix (◊). The applied rainfall rate (dash-dot-dot line) is also shown.

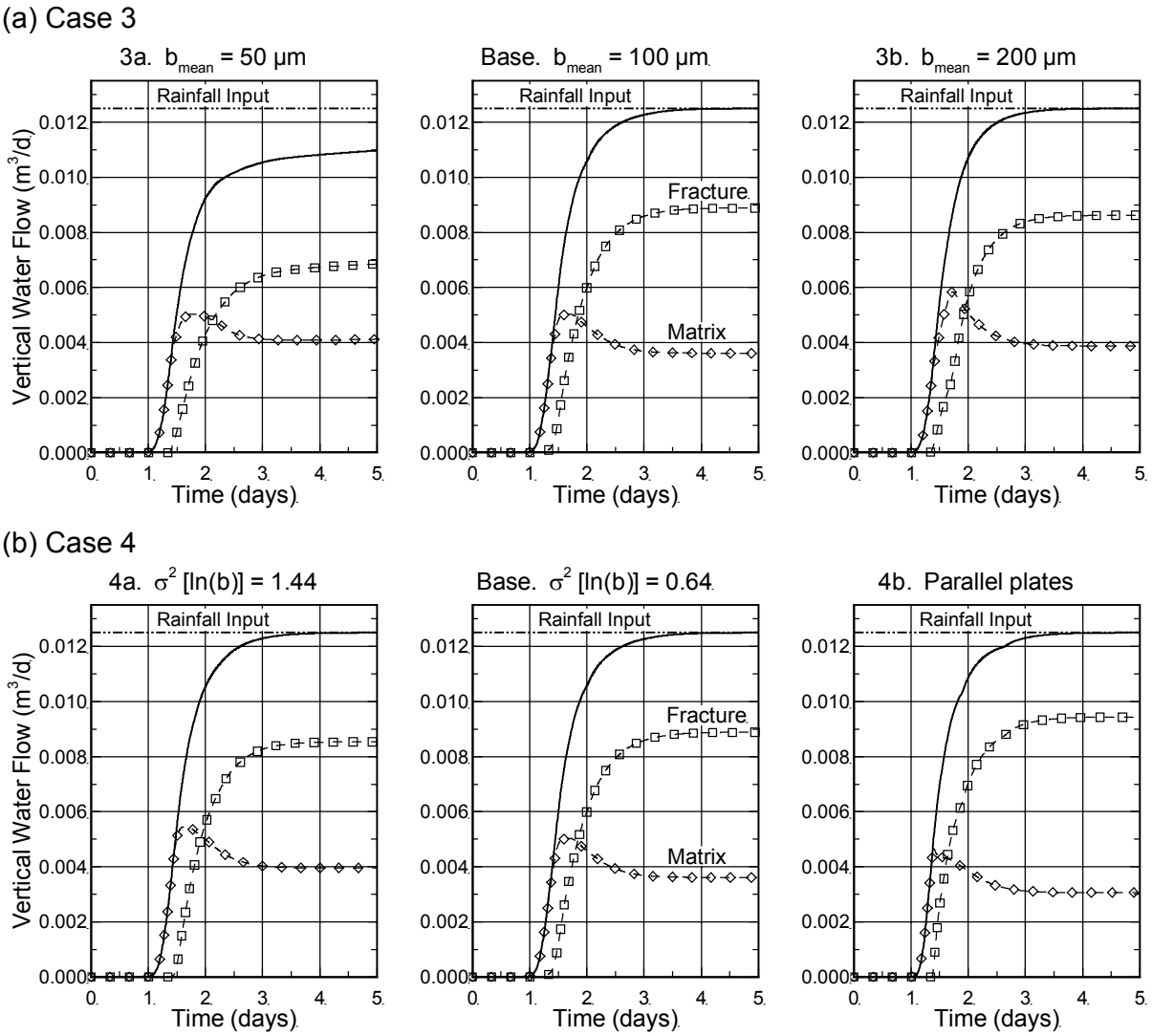

Figure 2.6. Transient vertical water flow rates at 0.5 m depth for varying values of (a) mean fracture aperture and (b) fracture aperture variance. The total vertical flow rate (solid line) is separated into contributions from the fracture (□) and matrix (◊). The applied rainfall rate (dash-dot-dot line) is also shown.

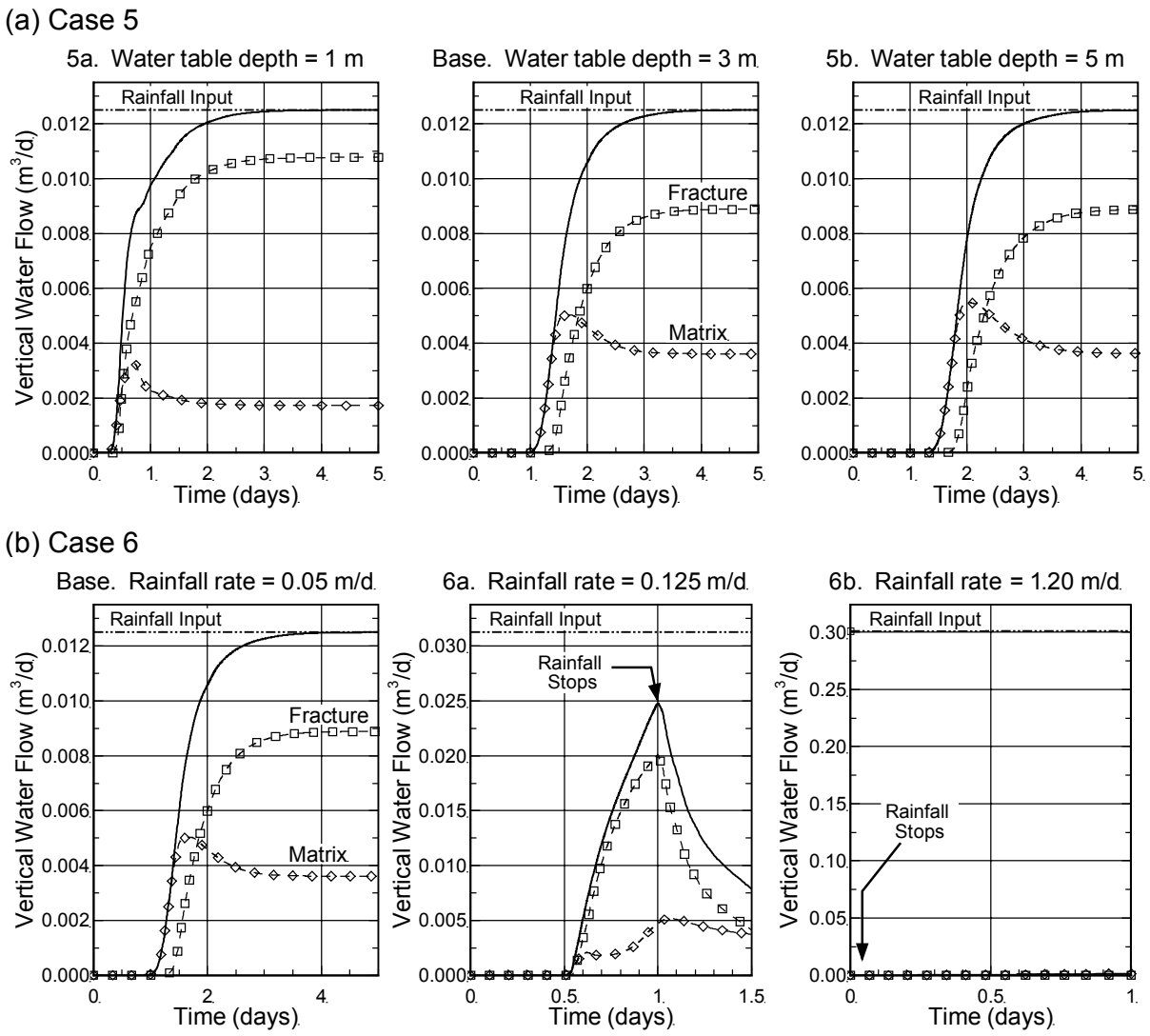

Figure 2.7. Transient vertical water flow rates at 0.5 m depth for varying values of (a) water table depth and (b) rainfall rate. The total vertical flow rate (solid line) is separated into contributions from the fracture (□) and matrix (◊). The applied rainfall rate (dash-dot-dot line) is also shown. Note that the time and flow rate axes for Cases 6a and 6b are different than the Base Case.

Table 2.1. Model Input Parameters for the Base Case

Parameter	Value
Water table depth	3.0 m
Applied rainfall rate	0.05 m/d
Rainfall duration	5 d
Porous Matrix	
Matrix K_s	0.02 m/d
Specific storage	1×10^{-4} m^{-1}
Porosity, θ_s	0.4
Residual water content, θ_r	0.08 m^3/m^3
α, van Genuchten parameter	1.0 m^{-1}
n, van Genuchten parameter	1.5
Fracture	
Geometric mean aperture	100 μm
Variance of ln(b)	0.64
Spatial correlation length	0.10 m
λ, Brooks-Corey pore size index	4.0
Fluids	
Density, ρ_w	1000 kg/m^3
Viscosity, μ_w	1.12×10^{-3} $N \cdot s/m^2$
Air-water interfacial tension, σ	0.0718 N/m
Solute Transport	
Free solution diffusion coefficient	1.73×10^{-4} m^2/d
Longitudinal dispersivity, α_L	0.01 m
Transverse dispersivity, α_T	0.001 m

Table 2.2. Model Input Parameters for Sensitivity Analyses

Case No.	Parameter Tested	Value
1a	Matrix K_s decreased 0.1x[a]	0.002 m/d
1b	Matrix K_s increased 10x	0.2 m/d
2a	Modified van Genuchten parameters ("coarser grained" material)	α=2.0 m^{-1}; n=2.0
2b	Modified van Genuchten parameters ("finer grained" material)	α=0.5 m^{-1}; n=1.3
3a	Fracture aperture decreased 0.5x	50 µm
3b	Fracture aperture increased 2x	200 µm
4a	Variance (ln b) increased 2.25x	1.44
4b	Parallel plate fracture	---
5a	Shallow water table	1.0 m
5b	Deep water table	5.0 m
6a	Increased rainfall rate 2.5x; Decreased duration 0.2x	0.125 m/d; 1.0 d
6b	Increased rainfall rate 24x; Decreased duration 0.0083x	1.20 m/d; 1.0 h

[a]0.1x indicates that parameter was multiplied by a factor of 0.1 compared to the Base Case

Chapter 3
Simulation of Processes and Physical Factors Influencing Transport of Nutrients and Pathogens in Thin Soil and Shallow Groundwater Settings

3.1 Introduction

In Ontario, the Nutrient Management Act was developed to provide a framework for managing nutrients from agricultural and non-agricultural sources throughout the province. Within this framework, provincial regulators (notably the Ministries of the Environment [MOE] and Agriculture, Food and Rural Affairs [OMAFRA]) are working to develop standards designed to control nutrient application on agricultural land while protecting the environment. Of particular concern is the development of standards in regions of thin soils over bedrock and/or shallow water tables. In these settings, there is increased risk for activities, such as the application of manure or biosolids and outdoor confinement of livestock, to have adverse impacts on groundwater resources. For this study, focus will be placed on agricultural land-use practices. Surface soils and other unconsolidated overburden deposits serve as a potential protective barrier to the vertical migration of water and contaminants. However, there is a possibility that agricultural contaminants applied to the soil surface could exceed the soil retention capacity and migrate through the soil profile into underlying groundwater. The agricultural contaminants of concern mainly include nutrients (nitrate, ammonium) and microorganisms (bacteria, viruses and other pathogens). The recent *E. coli* contamination of the drinking water supply in Walkerton represents a striking example of the significant impacts that farming practices can have on groundwater in southern Ontario [*O'Connor*, 2002].

The likelihood of groundwater impacts depends upon a variety of factors, including soil properties, depth to groundwater, topography, geology, and climate [*de Vries and Simmers*, 2002]. Another significant factor in the vertical migration of water and particularly contaminants is the presence of preferential flow along fractures and other macropores. In regions with fine-grained soils, where fractures and other macropores are prevalent, flow can bypass a large portion of the soil matrix and contaminants can very quickly be transported to depth. Field studies suggest that preferential flow through macropores has the potential to increase groundwater flow velocities, recharge rates and contaminant transport rates [*Coles and Trudgill*, 1985; *Kelly and Pomes*, 1998; *Gerber et al.*, 2001; *Jorgensen et al.*, 2002]. There is increasing evidence that flow along preferential paths is widespread and can represent a significant portion of the total flow system [*Flury et al.*, 1994; *Jury and Wang*,

2000]. With all of these factors to consider, it is difficult to ascertain which processes and physical parameters are the most important in controlling the behaviour of agricultural chemicals in the subsurface. There is a need for a consistent, defensible approach to assess the factors controlling the transport of surface applied contaminants in these types of systems before standards can be established.

The primary objective of this investigation is to improve our understanding of the vertical migration of agricultural contaminants in regions of thin soils and shallow groundwater in Ontario. This is achieved by:

- Using advanced groundwater simulation tools to investigate the transport of nutrients and pathogens through thin overburden soils;
- Simulating a variety of physical scenarios to establish the relevant importance of various factors such as soil type, presence or absence of macropores, overburden thickness, water table depth, and rainfall conditions;
- Assessing the sensitivity of the various physical parameters in controlling vertical contaminant transport in order to assess groundwater contamination risk and aid in establishing nutrient management standards; and,
- Providing recommendations, based on information gathered and the simulation results, to assist in the design of subsequent field-scale experiments to address areas of concern or uncertainty.

Section 3.2 of this report describes the model and the numerical simulation scenarios that were developed. The simulation results, along with a discussion of the important findings, are presented in Section 3.3. Finally, conclusions are provided in Section 3.4.

3.2 Model Description and Simulation Scenarios

Unsaturated flow system dynamics can be very complex, making it difficult to evaluate groundwater vulnerability at the field scale. Numerical modelling tools provide a means of evaluating these dynamic flow systems under a wide range of conditions. Valuable understanding of the hydraulic behaviour of the system and information on important processes or parameters can be derived through the use of numerical models. Here we employ a three-dimensional discrete fracture

model that is capable of describing both surface and subsurface flow and transport processes. The model was chosen because it allows investigation of fracture flow and transport, which is believed to be a significant factor in controlling vertical contaminant migration in finer-grained or structured soils. As such, the model is well suited for examination of the transient mobility of contaminants in a wide range of soil types.

The conceptual model employed is designed to represent flow of water and transport of contaminants through a typical soil profile during a large rainfall event. The model simulates transient infiltration into a simple rectangular soil block both during and following the rainfall event. It is assumed that the rainfall event closely follows the surface application of manure and infiltrating water transports potential contaminants with it. Factors related to manure application, such as liquid versus solid manure and manure incorporation methods, were not considered directly in this study. Instead, it was assumed that any application of manure would make nutrients and pathogens available at the soil surface, and subsequent infiltration of rainfall would provide a potential mechanism for transport of the contaminants to underlying groundwater.

3.2.1 Numerical Model

The numerical model employed in this study, designated HydroGeoSphere, is a three-dimensional fully integrated subsurface and overland flow and solute transport model. The subsurface component of the model is built upon the original model of *Therrien and Sudicky* [1996], which is capable of simulating variably saturated discretely-fractured porous media. A modified form of Richards equation is used to describe transient subsurface flow in both the matrix and the fracture. The model uses a common node approach, where fractures are discretized on the face of matrix blocks and they share common nodes. This ensures the continuity of hydraulic head at the fracture-matrix interface and no fluid leakage terms are required to account for mass exchange between fracture and matrix.

Simulations are performed on a simple three-dimensional soil block measuring 2.5 m high. The width and depth of each block was varied depending on the soil thickness and whether fractures were incorporated in the model or not. Where no fracturing was incorporated (*e.g.*, for sandy soils), flow and transport essentially becomes one-dimensional in the vertical direction. In this case, the dimensions of the soil block were reduced to 0.02 m in both width and depth to reduce computation time. In the case of fractured systems, a single vertical fracture is located through the middle of the domain (in the x-z plane). Figure 3.1 shows an example of a modelled soil block containing a single fracture. Since fracture frequency decreases with depth, the lateral size of the model domain is varied depending on the soil thickness. Refer to Section 3.2.3.1 for more details.

In all cases, the modelled domain is discretized into hexahedral block elements 0.02 m on each side. The mesh is refined near the fracture plane, where a nodal spacing of 0.002 m is used adjacent to the fracture in the y-direction, and gradually increased to a maximum of 0.02 m further from the fracture. Details of the model dimensions, fracture spacing and element sizes are provided in Table 3.1 for each of the simulations.

All lateral boundaries in the model are assigned a no-flow boundary condition. Infiltration along the upper boundary is simulated using a constant flux equivalent to the applied rainfall rate. Overland flow is incorporated into the simulations to enable ponding and possible overland flow of water applied in excess of the infiltration rate. Any infiltration excess is allowed to either pond on the surface or flow toward the fracture. However, runoff out of the model domain is not permitted since a detailed analysis of rainfall-runoff relationships is beyond the scope of this study. The bottom boundary is assigned a constant head to simulate the presence of a static water table either beneath or within the soil profile. Top and bottom boundary conditions for the simulations are provided in Table 3.1. Hydrostatic initial conditions are employed for all simulations.

3.2.2 Simulated Scenarios

This study is designed to provide insight into the important parameters controlling contaminant transport through thin agricultural soils. A large number of simulations are performed to evaluate the influence of various input parameters during hypothetical rainfall events. By varying individual system parameters, we assess the relative sensitivity of each parameter in shaping the flow system response. Using numerical tracers, the model is able to quantify the relative impact of each parameter on the concentration and mass flux of contaminants migrating through the soil profile. The input parameters investigated include:

- Soil type
- Soil thickness
- Water table depth
- Presence/absence of fractures
- Rainfall characteristics (intensity and duration)

Each of these parameters is expected to affect the flow of water and movement of contaminants to one degree or another. It should be noted that the simulation results are not intended to predict actual contaminant migration rates. More detailed, site-specific field data would be required for such

predictions. However, the results do provide valuable insight into important flow processes and can help identify the key parameters that control contaminant migration in these environments.

Simulation parameters for all cases are chosen to be representative of the hydrologic and soil conditions encountered in southern Ontario. Soil type is divided into the four main Hydrologic Soil Groups (see Section 3.2.3). For each soil type, both soil thickness and water table depth are varied independently. Relatively thin soils and shallow water table conditions are utilized since that is the focus of this work. Both soil thickness and water table depth are varied between 0.5 m and 2.0 m below ground surface (bgs). The 0.5 m soil thickness is consistent with earlier work presented by MOE, whereas a soil thickness of 2.0 m is chosen to represent a thicker soil that still may exhibit a potential for groundwater contamination. Varying the depth to the water table is analogous to varying antecedent soil moisture conditions. A water table depth of 0.5 m bgs is very shallow, indicative of a soil profile that is very wet and susceptible to leaching of contaminants. The deeper water table (2.0 m bgs) represents slightly drier initial soil conditions, increasing the soil moisture storage capacity and thereby reducing the likelihood and rate of contaminant migration. It is recognized that a 2.0 m deep water table is still relatively shallow and the drying affect of evapotranspiration on the soil profile during the growing season is not considered here. As such, the simulated conditions represent something of a worst-case scenario for migration of contaminants through the soil profile.

Macroporosity is incorporated into the model because many soil types, particularly fine-grained soils, contain numerous fractures or macropores generated by weathering, desiccation, biological activity and other processes. The presence or absence of fracturing in the model is determined by soil type and described in more detail in Section 3.2.3.1.

The influence of rainfall intensity and duration are also investigated with selected simulations. The simulated rainfall rates are chosen to represent relatively large rainfall events for southern Ontario. These large events are more likely to generate significant subsurface flow and transport and result in adverse impacts to groundwater. For the majority of simulations, a rainfall event of 1-hour duration and an intensity of 30 mm/hr (0.72 m/d) is selected. This is consistent with a rainfall return period of approximately 5 years. In other words, over the long term a rainfall event of this severity or greater is statistically expected to occur every 5 years on average. The affect of rainfall intensity is investigated by simulating rainfall events of 1-hour duration with a 100-year return period for selected soil types. Similarly, 24-hour long rainfall events with a 5-year return period are simulated for the same soil types to examine the influence of rainfall duration.

A total of 20 simulations were completed and the results of selected cases are presented here. The model input values used for each of the cases are shown in Table 3.1.

3.2.3 Soil Properties

There is a wide range of agricultural soil types throughout Ontario. One common method of classifying the different soil types is the use of hydrologic soil groups (HSGs), which were developed by the United Stated Department of Agriculture (USDA) and have been adopted in many regions, including Ontario. HSGs are designated by the letters A through D based on the ability of a soil to infiltrate, transmit, and drain water. HSG A soils are typically coarse-textured (*e.g.*, sand or gravel) and are the most permeable soils, while HSG D soils are fine-grained (*e.g.*, clay), relatively low permeability, and have poor drainage characteristics. The HSGs provide a reasonable means of representing the range in permeability of different soil types, which is a major control on water flow and contaminant leaching. Therefore, HSGs are adopted in this study.

Soil hydraulic parameters are required for each HSG in order to simulate variably saturated flow in porous media. These soil characteristics include saturated hydraulic conductivity (K_s), specific storage (S_s), saturated water content or porosity (θ_s), and parameters used to describe the unsaturated constitutive relations between capillary pressure, saturation and relative hydraulic conductivity. The common van Genuchten-Mualem (VGM) model [*Mualem*, 1976; *van Genuchten*, 1980] is used to describe these constitutive relations. The original VGM capillary pressure-saturation-hydraulic conductivity relationships are given by:

$$S_e(h) = \begin{cases} \left(1 + \alpha|h|^n\right)^{-m}, & h < 0, \\ 1, & h \geq 0, \end{cases} \tag{1a}$$

$$K(h) = \begin{cases} K_s \cdot S_e^{0.5}\left[1-\left(1-S_e^{1/m}\right)^m\right]^2, & h < 0, \\ K_s, & h \geq 0, \end{cases} \tag{1b}$$

where h is the pressure head, α, n and m are empirical fitting parameters, and $K(h)$ is the soil's hydraulic conductivity. The effective saturation, S_e, is given by

$$S_e(h) = \frac{\theta(h) - \theta_r}{\theta_s - \theta_r} \tag{2}$$

where θ is volumetric water content and θ_s and θ_r are the saturated and residual volumetric water contents, respectively. Additionally, applying Mualem's model for predicting unsaturated hydraulic conductivity [*Mualem*, 1976] yields $m = 1 - 1/n$.

The VGM relation for relative hydraulic conductivity can induce numerical instability for small values of the fitting parameter n (*i.e.*, n < 1.5), which are typical of relatively fine-grained soils [*Vogel et al.*, 2001]. A modified form of the VGM model was adopted by *Vogel et al.* [2001] to correct the shape of the *K(h)* function near saturation for small values of n, and consequently improve numerical stability. The modified VGM model involves the introduction of a minimum capillary height parameter, h_{min}, as well as the introduction of the parameter θ_m to replace θ_s in a revised form of the effective saturation equation as follows:

$$S_e^*(h) = \frac{\theta(h) - \theta_r}{\theta_m - \theta_r}. \tag{3}$$

The modified VGM equations then become

$$S_e^*(h) = \begin{cases} \left(1 + \alpha|h|^n\right)^{-m}, & h < h_{\min}, \\ 1, & h \geq h_{\min}, \end{cases} \tag{4a}$$

$$K(h) = \begin{cases} K_s \cdot S_e^{0.5}\left[\dfrac{1 - F(S_e)}{1 - F(1)}\right]^2, & h < h_{\min}, \\ K_s, & h \geq h_{\min}, \end{cases} \tag{4b}$$

$$F(S_e) = \left(1 - S_e^{*1/m}\right)^m. \tag{4c}$$

The parameters h_{min} and θ_m have little or no physical meaning and can be considered curve fitting parameters used to modify the shape of the water retention and hydraulic conductivity curves near saturation. *Vogel et al.* [2001] recommend using a small h_{min} value when no measured data are available. A value of h_{min} = -2.0 cm was adopted for this study. Accordingly, θ_m is set slightly larger than θ_s using the approximation

$$\theta_m = \theta_r + (\theta_s - \theta_r) \cdot \left[1 + (2\alpha)^n\right]^m \tag{5}$$

presented by *Vogel et al.* [2001]. In this study, the modified VGM model was employed for soils with small values of *n* (*i.e.*, $n \leq 1.5$). The original VGM model was employed for soils with *n* values greater than 1.5.

Each HSG was assigned soil characteristics based on the expected soil texture. These parameters were obtained by selecting approximate "average" values for each HSG using USDA HSG tabulated hydraulic conductivity values, other published soils information [*e.g., Carsel and Parrish*, 1988], and

class average values from the Rosetta soils database [*Schaap and Leij*, 1998]. The soil parameters used in the simulations are listed in Table 3.2.

This investigation focuses on shallow soils over bedrock. In discussions with MOE it is presumed that the bedrock is fractured and highly permeable, however, no distinction of bedrock type or geology is made. The choice of underlying material does play an important role in water movement through the soil profile, particularly in cases with a deeper water table where the unsaturated zone is larger. The unsaturated flow characteristics vary depending on the bedrock material type selected. This, in turn, will influence water and contaminant movement in the underlying bedrock and, to a lesser degree, in the overlying soil material. For the sake of consistency, the material underlying the soil profile was represented by sand (HSG A) in all simulated cases. The sand represents the presence of a conductive aquifer unit beneath the soil profile. Any contaminants leaching from the soil profile and entering the underlying sand are assumed to be transported readily to any nearby receptors (*e.g.*, water wells, streams).

3.2.3.1 Fracture Characteristics

Soil macropores, which are simply any large soil pores, have the potential to generate significant preferential flow and transport through soil profiles. Macropores can be separated into linear features, such as animal burrows and rootholes, and planar features, such as cracks and fractures. Soil macroporosity was incorporated into the model through the use of fractures, which have a relatively large surface area to volume ratio. Although not incorporated into the model, it is expected that linear macropore features would result in a greater degree of preferential flow and transport to depth due to their smaller surface area to volume ratio.

The presence or absence of fractures in the simulations was based on the soil texture. Fracturing tends to be ubiquitous in fine-grained soils and is much less common, or even absent, in coarse-grained soils due to a lack of cohesion. Thus, fractures are not included in HSG A (sand) simulations but are generally incorporated into all of the remaining HSGs (loam, clay loam, and clay). Preliminary simulations of fine-grained soil types without fracturing suggested that vertical contaminant migration was severely restricted in these situations. Consequently, detailed simulations of fine-grained soils without fractures were not carried out. One simulation of unfractured HSG B (loam) is included to provide a comparison between fractured and non-fractured soils.

In order to make numerical simulations more tractable, real fracture networks are often represented by a series of regular, repeating parallel or orthogonal fracture sets. In the simulations presented here, fracturing is incorporated in the model by emplacing a single vertical fracture in the centre of the soil block. This is equivalent to representing the fracture network as a series of parallel,

equally spaced fractures. Since there is only one fracture in the modelled soil block, the fracture spacing is equal to the lateral size of the model domain (in the y-direction).

It is the vertically continuous fractures, which extend throughout the entire soil profile, that control transport of contaminants to underlying groundwater resources. Field evidence suggests that the number of fractures decreases with depth [*McKay et al.*, 1993b; *Fidler*, 1997; *McKay et al.*, 1999]. Consequently, thin soils are expected to have more fractures extending throughout the entire soil profile depth than thicker soils. Since the modelled fracture penetrates from ground surface to the bottom of the soil profile, the fracture spacing is varied depending on the soil thickness. For example, 0.5 m thick soils were simulated with a fracture spacing of 0.2 m, whereas a fracture spacing of 0.5 m was used for 2.0 m thick soils. The fracture spacings used for all simulations are shown in Table 3.1. The selected fracture spacings are within the range of values obtained from field studies on fractured clayey soils in southern Ontario [*McKay et al.*, 1993b; *Fidler*, 1997].

The fracture aperture must also be specified in the numerical simulations. This is generally done by representing fractures as parallel plates [*e.g., Therrien and Sudicky*, 1996]. However, it is hypothesized that fracture roughness can lead to channelling of water in the plane of a fracture, resulting in increased flow velocities and transport rates down the fracture. Therefore, fracture roughness is incorporated into the model here by assigning spatially variable apertures within the fracture plane. Fracture apertures are generated stochastically using Fourier transform techniques developed by *Robin et al.* [1993]. The aperture distribution is assumed to follow a spatially correlated log-normal distribution. A log-normal distribution is chosen because it matches reasonably well with measured aperture distributions on rock fractures [*Gale*, 1987; *Keller*, 1998] and is consistent with earlier modelling studies [*Kueper and McWhorter*, 1991; *Abdel-Salam and Chrysikopoulos*, 1996; *Vandersteen et al.*, 2003]. The aperture field is mapped onto to the fracture plane, with each fracture element assigned an aperture that was assumed to be constant for that element (*i.e.*, a local parallel-plate approximation). Based on indirect field measurements of fracture apertures in silt- and clay-rich soils [*McKay et al.*, 1993b; *Fidler*, 1997], a geometric mean fracture aperture of 100 μm was selected for all simulations. Given that published information on fracture roughness (aperture variability statistics) for unconsolidated porous materials did not exist, these parameter values were selected from published fractured rock experiments. Figure 3.1 shows an example of a single realization of the aperture field within the fracture plane.

Fracture saturation and hydraulic conductivity are assigned on an element-by-element basis as functions of the elemental aperture. The Brooks-Corey model [1964] is used to describe the constitutive relations for the fracture. The capillary pressure-saturation relationship is given by

$$S_e(h) = \begin{cases} \left(h_{ae} / h \right)^{\lambda}, & h \le h_{ae}, \\ 1 \qquad\quad , & h > h_{ae}, \end{cases} \tag{6}$$

where h_{ae} is the air entry pressure head and λ is an empirical pore size distribution index. The air entry pressure head for each fracture element can be related to fracture aperture by a simplified form of the Young-Laplace equation

$$h_{ae} = -\frac{2\sigma \cos(\beta)}{b \rho_w g} \tag{7}$$

where σ is the interfacial tension between air and water, β is the contact angle measured through the wetting phase, b is the fracture aperture, ρ_w is water density, and g is acceleration due to gravity. For all simulations, the contact angle, β, is assumed to be zero (i.e., water is perfectly wetting).

The saturated hydraulic conductivity K_{fs} for a constant aperture fracture element is given by

$$K_{fs} = \frac{b^2 \rho_w g}{12 \mu_w} \tag{8}$$

where μ_w is the viscosity of water. Utilizing a modified form of the Brooks-Corey expression based on theory by *Mualem* [1976], the relative hydraulic conductivity, K_r, for the element can be written as

$$K_r = \left(\frac{h_{ae}}{h} \right)^{2.5\lambda+2}, \quad h \le h_{ae}. \tag{9}$$

The use of the Brooks-Corey model to describe constitutive relations for the fracture appears to be a reasonable approximation if each fracture element is considered a local macroscopic continuum. The reader is referred to Chapter 2 for a more detailed description of fracture roughness and the unsaturated fracture relations. A listing of fracture properties used in the simulations is provided in Table 3.3.

3.2.4 Implementation of Numerical Tracers

Numerical tracers were used to monitor movement of surface applied contaminants throughout the simulations. Two separate tracers were utilized; one for dissolved solutes (*e.g.*, nitrate) and one to represent movement of colloids (*e.g.*, microorganisms). The Solute tracer, which was assumed to be conservative (i.e., no decay or adsorption), was applied with the rainfall on the upper soil surface with a specified concentration of 1.0 kg/m^3. The Solute tracer concentration was assigned as 0.0 kg/m^3

throughout the soil block. The absolute concentration of solute input source is not defined, since the output results are expressed in relative mass-flux or relative concentration terms. The free solution diffusion coefficient of the Solute tracer was taken as 1.73×10^{-4} m^2/d. Given the relatively small size of the simulated soil block, the longitudinal and transverse dispersivity of both the soil and the fracture were taken as 5 mm and 1 mm, respectively.

The second numerical tracer was designed to evaluate the likelihood of pathogenic colloids breaking through the soil profile during the rainfall event. Transport of pathogens in unsaturated fractured porous media involves numerous complex processes, such as straining, attachment to solids or air-water interfaces, diffusion, ionic strength effects, and microorganism survival. Currently, the numerical model is unable to properly simulate these processes and therefore a simplified approach for tracking colloid movement through a fractured soil was developed for this study.

Research suggests that transport of pathogenic colloids through both saturated [*McKay et al.*, 1993c; *Becker et al.*, 1999; *McKay et al.*, 2000] and unsaturated [*Natsch et al.*, 1996; *Unc and Goss*, 2003; *Passmore*, 2005] porous media is strongly controlled by preferential flow through macropores. Therefore, we assume fractures are the dominant transport pathway for colloids in this study. Based on work by *Wan and Tokunaga* [1997] and *Veerapaneni et al.* [2000], the potential for colloid transport in unsaturated fractures can be related to the ratio of colloid diameter, d, to water film thickness, w. Where the ratio d/w is approximately 1.0 or greater, colloids are effectively strained. Conversely, colloids that are smaller than the water film thickness (i.e., $d/w < 1$) are readily transported with the moving water. If we assume the water film covers each side of the fracture uniformly, then the thickness of the water film can be related to the fracture aperture and saturation as

$$w = \frac{S_f \cdot b}{2}, \quad S_f < 1 \tag{10}$$

where S_f is the fracture saturation. This suggests that the likelihood of a colloid being transported through an unsaturated fracture is dependent on the size of the colloid, the fracture aperture, and fracture saturation. Regions of a fracture that have a relatively small aperture or thin water film are more likely to strain out colloids. This is shown schematically for an enlarged section of fracture in Figure 3.2.

Transport of hypothetical colloids is simulated using a particle tracking routine along the plane of the fracture. At any given simulation time, the groundwater velocity distribution and saturation conditions within the fracture plane can be calculated from the HydroGeoSphere simulation results. Numerical tracer particles are then applied across the top of the fracture and are transported through

the fracture according to the velocity field. The particle tracking was accomplished using Tecplot, a scientific plotting program. The particle tracking method assumes a steady-state velocity field. Although the infiltration process is transient, the assumption of steady state flow for colloid transport is reasonable since travel times for the particles through the soil profile are on the order of minutes. Using the transport pathway from the particle tracking routine and the water film thicknesses calculated from the HydroGeoSphere results, the likelihood of colloid breakthrough at the base of the soil profile can be evaluated for different sizes of particles.

3.2.4.1 Vertical Tracer Fluxes

In order to assess contaminant migration potential, the vertical flux of water and Solute tracer is estimated as a function of time. At each model time step, the Solute tracer flux crossing a horizontal slice at any specified depth may be calculated. The solute flux is obtained by multiplying the vertical water flux by the solute concentration at each model node and then summing the values for all nodes on the horizontal slice. For the purposes of this study, horizontal slices at depths of 0.2 m, 0.5 m, 1.0 m, and 2.0 m below ground surface (bgs) are considered. The total vertical fluxes are separated into contributions from the porous matrix elements and the fracture elements. The vertical tracer mass fluxes provide a reasonable measure of solute transport potential to underlying groundwater resources because they represent an integrated measure of both flow rate and contaminant concentration.

In this study, all Solute tracer fluxes are expressed relative to the input flux. That is, the tracer flux at depth is divided by the tracer flux input at the soil surface, providing a relative flux that ranges from zero to one. Use of relative tracer fluxes generally makes it easier to compare results from one scenario to the next. In some instances, such as when varying rainfall rates (i.e., input flux) are compared, careful interpretation of the results is necessary.

3.3 Results and Discussion

3.3.1 Fractured Versus Unfractured Soil

Figure 3.3 provides a comparison of the relative tracer fluxes observed at 0.2 m bgs for a fractured soil (Case B02) versus a non-fractured (Case B05) loam soil. It is clear that the tracer mass flux is greater in the case of fractured soil than the non-fractured soil. In both cases, the rainfall intensity for the 1-in-5 year rainfall event (0.72 m/d) exceeds the saturated hydraulic conductivity of the HSG B soil (0.26 m/d). In the case of the fractured soil (Figure 3.3a), this generates preferential flow along the fracture and results in the transport of the Solute tracer along the fracture to depth. The flux of Solute tracer at 0.2 m depth rises throughout the course of the rainfall event and reaches a maximum of about 10% of the input flux near the end of the one hour rainfall. Figure 3.3b shows that almost no

surface applied tracer reaches 0.2 m depth either during or following the rainfall event. This is a result of the relatively uniform plug or piston-type flow mechanism in the non-fractured case. According to the simulation results, a portion of the Solute laden water infiltrates the soil profile while the remainder ponds on the ground surface and slowly infiltrates the soil after rainfall ceases. Thus, plug flow serves to limit the depth of penetration of surficial contaminants. The Solute tracer remains in the upper portion of the soil profile in the non-fractured case, creating additional opportunity for nutrient uptake or die-off of pathogens.

Even with a relatively large rainfall event on a moderately permeable non-fractured soil, as in Case B05, there is essentially no tracer flux reaching even a relatively shallow depth of 0.2 m bgs. The Solute is retained in the soil profile and is only likely to be mobilized downward by subsequent rainfall events. The lack of contaminant flux observed during the rainfall event in the non-fractured soil case is not consistent with the majority of field evidence that shows preferential flow is common in many soils [*Flury et al.*, 1994; *Kung et al.*, 2000; *Weiler and Naef*, 2003b; *Jansson et al.*, 2005]. Fractures and other macropores tend to be ubiquitous in all but the sandiest soils, giving rise to significant potential for contaminant movement to groundwater. The simulation results show that where fractures are present they are likely to play an important role in the vertical movement of both water and contaminants. Fractures serve to increase contaminant fluxes and reduce travel times through the vadose zone. For these reasons, the remainder of the simulations for fine-grained soils (HSGs B through D) include the influence of fractures.

3.3.2 Influence of Soil Type and Thickness

The influence of soil type on the relative vertical Solute fluxes is shown in Figure 3.4 and Figure 3.5. The transient Solute tracer flux at 0.2 m bgs is shown in Figure 3.4 for a soil profile that is 0.5 m thick and for a water table located at a depth of 0.5 m below ground surface. Of the cases simulated, this represents the likely worst-case scenario for transport of contaminants from surface to groundwater. Breakthrough of contaminants at 0.2 m is observed in all four soil types. For HSG A (Figure 3.4a), transport occurs only through the soil matrix, as it is unfractured sand. The peak relative tracer flux of 0.08 occurs approximately 0.6 hours after the rainfall stops. The peak arrival at depth is delayed because of the plug flow conditions in such a soil. Solute transport behaviour is distinctly different in the remaining three soil types that contain fractures. The relative tracer flux shows a quicker, more peaked response due to preferential flow down the fracture. For example, in the clay soil of HSG D (Figure 3.4d) both the first arrival time and the peak of the tracer flux occur earlier than for HSG A (Figure 3.4a). In each of the three fractured soils, the peak tracer flux is more than three times greater than for the non-fractured sand (HSG A). In fact, the greatest tracer flux occurs in the finest-grained soil type: HSG D. This is counter to conventional non-fractured flow

systems, where contaminant flux would be expected to be greatest in the coarse-grained soils due to their greater hydraulic conductivity. However, when fractures are present vertical flow and transport tend to be greater in finer-grained, structured soils. Finer-grained soils have a greater moisture retention capacity and a smaller saturated hydraulic conductivity which helps to initiate and promote fracture flow as the dominant flow mechanism. This is shown in Figure 3.4b-d where the tracer flux for the three fractured soils is contributed almost entirely by the fracture. Only for HSG B is there any noticeable flux of tracer at 0.2 m depth through the soil matrix. Overall, the results suggest that contaminant breakthrough can occur to shallow depths in all soil types. Under the right soil and hydrologic conditions, very thin soils (*e.g.*, < 0.3 m) are likely to provide minimal protection for underlying groundwater resources.

As described in Section 3.2.3.1, the fracture spacing in the model is varied depending on the soil thickness. Figure 3.4 presents tracer fluxes for 0.5 m thick soil profiles where a fracture spacing of 0.2 m was used, while Figure 3.5 presents results for 2.0 m thick soils with a larger fracture spacing of 0.5 m. The response of HSG A is the same in both cases since it does not include fractures. The relative Solute fluxes for the three fractured soils are significantly reduced in the thicker soils due to the wider fracture spacing (Figure 3.5b-d). The reduction in relative flux in Figure 3.5 compared to Figure 3.4 is approximately 2.5 to 3.0 times, which is roughly the same as the reduction in fracture frequency. For a given soil type it appears that roughly the same amount of solute mass is transported down each fracture regardless of fracture spacing. In other words, the reduction in apparent contaminant flux is due to a reduction in the fracture frequency, not a decrease in the mass of tracer flowing down the individual fractures. Thus, thicker soils would be expected to offer some degree of additional protection to groundwater due to reductions in macropore frequency and continuity. For either soil thickness, however, surficial contaminants may still reach groundwater. The degree of protection provided by thicker soils may be mitigated by the presence of vertically connected fractures and other macropores.

3.3.2.1 Tracer Fluxes as a Function of Depth

To this point, only tracer flux results at a depth of 0.2 m bgs have been examined. The vertical extent of tracer migration is a critical factor in determining the likelihood of impacts to groundwater resources. Solute tracer fluxes at various depths for HSGs A and C are provided in Figure 3.6 and Figure 3.7, respectively. Figure 3.6 illustrates the affect that plug flow has on transport behaviour when no fractures are present. In this case, the Solute tracer front migrates downward through the soil profile, reaching the 0.2m depth plane after approximately 1.0 hour. Since the downward moving tracer front reaches a depth of only 0.35 m after 24 hours, the Solute tracer fluxes are essentially zero at depths of 0.5 m or greater. This does not indicate that there is no downward flow of water at

greater depths, but rather that any vertical water flow at depth is a result of *in-situ* water being displaced downward by the infiltrating rainfall. In the simulations, the Solute tracer originates at ground surface and is limited to relatively shallow depths. It is possible in field situations that solutes already present in the soil profile may be transported to greater depths during repeated infiltration events. However, these *in-situ* contaminants would be subject to other factors, such as plant uptake and chemical or biological degradation, making them less prone to cause adverse impacts to groundwater.

It is also important to consider the likelihood that plug flow conditions exist in an agricultural field setting. Other preferential flow mechanisms, such as flow funnelling or unstable flow fingering, have been shown to occur in relatively homogeneous, coarse-grained soils [*Hendrickx and Flury*, 2001]. These flow mechanisms would serve to increase the rate of solute transport through thin soils compared to the results presented here.

Figure 3.7 shows how tracer transport is influenced as it moves vertically through a fractured clay loam (HSG C) soil profile. The vertical flux is controlled entirely by flow through the fracture at all depths. The tracer flux decreases slightly at each successive depth due to dispersion in the plane of the fracture as well as diffusion of Solute mass into the soil matrix. The peak in the observed tracer flux arrives progressively later with depth, occurring after the rainfall event has ended at all depths. This suggests that much of the tracer transport to greater depths results during drainage of the fracture. In this case, the water table is shallow (0.5 m bgs) and the majority of the soil profile is relatively wet or even saturated. This reduces the capacity of the soil to imbibe water from the fracture and enhances vertical flow and transport along the fracture. Under these conditions, contamination from surficial sources can extend to considerable depth in fractured soils.

These results further demonstrate the critical role that flow mechanisms play in transporting contaminants through the vadose zone. The risk of adverse impacts to groundwater resources is much greater where preferential flow mechanisms exist. Where no preferential flow exists (Figure 3.6) transport is limited to less than 0.5 m depth. Conversely, surficial contaminants can be transported to depths of greater than 2.0 m where vertically connected fractures are present (Figure 3.7). The tracer flux reaching 2.0 m depth is only a small portion of the flux entering the soil profile (approximately 2% at the peak). Nevertheless, there is still a potential to adversely impact groundwater depending on surficial contaminant loadings and, perhaps more importantly, the presence of pathogenic organisms. The presence of fractures and other macropores raises questions about the suitability of thin soils for protection of groundwater resources. The question of "How thick is thick enough?" for protection of groundwater resources appears to be related more to the interconnectivity and vertical continuity of macropores.

3.3.3 Influence of Antecedent Moisture and Water Table Depth

The depth to the water table and antecedent moisture conditions in a soil profile are often closely linked, particularly in shallow water table environments. A shallower water table results in increased initial pressure heads throughout the soil profile and consequently higher initial soil matrix and fracture saturations. The depth to the water table has a significant affect on flow and transport behaviour as shown in Figure 3.8. A shallower water table is shown to result in increased vertical Solute tracer fluxes at all depths in the soil profile. In Figure 3.8a, Solute tracer flux is observed at all measurement depths through the soil profile under shallow water table conditions, yet there is no discernible tracer flux at even 1.0 m depth when the water table is deeper. This same effect is shown even more dramatically in the HGS B soil, where Solute tracer does not reach 0.5 m depth under deep water table (i.e., 2.0 m bgs) conditions. As water flows down the fracture there can be a large amount of mass transfer between the fracture and the matrix. During infiltration, water and contaminants moving down the fracture are imbibed into the drier soil matrix. This is the primary reason why vertical tracer fluxes decrease with depth in a soil profile. When the water table elevation is raised, the soil matrix is wetter and the soil has less capacity for imbibing water from the fracture. Under wetter soil conditions, fracture flow is enhanced and contaminants are more likely to be transported to considerable depth along the fracture. The end result is increased vertical tracer fluxes and greater depths of contaminant penetration under shallower water table conditions.

Variations in antecedent moisture conditions, whether induced by changes in water table depth or soil type, have a significant influence on contaminant fluxes and the depth of contaminant penetration. It is well known that soil saturation conditions vary for different soil types and are related to the pore size distribution. For a given water table depth, a finer-grained soil will have a higher antecedent moisture content than a coarser-grained soil. The ability of finer-grained soils to retain water reduces their capacity to imbibe and store infiltrating water. This is partly the basis of the HSG classification system. In comparing an HGS C soil (Figure 3.8a) to an HGS B soil (Figure 3.8b) for the same water table depths, the simulations show that Solute tracer fluxes are generally greater for the finer-grained HSG C soil, particularly deeper in the soil profile. For example, in the shallow water table diagram of Figure 3.8a there is a gradual decrease in the peak tracer flux from the 0.2 m depth slice to the 2.0 m depth slice. The decrease in vertical flux between measurement depths is much more dramatic in the HSG B soil (Figure 3.8b). Note that vertical transport is predominantly through the fracture in both soil types. The marked decrease in tracer flux with depth for HGS B can be explained by the soil's greater soil moisture storage capacity. The coarser-grained HSG B soil can imbibe more infiltrating water (and the contaminants it carries) into the soil matrix, thereby limiting the depth of contaminant migration. This imbibition effect is present for both shallow and deep water

table conditions, although it is much more prevalent where the water table is deeper and the soil is drier.

3.3.4 Influence of Rainfall Intensity and Duration

Rainfall intensity and duration are not measurable prior to a given rainfall event and thus cannot be readily used to assist in establishing guidelines for groundwater protection. Nevertheless, it is important to understand how rainfall characteristics affect flow and transport conditions in order to determine under what environmental conditions groundwater resources are most susceptible.

Figure 3.9 demonstrates the influence of varying rainfall conditions on vertical Solute transport characteristics at a depth of 0.2 m bgs for HGS B. Comparing rainfall events of equal duration (Figure 3.9a and b), the relative tracer flux responses are similar in shape and magnitude. In both cases, the matrix hydraulic conductivity is less than half the rainfall rate, resulting in preferential transport down the fracture. The 100 year return period (RP) event results in more ponding of water on ground surface, but not necessarily greater rates of contaminant transport than the 5 year RP event. In a typical field situation, there is the potential for ponded water from higher intensity rainfall events to flow overland to nearby surface watercourses, transferring a portion of the contaminant load from groundwater to surface water resources.

The relative tracer flux is considerably greater for the longer duration, low intensity rainfall event (Figure 3.9c). In this scenario, an appreciable portion of the tracer flux occurs through the soil matrix, particularly during the latter stages of the rainfall event. This is a consequence of the rainfall rate being less than the matrix hydraulic conductivity of the soil. Ponding conditions are not generated at the ground surface and a greater proportion of the flow and transport takes place through the soil matrix. It is worth restating that the fluxes are expressed relative to the input flux, making the total tracer flux appear much larger in Figure 3.9c compared to Figure 3.9a and Figure 3.9b. The actual tracer fluxes can be obtained by multiplying the relative tracer fluxes by the input flux (i.e., rainfall rate x source concentration). If these calculations are performed, the actual peak tracer fluxes are lowest for the 24-hour duration storm (Figure 3.9c) and largest for the 100 RP storm (Figure 3.9b). Still, the long duration, low intensity rainfall event results in proportionately more contaminant flux at depth in the soil profile. Longer duration rainfall events (of equal return period) have a larger amount of total rainfall. The increased volume of infiltration water can more readily overcome soil moisture deficits and generate preferential flow along macropores. The relationship between soil moisture conditions and the total volume of rainfall plays a pivotal in controlling the onset and extent of preferential flow.

3.3.5 Colloid Transport

Colloid transport was simulated using a particle tracking method where colloid tracer particles are released on the ground surface and their movement is tracked through the fracture using the velocity field generated by the HydroGeoSphere model. The results of particle tracking simulations for HSG B soil under shallow water table conditions are shown in Figure 3.10. Figure 3.10a illustrates the path of particles at the end of the rainfall event. The majority of the particles move very quickly through the soil and breakthrough at the base of the soil profile in approximately 5 to 10 minutes. Seven hours after the rainfall event has ended, significant portions of the fracture remain near saturation and pathways for rapid transport of particles from soil surface to the base of the soil profile remain open (Figure 3.10b).

The equivalent unsaturated water film thickness calculated from Equation 10 is included in Figure 3.10 for reference. Note that the equivalent water film thickness shown does not take into account the fact that the fracture is saturated below the water table (i.e, 0.5 bgs or below Z = 2.0). It is observed that colloids are generally transported where water films are thicker, which corresponds to the larger aperture regions of the fracture that remain near saturation. Larger aperture regions of the fracture have a significantly greater hydraulic conductivity when nearly saturated (see Equation 8) and this generates preferential flow or flow channelling within the plane of the fracture. The colloid particles are transported through regions of the fracture where equivalent water film thicknesses are greater than 10 μm. This has major implications for transport of microorganisms since most microorganisms of concern are less than 10 μm in size. This implies that most microorganisms are likely to be readily transported through the fracture with minimal straining or filtration. In most natural soils there will be mechanisms by which microbial transport is attenuated, whether by filtering, attachment to soil particles and air-water interfaces, adsorption, or inactivation. However, the results here suggest that microbes would potentially be transported very quickly to depth via macropores, limiting the time available for these attenuation processes. Consequently, the risk to groundwater resources from transport of microorganisms through macroporous soils, even those up to two metres in thickness, appears to be very large.

The influence of soil moisture conditions on colloid transport is shown in Figure 3.11. The depth of colloid penetration in a soil profile is a function of antecedent moisture conditions. When the water table is deeper, the drier soil matrix forces more mass transfer of water from the fracture to the matrix. This restricts the downward migration of the wetting front within the fracture as well as reduces the thickness of water films. Consequently, colloids are only able to migrate a relatively short distance into the fracture before encountering regions that are too dry to permit further migration. At the end of a rainfall event colloids are transported to a maximum depth of about 0.25 m

bgs (Figure 3.11a). Following drainage of the fracture for several hours, colloids are transported over only a small region of the fracture to a maximum depth of 0.15 m bgs.

The influence of soil moisture on colloid movement is similar when comparing different soil types. Colloid transport is enhanced in finer-grained soils, which generally have higher water contents and drain more slowly following rainfall. Figure 3.12 shows colloid transport along the fracture for a deep water table (2.0 m bgs) for HSG D (clay) soil. Both the fracture and soil matrix reach saturation more quickly following the onset of infiltration in the HSG D soil, giving rise to increased fracture flow. Colloids are readily transported through the fracture in the HGS D soil at the end of the rainfall event (Figure 3.12a) as well as after the soil has drained for 7.0 hours (Figure 3.12b). In general, shallow water tables are most susceptible to colloid transport. However, the combined influence of soil type and water table depth on antecedent moisture content should be considered when evaluating the potential for contaminant transport. The results show that a finer-grained HSG D soil with a deep water table (Figure 3.12) is just as susceptible to colloid transport as a coarser-grained HSG B soil under shallow water table conditions (Figure 3.10), owing to differences in soil water retention characteristics.

The primary difference between solute and colloid movement is the difference in time of travel. Solutes, due to their smaller size, are more subject to imbibition and matrix diffusion effects than colloids. The simulations suggest that the time for surficial solutes to travel through a 2 m thick fractured soil is on the order of hours, compared to travel times on the order of minutes for colloidal particles. These relatively quick transport velocities for colloids are consistent with field experiments in which colloid migration rates in excess of 100 m/d have been reported through fractured soil materials [*McKay et al.*, 2000]. An increasing number of column and field studies have demonstrated that macropores enhance pathogen transport [*e.g., Natsch et al.*, 1996; *McKay et al.*, 1999]. The simulations presented here appear to support the field evidence and indicate that groundwater is highly susceptible to microbial contamination in areas of thin soils or shallow groundwater.

3.3.6 Comment on Proposed Standards for Manure Application

Recommended standards for manure application were developed by a Provincial advisory committee and presented in a draft document dated March 2005. The draft standards address the need for restrictions on manure application in areas with shallow soils over bedrock (Table 3.4) and areas of shallow groundwater (Table 3.5 and Table 3.6). The proposed standards apply to soils that are less than one metre thick (Table 3.4) and regions in which the water table is less than one metre deep (Table 3.5). In terms of protection for groundwater resources, the standards do not appear to be conservative relative to the simulation results presented herein. For example, the draft standards

would propose no restrictions for solid manure application on soil profiles as thin as 0.3 m. Similarly, there would be no restrictions for manure application on HSG C and D soils in regions where the water table was as shallow as 0.6 m bgs. Based on the results of simulations in this study, breakthrough of surficial contaminants, both nutrients and pathogens, would be anticipated under these types of conditions (see Figure 3.8 and Figure 3.12) and could pose a significant risk to groundwater resources. Additional information, including field data and research, appears warranted in order to confirm this assessment and provide additional support for development of detailed standards.

3.4 Conclusions

Numerical simulations were employed in this study to investigate the transport of agricultural contaminants in regions of thin soils over bedrock and shallow groundwater in Ontario. The results indicate that macropores such as fractures play a critical role in controlling the rate of contaminant migration through soils. Contaminant fluxes are generally larger and extend to greater depths in fractured soils. The numerical model clearly demonstrates the importance of preferential flow along fractures, leading to potentially significant transport of surficial contaminants to depth. It is commonly believed that groundwater contamination potential is directly related to the permeability or drainage potential of a particular soil type (see Table 3.5). However, the widespread presence of macropores in finer-grained structured soils can drastically reduce the protective capacity of lower permeability soil types. As a result, shallow soils of all types generally provide little protection for groundwater. In fact, the simulation results suggest that a fractured lower permeability soils may pose a greater risk to groundwater owing to their lower permeability matrix and soil water retention characteristics.

Thicker soils provide some degree of additional protective capacity for groundwater; however, the amount of the increase depends heavily on the dominant flow mechanism. In non-fractured soils, where plug- or piston-type flow is presumed, thicker soils can provide significant additional protection. In fractured soil environments, contaminants may still reach groundwater as a result of preferential flow and transport. Simulations showed that surface applied tracers were able to reach the base of 2 m thick soil profiles containing fractures. Where soils contain fractures, much of the additional protective capacity afforded by thicker soils is a result of a reduction in the fracture frequency with depth. Accordingly, fracture continuity may be a more important measure than soil thickness in evaluating the susceptibility of soils to contamination from agricultural sources.

Antecedent soil moisture conditions have a significant impact on contaminant fluxes for both solutes and colloids. Drier soils have a greater capacity to imbibe and store infiltrating water along

with the contaminants they carry. Conversely, wetter soils reach saturation more quickly following the onset of rainfall, making them more susceptible to preferential flow and contaminant transport. This explains why low intensity, long duration rainfall events, which have a greater volume of total rainfall, are more likely to generate adverse impacts to groundwater.

Together water table depth and soil type strongly influence the antecedent soil moisture content. Under relatively shallow water table conditions (0.5 m bgs), most soil types are susceptible to contamination. When the water table is deeper (2.0 m bgs) there is less potential for groundwater contamination, but finer-grained soils may still be at risk due to their higher equilibrium saturation conditions. It is important that soil type and depth to the water table be considered in conjunction for evaluating groundwater contamination potential.

Although nutrients and pathogens both pose a potential risk to groundwater resources, the results of this study suggest that pathogens have a significantly shorter travel time through the soil. Colloids are less prone to the effects of imbibition and matrix diffusion and are able to migrate very quickly along fractures. Also, the thickness of water films estimated in the fractures is sufficient to support colloid transport, even under unsaturated conditions. The end result is that particles less than about 10 μm in size, which includes most microbes of interest, could be transported to depths of 2 metres or more in a matter of minutes via fractures.

Based on the results of this investigation, areas where overburden cover is thin, contain continuous macroporosity and have shallow water tables, likely represent conditions of high vulnerability with respect to potential impacts to water quality from nutrient application. This is true even if the native material has low permeability such as a clay loam. It is particularly the case where the underlying sediments are used locally as a groundwater resource. The simulation results can be used to assist in developing general criteria for identifying highly vulnerable areas where nutrient application may require some degree of restriction. Additional insight into the processes controlling the mobility of potential contaminants derived from nutrients, including manure, can be obtained through controlled field experimentation. This is the focus of a subsequent phase of the research work that is presented in Chapters 4 and 5.

3.5 References

Abdel-Salam, A. and C.V. Chrysikopoulos (1996), Unsaturated flow in a quasi-three-dimensional fractured medium with spatially variable aperture, *Water Resour. Res.*, *32*(6), 1531-1540.

Becker, M.W., P.W. Reimus, and P. Vilks (1999), Transport and attenuation of carboxylate-modified latex microspheres in fractured rock laboratory and field tracer tests, *Ground Water*, *37*(3), 387-395.

Brooks, R.H. and A.T. Corey (1964), Hydraulic properties of porous media, Hydrology Papers No. 3, University of Colorado, Fort Collins, Colorado, USA.

Carsel, R.F. and R.S. Parrish (1988), Developing joint probability distributions of soil water retention characteristics, *Water Resour. Res.*, *24*(5), 755-769.

Coles, N. and S. Trudgill (1985), The movement of nitrate fertiliser from the soil surface to drainage waters by preferential flow in weakly structured soils, Slapton, S. Devon, *Agr. Ecosyst. Environ.*, *13*(3-4), 241-259.

de Vries, J.J. and I. Simmers (2002), Groundwater recharge: an overview of processes and challenges, *Hydrogeol. J.*, *10*(1), 5-17.

Fidler, S.R. (1997), Spatial and temporal variability of hydraulic response in fractured low permeability sediments, PhD thesis, University of Waterloo, Waterloo, Ontario, Canada.

Flury, M., H. Fluhler, W.A. Jury, and J. Leuenberger (1994), Susceptibility of soils to preferential flow of water: a field study, *Water Resour. Res.*, *30*(7), 1945-1954.

Gale, J.E. (1987), Comparison of coupled fracture deformation and fluid flow models with direct measurements of fracture pore structure and stress-flow properties, in *Proceedings of the 28th U.S. Symposium on Rock Mechanics*, edited by Farmer, Ian W., Daemen, Jaak J. K., Desai, C. S., Glass, C. E., and Neuman, Shlomo P., pp. 1213-1222, A.A. Balkema, Rotterdam, Netherlands, 29 June 1987.

Gerber, R.E., J.I. Boyce, and K.W. Howard (2001), Evaluation of heterogeneity and field-scale groundwater flow regime in a leaky till aquitard, *Hydrogeol. J.*, *99*(1), 60-78.

Hendrickx, J.M.H. and M. Flury (2001), Uniform and preferential flow mechanisms in the vadose zone, in *Conceptual Models of Flow and Transport in the Fractured Vadose Zone*, edited by National Research Council, pp. 149-187, National Academy Press, Washington, D.C.

Jansson, C., B. Espeby, and P.E. Jansson (2005), Preferential water flow in a glacial till soil, *Nord. Hydrol.*, *36*(1), 1-11.

Jorgensen, P.R., M. Hoffmann, J.P. Kistrup, C. Bryde, R. Bossi, and K.G. Villholth (2002), Preferential flow and pesticide transport in a clay-rich till: Field, laboratory, and modeling analysis, *Water Resour. Res.*, *38*(11), 1246, doi:10.1029/2001WR000494.

Jury, W.A. and Z. Wang (2000), Unresolved problems in vadose zone hydrology and contaminant transport, in *Dynamics of Fluids in Fractured Rock*, Geophysical Monograph 122, edited by B. Faybishenko, P.A. Witherspoon, and S.M. Benson, pp. 67-72, American Geophysical Union, Washington, DC, USA.

Keller, A. (1998), High resolution, non-destructive measurement and characterization of fracture apertures, *Int. J. Rock Mech. Min. Sci. & Geomech. Abstr.*, *35*(8), 1037-1050.

Kelly, B.P. and M.L. Pomes (1998), Preferential flow and transport of nitrate and bromide in claypan soil, *Ground Water*, *36*(3), 484-494.

Kueper, B.H. and D.B. McWhorter (1991), Behavior of dense, nonaqueous phase liquids in fractured clay and rock, *Ground Water* , *29*(5), 716-728.

Kung, K.-J.S., E.J. Kladivko, T.J. Gish, T.S. Steenhuis, G. Bubenzer, and C.S. Helling (2000), Quantifying preferential flow by breakthrough of sequentially applied tracers: Silt loam soil, *Soil Sci. Soc. Am. J.*, *64*(4), 1296-1304.

McKay, L.D., J.A. Cherry, and R.W. Gillham (1993a), Field experiments in a fractured clay till: 1. Hydraulic conductivity and fracture aperture, *Water Resour. Res.*, *29*(4), 1149-1162.

McKay, L.D., J. Fredericia, M. Lenczewski, J. Morthorst, and K.E.S. Klint (1999), Spatial variability of contaminant transport in a fractured till, Avedøre Denmark, *Nord. Hydrol.*, *30*(4-5), 333-360.

McKay, L.D., W.E. Sanford, and J.M. Strong (2000), Field-scale migration of colloidal tracers in a fractured shale saprolite, *Ground Water*, *388*(1), 139-147.

McKay, L.D., R.W. Gillham, and J.A. Cherry (1993b), Field experiments in a fractured clay till; 2, Solute and colloid transport, *Water Resour. Res.*, *29*(12), 3879-3890.

Mualem, Y. (1976), A new model for predicting the hydraulic conductivity of unsaturated soils, *Water Resour. Res.*, *12*(3), 513-522.

Natsch, A., C. Keel, J. Troxler, M. Zala, N. Von Albertini, and G. Défago (1996), Importance of preferential flow and soil management in vertical transport of a biocontrol strain of *Pseudomonas fluorescens* in structured field soil, *Applied and Environmental Microbiology*, *62*(1), 33-40.

O'Connor, D. (2002), Report of the Walkerton Inquiry Part One: The Events of May 2000 and Related Issues, Ontario Ministry of the Attorney General, Toronto, Ontario.

Passmore,J. (2005), An analysis of the transport of bacteria from biosolids through the unsaturated profiles of three different soils, MSc thesis, University of Guelph, Guelph, Ontario, Canada.

Robin, M.J.L., A.L. Gutjahr, E.A. Sudicky, and J.L. Wilson (1993), Cross-correlated random field generation with the direct fourier transform method, *Water Resour. Res.*, *29*(7), 2385-2397.

Schaap, M.G. and F.J. Leij (1998), Database-related accuracy and uncertainty of pedotransfer functions, *Soil Sci.*, *163*(10), 765-779.

Therrien, R. and E.A. Sudicky (1996), Three-dimensional analysis of variably-saturated flow and solute transport in discretely-fractured porous media, *J Contam. Hydrol.*, *23*(1-2), 1-44.

Unc, A. and M.J. Goss (2003), Movement of faecal bacteria through the vadose zone, *Water, Air, and Soil Pollution*, *149*(1-4), 327-337.

van Genuchten, M.T. (1980), A closed-form equation for predicting the hydraulic conductivity of unsaturated soils, *Soil Sci. Soc. Am. J.*, *44*, 892-898.

Vandersteen, K., J. Carmeliet, and J. Feyen (2003), A network modeling approach to derive unsaturated hydraulic properties of a rough-walled fracture, *Transport Porous Med.*, *50*(3), 197-221.

Veerapaneni, S., J. Wan, and T.K. Tokunaga (2000), Motion of particles in film flow, *Environ. Sci. Technol.*, *34*(12), 2465-2471.

Vogel, T., M.T. van Genuchten, and M. Cislerova (2001), Effect of the shape of the soil hydraulic functions near saturation on variably-saturated flow predictions, *Adv. Water Resour.*, *24*(2), 133-144.

Wan, J. and T.K. Tokunaga (1997), Film straining of colloids in unsaturated porous media: Conceptual model and experimental testing, *Environ. Sci. Technol.*, *31*(8), 2413-2420.

Weiler, M. and F. Naef (2003), An experimental tracer study of the role of macropores in infiltration in grassland soils, *Hydrol. Process.*, *17*(2), 477-493.

3.6 Figures and Tables

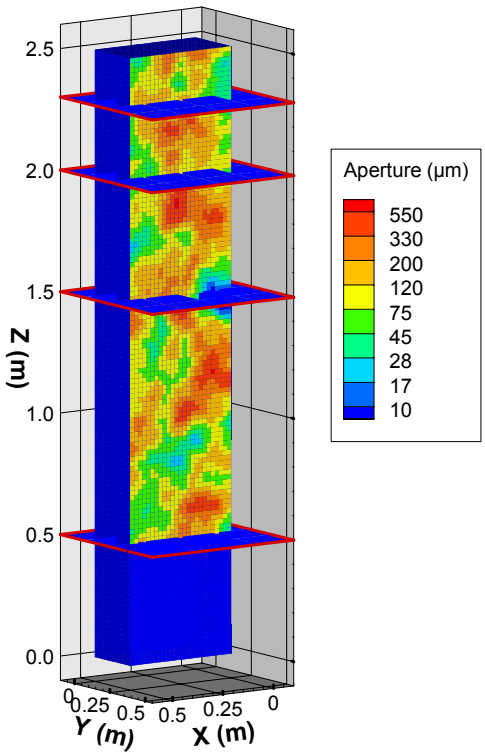

Figure 3.1. An example of half of a modelled soil block showing the spatial aperture distribution within the fracture plane, located at Y = 0.25 m, for Case B02. Vertical water and tracer flow rates are calculated at the location of the horizontal slices (Z = 0.5, 1.5, 2.0, and 2.3 m).

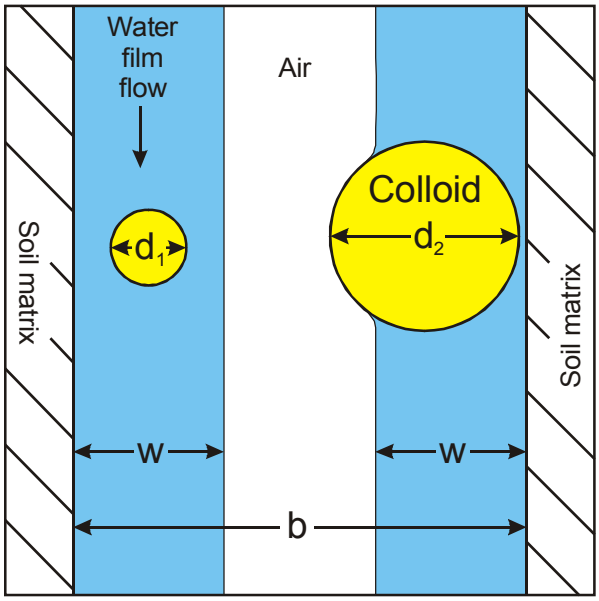

Figure 3.2. Conceptual model of water film flow and colloid transport within a fracture (after Wan and Tokunaga, 1997). The smaller colloid on the left is transported in the water film since $d_1/w < 1$, while transport of the larger colloid on the right is retarded because $d_2/w > 1$.

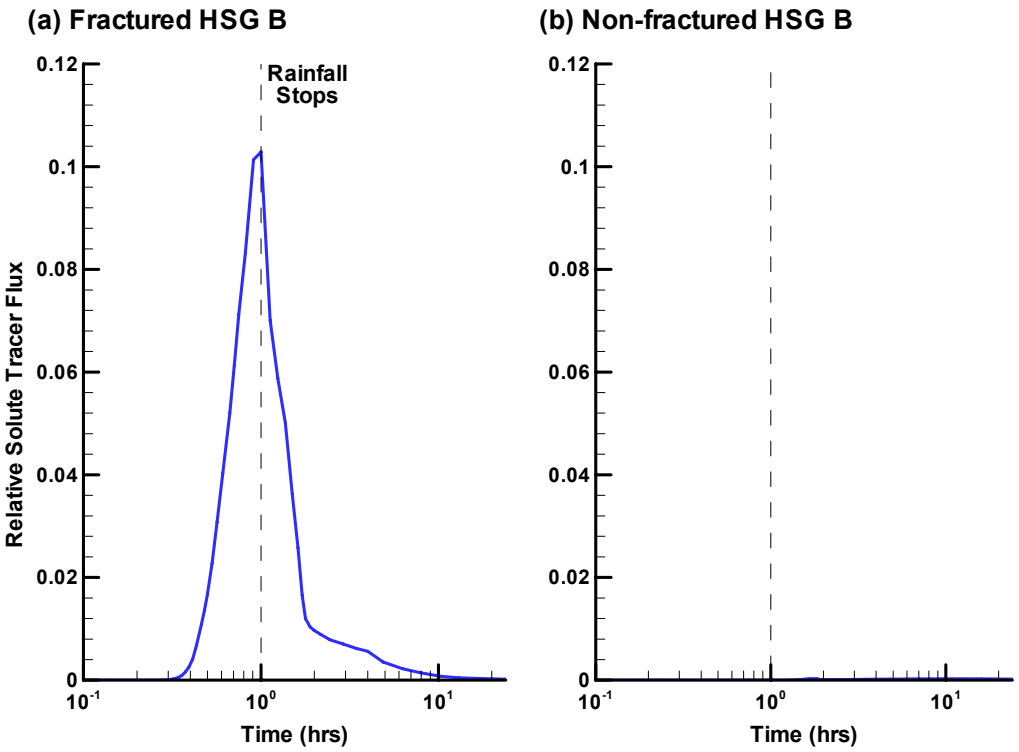

Figure 3.3. Comparison of total Solute flux crossing a horizontal slice at 0.2 m depth for (a) fractured HSG B soil [Case B02], and (b) non-fractured HSG B soil [Case B05]. The vertical dashed line indicates the time when rainfall stopped.

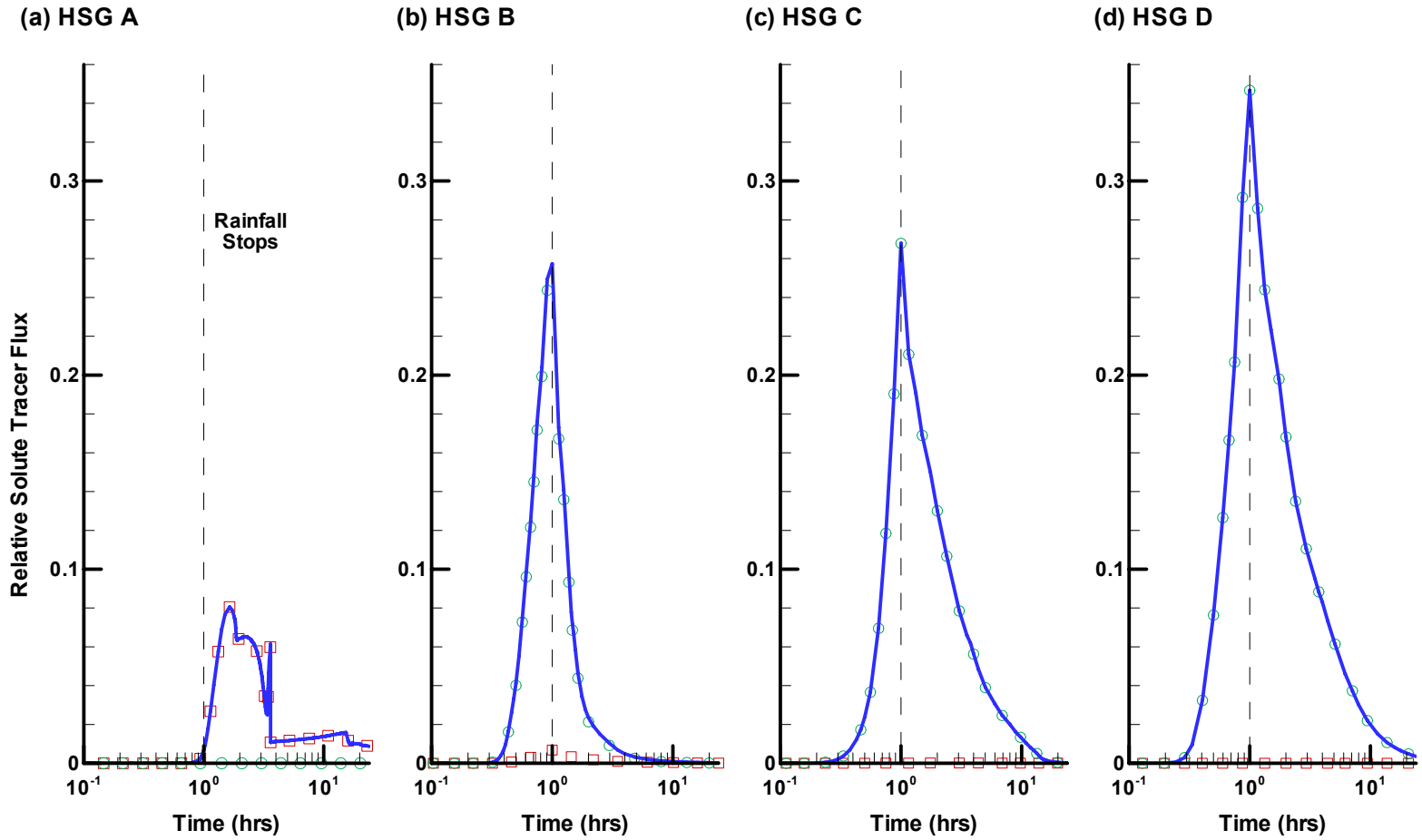

Figure 3.4. Transient relative Solute fluxes for each soil type with a 0.5 m thick soil profile and the water table 0.5 m below ground surface. The Solute fluxes are calculated for a horizontal slice at 0.2 m depth for soil types (a) HSG A [Case A01], (b) HSG B [Case B01], (c) HSG C [Case C01], and (d) HSG D [Case D01]. The total Solute flux (solid line) is separated into contributions from the soil matrix (□) and the fracture (○). The vertical dashed line indicates the time when rainfall stopped.

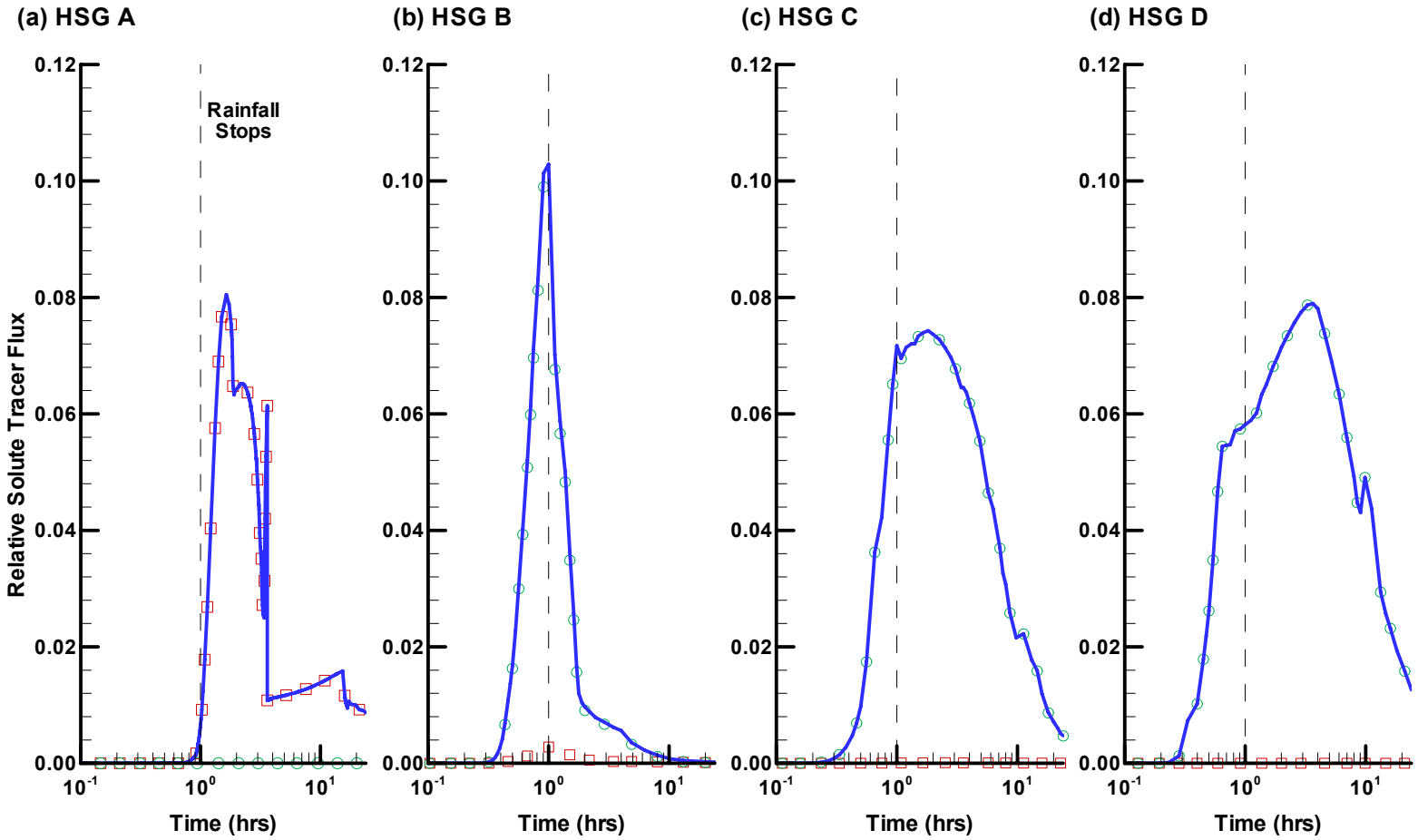

Figure 3.5. Transient relative Solute fluxes for each soil type with a 2.0 m thick soil profile and the water table 0.5 m below ground surface. The Solute fluxes are calculated for a horizontal slice at 0.2 m depth for soil types (a) HSG A [Case A01], (b) HSG B [Case B02], (c) HSG C [Case C02], and (d) HSG D [Case D02]. The total Solute flux (solid line) is separated into contributions from the soil matrix (□) and the fracture (○). The vertical dashed line indicates the time when rainfall stopped.

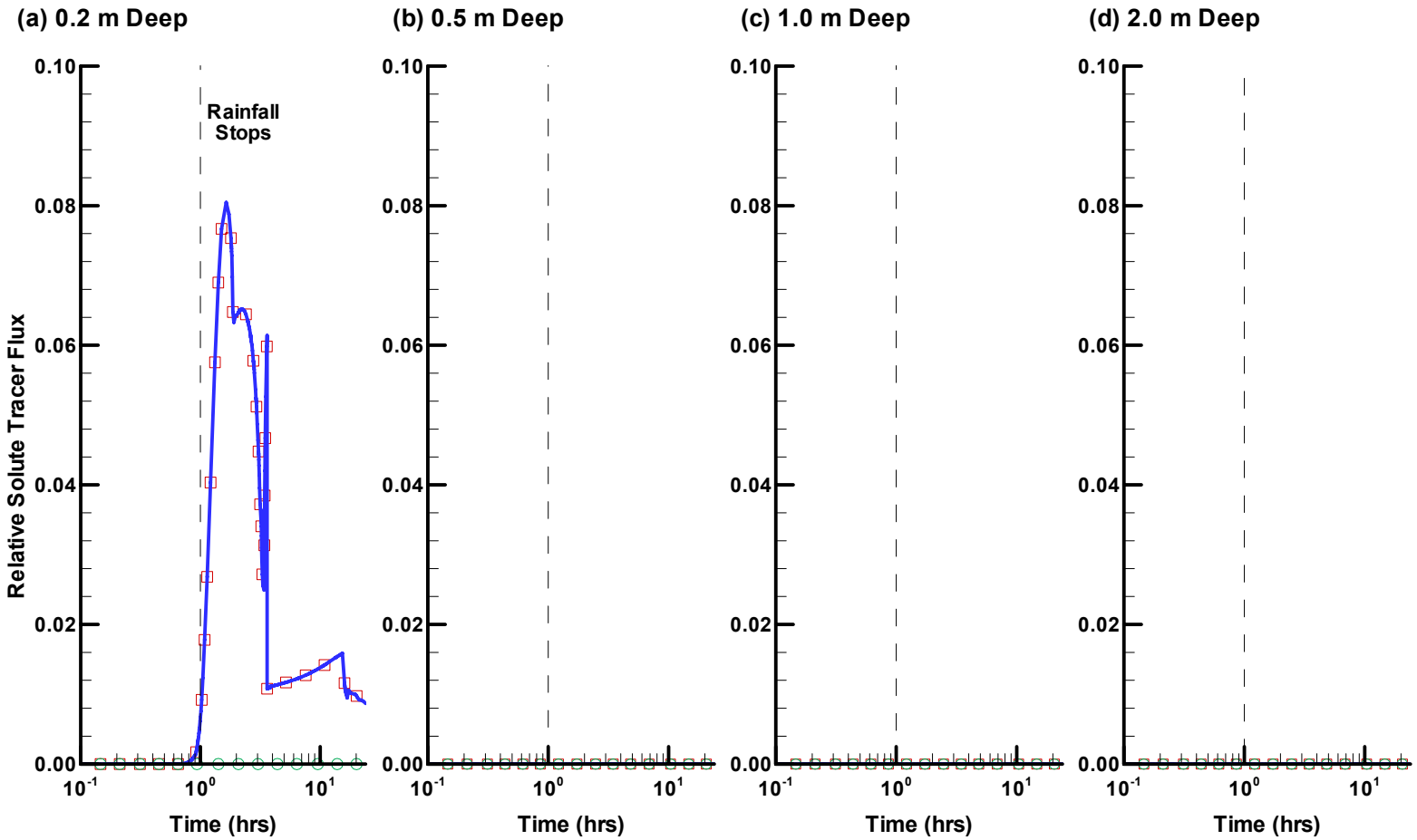

Figure 3.6. Transient relative Solute fluxes in HSG A soil at depths of (a) 0.2 m, (b) 0.5 m, (c) 1.0 m, and (d) 2.0 m below ground surface. The soil profile is 2.0 m thick and the water table is 0.5 m below ground surface [Case A01]. The total Solute flux (solid line) is separated into contributions from the soil matrix (□) and the fracture (○). The vertical dashed line indicates the time when rainfall stopped.

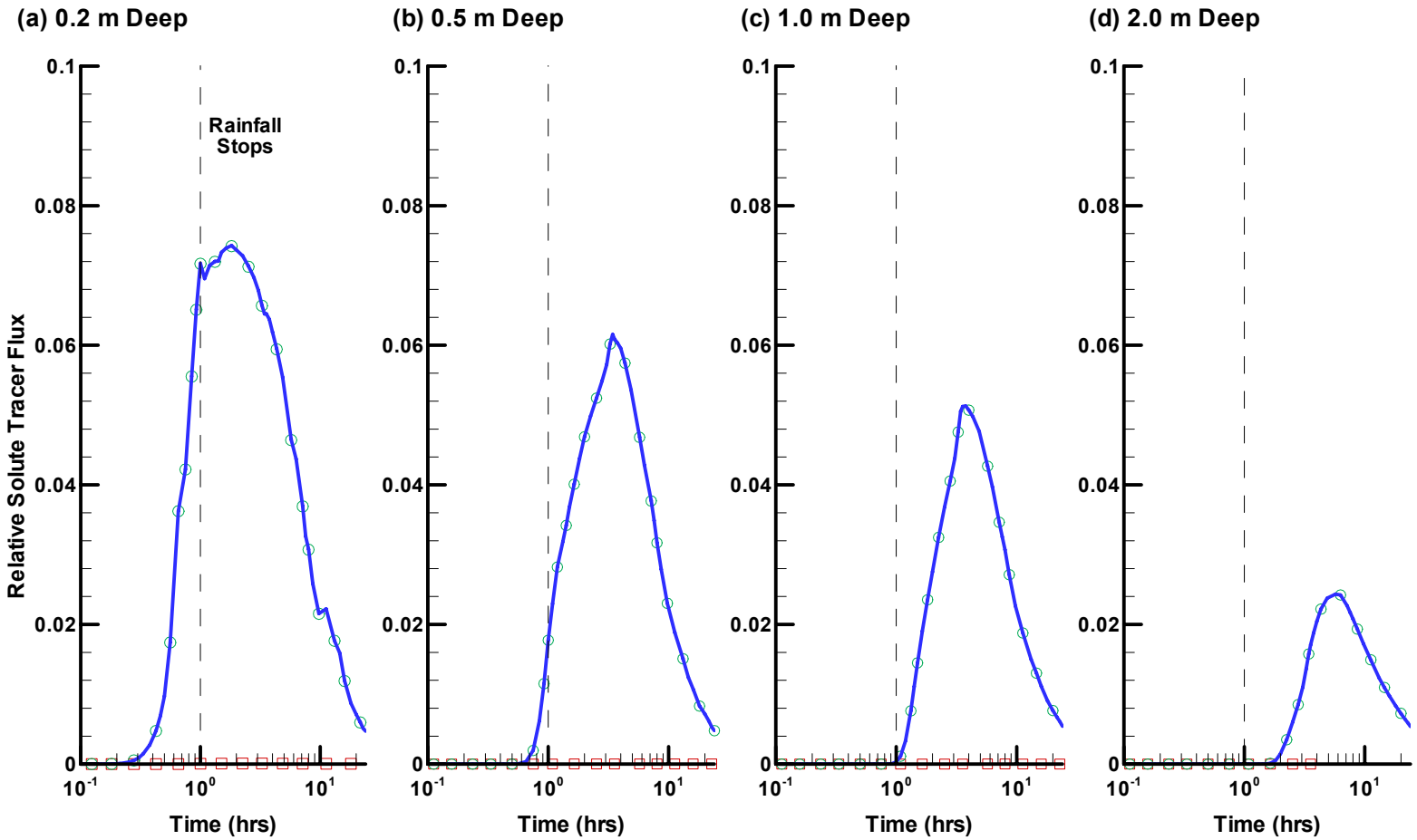

Figure 3.7. Transient relative Solute fluxes in HSG C soil at depths of (a) 0.2 m, (b) 0.5 m, (c) 1.0 m, and (d) 2.0 m below ground surface. The soil profile is 2.0 m thick and the water table is 0.5 m below ground surface [Case C01]. The total Solute flux (solid line) is separated into contributions from the soil matrix (□) and the fracture (○). The vertical dashed line indicates the time when rainfall stopped.

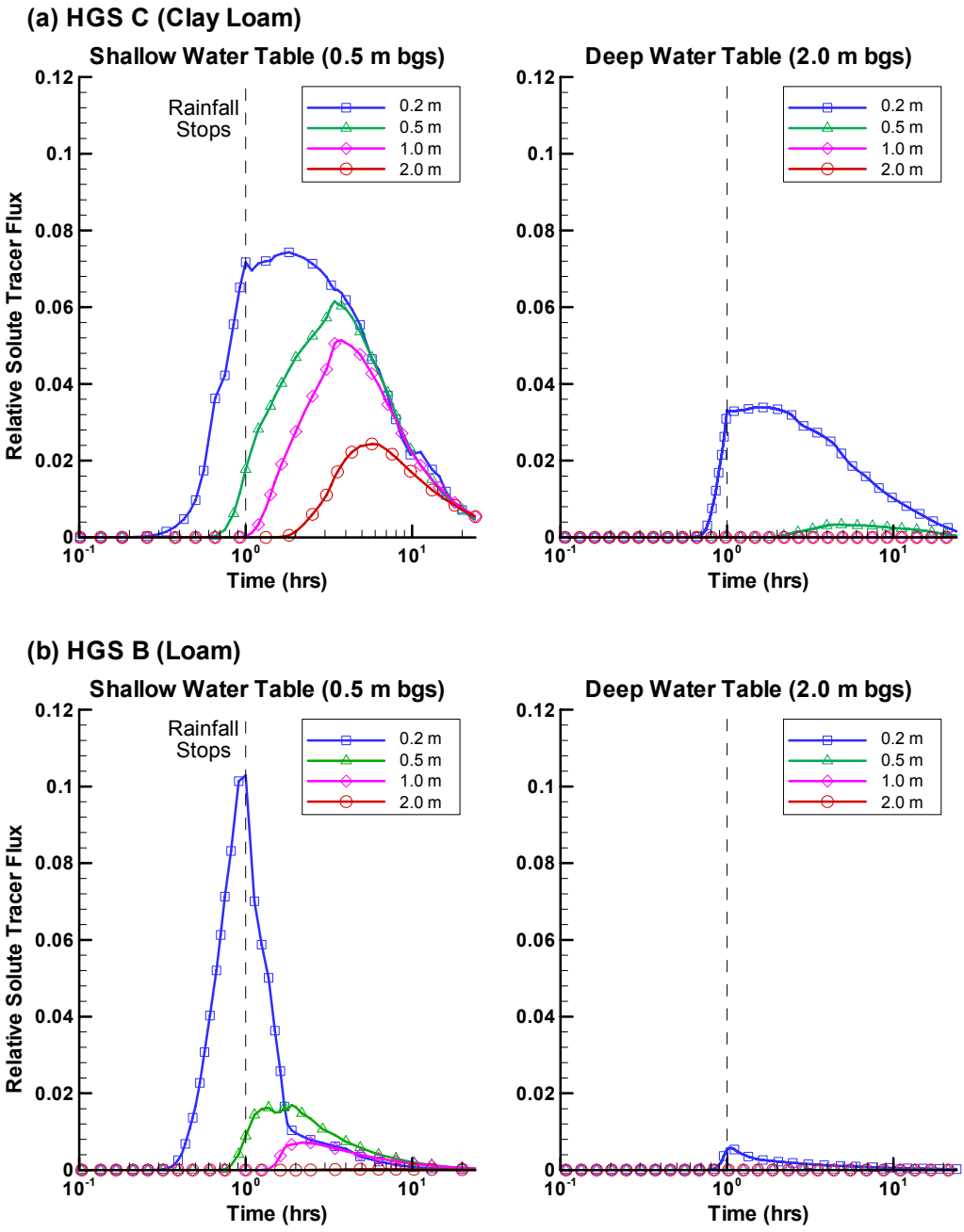

Figure 3.8. Plots of total relative Solute fluxes versus time showing two sets of water table depths: shallow (left panel) and deep (right panel) for soil types (a) HSG C [Cases C02 and C04] and (b) HSG B [Cases B02 and B04]. The soil profile is 2.0 m thick and fluxes are shown for horizontal slices at 0.2 m, 0.5 m, 1.0 m, and 2.0 m depth. The vertical dashed line indicates the time when rainfall stopped.

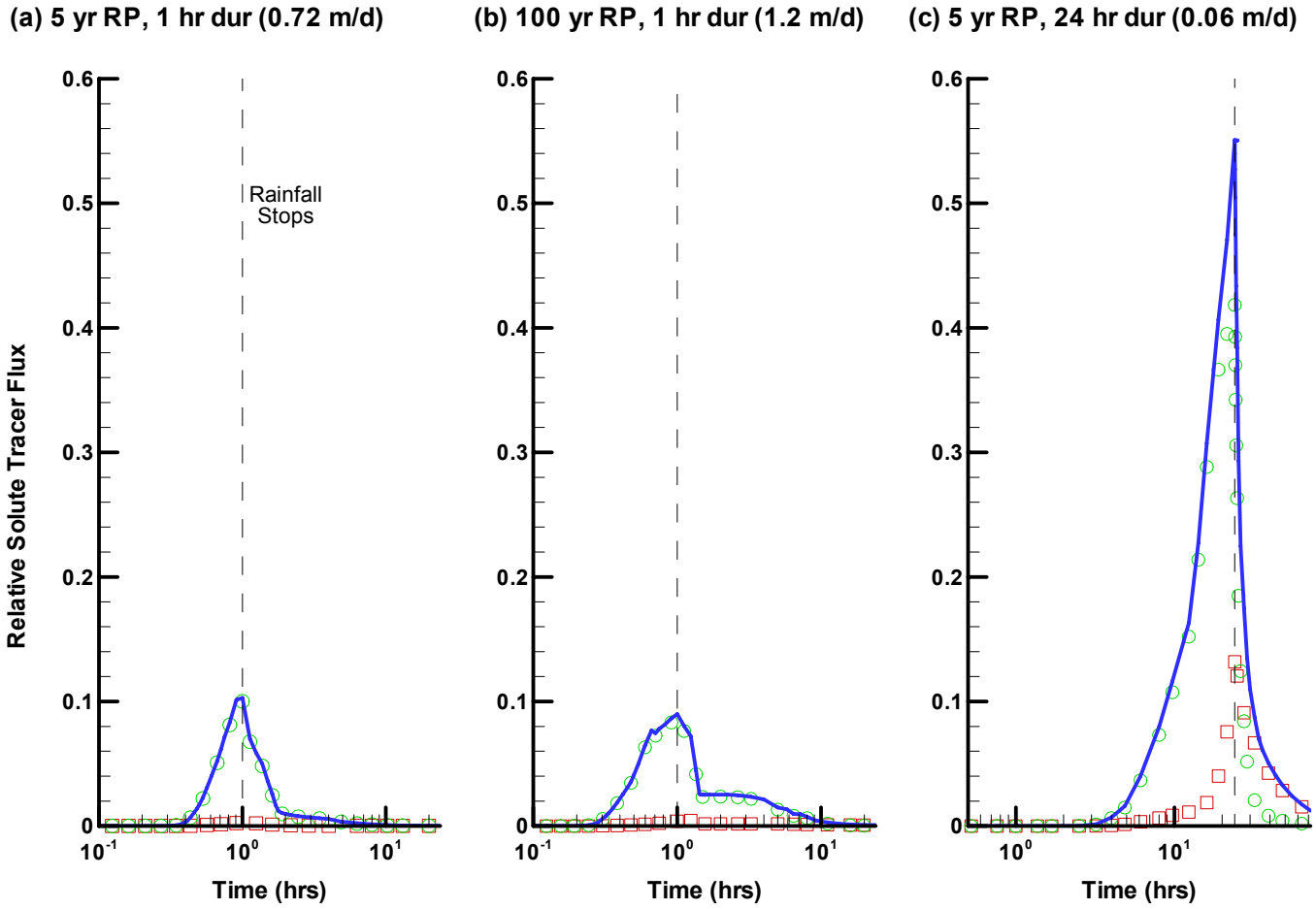

Figure 3.9. Transient relative Solute fluxes crossing a horizontal slice at 0.2 m depth in HSG B soil for varying rainfall events: (a) 5 year return period (RP) event of 1.0 hour duration [Case B02], (b) 100 year RP event of 1.0 hour duration [Case B06], and (c) 5 year RP event of 24.0 hour duration [Case B07]. The soil profile is 2.0 m thick and the water table is 0.5 m below ground surface. The total Solute flux (solid line) is separated into contributions from the soil matrix (□) and the fracture (○). The vertical dashed line indicates the time when rainfall stopped.

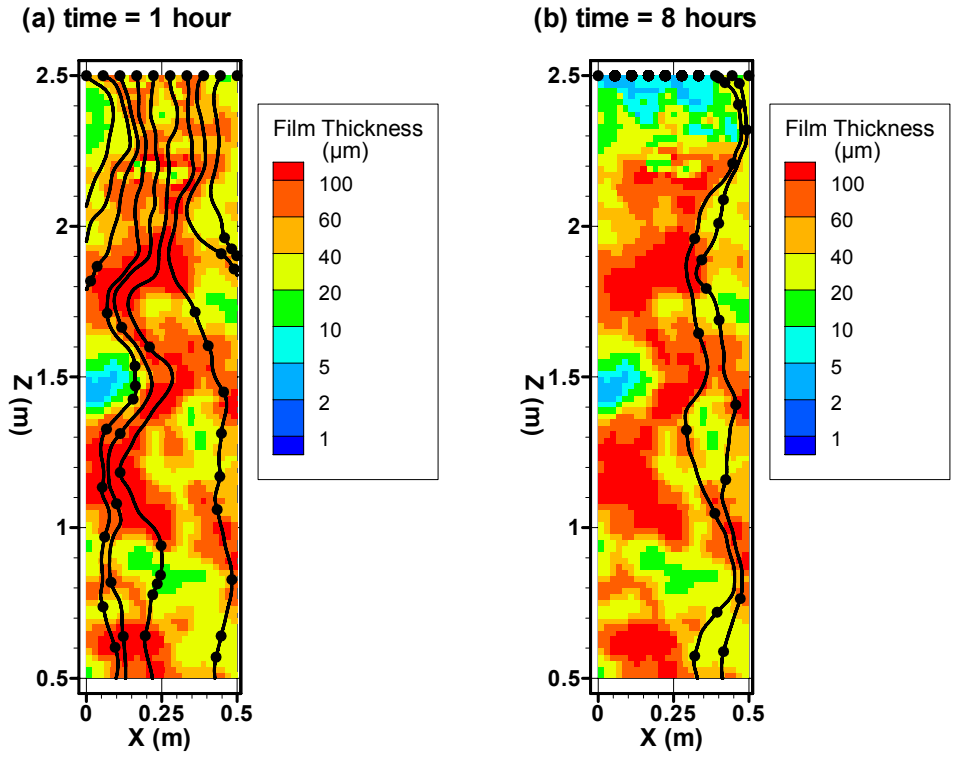

Figure 3.10. Contour plots of equivalent unsaturated water film thickness in the fracture plane for a 2.0 m thick HSG B soil under shallow water table (0.5 m bgs) conditions [Case B02]. Film thicknesses are shown for times (a) 1.0 hour (end of the rainfall event), and (b) 8 hours after the start of the simulations. The black lines represent Colloid tracer particle pathways in the fracture and each circle represents 1.0 minute of travel time.

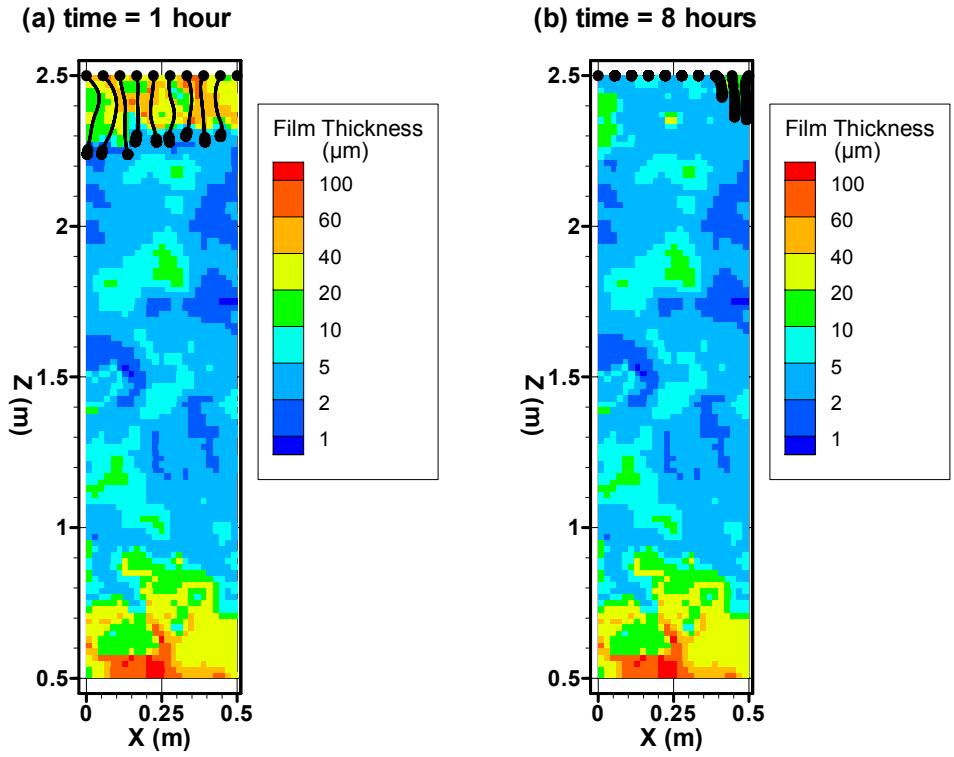

Figure 3.11. Contour plots of equivalent unsaturated water film thickness in the fracture plane for a 2.0 m thick HSG B soil under deep water table (2.0 m bgs) conditions [Case B04]. Film thicknesses are shown for times (a) 1.0 hour (end of the rainfall event), and (b) 8 hours after the start of the simulations. The black lines represent Colloid tracer particle pathways in the fracture and each circle represents 1.0 minute of travel time.

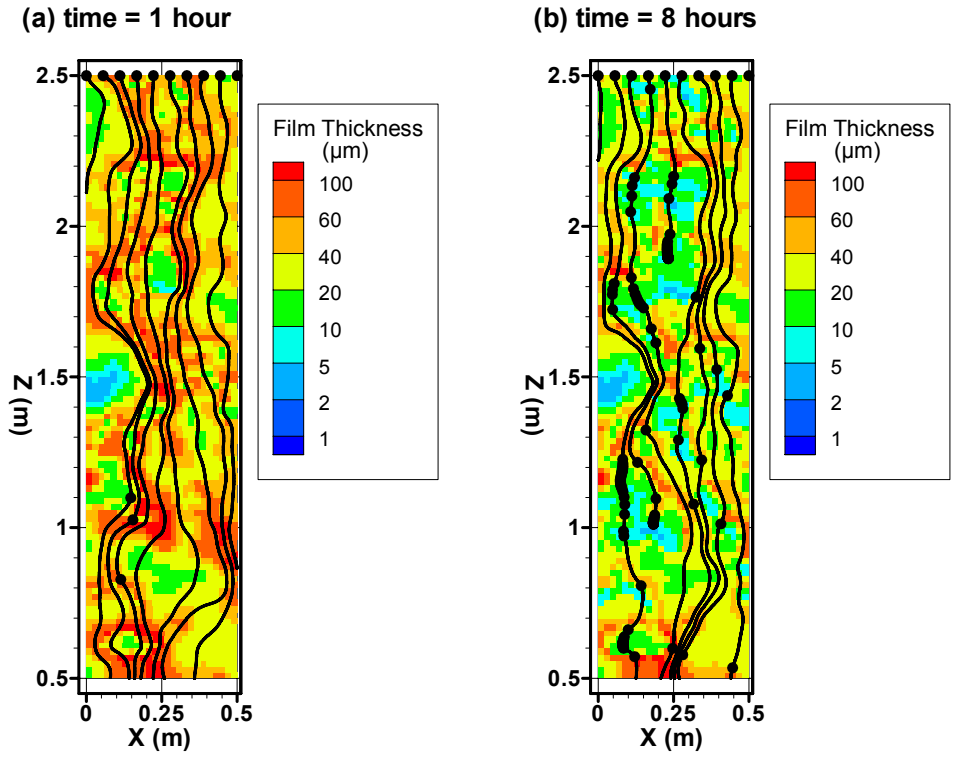

Figure 3.12. Contour plots of equivalent unsaturated water film thickness in the fracture plane for a 2.0 m thick HSG D soil under deep water table (2.0 m bgs) conditions [Case D04]. Film thicknesses are shown for times (a) 1.0 hour (end of the rainfall event), and (b) 8 hours after the start of the simulations. The black lines represent Colloid tracer particle pathways in the fracture and each circle represents 1.0 minute of travel time.

Table 3.1. Model dimensions and input parameters.

Case	Soil Properties			Grid Dimensions			Initial Conditions	Boundary Conditions				
	HSG[a]	Depth	Fracture Spacing	X	Y	Z	Water Table Depth	Rainfall Intensity	Rainfall Duration		Return Period[b]	Lower Boundary Head
		(m)	(m)	(m)	(m)	(m)	(m)	(m/d)	(d)	(hr)	(yr)	(m)
A01	A	2.0	na	0.02	0.02	2.5	0.5	0.72	0.0417	1.0	5	2.0
A02	A	2.0	na	0.02	0.02	2.5	2.0	0.72	0.0417	1.0	5	0.5
A03	A	2.0	na	0.02	0.02	2.5	0.5	1.20	0.0417	1.0	100	2.0
B01	B	0.5	0.2	0.5	0.2	2.5	0.5	0.72	0.0417	1.0	5	2.0
B02	B	2.0	0.5	0.5	0.5	2.5	0.5	0.72	0.0417	1.0	5	2.0
B03	B	0.5	0.2	0.5	0.2	2.5	2.0	0.72	0.0417	1.0	5	0.5
B04	B	2.0	0.5	0.5	0.5	2.5	2.0	0.72	0.0417	1.0	5	0.5
B05	B	2.0	na	0.02	0.02	2.5	0.5	0.72	0.0417	1.0	5	2.0
B06	B	2.0	0.5	0.5	0.5	2.5	0.5	1.20	0.0417	1.0	100	2.0
B07	B	2.0	0.5	0.5	0.5	2.5	0.5	0.06	1.00	24.0	5	2.0
C01	C	0.5	0.2	0.5	0.2	2.5	0.5	0.72	0.0417	1.0	5	2.0
C02	C	2.0	0.5	0.5	0.5	2.5	0.5	0.72	0.0417	1.0	5	2.0
C03	C	0.5	0.2	0.5	0.2	2.5	2.0	0.72	0.0417	1.0	5	0.5
C04	C	2.0	0.5	0.5	0.5	2.5	2.0	0.72	0.0417	1.0	5	0.5
C05	C	2.0	0.5	0.5	0.5	2.5	0.5	1.20	0.0417	1.0	100	2.0
C06	C	2.0	0.5	0.5	0.5	2.5	0.5	0.06	1.00	24.0	5	2.0
D01	D	0.5	0.2	0.5	0.2	2.5	0.5	0.72	0.0417	1.0	5	2.0
D02	D	2.0	0.5	0.5	0.5	2.5	0.5	0.72	0.0417	1.0	5	2.0
D03	D	0.5	0.2	0.5	0.2	2.5	2.0	0.72	0.0417	1.0	5	0.5
D04	D	2.0	0.5	0.5	0.5	2.5	2.0	0.72	0.0417	1.0	5	0.5

na indicates not applicable

[a]Hydrologic Soil Group (refer to Table 2 for soil properties)

[b]Return period indicates the average interval of time within which the given rainfall event is likely to be equalled or exceeded once

Table 3.2. Hydrologic soil group properties.

HSG[a]	Texture	K_s		S_s	θ_s	VGM[b] Values		
						θ_r	α	n
		(m/d)	(cm/s)	(m^{-1})	(-)	(-)	(m^{-1})	(-)
A	Sand	8.6	$1.0x10^{-2}$	$1x10^{-4}$	0.35	0.05	12	3.0
B	Loam	0.26	$3.0x10^{-4}$	$1x10^{-4}$	0.4	0.07	4	1.5
C	Clay Loam	$8.6x10^{-3}$	$1.0x10^{-5}$	$1x10^{-4}$	0.45	0.09	1.0	1.25
D	Clay	$2.6x10^{-4}$	$3.0x10^{-7}$	$1x10^{-3}$	0.45	0.1	0.6	1.1

[a]Hydrologic Soil Group
[b]van Genuchten-Mualem Model

Table 3.3. Fracture properties.

Fracture Parameter	Value
Geometric mean aperture	100 μm
Variance of ln(b)	0.64
Spatial correlation length	0.10 m
λ, Brooks-Corey pore size index	4.0
Residual fracture saturation	0.05

Table 3.4. Draft restrictions for manure applications on shallow soils over bedrock.

Depth to Bedrock (m)	Liquid Manure	Solid Manure
0.0-0.15	No application	No application Oct. - May; <22 t/ha June-Sept.
0.15-0.30	No application Oct. - May; Pre-till or <40 m^3/ha	Pre-till or <45 t/ha
0.30-0.90	Pre-till or <40 m^3/ha	No restriction

Table 3.5. Draft assessment of groundwater contamination potential.

HSG[a]	Depth of Unsaturated Soil at the Time of Application[b]		
	< 0.30 m	0.3-0.6 m	0.6-0.9 m
A	No application	High	Moderate
B	No application	Moderate	Low
C	No application	Low	Very low
D	No application	Low	Very low

[a]Hydrologic Soil Group
[b]Taken as equivalent to the depth of the water table

Table 3.6. Draft restrictions for manure application in areas of shallow groundwater.

Groundwater Contamination Potential	Liquid Manure	Solid Manure
High	No application	Pre-till and <45 t/ha
Moderate	Pre-till and <40 m^3/ha	Pre-till
Low	Pre-till or <40 m^3/ha	No restriction
Very low	No restriction	No restriction

Chapter 4
Field Investigations of Partially Saturated Flow Through Macroporous Soil Beneath a Tension Infiltrometer

4.1 Introduction

Macropores are large soil voids, often distinct in some manner from the soil matrix, that can permit preferential flow of water and contaminants through the soil profile. They are formed by a variety of weathering and biological processes [*Beven and Germann*, 1982] and are common in most natural soils. Preferential flow through macroporous soils has been identified or inferred in a large number of field studies [*Bouma and Dekker*, 1978; *Coles and Trudgill*, 1985; *Edwards et al.*, 1993; *Flury et al.*, 1994; *Scanlon and Goldsmith*, 1997; *Perillo et al.*, 1999; *Kung et al.*, 2000; *Buttle and McDonald*, 2000; *Haria et al.*, 2003; *Unc and Goss*, 2003]. Macropores are a very important feature in hydrologic systems, as they affect the rate and depth of infiltration, rainfall-runoff relationships, groundwater recharge, and the preferential transport of contaminants to groundwater. Although mechanisms controlling flow behaviour in saturated macroporous sediments is fairly well understood [*McKay et al.*, 1993b; *Hinsby et al.*, 1996; *Jorgensen et al.*, 2002], flow phenomena under partially saturated conditions within the macropore domain have not been well characterized.

There are several physical processes that play an important role in preferential flow through macroporous soils. Many of the relevant flow processes occur at the pore scale, but have important consequences for field-scale flow and transport. Antecedent soil moisture, macropore flow initiation, and macropore-matrix interaction are interrelated and have been identified as important mechanisms in controlling the extent of preferential flow [*Shipitalo et al.*, 1990; *Ghodrati et al.*, 1999; *Heppell et al.*, 2002; *Weiler and Naef*, 2003a; *Weiler and Naef*, 2003b; *Tallon et al.*, 2007]. Other studies have shown that macropore connectivity is also important [*Faeh et al.*, 1997; *Cameira et al.*, 2000; *Nobles et al.*, 2004]. While these processes are critical, accurate descriptions of their function remain elusive. One area that has received relatively little attention is the water configuration within individual macropores. Highly simplistic capillary tube or parallel plate models, where pores are either completely filled with air or water depending on soil water potential, are widely adopted to describe flow in macropores [*Bodhinayake et al.*, 2004; *Kung et al.*, 2006]. These models are unrealistic in that the larger macropores do not contribute to flow until they become completely water filled. The result is that preferential flow observations are often attributed to either ponded infiltration on surface or, more commonly, a saturated soil layer below surface [*e.g., Tallon et al.*,

2007]. A more realistic conceptual model considers a continuum of pore sizes, from microscopic up to macroscopic pores, with each pore increasingly contributing to flow as the soil becomes wetter. In other words, even the largest macropores can contribute to flow even though they are not fully saturated. Recent field and laboratory studies conducted under partially saturated conditions suggest that flow can occur as thin films or pulses along macropore walls [*Tokunaga and Wan*, 1997; *Villholth et al.*, 1998; *Leonard et al.*, 2001; *Tofteng et al.*, 2002; *Gjettermann et al.*, 2004]. This changing paradigm suggests that macropores could play a much more active role in water and contaminant movement than previously thought. The practical relevance of flow in macropores under partially saturated conditions remains unknown and requires additional work. Proper mechanistic descriptions of liquid configuration within macropores are needed to accurately describe the dynamics of flow along macropores and between macropores and matrix.

One of the main factors limiting our understanding is the difficulty in observing and quantifying of macropore flow phenomena in the field. For example, there are few (if any) methods for monitoring in situ flow rates or water contents for individual macropores. In natural soils it is difficult to control the extent to which macropores contribute to preferential movement of water. Once initiated, preferential flow through macropores is notorious for its variability in time and space [*e.g., Dahan et al.*, 1999; *Podgorney et al.*, 2000]. In this study, we propose combining field methods for characterizing the spatial and temporal variability of subsurface flow with techniques for controlling the degree of macropore flow in order to improve our understanding of macropore flow processes. The tension infiltrometer provides an effective method for controlling flow in pores of different sizes [*Watson and Luxmoore*, 1986; *Jarvis et al.*, 1987; *Buttle and McDonald*, 2000]. The device permits infiltration of water at negative pressures (or tensions), thereby limiting saturated flow to pores below a certain size based on capillary theory (of course remembering that flow will still occur in pores of all sizes as described above). With increasing pressure potentials, relatively larger and larger pores contribute to infiltration. The measured flow rates describe the transient response of the system at different tensions, and are most often used to estimate unsaturated hydraulic conductivity or to characterize the degree of macroporosity [*Watson and Luxmoore*, 1986; *Ankeny et al.*, 1991; *Reynolds and Elrick*, 1991; *Vandervaere et al.*, 2000; *Bodhinayake et al.*, 2004]. Dye tracers have also been shown to be useful for assessing macropore flow in the field [*Bouma and Dekker*, 1978; *Flury et al.*, 1994; *Weiler and Naef*, 2003b; *Nobles et al.*, 2004], as the dye patterns reflect the spatial variability of flow at all scales. All dye compounds undergo sorption to mineral surfaces and thus are retarded relative to the infiltrating water. Nevertheless, they provide excellent visualization of flow pathways. Subsurface dye patterns can provide insights into pore scale phenomena, such as macropore-matrix interaction, and at the same time be used to delineate the extent of flow in the bulk soil. Few studies have combined tension infiltration with the use of dye tracers [*Jarvis et al.*, 1987; *Lin and McInnes*,

1995], yet together they have the potential to provide valuable information about the hydraulic behaviour of macroporous soils.

In this study, small-scale dye infiltration experiments were conducted using a tension infiltrometer at two field sites in southern Ontario. The primary objective was to investigate the influence of macropores on subsurface flow through structured, low permeability soils during episodic infiltration at different soil water potentials. Tension infiltration was used to control macropore flow, while detailed spatial (i.e., dye patterns) and temporal (i.e., infiltration rates) data sets were collected to characterize flow behaviour. By comparing flow regimes with and without the influence of macropores, the nature of different physical processes, such as macropore connectivity, flow initiation, and macropore-matrix interaction, was assessed. In addition, the concept of flow in macropores under negative pressures is discussed with regard to the potential for flow under fully or partially saturated conditions.

4.2 Methods

4.2.1 Site Descriptions

Controlled tension infiltration experiments were conducted at two field sites in southern Ontario, Canada. Infiltration tests were first conducted in October 2005 at the Elora Research Station (latitude 43° 38′ 25" N, longitude 80° 24′ 34" W), an active agricultural research facility located approximately 20 km northwest of Guelph, Ontario. The infiltration tests were located on a regularly mowed turfgrass site that was surrounded by agricultural fields. The soil was a slightly stony, imperfectly drained Guelph silt loam [*Hoffman et al.*, 1963] that overlies approximately 20 to 22 m of Port Stanley Till. The depth to the water table was approximately 1.4 m below ground surface at the time of the experiments.

A second series of infiltration experiments was conducted in July and August 2006 at a small farm near the western edge of Walkerton, Ontario (latitude 44° 07′ 01" N, longitude 81° 9′ 50" W). The tests were conducted on a conservation tilled field that is typically cropped in a corn-soybean rotation and was planted with soybeans in the 2006 cropping season. The soil was described as imperfectly drained Listowel loam [*Hoffman and Richards*, 1954] that is derived from Elma Till parent material. Bedrock of the Upper Silurian Bass Island Formations was encountered at depths between 2.7 and 3.2 m near the infiltration sites. The water table at Walkerton was 1.1 m below surface in spring and gradually receded to a maximum depth of 1.5 m over the growing season.

4.2.2 Tension Infiltration Experiments

All infiltration tests in this study were conducted using a tension infiltrometer (TI) with a 209 mm diameter disc (Soil Measurement Systems model SW-080B). The water level in the TI tower was recorded with a differential pressure sensor (Honeywell 26PC series) connected to a datalogger (Campbell Scientific CR10X) for automated recording of infiltration rates [*Casey and Derby*, 2002]. All tension infiltrometers and pressure sensors used were calibrated in the laboratory prior to use in the field. The infiltration soil surfaces were prepared by carefully removing any vegetation (*e.g.*, grass, soybeans) and then scraping away a thin layer (approximately 0-2 cm) of soil to ensure a level surface. Although the infiltration surface was altered, care was taken to minimize the disturbance to the soil structure and prevent smearing or clogging of macropore features. A 3 mm thick layer of uniform glass beads (Spheriglass No. 2024) was applied on the soil surface within a 209 mm inside diameter metal retaining ring, which was subsequently removed prior to emplacement of the infiltrometer disc. The glass beads improve hydraulic contact between the soil and the infiltrometer disc [*Perroux and White*, 1988]. The Spheriglass No. 2024 beads were chosen because they have similar size and hydraulic characteristics to the glass beads recommended by Reynolds and Zebchuk [1996] for tension infiltration experiments. Three time domain reflectometry (TDR) probes were installed at equal distances around the perimeter of the TI disc during each experiment. The 10.0 cm long TDR probes were installed in the soil at a 45° angle (from horizontal) pointing toward the centre of the infiltration disc area. The TDR probes were connected to the datalogger via a multiplexor and regular water content measurements were recorded prior to and during the infiltration tests.

In order to assess subsurface flow patterns, Brilliant Blue FCF dye (C.I. Acid Blue 9, 42090) was added to the infiltration water at a concentration of 4.0 g/L. Brilliant Blue FCF has been identified as a useful tracer for water flow in the vadose zone [*Flury and Fluhler*, 1995; *Flury and Wai*, 2003] and has been used in other hydrologic studies [*Flury et al.*, 1994; *Forrer et al.*, 2000; *Kulli et al.*, 2003; *Weiler and Naef*, 2003b; *Nobles et al.*, 2004]. It was selected for use because it has low toxicity [*Flury and Fluhler*, 1994] and is a reasonable compromise between the competing effects of mobility and visibility [*Flury and Fluhler*, 1995; *German-Heins and Flury*, 2000]. Preliminary staining tests indicated the dye was readily visible in the subsurface materials at both sites.

Two infiltration tests situated approximately 2.3 m apart were conducted at the Elora site (EL-D1 and EL-D2) on October 17 and 18, 2005. A total of four infiltration tests were conducted at the Walkerton site. From July 11 to 13, 2006, three infiltration tests (WK-D1, WK-D2, and WK-D3) were conducted, each approximately 1.5 m apart. As part of a subsequent rainfall simulation experiment (see Chapter 5), a fourth infiltration test (WK-D4), located approximately 13 m east of WK-D1, was conducted on August 17, 2006. It is notable that surface soils at Walkerton were much

drier at the time of test WK-D4 as a result of increased crop growth and evapotranspiration between the two test periods. Water was infiltrated at successively increasing pressure potentials for all tests. The maximum pressure head applied to the TI disc was varied between the tests at each site to evaluate the influence of macropores on subsurface flow patterns at different tensions. In most tests, infiltration was limited to two applied pressure potentials, with the bulk of the infiltrated water applied at the maximum pressure potential. Four pressure potentials were applied for test EL-D2 to assist in evaluating flow rates over a range of tensions. The range of pressure heads applied in all tests at Elora (-16.4 cm to -0.6 cm) was similar to the range used at Walkerton (-12.8 cm to -0.4 cm). A total of 1.0 L of dye solution was applied for all tests, with the exception of test EL-D2 where about 2.0 L of dye solution was applied as a result of the infiltration period being extended due to a malfunction in the monitoring system. The larger volume of fluid applied in test EL-D2 likely influenced the extent of the dye patterns and saturation changes observed in the subsurface, but it was not expected to change the relative contributions of macropores versus matrix flow and the characteristic dye patterns that resulted.

4.2.3 Excavation, Mapping and Photographs of Soil Sections

Following completion of infiltration, excavations were completed to examine the dye-stained flow patterns and to map soil features. Plastic covers were placed over the individual infiltration sites and the excavation areas were covered with tarps to protect from evaporation and rainfall during excavation. Parallel vertical soil sections were first excavated at distances of 20, 10, and 0 cm away from the center of each disc area. Beneath the remaining half of the infiltration area, horizontal soil sections were prepared at 2, 5, and 10 cm below the infiltration surface and every 10 cm thereafter until no further dye staining was observed. All soil sections were carefully cut using hand tools in order to reduce damage to soil structure. During excavation, macropore locations and characteristics were mapped for all horizontal soil sections. All soil sections were photographed using procedures modified from Forrer et al. [2000]. Photographs of the soil profiles were taken during the day using an opaque white tarp to diffuse the light. A gray frame with ruled markings was placed on the soil profile to assist with the correction of geometric distortion and uneven illumination in the photographs. White reflection panels were also used either beneath or beside the soil profiles to permit more even lighting of the soil profiles. Photographic color and gray scales (Kodak Q-14 Color separation guide and gray scale) were pinned to the soil surface to ensure consistency in subsequent image analysis procedures. Photographs were taken with a 5.0 megapixel digital camera (Canon Powershot A95) using consistent manual exposure settings. All original photographs were stored digitally with a resolution of 2592 by 1944 pixels.

At the Walkerton site, dye calibration patches were prepared and photographed for the A and B soil horizons as described by Weiler and Fluhler [2004]. On horizontal soil sections adjacent to the infiltration tests, six 8-by-8 cm patches of soil were excavated approximately 5 mm deep. Approximately 100 ml of Brilliant Blue FCF dye solution with concentrations of 4.0, 2.0, 1.0, 0.5, 0.2, and 0.05 g/L were poured onto the patches and allowed to infiltrate. The dye stained soil was then photographed using the methods described above. The dye calibration patches were used during image analysis to define concentration categories for dye stained soil regions.

4.2.4 Infiltration on an Open Vertical Soil Section

In order to better assess the transient development of flow pathways in the subsurface, an additional tension infiltration test was conducted at Walkerton on an exposed vertical soil section. This infiltration test is hereafter referred to as the transient dye test. First, a smooth vertical face was excavated within a shallow trench, about 3 m away from test WK-D4. The TI disc was then placed on the soil surface with the edge of the disc extending approximately 4.5 cm beyond the vertical face. A dye solution was infiltrated in a similar manner as described above for tests WK-D3 and WK-D4. Following initial setup, the large majority (over 95%) of the dye solution was infiltrated over a 29.7 min period at a pressure head of -0.4 cm. Time lapse photographs of the vertical soil section were taken at one minute intervals to record the advancement of the wetting front and subsequent redistribution following cessation of infiltration.

4.2.5 Soil Physical Property Testing

Following the infiltration tests, undisturbed core samples and bulk soil samples were collected from the A, B and C horizons at both sites to measure soil physical properties. A total of ten intact core samples were collected and analyzed from each site. The core samples were collected by pushing a cylindrical aluminum tube, 25 mm tall by 47 mm inside diameter, into the soil and carefully removing it by excavating around the core tube. Soil at each end of the core was trimmed flush with the core tube and one end was covered with fine cloth that was secured to the core. The cores were then oven dried and weighed. Bulk density ρ_b was calculated by dividing the dry soil mass by the core volume [*Blake and Hartge*, 1986]. Total porosity n was calculated using the equation provided by Carter and Ball [1993]

$$n = 1 - \frac{\rho_b}{\rho_p} \tag{13}$$

where ρ_p is the particle density, which was assumed equal to 2.65 g cm^{-3}. Saturated hydraulic conductivity K_{sat} of the core samples was determined in the laboratory using either a constant head

(Elora) or falling head (Walkerton) permeameter [*Reynolds*, 1993]. A minimum of three repetitions were completed for each core sample. In addition, soil water retention curves were measured on the intact soil cores according to the pressure plate method described by Topp et al. [1993]. The retention curves were measured at pressure heads of 0, -0.1, -0.2, -0.5, -1.0, and -3.0 m.

Bulk soil samples were collected from the open excavations using a shovel or hand trowel and the soil was placed in clean, sealable plastic bags. The grain size distribution of the bulk samples was determined using a combination of sieve analysis and the hydrometer method [*Sheldrick and Wang*, 1993].

4.2.6 Image Analysis of Dye Stain Patterns

The image analysis procedures used closely followed those outlined by Weiler and Fluhler [2004] and, to a lesser extent, Forrer et al. [2000], with selected modifications to improve discrimination of dye patterns and ensure consistency between images. A detailed description of the image analysis procedure is provided in Appendix B. Briefly, all images underwent the following procedures: geometric correction, background subtraction, color adjustment, histogram stretching, dye classification, and a final visual check. Image processing was completed using IDL software (ITT Visual Information Solutions version 6.2) along with standard photo-editing software packages. The resulting images were separated into dyed and non-dyed regions, with the dyed regions further divided into three classes based on the intensity of dye staining. At the Walkerton site, dye stained soil calibration patches were used to determine concentration categories for the three dye stained soil classes (0.2-1.5 g/L, 1.5-3.0 g/L, and >3.0 g/L). Based on detailed visual inspection, the area of misclassified pixels was small in all images and generally limited to very dark soil regions (*e.g.*, shadows) or stained areas around cobbles and rocks.

4.3 Results and Discussion

4.3.1 Soil Conditions and Macroporosity

The soil physical properties measured from samples collected at both the Elora and Walkerton sites are provided in Table 4.1. A summary of all soil data, including soil water retention curves and grain size distribution plots for each soil horizon, is compiled in Appendix C. In general, the soil characteristics were very similar between the two sites. The Elora A and B horizons can be described as silt loam and loam based on their textural composition, while the A and B horizons at Walkerton are described as loam. Average saturated hydraulic conductivity, K_{sat}, values at Elora ranged between 2×10^{-6} m s^{-1} (B horizon) and 9×10^{-7} m s^{-1} (C horizon). Soils from the Walkerton site had higher average K_{sat} values, between 5×10^{-5} m s^{-1} and 9×10^{-5} m s^{-1}. The laboratory determined K_{sat} values

from Walkerton were higher than expected and may be due to the higher sand content and lower clay content at the Walkerton site. Alternately, the results may have been affected by soil shrinkage and subsequent short-circuiting of water along the walls of the core tube during permeameter testing as the soil cores from Walkerton were subjected to oven drying and rewetting prior to testing. In addition, the van Genuchten-Mualem constitutive relationship model [*Mualem*, 1976; *van Genuchten*, 1980] was fitted to the average soil water retention data for each soil horizon (Appendix C) using least squares optimization. The resulting empirical fitting parameters, α and n, are provided in Table 4.1.

Soil macropore features were photographed and recorded during the test excavations. An example of a typical excavated soil section and the macropore features encountered is shown in Figure 4.1. The dominant macropore type at both sites was earthworm burrows, although preferential flow along root holes and fractures was also identified close to the soil surface. The wormholes were circular and ranged in size from about 2 to 10 mm in diameter. Numerous burrows extended beyond the maximum depth of excavations (approximately 1.2-1.4 m). Individual existing or abandoned root holes tended to be smaller with diameters between 1 and 4 mm. Many earthworm burrows were lined with a coating of finer-grained organic material that has been identified and examined in other studies [*Stehouwer et al.*, 1994; *Jensen et al.*, 2002; *Schrader et al.*, 2007]. Other burrows, such as the one shown in Figure 4.1b, appeared to contain no such coating and were connected directly to unaltered soil matrix material.

The number and type of observed macropores as a function of depth are given in Table 4.2 and plotted in Figure 4.2. The trends in macropore density were similar at both field sites. The density of cylindrical macropores increased with depth to the maximum at 30 cm below ground surface, and decreased thereafter. The peak in macropore density at 30 cm is partly attributed to increased wormhole stability in the B and C soil horizons, and the fact that historical tillage depths were approximately 20 cm below surface. The variability in macropore density with depth suggests that a large number of dead end macropores were likely encountered, particularly below 30 cm depth. Vertically oriented earthworm burrows were by far the dominant macropore feature, constituting over 85% of the cylindrical macropores at both sites. Fractures and root holes were most prevalent in the top 20 cm of the soil profile, with fracture density peaking at 10 cm depth (Figure 4.2).

The vegetative growth stage was also recorded for each experiment. At the Elora site, the infiltration experiments were conducted on turfgrass that was regularly mowed to a height of approximately 5-8 cm. A very large number of hair-like roots were encountered in the top 2 to 5 cm of the soil due to presence of the mature turfgrass. These small roots were too numerous to count and are not included in the totals listed in Table 4.2 or shown in Figure 4.2. At the Walkerton site, the

soybean crop canopy was approximately 25-30 cm high at the time tests WK-D1 through WK-D3 were conducted (July 11-13). At the same time, the crop roots were concentrated in the top 10 cm of the soil profile. The canopy height increased to a height of approximately 60-70 cm and the crop roots extended to 15-20 cm depth by the time test WK-D4 was conducted on August 17. Although the roots tended to extend more laterally than vertically, individual roots were discovered at depths more than 50 cm below surface. The deepest roots were commonly seen within existing worm burrows. The increased vegetative growth and associate evapotranspiration that occurred between the first three TI tests (WK-D1 through WK-D3) and test WK-D4 caused a marked decrease in the soil water content in the top 10-15 cm of the soil profile.

4.3.2 Infiltration Rate and Soil Moisture Measurements

The cumulative infiltration volumes and changes in water content recorded during the tests at Elora and Walkerton are presented in Figure 4.3 and Figure 4.4, respectively. The infiltration rates are indicated by the slope of the cumulative infiltration curve in the figures. Details of the applied pressure heads and quasi-steady flow rates for each test are summarized in Table 4.3. The plots show distinct flow characteristics that are dependent on the pressure head applied with the TI. The discussion here will focus primarily on the Walkerton results, but the same general trends were observed at both sites. As expected, the infiltration rates were highest for tests conducted at higher (less negative) pressure heads, and significantly lower for tests at the lowest (most negative) pressure heads. For example, quasi-steady infiltration rates were 0.52, 2.47, and 4.14 cm hr^{-1} at the maximum applied pressure heads for tests WK-D1, WK-D2, and WK-D3, respectively (Table 4.3). Based on the duration and intensity of infiltration, tests WK-D1, WK-D2, and WK-D3 are representative of rainfall events with return periods of approximately <2, 2, and 5 years, respectively.

The variability in the measured infiltration rates was also a function of the applied pressure head. The infiltration rate was generally steadier and the changes in water content were more uniform at lower infiltration pressures (see for example test WK-D1 in Figure 4.4a). At the highest water supply pressures, the measured changes in soil water content were more erratic in both space and time. For example, changes in water content were different for each of the three TDR probes in test WK-D3, with total increases of 0.13, 0.15, and 0.08 during infiltration. The timing of the water content changes during infiltration and drainage were also significantly different among the three measurement locations. Conversely, the water content showed a consistent increase of 0.15 along all three TDR probes in test WK-D1, suggesting fairly uniform spatial infiltration. The increased variability in measured soil water contents is indicative of increased preferential flow encountered at the higher water supply potentials, which results in significant spatial variability in the wetting front beneath the TI disc.

There was less spatial variability in the measured soil water contents at the Elora site (Figure 4.3) compared to Walkerton (Figure 4.4), particularly for tests with higher infiltration pressures. The water content response in test EL-D2 (Figure 4.3b), for example, was much more consistent among the three TDR probes than either tests WK-D3 or WK-D4 (Figure 4.4c and d) conducted at Walkerton using similar maximum infiltration pressures. This too is attributed to the role of antecedent moisture and the manner in which the TI tests were performed. Test EL-D2 had the highest antecedent moisture content and was also conducted using four different applied pressures, which caused more gradual wetting of the soil. As a result, the shallow soil matrix was likely wetted in a spatially uniform manner and was very close to saturation by the time the final infiltration pressure head (h_{max} = -0.6 cm) was applied. The reduction in available soil moisture storage limited capillary forces and enhanced vertical macropore flow because of the reduction in water exchange between macropores and the matrix, at least near the soil surface (i.e., above the matrix wetting front). So, although macropore flow likely was prevalent during test EL-D2, it did not result in as much spatial variability in shallow soil moisture as the tests at Walkerton.

Tests WK-D3 and WK-D4 were conducted at similar pressure heads, but the surficial soil was much drier prior to test WK-D4 (Figure 4.4). Both tests had similar infiltration rates and showed considerable variability in the observed water content changes between the different TDR measurement locations. However, the average water content increase measured in the top 8 cm of soil beneath the TI disc was much larger for test WK-D4 (0.19) than for test WK-D3 (0.12). Obviously, the drier soil conditions for WK-D4 resulted in increased imbibition of water into the surficial soil during infiltration. It is not clear, however, whether the increased imbibition was the result of increased infiltration directly from the TI disc into the soil matrix, or the result of increased water transfer between the soil matrix and macropores. Given the similar infiltration rates observed during the two tests, it is suspected that the latter process is more prevalent.

The shape of the cumulative infiltration and soil moisture content curves, during both infiltration and redistribution, provide additional insights into flow processes. During infiltration, the slope of the cumulative infiltration plots changed each time the applied pressure head was increased. The most dramatic changes in slope (i.e. infiltration rate) occurred at the largest pressure heads (or smallest tensions). This is shown most clearly in test EL-D2 (Figure 4.3b) which had four applied pressure heads ranging from -16.4 to -0.6 cm (Table 4.3). As the applied pressure heads increased, the infiltration rates increased significantly as the flow system transitioned from nearly 100% matrix flow to a combined matrix and macropore flow system. This suggests the permeability of the macropores is much greater than micro- and mesopores. The soils at both sites, although relatively fine-grained, clearly have the capacity to transmit water at relatively high rates as the macropore

network becomes increasingly engaged in flow. This implies that it would take either a very long or very high intensity rainfall event to exceed the infiltration capacity of these macroporous soils.

Once infiltration stopped, the water content measurements from the Walkerton tests gave an indication of the transient flow behaviour during redistribution (soil water content was not recorded following infiltration in the Elora tests). Figure 4.4 shows that drainage and redistribution was a much slower process than infiltration. In tests WK-D1 and WK-D2, each of the three TDR probes showed a similar monotonic decline in water content as redistribution occurred under gravitational and capillary pressure gradients. This again suggests a more spatially uniform infiltration and redistribution pattern under lower infiltration pressure conditions. However, in tests WK-D3 and WK-D4 with the higher infiltration pressures, the water content measurements showed more variation. For instance, the response of each of the probes in test WK-D4 (Figure 4.4d) was distinct. TDR probe 3 showed a water content peak at the end of the infiltration period and then steadily declined in much the same manner as tests WK-D1 and WK-D2. The water content measured by TDR probe 2 continued to increase for a short period following infiltration and then began to decline, whereas the water content along TDR probe 1 slowly increased to the end of the measurement period nearly 80 minutes after infiltration ceased. The three water content curves were converging, but at an ever decreasing rate. The internal drainage and redistribution discussed here are considered to represent the response of the soil matrix. The macroporosity is expected to drain much more quickly and, because of the relatively small volume of macroporosity, would not likely be detected by the TDR probes. Macropores are clearly an important feature during infiltration, but once the water input source is removed, capillary forces cause the flow system to quickly transition to the smaller pores and the hydraulic conductivity decreases correspondingly. Macropore-matrix interaction must be significant in order for the quick transition from macropore to matrix dominated flow to occur.

The cumulative infiltration curves for tests WK-D1, WK-D2 and WK-D3 (Figure 4.4) are concave upward, indicating a gradual increase in infiltration rate with time. The reason for increasing infiltration rates with time is not clear and counter to conventional infiltration theory. It was initially speculated that the apparent increase in infiltration rate could be the result of a decrease in the kinematic viscosity of the fluid due to temperature increases over the period of the tests. However, similar temperature increases were also noted during test WK-D4 and yet the infiltration rate gradually decreased with time during this test.

A second possible explanation for the concave upward infiltration curves is the role of antecedent soil moisture and its influence on permeability. Infiltration rates tend to decrease over time as capillary forces decrease and available storage is filled. As infiltration proceeds in the wetter soils (i.e., WK-D1, WK-D2 and WK-D3), progressively more of the macropore network becomes active

and the resulting effective permeability could increase at a rate that outpaces the influence of decreasing capillarity and available storage. As a result, infiltration rates continue to increase and the system never reaches steady state during the infiltration period. If this was the case, we would expect the influence to be greatest for higher antecedent moisture conditions and higher infiltration pressures. This is generally true for this study, but there are notable exceptions in the concave upward infiltration curve of test WK-D1 (Figure 4.4a) and the lack of any apparent infiltration rate increases during test EL-D2 (Figure 4.3b), which had the highest antecedent moisture content of any of the tests. The exact reason for the infiltration rate increases cannot be conclusively determined from the existing data.

4.3.3 Subsurface Dye Patterns

Brilliant Blue FCF dye is known to undergo adsorption [*German-Heins and Flury*, 2000] and has been shown to have a retardation factor of 1.2 relative to a conservative iodide tracer [1995]. Nevertheless, the resulting dye stained soil patterns are considered to reasonably reflect the underlying flow patterns that occurred during infiltration and are conservative in the sense that the actual movement of water or a non-sorbing tracer would be even greater than the dye.

The classified dye stain patterns for vertical soil sections cut along the centerline of the TI disc are shown in Figure 4.5 and Figure 4.6 for the Elora and Walkerton sites, respectively. Classified dye patterns for all vertical sections are provided in Appendix D. It is readily apparent that the subsurface flow patterns are not spatially uniform, owing to soil heterogeneity and macroporosity. There are distinct differences in the dye patterns observed for infiltration at different applied pressure heads. Dye patterns were most uniform and generally confined to the upper 10 cm of the soil profile under infiltration at the lowest pressure heads (Figure 4.5a and Figure 4.6a). With an increase in the maximum applied pressure head, the depth of dye staining increased and the observed flow patterns became more irregular, particularly below 5-10 cm depth. The depths of dye staining were a function of the applied infiltration pressure head. The maximum depths of dye staining encountered for each test are given in Table 4.3. In the three tests conducted with maximum pressure heads greater than -1.0 cm (EL-D2, WK-D3, and WK-D4), the maximum depth of dyed soil was equal to or greater than 70 cm below surface. There was deeper propagation of dye in test EL-D2, compared to WK-D3 and WK-D4, likely as a result of the higher antecedent soil moisture content and larger volume of water applied in test EL-D2. Test WK-D2, which had a maximum infiltration pressure head of -2.5 cm, showed dye staining to 30 cm depth (Figure 4.6b and Table 4.3) as a direct result of flow along macropores. The critical finding is that the dye patterns clearly demonstrate the occurrence of macropore flow at infiltration pressures less than atmospheric, resulting in much deeper propagation of infiltrating fluid than would be expected under uniform, plug flow conditions.

The dye patterns along the horizontal soil sections showed similar features. The horizontal dye patterns for the first three tests at Walkerton, given in Figure 4.7, show the same relationship between the depth of dye staining and the pressure applied to the TI disc. The dye patterns for all other horizontal sections are provided in Appendix D. In all cases, the greatest depths of staining occur under the largest supply pressures. These results are consistent with other studies that have shown the depth of infiltration is dependent on small pressure differences at the infiltration surface under near-saturated conditions [*Trojan and Linden*, 1992; *Lin and McInnes*, 1995]. In this study, the largest pressures (although still negative) produced near-saturated conditions in the soil, triggering flow in larger soil pores. The dye patterns from test WK-D2 suggest that preferential flow along macropores is significant for infiltration at pressure heads as low as -2.5 cm. Jarvis et al. [1987] used a similar experimental design in a clay soil to show preferential flow in macropores at pressure heads of -0.5 and -2 cm, but not at -9 cm. It is clear from the dye patterns that the tension infiltrometer is a useful tool for controlling the initiation of macropore flow in field soils.

In the upper 5 to 10 cm of the soil profile a large portion of the soil area beneath the disc was dye covered, including both the soil matrix and macropores (see Figure 4.7). Given the extent of dye staining near surface it was difficult to tell whether flow in macropores was initiated directly beneath the TI disc or deeper in the subsurface. Both surface and subsurface [*Logsdon*, 1995; *Allaire-Leung et al.*, 2000; *Weiler and Naef*, 2003a] initiation of flow have been suggested in other studies. It is clear from these results that macropore flow was initiated very near the soil surface. The horizontal dye patterns in test WK-D3, which exhibited clear evidence of preferential flow, were more irregular at 2 and 5 cm depth than tests WK-D1 or WK-D2. The irregular dye patterns in test WK-D3, especially the higher dye concentration regions, were centered on macropore features, signifying that flow along macropores was initiated within a few centimeters of the soil surface. In all tests where macropore flow was identified, dye staining along vertical macropores was observed at less than 10 cm depth. This is well above the A-B soil horizon boundary (about 20 cm depth) where flow convergence or local soil saturation might be expected to initiate macropore flow.

Below 10 cm depth, the dye patterns were obviously related to the presence of vertically oriented macropores. Dye stain patterns could be clearly traced from near surface to the maximum depth of dye staining along an individual macropore or, more commonly, a series of closely connected macropores. For example, the notable finger of dye extending from 20 to 60 cm depth in test WK-D4 (Figure 4.6d) followed a single vertical wormhole. Dye was traced in this wormhole to a maximum depth of 74 cm below ground surface. The dye stain patterns in test EL-D2 (Figure 4.5b), on the other hand, tended to follow a series of subvertical macropores where the dye patterns surrounding individual macropores were clearly connected. In addition, only a portion of the macropores beneath

the TI disc were dye stained at any given depth, and the percentage that were stained decreased with depth. In many cases, unstained macropores could be attributed to a lack of continuity and connectivity of the macropore network. However, several instances were noted where macropores were connected to dyed soil matrix near surface, yet they did not conduct flow to greater depths. At other locations, dye staining dissipated with depth in macropores that appeared to continue vertically downward, and connected laterally to other nearby vertical macropores. No visible macropores or soil heterogeneities were identified directly linking the vertical macropores, but it was difficult to assess three-dimensional macropore connectivity on the soil sections.

A unique feature identified on the classified dye images was the presence of regions of greater dye concentration near the bottom of several vertical fingers. These dye stained "bulbs" were often present near the maximum vertical extent of staining (e.g., Figure 4.6c) as well as the lower portion of shallower fingers of dyed soil (e.g., Figure 4.5b). The origin of the more intense dye staining at depth is speculated to result from the dye solution reaching the bottom of dead-end macropores. The presence of dye staining along vertical macropores demonstrated that fluid was transferred from the macropores into the soil matrix (Figure 4.1b). Once dye solution reached the bottom of a macropore it would begin to accumulate as long as the rate of infiltration along the macropore exceeded the rate of fluid transfer into the matrix. This would in turn increase pressure within the macropore and enhance flow from macropore to matrix, resulting in the observed "bulb" of dye stained soil. The proposed mechanism for generating these features is based on field observations of flow into and along vertical macropores, and the results of preliminary numerical simulations using a subsurface flow and transport model incorporating discrete macropores (not shown). Other studies have also shown dead-end macropores can enhance macropore-matrix interaction and that macropore continuity is important in order to accurately simulate flow and transport in macroporous soils [*Faeh et al.*, 1997; *Cameira et al.*, 2000].

Dye patterns varied considerably with the applied water supply potential, but for a given supply potential the dye patterns were remarkably consistent between the two sites. This is illustrated most clearly in the dye stained width plots of Figure 4.8. Tests EL-D1 and WK-D1, conducted at the lowest pressure heads, showed very similar extents of dye staining, both vertically and horizontally. Since flow was restricted primarily to the soil matrix, which was similar in nature at both sites, and the same volume of dye solution was applied in both tests, the result is not surprising. On the opposite end of the flow spectrum, tests EL-D2 and WK-D3 were both conducted under very small negative pressure heads and had similar antecedent moisture conditions. The resulting flow patterns showed more irregularity as a result of macropore flow, but the same general trends were observed in

each of the tests. That is, dye stained width fluctuated a great deal with peaks spaced roughly every 10 cm, and the maximum depth of dye staining was approximately 60 cm below surface.

In all infiltration tests there was a significant amount of lateral infiltration directly beneath the TI disc due to soil capillary forces. Figure 4.9 shows the variation in dye stained soil width in the top 10 cm of the soil profile for the four tests conducted at Walkerton. The degree of lateral flow and resulting width of dye stained soil is affected by the amount of vertical preferential flow and antecedent moisture conditions. The first three tests (WK-D1, -D2, and -D3) were conducted under the same soil moisture conditions. Tests WK-D1 and WK-D2 showed increased lateral flow in the top 5 cm, compared to WK-D3, because the lower infiltration supply pressures were more conducive to soil matrix flow. Test WK-D3 had greater vertical preferential flow, thereby reducing the amount of time and contact area for lateral flow into the soil matrix. In comparing tests WK-D3 and WK-D4, with similar infiltration supply pressures but different initial soil moisture contents, the greater width of dyed soil in WK-D4 showed that drier soils enhanced lateral infiltration. Given the increased lateral flow in the upper portion of WK-D4, a decrease in preferential flow below 10 cm depth was expected relative to test WK-D3. The results, however, are not conclusive in this regard. WK-D4 showed approximately the same maximum depth of dye staining, but had considerably less dye coverage below 10 cm depth, as compared to WK-D3 (Figure 4.6 and Figure 4.8). Perhaps the increased lateral flow near surface in WK-D4 resulted in a decrease in the volume of dye solution available, thus fewer macropores contributed to flow and the lateral extent of dye staining was reduced at depth. At the same time, the depth of dye penetration within flowing macropores was controlled by the infiltration supply pressure and the antecedent soil moisture content deeper in the soil profile (i.e., greater than 10 cm depth), which appeared to be similar during both tests. The literature reports conflicting data on the influence of antecedent moisture on preferential flow along macropores. Certain studies demonstrate that wetter soils promote macropore flow [*Coles and Trudgill*, 1985; *Kung et al.*, 2000; *Haria et al.*, 2003; *Weiler and Naef*, 2003b], others point out that the initial water content has little influence [*Flury et al.*, 1994; *Heppell et al.*, 2002], and still others seem to show that macropore contributions are greatest under dry soil conditions [*Shipitalo and Edwards*, 1996; *Katterer et al.*, 2001]. Given the conflicting literature data and the inconclusive results in this study, this remains a worthwhile topic for future research.

4.3.4 Transient Infiltration Observations on a Vertical Soil Section

The dye patterns presented to this point gave a detailed view of spatial flow patterns, however, because of the time frame required for the excavations they represent a period of one day to several days after infiltration occurred. As such, they did not represent the tracer infiltration flow paths alone, but rather a combination of the infiltration and redistribution processes. There remained a need

to obtain information on the transient nature and velocity of subsurface flow processes and, therefore, the transient dye test was conducted to visualize flow along an exposed vertical soil section. Figure 4.10 shows the development of dye staining during the infiltration period as well as during redistribution after flow from the TI disc was stopped. The experiment is not ideal, in that the dye solution can preferentially flow down the exposed vertical face in a manner analogous to flow down one side of a large fracture, such as a desiccation crack. Nevertheless, the results provide valuable information that could not be obtained from either transient monitoring (flow rates and water contents) or steady state dye patterns following infiltration.

The photographs provide visual confirmation of preferential flow along macropores and highlight the relatively large vertical flow velocities. Figure 4.10a shows dye emerging from an earthworm burrow at a depth of nearly 20 cm after only six minutes. The associated flow velocity of 46 m/d in the burrow is nearly twice that of the wetting front advancing down the vertical face, even though both could be considered preferential flow. The flow characteristics remained steady throughout the course of the infiltration event. Early breakthrough of dye was also identified in two separate earthworm burrows between 30 and 40 cm depth after 15 minutes (Figure 4.10b). Imbibition of dye from the wormholes into the surrounding soil matrix was clearly visible. The mechanisms of flow were evaluated from observations of flow down the soil face and near the terminus of the macropores. Flow occurred primarily as a thin film down the exposed soil face. Intermittent flow as rivulets or large drops was also observed over short vertical distances at noticeably higher velocities. These intermittent flows were very likely non-Darcian. In the earthworm burrows, flow first emerged in the form of thin films and occasional small droplets, which then spread laterally on the exposed face. The fact that the dye solution did not appear to fully saturate the burrow has implications for flow rates and velocities and will be discussed further in the next section.

The transient dye test shows the primary mechanism for delivery of water to the macropores under negative (sub-atmospheric) pressure conditions. Water leaving the TI disc first flowed into the glass bead contact material and then into either the soil matrix or macropores (i.e., earthworm burrows, open face, etc.). The water reaching the exposed soil face must flow through the glass beads, the soil matrix, or some combination of the two. In order for this to occur, the infiltrating water is drawn away from the TI disc by capillarity and gravitational gradients. The macropore that is the open vertical face applies these same capillary forces and is able to draw water from the matrix toward the macropore. This may have been aided by evaporation from the soil face in this instance, but the influence is expected to be minor given the short time frame of the experiment. The sheen that eventually formed on the open face (Figure 4.10a-c) and the resulting film/rivulet flow down the face

are clear indications that macropore flow can be initiated at pore pressures less than atmospheric pressure.

Near the end of the infiltration period, the dye had reached a depth of 45 cm (Figure 4.10c), giving an average vertical flow velocity of 22 m/d. Once flow from the TI disc was stopped, subsurface flow quickly ceased. The photographs taken at the end of the infiltration period (t=29 min) and after redistribution (t=51 min) show little difference in the lateral or vertical extent of dye staining (Figure 4.10). The resulting dye patterns from this experiment are much more diffuse than those obtained from the other TI tests (*e.g.*, EL-D2, WK-D3). This is due to the combined influence of preferential flow along the face combined with lateral flow, both on the exposed face and into the soil matrix. The quick cessation of flow following infiltration is ascribed to redistribution of water from the macropores into the smaller pores of the soil matrix. The redistribution of water is demonstrated by the abrupt change in water content along the exposed face. The sheen visible on the soil face during infiltration (Figure 4.10a-c) was indicative of near-saturated soil conditions. After stopping flow from the TI disc, the sheen immediately began to dissipate and had disappeared in less than three minutes as dye solution was drawn away from the vertical face by soil capillary forces (see Figure 4.10d). Two important conclusions can be drawn from the swift flow response at the conclusion of infiltration. First, it indicates that mass exchange between macropores and matrix was a significant process throughout the infiltration period and would serve to effectively retard the advance of water flowing downward through macropores. Second, the vertical extent of dye staining observed in the other tests probably occurred during the infiltration period, not as a result of subsequent drainage and redistribution. A reasonable estimate of vertical transport velocity can therefore be estimated based on the maximum depth of dye staining and length of the infiltration period.

4.3.5 Conceptualization of Flow Along Macropores

Undoubtedly, the vertical flow velocities along the macropores were large in comparison to flow in the soil matrix. It is worth considering how these large flow velocities could be achieved and whether the macropores are likely to achieve these velocities under partially or fully saturated conditions. If macropores are considered as smooth, cylindrical tubes, the relationship between the radius of the largest water filled pore, r, and pressure head, ψ, is given by

$$r = -\frac{2\sigma \cos\beta}{\rho_w g \psi} \tag{14}$$

where σ is the interfacial tension between air and water, β is the contact angle between water and solid (assumed to be zero), ρ_w is the density of water, and g is acceleration due to gravity. The

corresponding average velocity for laminar flow through a water filled macropore is given by the Hagen-Poiseuille equation as

$$\bar{v} = \frac{r^2 \rho_w g}{8\mu}\left(-\frac{dh}{dz}\right) \tag{15}$$

where μ is the viscosity of water, and dh/dz is the hydraulic head gradient in the direction of flow (assumed equal to one for vertical gravity driven flow). The linear macropores (earthworm burrows and root holes) encountered at the sites generally ranged between 0.1 and 1.0 cm diameter. Using Equations 14 and 15, a macropore with a diameter of 0.1 cm would be water filled at pressure heads greater than -3.0 cm with an average flow velocity of 0.31 m/s (26 km/d). Increasing the macropore diameter to 1.0 cm equates to the pore filling at a pressure head of -0.3 cm, however, the resulting velocity is large enough for flow to become turbulent (Reynolds number, *Re*, greater than ≈2000). The flow velocity for turbulent conditions can be calculated as 2.8 m/s (240 km/d) using equations taken from Wang et al. [1994]. The associated volumetric flow rates would be 14 and 1.3 x 10^4 cm^3/min for the 0.1 cm and 1.0 cm diameter macropores, respectively. The theoretical calculations compare favourably with field measurements of peak flow rates into individual earthworm burrows from other studies, which ranged between 8 and 1050 cm^3/min, with averages near 100-500 cm^3/min [*Wang et al.*, 1994; *Shipitalo and Gibbs*, 2000]. For comparison, tests WK-D2 and WK-D3 were conducted at maximum pressure heads of -2.5 and -0.4 cm, respectively. According to the above calculations, the smaller (0.1 cm) macropores would have been filled during both tests and the larger (1.0 cm) macropores would have been filled for test WK-D3 only. Based on the measured infiltration rates from these same tests (see Table 4.3), two 0.1 cm diameter macropores would have been sufficient to carry the entire flow from the TI disc. A single 1.0 cm diameter macropore flowing full could potentially transmit water far in excess of the measured infiltration rates. This is not consistent with the field data in which several dye stained macropores, including larger macropores (see for example Figure 4.1), were identified in each test. Likewise, the calculated flow velocities within the macropores (in the order of kilometers per day) are much higher than those measured in the earthworm burrow (46 m/d) and along the exposed soil face (22 m/d) during the transient dye test. It is readily apparent that the larger dye stained macropores could not have been fully saturated.

An alternative explanation to describe the flow along macropores is proposed considering (1) the macropores, especially the larger ones, conducted fluid while only partially saturated, and (2) water transfer between the macropore and the soil matrix reduced the velocity of the water advancing in the macropore. Both mechanisms likely played a role depending on the size of the macropore and the local soil pressure conditions. Although the often used capillary tube model assumes that pores are

either completely full or completely drained depending on pressure, most real pore spaces are angular or will have surface roughness that will retain water by capillary forces and adsorption even when drained [*Tuller et al.*, 1999]. Using the physically-based liquid configuration model of Tuller and Or [*Tuller et al.*, 1999; *Or and Tuller*, 2000; *Tuller and Or*, 2001], the saturation and flow velocity in vertical macropores with varying cross-sections (*e.g.*, flat surface, angled corners, triangles, squares, etc.) can be calculated. The earthworm burrows encountered at the Walkerton and Elora sites had circular cross-sections, but closer examination revealed many small irregularities along the walls of the burrows (see Figure 4.1b). These irregularities, although very small, are sufficient to conduct relatively large fluid volumes. Assuming that a rough-walled circular worm burrow can be represented by a regular polygon with 10 sides, the flow velocity and water-filled area can be calculated for partially saturated conditions. With no water loss to the matrix and an applied pressure head of -4.0 cm, all macropores between 0.1 and 1.0 cm in diameter would be partially filled with a vertical flow velocity of 9.0 m/d and a volumetric flow rate of 2.3×10^{-5} cm^3/min. It is interesting that for a given pressure potential the velocity and flow rate are independent of the size of the pore, as long as the pore is unsaturated. With an increase in pressure head to -0.4 cm (a factor of 10), only the larger 1.0 cm diameter macropore remains unsaturated and the associated velocity and volumetric flow rate increase by factors of 10^2 and 10^4, respectively. These values appear more consistent with the field data from the TI tests, in that both the velocities and flow rates appear to bracket the field measured values. The emergence of dye from earthworm burrows as thin films during the transient test further supports the proposed concept of partially saturated macropore flow. Flow into termite holes was similarly observed as thin films, rather than saturated flow, by Léonard and Rajot during infiltration experiments in Niger [*as described and cited by Leonard et al.*, 2001]. In laboratory experiments using rough, fractured rock surfaces, Tokunaga and Wan [1997] demonstrated water flow in thin films with velocities between 2 and 40 m/d. Film flow was considered significant at pressure potentials greater than about -2.5 cm. Tokunaga and Wan concluded that surface roughness had a major influence on gravity driven flows at near-zero pressures, lending further support to the notion that irregular pore geometries play an important role in unsaturated macropore flow.

In comparison to field-measured values, the unsaturated flow velocities calculated with the Tuller and Or model still seem unreasonably large as pressure heads approach zero. Macropore-matrix interaction can help explain the apparent reduction in flow velocities in natural pores. The model of Tuller and Or assumes equilibrium between matrix and macropores, and does not consider dynamic transfer processes that would limit the speed at which water travels down along the macropore walls. Simple mass balance calculations show that water drawn into the soil matrix by capillary forces can potentially yield significant reductions in the vertical flow velocity within the macropore. For example, consider a 1 cm diameter pore (represented as a 10 sided regular polygon) with a pressure

head of -0.4 cm as before. Using data from the transient dye test at Walkerton, a specific discharge (or Darcy velocity) of 2 x 10^{-6} m/s through the macropore wall is capable of reducing the vertical flow velocity from the predicted value of 900 m/d at the source to the measured value of 46 m/d based on the time for dye breakthrough. Reasonable values for soil hydraulic conductivity (*e.g.*, 10^{-5}-10^{-6} m/s) and lateral hydraulic gradient (*e.g.*, 10^{-1}-10^{-2}) could easily give the required specific discharge through the macropore wall. Under these conditions, the volumetric flow rate at the source is 0.23 cm^3/min, of which 95% is imbibed into the soil matrix. Because of its near circular shape, water saturation is less than 1% within the macropore, but the capillary-held water covers 38% of the macropore wall area. These calculations represent only the capillary contributions to liquid retention and do not consider the adsorptive component, which is considered negligible at the pressure potentials under consideration (i.e., near saturation). Macropore-matrix interaction may also serve to limit the supply of water into the upper portions of the macropore. Where macropores are not connected to surface, the lower permeability soil matrix restricts the flow of water into the macropore, thereby further reducing the potential for large flow velocities. Various coatings on the macropore walls may inhibit or enhance these transfer processes to one degree or another, but the proposed mechanisms remain the same.

The concentration of flow along angular notches predicted by the model may also explain why many of the dye halos surrounding macropores were not centered directly on the macropores (see for example Figure 4.1b). A natural worm or root hole is expected to have a slightly irregular cross-section, including small notches or other features, that could potentially channel much of the flow along one side of the macropore. This would result in preferential infiltration through one portion of the macropore wall, giving rise to the eccentric halos of dye that were observed.

The flow velocities measured in this study are similar to the mean maximum transport rate of 13 m/d reported by Nimmo [2007] for a large number of field studies of preferential flow and transport in unsaturated porous media. Nimmo argues that the maximum flow velocity for preferential flow in unsaturated materials falls within a narrow range because it is constrained by various physical mechanisms, similar to the concept of a terminal velocity for an object in a fluid. The fact that unsaturated flow in macropores is not geometrically bounded by solid surfaces or capillary interfaces is put forward by Nimmo as a major factor. This is supported by the findings of the current study. The role of liquid configuration appeared to play a significant role in regulating preferential flow along macropores. In addition, the results presented herein would indicate that macropore-matrix interaction is another potentially important self-regulating mechanism for vertical flow and transport rates.

The results presented here bring into question the usefulness of using TI data to estimate unsaturated hydraulic conductivity or effective macroporosity. The measured infiltration rates at different tensions are typically used to estimate the unsaturated hydraulic conductivity relation $K(\psi)$, particularly near saturation [*Ankeny et al.*, 1991; *Reynolds and Elrick*, 1991; *Angulo-Jaramillo et al.*, 2000; *Vandervaere et al.*, 2000]. The problem with these estimates is that preferential flow along macropores invalidates the assumption of uniform flow on which the solutions are based. This can lead to erroneous predictions because results are based on a single-domain analysis of a system with multiple domains. Lin and McInnes [1995] have shown that the estimation and application of a single hydraulic conductivity function to predict infiltration into macroporous soil is tenuous at best. Likewise, methods for estimating macroporosity are also based on erroneous assumptions. It is generally assumed that at a given pressure head, pores larger than a certain size (calculated from Equation 14) are empty and do not contribute to the water flux [*Watson and Luxmoore*, 1986; *Bodhinayake et al.*, 2004]. The estimates of macroporosity do not consider flow in partially saturated macropores, which can contribute significantly to the total flow. Estimates of macroporosity based on flow in completely filled macropores are likely to underestimate the true effective macroporosity. In addition to variable flow geometry, flow within the macropores near saturation is potentially non-Darcian (*e.g.*, drops, rivulets). This would further limit the application of analytical expressions for estimating $K(\psi)$ or macroporosity based on tension infiltration data.

4.4 Summary and Conclusions

Analyses of dye patterns from tension infiltration tests using equal infiltration volumes illustrated a clear relationship between the vertical extent of dye staining and the applied pressure head. Larger (but always negative) infiltration pressures gave rise to increased infiltration rates, greater variability in soil water content measurements in both time and space, and increased depths of dye penetration, all of which were attributed to preferential flow along macropores. The main preferential pathways were earthworm burrows, with root holes and fractures also contributing to flow. Preferential flow in macropores was limited to infiltration with applied pressure heads greater than -3 cm. Undoubtedly, near-zero soil water potentials were needed to initiate macropore flow, but the results suggest that surface ponding or saturation of the soil matrix are not necessarily required. There was considerable evidence for partially saturated flow in the macropores under these small negative pressures. Traditional capillary theory can still be applied and a conceptual model for flow along the walls and corners of rough macropores is proposed. Slower flow in thin films and corners, as opposed to full macropores, consequently has implications for vertical transport velocities, colloid retention along macropore walls (i.e., attachment, film straining [*Wan and Tokunaga*, 1997]), and macropore-matrix interaction.

Macropore-matrix interaction was a very important process throughout the experiments. Imbibition of dye from the macropores into the matrix was noticed during a transient infiltration test on an exposed soil face, and dye stained halos around wormholes were repeatedly seen on the excavated soil sections. Mass transfer of water through the macropore walls significantly retarded the downward movement of water in the macropores. It is also believed that flow from the matrix into the macropores near the soil surface contributed to preferential flow. Drier soil enhanced the degree of lateral infiltration into the soil matrix near surface, but did not appear to affect the overall depth of dye staining. These findings point to the soil matrix as a significant factor in controlling the initiation and extent of flow in macropores. This view is supported by earlier modeling studies (see Chapters 2 and 3), but requires additional field studies on a wider range of soil types for confirmation. Given the importance and complexity of the exchange process, further research in this area is sorely needed.

The infiltration potential of macroporous soils is very high. Dye penetrated to depths between 0.7 and 1.0 m at the highest supply pressures. Based on direct observations of infiltration processes during the transient dye test, it is believed the maximum depths of dye staining were achieved during or very shortly after the infiltration period. This would imply peak vertical transport rates on the order of tens of meters per day, which in turn has implications for the fate of chemicals or microorganisms in the vadose zone. On the other hand, only a fraction of the visible macropores contributed to flow at these depths. At first glance, this might suggest that mass fluxes of water or contaminants would be limited. However, the cumulative impact of transport in macropores at the field scale is potentially very large, and has the capacity to continue increasing with increased water inputs at surface.

Based on the observed flow structure and mechanisms, the use of TI data for estimating unsaturated hydraulic conductivity and macroporosity is difficult to justify. At sufficiently large scales, where a representative elementary volume encompassing numerous macropores can be defined, estimating a single hydraulic conductivity-pressure potential relationship may be valid. Unfortunately, this condition is not likely to be met for most TI applications in macroporous soils. Improvements in estimating macroporosity and flow rates may come from including irregular macropore geometries into conceptual models of unsaturated flow. Physically-based models, such as that developed by Tuller and Or [2002], show promise for improving flow and transport predictions. This study provided a detailed picture of infiltration rates, macropore geometry, and flow patterns. The experimental data set can be used in the future to evaluate conceptual and numerical models of macropore flow that include realistic descriptions of flow in partially saturated pores.

The TI performed extremely well as a tool for controlling macropore flow in situ and, together with the dye tracer, permitted detailed examination of small-scale flow processes. The question can

be asked whether the subsurface flow system that develops beneath a TI mimics the conditions that would occur during a natural infiltration event. Certainly the surface boundary conditions imposed by the TI are different than natural rainfall on the soil surface, but it remains to be seen how this influences the flow pathways that develop. This will be addressed further in Chapter 5.

4.5 References

Allaire-Leung, S.E., S.C. Gupta, and J.F. Moncrief (2000), Water and solute movement in soil as influenced by macropore characteristics - 1. Macropore continuity, *J. Contam. Hydrol.*, *41*(3-4), 283-301.

Angulo-Jaramillo, R., J.P. Vandervaere, S. Roulier, J.L. Thony, J.P. Gaudet, and M. Vauclin (2000), Field measurement of soil surface hydraulic properties by disc and ring infiltrometers; A review and recent developments, *Soil Till. Res.*, *55*(1-2), 1-29.

Ankeny, M.D., M. Ahmed, T.C. Kaspar, and R. Horton (1991), Simple field method for determining unsaturated hydraulic conductivity, *Soil Sci. Soc. Am. J.*, *55*(2), 467-470.

Beven, K. and P. Germann (1982), Macropores and water flow in soils, *Water Resour. Res.*, *18*(5), 1311-1325.

Blake, G.R. and K.H. Hartge (1986), Bulk density, in *Methods of soil analysis. Part 1.*, Agronomy No. 9, edited by A. Klute, pp. 363-375, American Society of Agronomy, Madison, WI.

Bodhinayake, W., B.C. Si, and C.J. Xiao (2004), New method for determining water-conducting macro- and mesoporosity from tension infiltrometer, *Soil Sci. Soc. Am. J.*, *68*(3), 760-769.

Bouma, J. and L.W. Dekker (1978), A case study on infiltration into dry clay soil; I, Morphological observations, *Geoderma*, *20*(1), 27-40.

Buttle, J.M. and D.J. McDonald (2000), Soil macroporosity and infiltration characteristics of a forest podzol, *Hydrol. Process.*, *14*(5), 831-848.

Cameira, M.R., L. Ahuja, R.M. Fernando, and L.S. Pereira (2000), Evaluating field measured soil hydraulic properties in water transport simulations using the RZWQM, *J. Hydrol.*, *236*(1-2), 78-90.

Carter, M.R. and B.C. Ball (1993), Soil porosity, in *Soil sampling and methods of analysis*, edited by M.R. Carter, pp. 581-588, Lewis Publishers, Boca Raton, FL.

Casey, F.X.M. and N.E. Derby (2002), Improved design for an automated tension infiltrometer, *Soil Sci. Soc. Am. J.*, *66*(1), 64-67.

Coles, N. and S. Trudgill (1985), The movement of nitrate fertiliser from the soil surface to drainage waters by preferential flow in weakly structured soils, Slapton, S. Devon, *Agr. Ecosyst. Environ.*, *13*(3-4), 241-259.

Dahan, O., R. Nativ, E.M. Adar, B. Berkowitz, and Z. Ronen (1999), Field observation of flow in a fracture intersecting unsaturated chalk, *Water Resour. Res.*, *35*(11), 3315-3326.

Edwards, W.M., M.J. Shipitalo, L.B. Owens, and W.A. Dick (1993), Factors affecting preferential flow of water and atrazine through earthworm burrows under continuous no-till corn, *J. Environ. Qual.*, *22*(3), 453-457.

Faeh, A.O., S. Scherrer, and F. Naef (1997), A combined field and numerical approach to investigate flow processes in natural macroporous soils under extreme precipitation, *Hydrol. Earth Syst. Sci.*, *1*(4), 787-800.

Flury, M. and H. Fluhler (1994), Brilliant Blue FCF as a dye tracer for solute transport studies - a toxicological overview, *J. Environ. Qual.*, *23*(5), 1108-1112.

Flury, M. and H. Fluhler (1995), Tracer characteristics of Brilliant Blue FCF, *Soil Sci. Soc. Am. J.*, *59*(1), 22-27.

Flury, M., H. Fluhler, W.A. Jury, and J. Leuenberger (1994), Susceptibility of soils to preferential flow of water: a field study, *Water Resour. Res.*, *30*(7), 1945-1954.

Flury, M. and N.N. Wai (2003), Dyes as tracers for vadose zone hydrology, *Rev. Geophys.*, *41*(1), 1002, doi:10.1029/2001RG000109.

Forrer, I., A. Papritz, R. Kasteel, H. Fluehler, and D. Luca (2000), Quantifying dye tracers in soil profiles by image processing, *Eur. J. Soil Sci.*, *51*(2), 313-322.

German-Heins, J. and M. Flury (2000), Sorption of Brilliant Blue FCF in soils as affected by pH and ionic strength, *Geoderma* , *97*(1-2), 87-101.

Ghodrati, M., M. Chendorain, and Y.J. Chang (1999), Characterization of macropore flow mechanisms in soil by means of a split macropore column, *Soil Sci. Soc. Am. J.*, *63*(5), 1093-1101.

Gjettermann, B., H.C.B. Hansen, H.E. Jensen, and S. Hansen (2004), Transport of phosphate through artificial macropores during film and pulse flow, *J. Environ. Qual.*, *33*(6), 2263-2271.

Haria, A.H., M.G. Hodnett, and A.C. Johnson (2003), Mechanisms of groundwater recharge and pesticide penetration to a chalk aquifer in southern England, *J. Hydrol.*, *275*(1-2), 122-137.

Heppell, C.M., F. Worrall, T.P. Burt, and R.J. Williams (2002), A classification of drainage and macropore flow in an agricultural catchment, *Hydrol. Process.*, *16*(1), 27-46.

Hinsby, K., L.D. McKay, P. Jorgensen, M. Lenczewski, and C.P. Gerba (1996), Fracture aperture measurements and migration of solutes, viruses, and immiscible creosote in a column of clay-rich till, *Ground Water*, *34*(6), 1065-1075.

Hoffman, D.W., B.C. Matthews, and R.E. Wicklund (1963), Soil survey of Wellington County, Ontario, Report No. 35 of the Ontario Soil Survey, Canada Department of Agriculture and the Ontario Agricultural College, Guelph, Ontario.

Hoffman, D.W. and N.R. Richards (1954), Soil survey of Bruce County, Ontario, Report No. 16 of the Ontario Soil Survey, Canada Department of Agriculture and the Ontario Agricultural College, Guelph, Ontario.

Jarvis, N.J., P.B. Leeds-Harrison, and J.M. Dosser (1987), The use of tension infiltrometers to assess routes and rates of infiltration in a clay soil, *J. Soil Sci.*, *38*(4), 633-640.

Jensen, M.B., H.C.B. Hansen, and J. Magid (2002), Phosphate sorption to macropore wall materials and bulk soil, *Water Air Soil Pollut.*, *137*(1-4), 141-148.

Jorgensen, P.R., M. Hoffmann, J.P. Kistrup, C. Bryde, R. Bossi, and K.G. Villholth (2002), Preferential flow and pesticide transport in a clay-rich till: Field, laboratory, and modeling analysis, *Water Resour. Res.*, *38*(11), 1246, doi:10.1029/2001WR000494.

Katterer, T., B. Schmied, K.C. Abbaspour, and R. Schulin (2001), Single- and dual-porosity modelling of multiple tracer transport through soil columns: effects of initial moisture and mode of application, *Eur. J. Soil Sci.*, *52*(1), 25-36.

Kulli, B., C. Stamm, A. Papritz, and H. Fluehler (2003), Discrimination of flow regions on the basis of stained infiltration patterns in soil profiles, *Vadose Zone J.*, *2*(3), 338-348.

Kung, K.-J.S., E.J. Kladivko, T.J. Gish, T.S. Steenhuis, G. Bubenzer, and C.S. Helling (2000), Quantifying preferential flow by breakthrough of sequentially applied tracers: silt loam soil, *Soil Sci. Soc. Am. J.*, *64*(4), 1296-1304.

Kung, K.J.S., E.J. Kladivko, C.S. Helling, T.J. Gish, T.S. Steenhuis, and D.B. Jaynes (2006), Quantifying the pore size spectrum of macropore-type preferential pathways under transient flow, *Vadose Zone J.*, *5*(3), 978-989.

Leonard, J., E. Perrier, and G. de Marsily (2001), A model for simulating the influence of a spatial distribution of large circular macropores on surface runoff, *Water Resour. Res.*, *37*(12), 3217-3225.

Lin, H.S. and K.J. McInnes (1995), Water flow in clay soil beneath a tension infiltrometer, *Soil Sci.*, *159*(6), 375-382.

Logsdon, S.D. (1995), Flow mechanisms through continuous and buried macropores, *Soil Sci.*, *160*(4), 237-242.

McKay, L.D., J.A. Cherry, and R.W. Gillham (1993), Field experiments in a fractured clay till: 1. Hydraulic conductivity and fracture aperture, *Water Resour. Res.*, *29*(4), 1149-1162.

Mualem, Y. (1976), A new model for predicting the hydraulic conductivity of unsaturated soils, *Water Resour. Res.*, *12*(3), 513-522.

Nimmo, J.R. (2007), Simple predictions of maximum transport rate in unsaturated soil and rock, *Water Resour. Res.*, *43*(5), W05426, doi:10.1029/2006WR005372.

Nobles, M.M., L.P. Wilding, and K.J. McInnes (2004), Pathways of dye tracer movement through structured soils on a macroscopic scale, *Soil Sci.*, *169*(4), 229-242.

Or, D. and M. Tuller (2000), Flow in unsaturated fractured porous media: hydraulic conductivity of rough surfaces, *Water Resour. Res.*, *36*(5), 1165-1177.

Perillo, C.A., S.C. Gupta, E.A. Nater, and J.F. Moncrief (1999), Prevalence and initiation of preferential flow paths in a sandy loam with argillic horizon, *Geoderma*, *89*(3-4), 307-331.

Perroux, K.M. and I. White (1988), Designs for disc permeameters, *Soil Sci. Soc. Am. J.*, *52*(5), 1205-1215.

Podgorney, R.K., T.R. Wood, B. Faybishenko, and T.M. Stoops (2000), Spatial and temporal instabilities in water flow through variably saturated fractured basalt on a one-meter scale, in *Dynamics of Fluids in Fractured Rock*, Geophysical Monograph 122, edited by B. Faybishenko,

P.A. Witherspoon, and S.M. Benson, pp. 129-146, American Geophysical Union, Washington, D.C., USA.

Reynolds, W.D. (1993), Saturated hydraulic conductivity: laboratory measurement, in *Soil sampling and methods of analysis*, edited by M.R. Carter, pp. 589-597, Lewis Publishers, Boca Raton, FL.

Reynolds, W.D. and D.E. Elrick (1991), Determination of hydraulic conductivity using a tension infiltrometer, *Soil Sci. Soc. Am. J.*, *55*(3), 633-639.

Reynolds, W.D. and W.D. Zebchuk (1996), Use of contact material in tension infiltrometer measurements, *Soil Technol.*, *9*(3), 141-159.

Scanlon, B.R. and R.S. Goldsmith (1997), Field study of spatial variability in unsaturated flow beneath and adjacent to playas, *Water Resour. Res.*, *33*(10), 2239-2252.

Schrader, S., H. Rogasik, I. Onasch, and D. Jegou (2007), Assessment of soil structural differentiation around earthworm burrows by means of X-ray computed tomography and scanning electron microscopy, *Geoderma*, *137*(3-4), 378-387.

Sheldrick, B.H. and C. Wang (1993), Particle size distribution, in *Soil sampling and methods of analysis*, edited by M.R. Carter, pp. 499-511, Lewis Publishers, Boca Raton, FL.

Shipitalo, M.J. and W.M. Edwards (1996), Effects of initial water content on macropore/matrix flow and transport of surface-applied chemicals, *J. Environ. Qual.*, *25*(4), 662-670.

Shipitalo, M.J., W.M. Edwards, W.A. Dick, and L.B. Owens (1990), Initial storm effects on macropore transport of surface-applied chemicals in no-till soil, *Soil Sci. Soc. Am. J.*, *54*(6), 1530-1536.

Shipitalo, M.J. and F. Gibbs (2000), Potential of earthworm burrows to transmit injected animal wastes to tile drains, *Soil Sci. Soc. Am. J.*, *64*(6), 2103-2109.

Stehouwer, R.C., W.A. Dick, and S.J. Traina (1994), Sorption and retention of herbicides in vertically oriented earthworm and artificial burrows, *J. Environ. Qual.*, *23*(2), 286-292.

Tallon, L.K., B.C. Si, D. Korber, and X. Guo (2007), Soil wetting state and preferential transport of Escherichia coli in clay soils, *Can. J. Soil Sci.*, *87*(1), 61-72.

Tofteng, C., S. Hansen, and H.E. Jensen (2002), Film and pulse flow in artificial macropores, *Nord. Hydrol.*, *33*(4), 263-274.

Tokunaga, T.K. and J. Wan (1997), Water film flow along fracture surfaces of porous rock, *Water Resour. Res.*, *33*(6), 1287-1295.

Topp, G.C., Y.T. Galganov, B.C. Ball, and M.R. Carter (1993), Soil water desorption curves, in *Soil sampling and methods of analysis*, edited by M.R. Carter, pp. 569-579, Lewis Publishers, Boca Raton, FL.

Trojan, M.D. and D.R. Linden (1992), Microrelief and rainfall effects on water and solute movement in earthworm burrows, *Soil Sci. Soc. Am. J.*, *56*(3), 727-733.

Tuller, M. and D. Or (2001), Hydraulic conductivity of variably saturated porous media: Film and corner flow in angular pore space, *Water Resour. Res.*, *37*(5), 1257-1276.

Tuller, M., D. Or, and L.M. Dudley (1999), Adsorption and capillary condensation in porous media: Liquid retention and interfacial configurations in angular pores, *Water Resour. Res.*, *35*(7), 1949-1964.

Tuller, M. and D. Or (2002), Unsaturated hydraulic conductivity of structured porous media: a review of liquid configuration-based models, *Vadose Zone J.*, *1*, 14-37.

Unc, A. and M.J. Goss (2003), Movement of faecal bacteria through the vadose zone, *Water Air Soil Pollut.*, *149*(1-4), 327-337.

van Genuchten, M.T. (1980), A closed-form equation for predicting the hydraulic conductivity of unsaturated soils, *Soil Sci. Soc. Am. J.*, *44*, 892-898.

Vandervaere, J.P., M. Vauclin, and D.E. Elrick (2000), Transient flow from tension infiltrometers; II, Four methods to determine sorptivity and conductivity, *Soil Sci. Soc. Am. J.*, *64*(4), 1272-1284.

Villholth, K.G., K.H. Jensen, and J. Fredericia (1998), Flow and transport processes in a macroporous subsurface-drained glacial till soil I: Field investigations, *J. Hydrol.*, *207*(1-2), 98-120.

Wan, J. and T.K. Tokunaga (1997), Film straining of colloids in unsaturated porous media: Conceptual model and experimental testing, *Environ. Sci. Technol.*, *31*(8), 2413-2420.

Wang, D., J.M. Norman, B. Lowery, and K. McSweeney (1994), Nondestructive determination of hydrogeometrical characteristics of soil macropores, *Soil Sci. Soc. Am. J.*, *58*, 294-303.

Watson, K.W. and R.J. Luxmoore (1986), Estimating macroporosity in a forest watershed by use of a tension infiltrometer, *Soil Sci. Soc. Am. J.*, *50*(3), 578-582.

Weiler, M. and F. Naef (2003a), Simulating surface and subsurface initiation of macropore flow, *J. Hydrol.*, *273*(1-4), 139-154.

Weiler, M. and H. Fluhler (2004), Inferring flow types from dye patterns in macroporous soils, *Geoderma*, *120*(1-2), 137-153.

Weiler, M. and F. Naef (2003b), An experimental tracer study of the role of macropores in infiltration in grassland soils, *Hydrol. Process.*, *17*(2), 477-493.

4.6 Figures and Tables

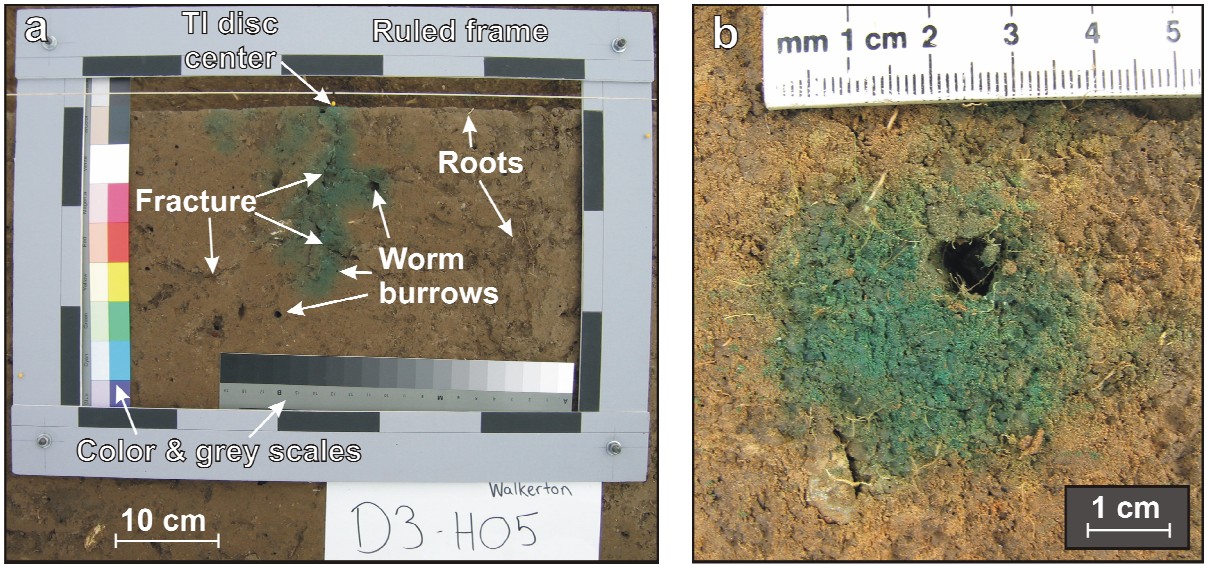

Figure 4.1. Photographs of (a) a typical excavated horizontal soil section and (b) a large earthworm burrow and associated dye stained halo on a horizontal section at 20 cm depth from test EL-D2. Various macropore features are highlighted in the horizontal section in (a) along with the frame and scales used to perform image correction. Also, note the eccentricity of the dye stained halo in (b).

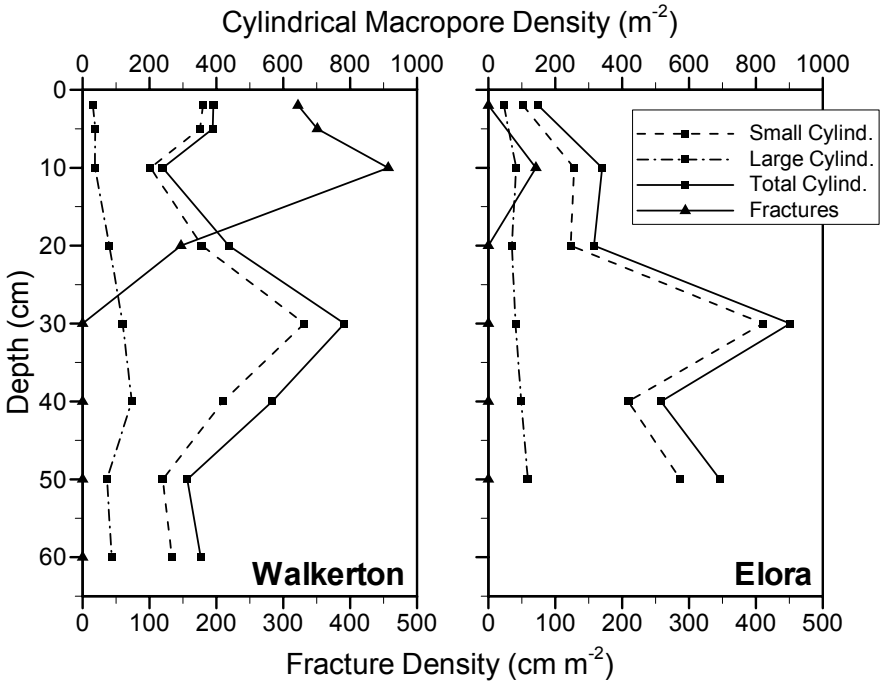

Figure 4.2. Plot of macropore density versus depth. The square (■) symbols represent linear cylindrical macropores and the triangle (▲) symbols represent planar fractures. The cylindrical macropores are subdivided further into small (dash-dot line), large (dashed line), and total (solid line) macropore numbers. Small macropores are assigned as those with diameters less than 5 mm, while large macropore diameters have diameters equal to or greater than 5 mm.

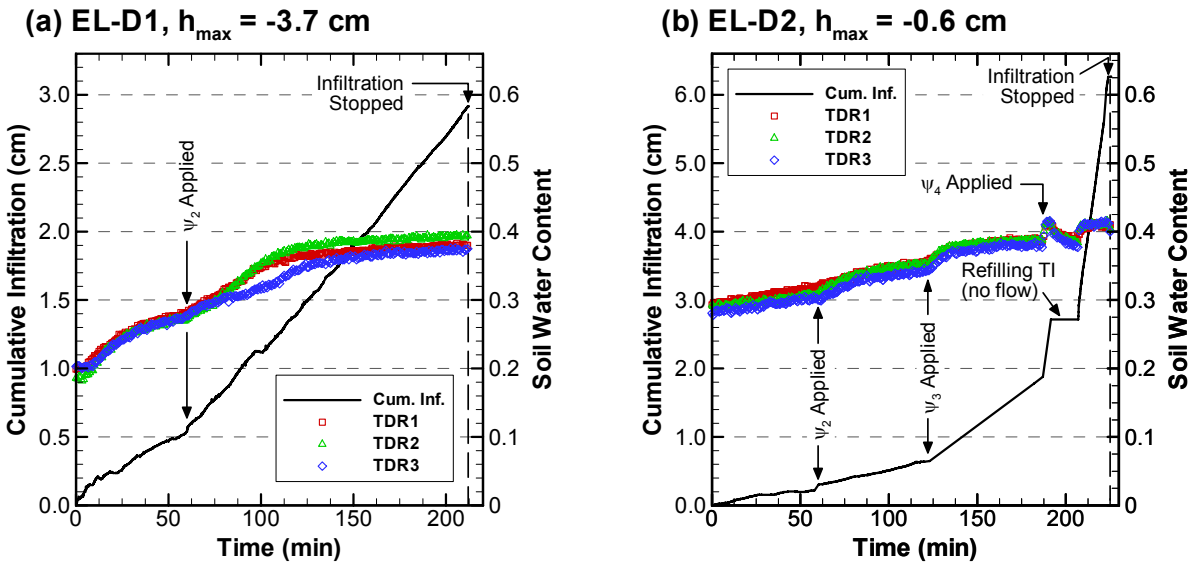

Figure 4.3. Measured infiltration volume (solid line) and soil water content along the three TDR probes (symbols) for the infiltration tests at Elora. The times when the applied tensions were changed and infiltration was stopped are indicated with arrows.

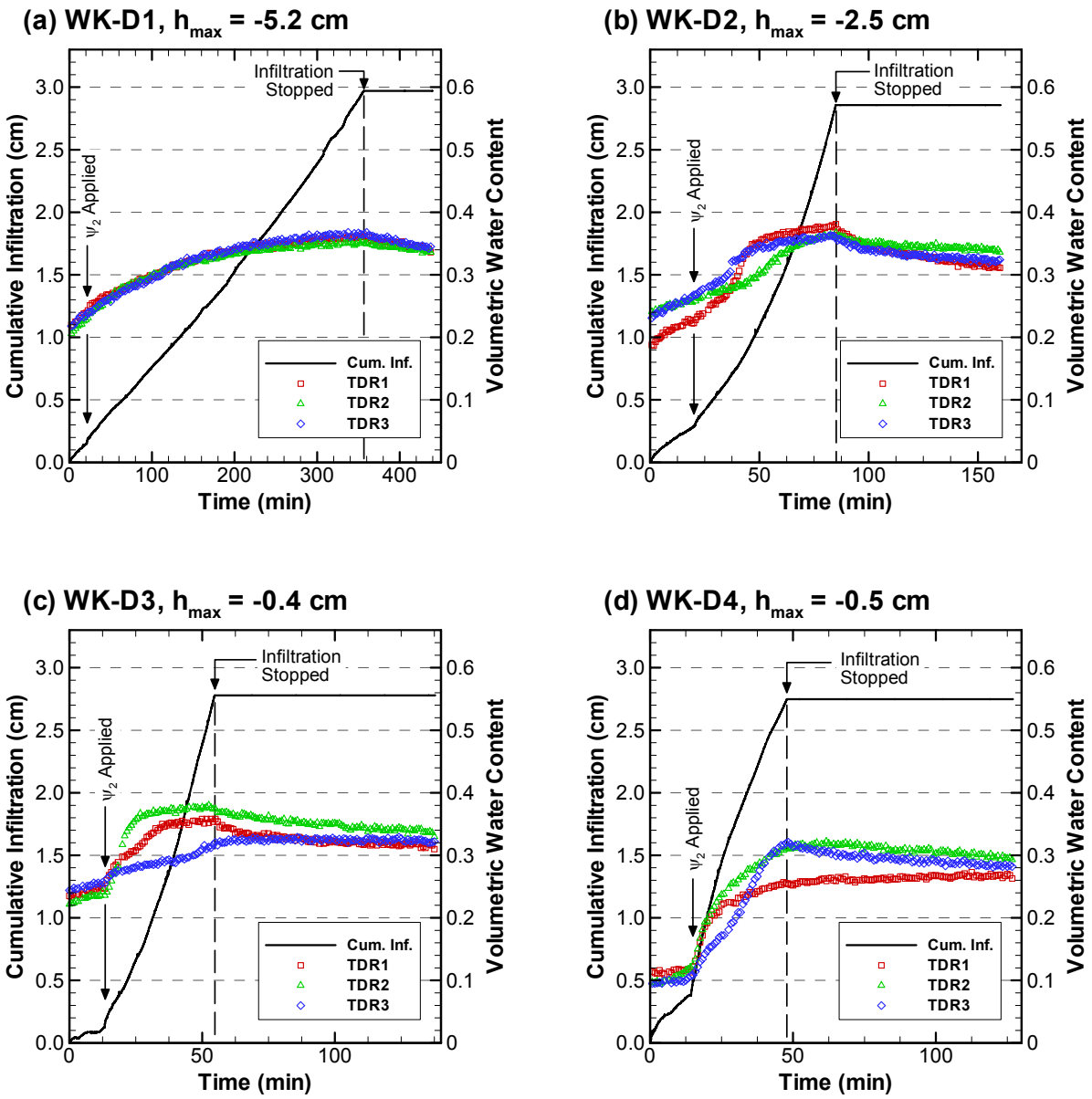

Figure 4.4. Measured infiltration volume (solid line) and soil water content along the three TDR probes (symbols) for the infiltration tests at Walkerton. The times when the applied tensions were changed and infiltration was stopped are indicated with arrows.

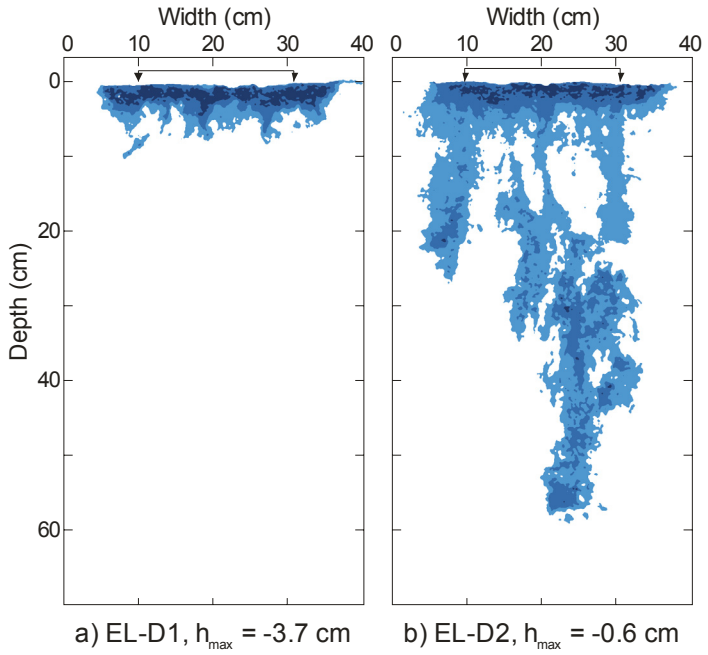

Figure 4.5. Classified dye patterns for vertical soil sections from the Elora site. All soil sections were located along the centreline of the tension infiltrometer disc, with the location of the disc indicated on the soil surface.

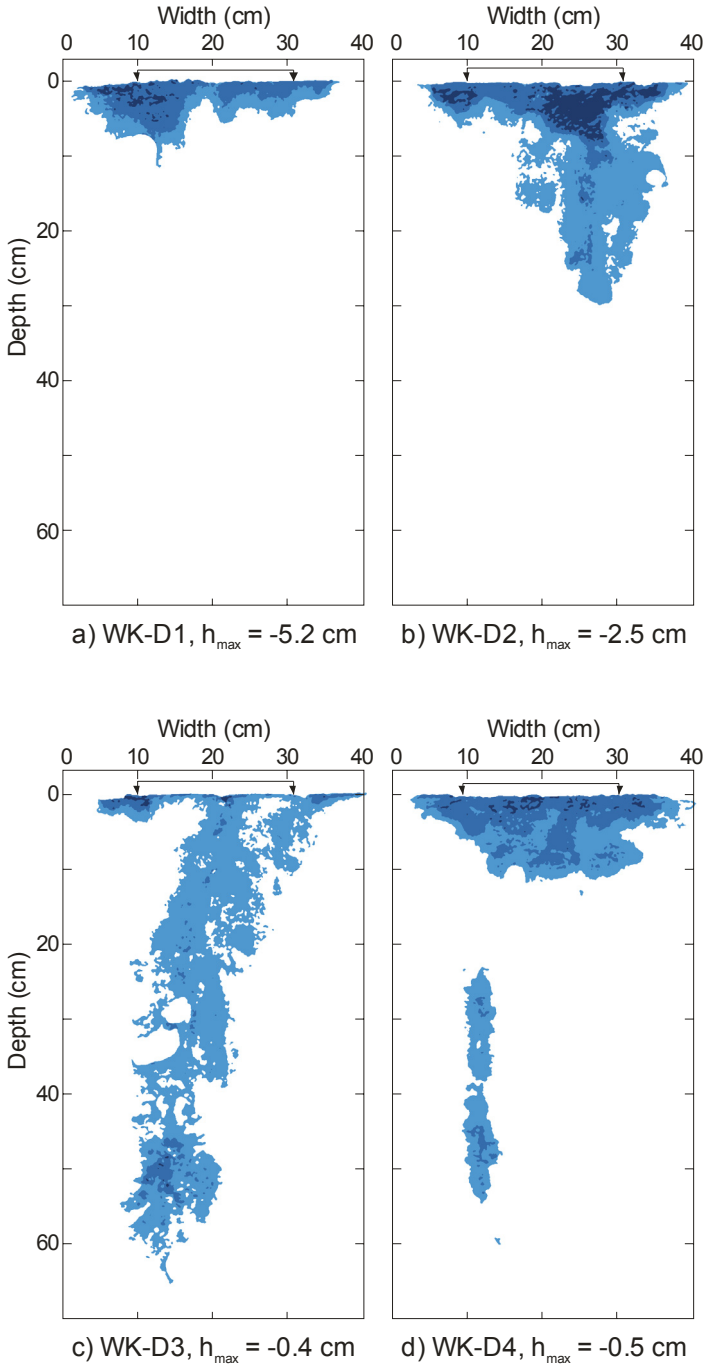

Figure 4.6. Classified dye patterns for vertical soil sections from the Walkerton site. All soil sections were located along the centreline of the tension infiltrometer disc, with the location of the disc indicated on the soil surface.

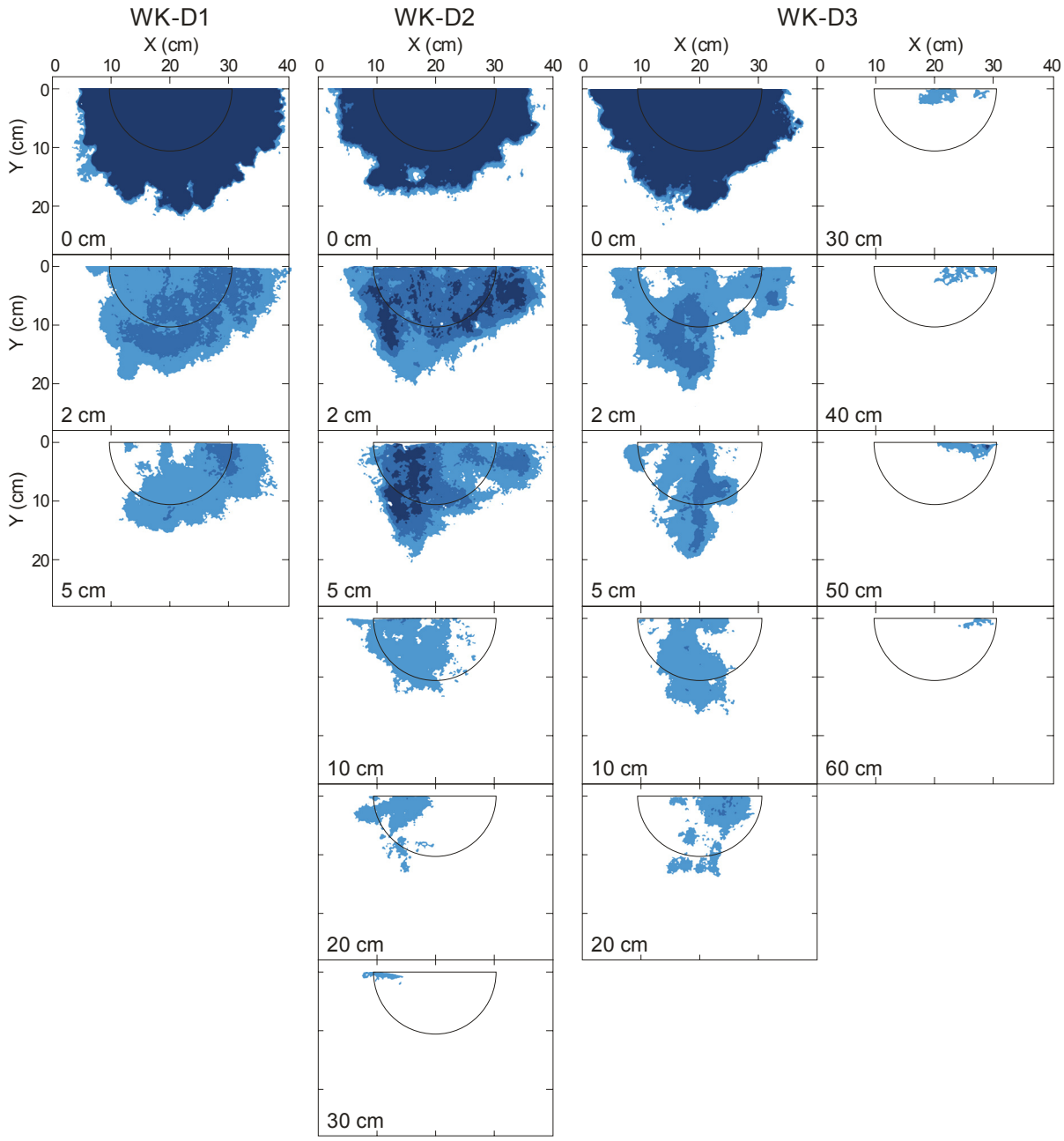

Figure 4.7. Classified dye patterns for horizontal soil sections for tests (a) WK-D1, (b) WK-D2, and (c) WK-D3. The infiltration area is indicated by the semi-circle and the depth is given in the lower left hand corner of each section.

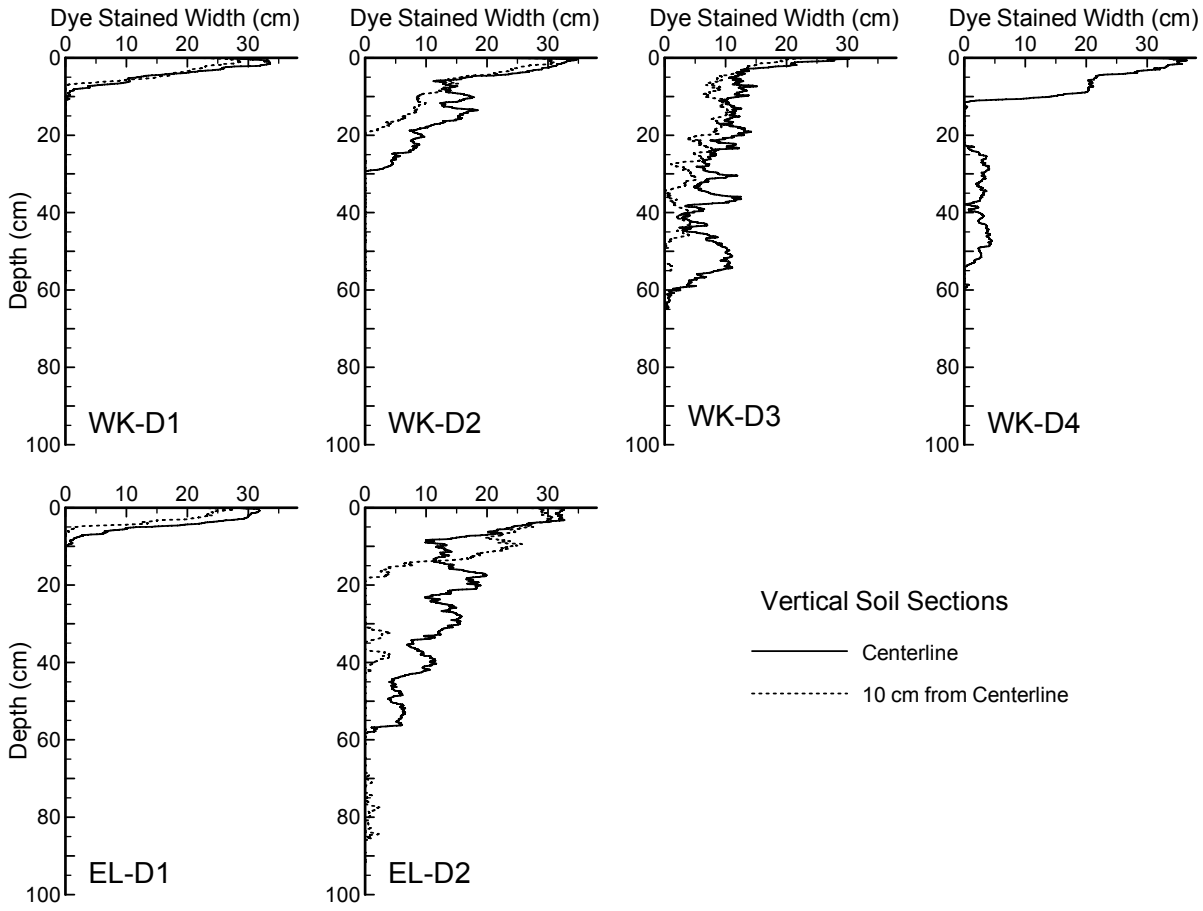

Figure 4.8. Width of dye stained soil versus depth for all vertical soil sections from the Walkerton and Elora sites.

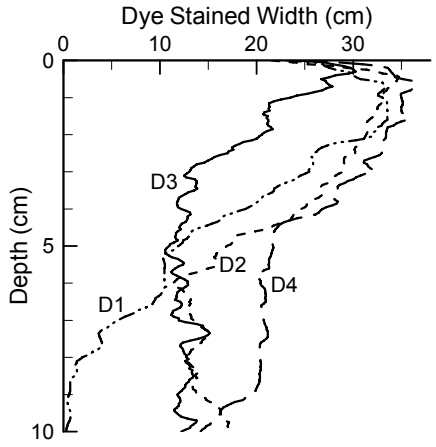

Figure 4.9. Dye stained width in the top 10 cm of the soil profile for the Walkerton infiltration tests.

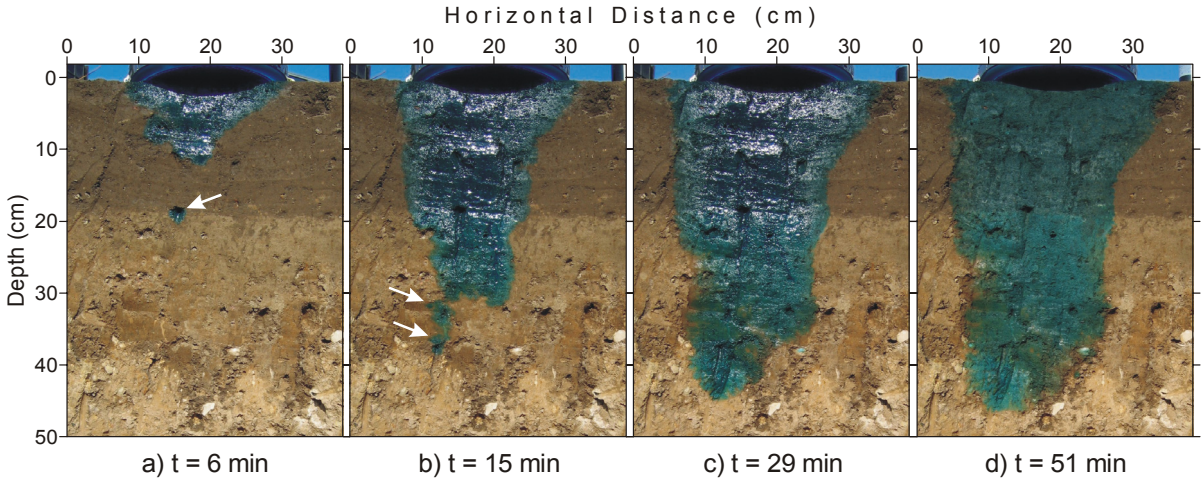

Figure 4.10. Time lapse photographs of infiltration along a vertical soil section at Walkerton. The times indicated are in minutes after the application of the -0.4 cm pressure head and represent periods (a and b) during infiltration, (c) at the end of infiltration, and (d) following redistribution. Light arrows indicate the locations of early dye solution breakthrough in worm burrows. Note the TI disc extended over the vertical soil face at the top of the photographs.

Table 4.1. Average soil properties determined from core and bulk samples collected at the infiltration sites.

Soil Horizon	Depth (cm)	Porosity ($cm^3\ cm^{-3}$)	Bulk Density ($g\ cm^{-3}$)	K_{sat} ($m\ s^{-1}$)	Clay/Silt/ Sand/Gravel (%)	VGM Parameters[b] α (1/m)	n (-)
Elora							
A	0-20	0.48	1.47	8×10^{-6}	13/64/22/1	10.3	1.20
B	20-45	0.45	1.55	2×10^{-6}	22/46/31/1	3.20	1.24
C	45-80	0.33	1.84	9×10^{-7}	21/44/29/6	17.9	1.18
Walkerton							
A	0-25	0.45	1.48	9×10^{-5}	7/46/47/0	3.81	1.19
B	25-45[a]	0.41	1.60	5×10^{-5}	16/36/48/0	15.6	1.16
C	45[a]-80	0.39	1.67	6×10^{-5}	9/44/35/12	10.7	1.15

[a]The B-C soil horizon boundary at the Walkerton site varied with location from 25-55 cm below ground surface.
[b]Parameters obtained by least squares fitting of van Genuchten-Mualem model to average soil water retention data.

Table 4.2. Macropore type and density as a function of depth.

Site	Depth	Cylindrical Macropore Density			Fracture
		Small[a]	Large[b]	Total	Trace Length
	(cm)	(m^{-2})	(m^{-2})	(m^{-2})	(cm m^{-2})
Elora	2	103	46	149	0
	10	256	83	340	71
	20	246	70	316	0
	30	821	81	902	0
	40	418	98	516	0
	50	574	118	692	0
Walkerton	2	360	31	391	322
	5	351	38	389	351
	10	203	37	240	457
	20	357	80	437	147
	30	663	120	783	0
	40	420	147	567	0
	50	240	73	313	0
	60	267	87	353	0

[a]Macropores less than 5 mm in diameter, consisting of mainly wormholes and root holes.
[b]Macropores greater than 5 mm in diameter, consisting entirely of wormholes.

Table 4.3. Infiltration characteristics and depth of dye staining for the tension infiltration tests.

Test	Pressure Head[a], ψ (cm H_20)	Time Period of Application (min)	Infiltration Rate[b] (cm^3 min^{-1})	Infiltration Rate[b] (cm hr^{-1})	Maximum Depth of Dye (cm)
EL-D1	-8.8	60	2.7	0.48	10
	-3.7	152	5.55	0.97	
EL-D2	-16.4	60	1.4	0.24	98
	-11.2	62	1.9	0.34	
	-4.8	65	6.59	1.15	
	-0.6	22	63.8	11.2	
WK-D1	-10.3	23	2.4	0.42	11
	-5.2	335	2.99	0.52	
WK-D2	-6.4	20	4.0	0.69	31
	-2.5	65	14.1 (23.1)[c]	2.47 (4.04)[c]	
WK-D3	-11.5	15	2.5	0.45	70
	-0.4	41	23.7 (29.3)[c]	4.14 (5.12)[c]	
WK-D4	-12.8	15	7.8	1.4	74
	-0.5	32.8	24.2	4.23	

[a]The pressure head, ψ, is taken at base of the tension infiltrometer disc where it touches the glass bead contact material.

[b]Represents the quasi-steady rate of infiltration based on the measured change in water level with time in the TI reservoir.

[c]Value in brackets was the maximum infiltration rate observed near the end of the infiltration period.

Chapter 5
Influence of Macroporosity on Dye and Microsphere Transport Through Partially Saturated Soils

5.1 Introduction

In agricultural areas, land application of manure or biosolids can lead to contamination of aquifers and water supply wells by solutes and microbial contaminants [*Goss et al.*, 1998; *Rudolph et al.*, 1998; *Macler and Merkle*, 2000; *Unc and Goss*, 2003]. In an extreme example, thousands of residents became ill and seven individuals died in the town of Walkerton, Ontario in May of 2000 after drinking groundwater contaminated with *Eschericia coli* O157:H7 and *Campylobacter jejuni* [*Hrudey et al.*, 2003]. The cause of the Walkerton outbreak was primarily attributed to pathogens from cattle manure reaching a shallow water supply well (Well #5 completed at 5-8 m depth) following a heavy rainfall [*Hrudey et al.*, 2003]. The microorganisms are traditionally conceptualized as individual migrating particles or colloids [*Ginn et al.*, 2002]. The processes controlling the fate and transport of these colloidal contaminants in the subsurface is poorly understood, especially under partially saturated conditions. Understanding colloid transport processes in the vadose zone is important in other areas as well, such as colloid-facilitated transport of metals, radionuclides and pesticides [*Villholth et al.*, 2000; *de Jonge et al.*, 2004]. Research on colloid transport through natural field soils is required to assess the vulnerability of groundwater resources and mitigate potential adverse effects to water quality.

Flow and transport through the vadose zone is dependent on a number of factors, including climatic conditions, vegetation, and soil properties. Under conditions of uniform plug- or piston-type flow, surficial soils can serve as an effective barrier to migration of surface applied contaminants, particularly colloids. However, there is growing evidence that preferential flow in natural soils is ubiquitous [*Coles and Trudgill*, 1985; *Flury et al.*, 1994; *Petersen et al.*, 1997; *Perillo et al.*, 1999; *Kung et al.*, 2000; *Kulli et al.*, 2003]. Under these conditions, contaminants can be rapidly transported through the soil profile, thus compromising the protective capacity of the soil. Macropores formed by weathering, vegetation and soil fauna are a common cause of preferential flow in many soils [*Beven and Germann*, 1982; *Hendrickx and Flury*, 2001]. Macroporous soils result in highly transient, irregular flow paths, as shown in Chapter 4, which make descriptions of contaminant transport difficult. McCarthy and McKay [2004] and DeNovio et al. [2004] identified preferential

flow in structured or macroporous soil as a key challenge for future colloid transport investigations in the vadose zone.

Individual processes affecting colloid transport in homogeneous saturated media (*e.g.*, ionic strength and solution chemistry, surface charge, pore size exclusion, filtration) are well documented and summarized in reviews by Ryan and Elimelech [1996], Ginn et al. [2002], and Sen and Khilar [2006]. Recently, there have been an increasing number of studies dealing with colloid transport in partially saturated porous media. A variety of laboratory experiments using micromodels or columns packed with homogeneous media (*e.g.*, glass beads or sand) have provided insights into pore-scale transport and retention mechanisms that are specific to partially saturated media. In particular, film straining and colloid attachment to air-water (AW) or air-water-solid (AWS) interfaces have been recognized as key retention mechanisms [*Wan and Wilson*, 1994a; *Wan and Wilson*, 1994b; *Wan and Tokunaga*, 1997; *Zevi et al.*, 2005; *Steenhuis et al.*, 2006]. Colloid behaviour becomes even more complex in natural soils due to soil structure and transient flow conditions [*DeNovio et al.*, 2004]. While studies of natural soils have generally been limited to colloid breakthrough experiments on undisturbed soil columns, they consistently demonstrate that preferential flow along macropores is a significant factor in colloid transport [*van Elsas et al.*, 1991; *Jacobsen et al.*, 1997; *McMurry et al.*, 1998; *Laegdsmand et al.*, 1999; *Passmore*, 2005; *Poulsen et al.*, 2006; *Karathanasis and Johnson*, 2006]. There is a need for field-based studies to improve our understanding of the role that macropores play in transporting colloids in the vadose zone.

To examine the influence of macropores on colloid transport under partially saturated conditions, a series of controlled infiltration experiments were conducted at two field sites in southern Ontario. The two field sites, one a conservation-tilled soybean field near Walkerton, Ontario and the other a grassland site on an agricultural research farm near Elora, Ontario, had similar soil characteristics. Microsphere tracers, along with a soluble dye, were applied to the soil using a tension infiltrometer (TI), which provided a means of controlling the degree of macropore flow. A simulated rainfall test using the same tracers was conducted at the Walkerton site for comparison. The primary goal of this study was to investigate the depth of migration and principal transport pathways of chemical and colloid tracers following infiltration events in macroporous soils. The infiltration conditions (pressure head or water content) under which preferential flow becomes important for vertical contaminant movement are demonstrated. Detailed tracer distribution data are evaluated to determine whether there are significant differences between the transport of dye versus microspheres, and to assess the role that macropore-matrix interaction plays in transport processes (particularly for microspheres). In addition, the simulated rainfall results are compared to the TI method to assess whether the TI can realistically represent solute and colloid transport that would occur under natural infiltration

conditions. The results are discussed in terms of their potential implications for shallow groundwater quality.

5.2 Methods

5.2.1 Description of Field Sites

This study was conducted at two field sites in southern Ontario, Canada. An initial series of tension infiltration tests were conducted in the fall of 2005 at the Elora Research Station (latitude 43° 38′ 25" N, longitude 80° 24′ 34" W), located approximately 20 km northwest of Guelph, Ontario. The tests were conducted on turfgrass plots that were mowed regularly during the growing season. The soil is described as slightly stony, imperfectly drained Guelph silt loam [*Hoffman et al.*, 1963] that overlies approximately 20 to 22 m of Port Stanley Till. The water table was approximately 1.4 m deep at the time of the experiments.

The majority of the experiments were conducted at a second site located on a small farm near the western edge of Walkerton, Ontario (latitude 44° 07′ 01" N, longitude 81° 9′ 50" W). The site was selected for two reasons; (1) it had similar soil properties to the Elora site, which are considered typical of those commonly encountered in southern Ontario, and (2) the site had a shallow water table and relatively thin overburden materials overlying a bedrock aquifer. Furthermore, the field under investigation was suspected to be a potential source of the bacteria that eventually contaminated Walkerton's Well #5, located immediately adjacent to the property. The infiltration tests were conducted on a conservation tilled field that is cropped in a corn-soybean rotation and was planted with soybeans at the time of the study. The soil is described as imperfectly drained Listowel loam [*Hoffman and Richards*, 1954] that is derived from Elma Till parent material. Bedrock of the Upper Silurian Bass Island Formation was encountered at depths between 2.7 and 4.8 m across the site, and was typically about 3.0 m deep near the infiltration test sites. The fractured dolomite of the Bass Island Formation forms a regional aquifer in which Well #5 was completed (Well #5 since decommissioned). The water table at Walkerton was 1.1 m below surface in spring and gradually decreased to a maximum depth of 1.5 m over the growing season.

5.2.2 Tension Infiltration Experiments

A tension infiltrometer (TI) was used at both sites to infiltrate water under negative pressures, thereby limiting or promoting flow in the macropores depending on the applied pressure head (see Chapter 4). The maximum pressure applied to the TI disc was varied in each test in an effort to control the extent of macropore flow and transport. At the Elora site, two TI tests were conducted (designated EL-D1 and EL-D2) using maximum pressure heads of -3.7 and -0.6 cm, respectively. A

total of four TI tests were conducted at Walkerton. Initially, three tests (designated WK-D1, WK-D2, and WK-D3) were conducted with maximum infiltration pressure heads of -5.2, -2.5, and -0.4 cm, respectively. A fourth test (designated WK-D4), with a maximum supply pressure similar to test WK-D3, was conducted approximately one month later to coincide with the simulated rainfall experiment described in the next section. The intent of test WK-D4 was to provide a reference for comparison of subsurface flow conditions between TI and simulated rainfall tests using similar infiltration rates. The near surface soils were drier at the time of test WK-D4 as a result of increased crop growth and evapotranspiration between the two test periods.

The methodology for the TI tests is discussed briefly here. Readers are referred to Chapter 4 for more details. Prior to the tests, each infiltration surface was prepared by removing surface vegetation (*e.g.*, grass, soybeans) and a thin layer (approximately 0-2 cm) of soil to obtain a level surface. Care was taken to prevent alteration of the soil structure. A layer of uniform glass beads (Spheriglass No. 2024) 209 mm in diameter and 3 mm thick was applied on the soil surface to improve hydraulic contact with the infiltrometer disc [*Perroux and White*, 1988]. Three time domain reflectometry (TDR) probes were installed at equal distances around the perimeter of the disc to monitor transient soil moisture content beneath the infiltrometer. The 10 cm long TDR probes were installed into the soil at a 45° angle (from horizontal) and pointed toward the centre of the infiltration area. Infiltration rate and volumetric soil water content were automatically recorded at regular intervals using a datalogger (Campbell Scientific CR10X).

Both solute and colloid tracers were used in this study. A dye solution consisting of Brilliant Blue FCF (C.I. Acid Blue 9, 42090; 4.0 g L^{-1}) was applied through the TI. Microspheres (Bangs Laboratories, Inc., Fishers, Indiana) were used to monitor colloid transport. Microspheres can serve as a reasonable surrogate for bacterial transport [*Hinsby et al.*, 1996; *Becker et al.*, 2004] and have many advantages as a field tracer. Microspheres come in a variety of sizes, have known surface characteristics, can be readily counted by fluorescent microscopy, do not grow or die in the subsurface, and the application rates can be easily controlled. Fluorescent polystyrene microspheres suspended in solution were applied directly to the soil surface. Microspheres with diameters of 3.7 μm (480 nm wavelength excitation maximum, 520 nm emission maximum) and 0.53 μm (360 nm wavelength excitation maximum, 420 nm emission maximum) were applied at densities of 2.6×10^5 spheres cm^{-2} and 3.5×10^7 spheres cm^{-2}, respectively. The 3.7 and 0.53 μm sizes will hereafter be referred to as the large and small microspheres, respectively, when discussing the TI tests. The microsphere sizes were selected because they encompass the size range of bacterial pathogens in manure or biosolids, and the amounts approximate the application intensities of bacteria found in these materials [*Passmore*, 2005]. Microspheres were applied in all cases except for test WK-D4.

All TI tests were conducted using two successively increasing pressure heads, with the exception of EL-D2 where four supply pressures were used to aid in evaluating flow rates over a range of tensions. The goal was to infiltrate the same volume of dye solution in each test (approximately 1.0 L), with the bulk of the solution applied at the maximum pressure head. As a result of an equipment malfunction, the infiltration period for test EL-D2 was extended and about 2.0 L of dye solution was applied. Characteristics for each of the TI tests are provided in Table 5.1.

5.2.3 Simulated Rainfall Experiment

As noted above, the TI has the ability to control the infiltration pressure at the soil surface, thus providing a simple and valuable tool for investigating macropore flow and transport processes. However, the TI can only test a relatively small volume of soil and it is not clear whether the infiltration conditions beneath the TI can be considered representative of the infiltration conditions that occur during rainfall. Therefore, a simulated rainfall experiment (designated WK-RS1) was conducted on a small plot at Walkerton for comparison with the TI tests.

The rainfall simulator was constructed with four nozzles mounted onto a frame and calibrated for the appropriate height, spray overlap, areal coverage, and irrigation rate. The rainfall apparatus was capable of evenly sprinkling the dye solution over a 1.3 x 1.3 m plot. A level plot for test WK-RS1 was selected adjacent to the location of the TI tests. Prior to the test, eight TDR probes were installed below the plot at 10, 25, and 42 cm depths. The 30 cm long TDR probes were inserted horizontally from a shallow trench excavated next to the plot. Changes in soil water content were recorded automatically prior to and during the experiment. In order to be consistent with the TI tests and remove infiltration variability associated with surface vegetation, the soybean crop was cut off just above the ground surface prior to sprinkling. Again, Brilliant Blue dye and fluorescent microspheres were used as tracers. Two sizes of fluorescent microspheres, with diameters of 3.7 μm (480 nm wavelength excitation maximum, 520 nm emission maximum) and 1.5 μm (425 nm wavelength excitation maximum, 480 nm emission maximum), were applied to a 1.2 x 0.4 m wide strip of soil along the center of the plot at a density of 1.1×10^5 spheres cm^{-2}. Brilliant Blue dye was added to the infiltration water at a concentration of 4.0 g/L. The plot was irrigated at a rate of 38 mm/hr for a period of 57 minutes. This application rate was similar to the infiltration rate measured in TI tests WK-D3 (conducted one month earlier) and WK-D4 (conducted the same day), and represents a storm with a return period of approximately 7 to 8 years for the area. During rainfall, the plot area was covered with a temporary greenhouse to prevent spray drift and reduce evaporation. A separate plastic sheet surrounded the rainfall simulator to control and collect the spray along the boundaries of the plot. The excess spray was collected in eaves that were periodically emptied and the collection volume recorded throughout the course of the experiment. Small areas of localized ponding occurred,

but no runoff from the plot was observed during the test. As with all of the TI tests, the infiltration plot and surrounding area were covered to protect from rain following the application of the tracers.

5.2.4 Excavation and Sampling of Soil Sections

All infiltration test sites were excavated to examine and photograph dye-stained flow patterns, map soil features, and collect samples for microsphere enumeration. Where the tension infiltrometer was used, parallel vertical slices were first excavated under one half of the disc along the centerline and 10 cm away from the centerline. Beneath the other half of the infiltration area, horizontal soil sections were prepared at 2, 5, and 10 cm below ground surface and every 10 cm thereafter until the dye was no longer visible. For the rainfall simulation plot, one vertical slice was cut down the center of the plot where the microspheres had been applied. Three horizontal sections were excavated in the remaining half of the plot at 5, 20, and 42 cm below ground surface. All soil sections were carefully cut using hand tools in order to reduce damage to soil structure and prevent cross-contamination with the microspheres. During excavation, the number, type, and location of macropores was mapped for all horizontal soil sections. The soil sections were photographed using procedures modified from Forrer et al. [2000]. Photographs were taken under diffuse light using a 5.0 megapixel digital camera. A ruled gray frame was placed on the soil profile to assist with the correction of geometric distortion and uneven illumination in the images. Photographic color and gray scales were pinned to the soil surface to ensure consistency in subsequent image analysis procedures.

Few sampling techniques for colloids in the vadose zone have been developed or tested [*McCarthy and McKay*, 2004]. For this study, microspheres were sampled and analyzed in the soil. Each sample was comprised of approximately 2 to 5 g of soil collected using a small clean metal scoop. The samples were placed in a plastic bag and stored in a cool, dark container. Generally, four to eight soil samples were collected from each soil section. Sampling locations were selected based on the observed dye patterns and were taken from a wide range of locations that varied in terms of depth, dye stain intensity (e.g., non-dyed to heavily dye stained soil), and proximity to macropores. A non-dyed control sample not expected to contain microspheres was also collected from each slice for quality assurance purposes. The horizontal sections from test WK-RS1 could not be reliably sampled because of the limited area over which the microspheres were applied. The location of all samples was marked and photographed.

5.2.5 Image Analysis of Dye Patterns

The image analysis procedures used closely followed those outlined by Weiler and Fluhler [2004] and, to a lesser extent, Forrer et al. [2000], with selected modifications to improve discrimination of dye patterns and ensure consistency between images. A detailed description of the image analysis

procedure is provided in Appendix B. Briefly, all images underwent the following procedures: geometric correction, background subtraction, color adjustment, histogram stretching, dye classification, and a final visual check. The resulting images were separated into dyed and non-dyed regions, with the dyed regions further divided into three classes based on the intensity of dye staining. At the Walkerton site, dye stained soil calibration patches were used to determine concentration categories for the three dye stained soil classes (0.2-1.5 g/L, 1.5-3.0 g/L, and >3.0 g/L).

5.2.6 Microsphere Enumeration

There is not yet a standard analysis technique for microspheres in soil samples, so the following method was developed. The method is partly based on studies conducted by Bales et al. [1997], Cumbie et al. [1999], McCarthy et al. [2002], and Passmore [2005]. Each soil sample was mechanically homogenized, diluted 1:20 in 0.01% Tween 20, and sonically agitated for two minutes to separate the microspheres from the soil particles. Samples were then shaken by hand for 10 s and let stand for 30 min to allow larger particles to settle. Using a membrane filtration unit, 0.5 mL of the sample solution was filtered onto a 2 μm mesh size filter. Two replicate filters were made for each sample, placed on a microscope slide, and mounted with a cover slip. An epifluorescent microscope was used to detect the microspheres, using different excitation filters to distinguish between the different microsphere colors. For the larger microspheres the entire filter was counted and the results represent the average of the two filter samples. The smaller 0.53 μm microspheres were clearly visible, but too small to count directly. Therefore, each sample was analysed for the presence or absence of microspheres by making two passes across the filter, one through the centre and another halfway to the edge of the filtered area. The smaller microspheres were considered present if they were detected on one or both filter samples. Laboratory control samples were prepared using mixtures of soil with and without microspheres, and subsequently counted in order to refine and verify the procedure. The lower detection limit is considered to be 20 microspheres per gram of soil.

5.2.7 Soil Physical Property Testing

Following the infiltration tests, undisturbed core samples and bulk soil samples were collected from the A, B and C horizons at both sites to measure soil physical properties. A total of ten intact core samples were collected and analyzed from each site. The core samples were collected by pushing a cylindrical aluminum tube, 25 mm tall by 47 mm inside diameter, into the soil and carefully removing it by excavating around the core tube. Soil at each end of core was trimmed flush with the core tube and one end was covered with fine cloth that was secured to the core. The cores were then oven dried and weighed. Bulk density ρ_b was calculated by dividing the dry soil mass by the core volume [*Blake and Hartge*, 1986]. Total porosity n was calculated using the equation provided by Carter and Ball [1993]

$$n = 1 - \frac{\rho_b}{\rho_p} \tag{16}$$

where ρ_p is the particle density, which was assumed equal to 2.65 g cm^{-3}. Saturated hydraulic conductivity K_{sat} of the core samples was determined in the laboratory using either a constant head (Elora) or falling head (Walkerton) permeameter [*Reynolds*, 1993]. A minimum of three repetitions were completed for each coil sample. In addition, soil water retention curves were measured on the intact soil cores according to the pressure plate method described by Topp et al. [1993]. The retention curves were measured at pressure heads of 0, -0.1, -0.2, -0.5, -1.0, and -3.0 m.

Bulk soil samples were collected from the open excavations using a shovel or hand trowel and the soil was placed in clean, sealable plastic bags. The grain size distribution of the bulk samples was determined using a combination of sieve analysis and the hydrometer method [*Sheldrick and Wang*, 1993].

5.3 Results and Discussion

5.3.1 Soil Conditions and Macroporosity

The soil physical properties measured from samples collected at both the Walkerton and Elora sites are provided in Table 5.2. Average soil water retention curves for each soil horizon are shown in Figure 5.1. A summary of all soil data, including soil water retention curves and grain size distribution plots, is compiled in Appendix C. In general, the soil characteristics were very similar between the two sites. Soil from the Walkerton site had a larger average saturated hydraulic conductivity K_{sat} compared to Elora, likely owing to the higher sand content and lower clay content at Walkerton.

Soil macropore features were photographed and recorded during the excavations. Both sites had significant macroporosity that was comprised of earthworm and insect burrows, root holes, and fractures. The number and type of observed macropores with depth are given in Table 5.3 and plotted in Figure 5.2. The trends in macropore density were similar at both sites. The areal density of linear macropores, most notably earthworm burrows and root holes, increased with depth to the maximum at 30 cm below ground surface, and decreased thereafter. The peak in macropore density at 30 cm is partly attributed to increased wormhole stability in the B and C soil horizons, and the fact that the maximum historical tillage depths were approximately 20 cm below surface. Fractures and root holes were most prevalent in the top 20 cm of the soil profile, with fracture density peaking at 10 cm depth (Figure 5.2). Vertically oriented earthworm burrows were by far the dominant macropore feature,

constituting over 85% of the linear macropores at both sites. It is not surprising then that earthworm burrows were the most significant pathways for preferential transport of dye and microspheres as will be shown later.

The observed wormholes were circular and ranged in size from about 2 to 10 mm in diameter. Individual root holes tended to be smaller with diameters between 1 and 4 mm. Roots were commonly seen within existing worm burrows. A small portion of the worm burrows were still occupied by living worms. Typical examples of earthworm burrows are shown in Figure 5.3. It was difficult to quantify macropore connectivity based on individual soil sections, however, earthworm burrows could frequently be tracked between soil sections at different depths. Numerous burrows extended beyond the maximum depth of excavations (approximately 1.2-1.4 m). At the same time, the variability in macropore density with depth (Figure 5.2) suggests that a large number of dead end macropores were likely encountered, particularly below 30 cm depth. Many worm burrows were lined with a coating of finer-grained organic material (*e.g.*, Figure 5.3c) that has been identified and examined in other studies [*Stehouwer et al.*, 1994; *Jensen et al.*, 2002; *Schrader et al.*, 2007], while others appeared to contain no such coating and be connected directly to unaltered soil matrix material (*e.g.*, Figure 5.3a).

The prevalence of linear, cylindrical macropores represents a fundamental change from the fracture-based macroporosity that was modeled in Chapters 2 and 3. In the relatively fine-grained soils studied here, it was initially expected that there would be a higher density of fractures extending from surface to several meters depth. This is commonly seen in more clay-rich sediments in southern Ontario [*McKay et al.*, 1993b; *Fidler*, 1997; *McKay et al.*, 1998]. The shift to predominantly cylindrical macropores changes the conceptual model of how flow and transport occur. Numerical modelling of saturated porous media by Fidler [1997] has shown that macropore geometry (i.e., cylindrical versus planar) is an important control on the pressure response and transport of solutes in macroporous systems. Cylindrical macropores have a much lower contact area between the matrix and macropore than fractures of equivalent volume. As a result, less macropore-matrix exchange of fluid or solute occurs in systems with cylindrical macropores. It is not clear how this same behaviour will affect partially saturated systems, where capillary pressures enhance mass transfer between macropores and matrix during infiltration. In any event, the presence of cylindrical macropores is likely to lead to a reduction in macropore-matrix interaction and potentially result in deeper than expected migration of the surface tracers than in an equivalent fractured system. Additional numerical simulations would be required to evaluate the potential significance of differences in macropore geometry on flow and transport under partially saturated conditions. This represents a significant opportunity for future research.

5.3.2 Water Content Measurements

A detailed discussion of infiltration rates and soil moisture content response during infiltration and redistribution during the TI tests was presented in Chapter 4 and will not be repeated. Rather, the discussion here will focus primarily on the results of water content measurements from the rainfall simulation experiment along with test WK-D4 for comparison. Overall, the response of the TDR probes to changes in soil water content showed evidence of preferential flow in both the TI and simulated rainfall experiments. Figure 5.4 shows the water content changes for the rainfall simulator test WK-RS1 and the TI test WK-D4. The two tests were conducted the same day and the infiltration rates were designed to be similar (Table 5.1). All shallow (i.e., 10 cm deep or less) TDR probes showed a significant response due to passage of the infiltration wetting front, although the changes in water content were highly variable in both time and space. During the simulated rainfall test WK-RS1, water content measured by TDR probe P2 in the center of the plot exhibited a delayed response relative to TDR probes P1 and P3 at the same depth (Figure 5.4a). Probes P1 and P3 showed a distinct peak in water content near the end of the rainfall period, followed by a steady decline as drainage and redistribution occurred. On the other hand, water content at P2 continued to increase for approximately 15 minutes after rainfall ended and remained nearly constant throughout the drainage period. Likewise, the timing and magnitude of the water content changes beneath the TI disc in test WK-D4 were significantly different for each of the three probes. For example, probe P1 had a rapid initial increase followed by a gradual increase that continued well beyond the end of the infiltration period, whereas probe P3 showed a more traditional increase throughout the infiltration period and subsequent decline after flow to the TI disc was stopped. Water content changes were measured deeper in the soil profile during test WK-RS1, but only probe P5 at 25 cm depth showed a marked response (Figure 5.4). There were small (i.e., $\Delta\theta < 0.015$) and very gradual water content increases at other probes, most notably P7 at 40 cm depth. These water content changes deeper in the subsurface were likely the result of localized preferential flow paths that intersected the TDR probes.

Water content measurements alone were not sufficient to demonstrate flow along macropores. The spatial and temporal variability of the water content readings at shallow depth implies preferential flow occurred, however, it could have been generated by features other than macropores, such as flow funneling by soil layers, fingering caused by flow instability, or natural geologic heterogeneity [*Hendrickx and Flury*, 2001]. Preferential flow phenomena by a variety of mechanisms have been observed in other field studies [*Ghodrati and Jury*, 1990; *Kung*, 1990; *Flury et al.*, 1994]. For example, Rudolph et al. [1996] used a dense TDR monitoring network to demonstrate highly variable infiltration patterns and solute transport in heterogeneous sand and gravel sediments. Although there are a number of potential preferential flow mechanisms, macropores are considered the most likely mechanism for preferential flow in fine-grained soils. Flury et al. [1994] showed in

dye tracing experiments at 14 field sites that dye penetrated deeper in finer-grained structured soils compared to unstructured soils, likely as a result of preferential flow along macropores. It is also worth noting that not all of the infiltration events in this study had evidence of preferential flow. The TI tests conducted at lower infiltration pressures had relatively uniform changes in water content both spatially and temporally, which was a strong indication of uniform piston-type flow (see for example Figure 4.4a in Chapter 4). This is described in more detail in Chapter 4 and suggests that the potential for preferential flow was a direct function of the applied pressure head.

5.3.3 Dye and Microsphere Tracer Transport

5.3.3.1 Tension Infiltration Experiments

The applied pressure heads and infiltration rates for the TI tests are given in Table 5.1. The degree of macropore flow and the depth of dye staining in the TI experiments were dependent on the applied pressure head as shown in Figure 5.5 and Figure 5.6 for the Elora and Walkerton sites, respectively. The relationship between the applied pressure head, infiltration rate, macropore flow observations, and depth of dye staining was discussed in detail in Chapter 4. Briefly, increases in the infiltration pressure, although still negative, promoted the initiation of flow along macropores and resulted in increased depths of dye penetration. Significant macropore flow was not observed in tests WK-D1 and EL-D1 that were conducted at maximum pressure heads of -5.2 and -3.7 cm, respectively. All of the remaining tests were conducted with maximum pressure heads greater than -3.0 cm and exhibited substantial flow along macropores. The deepest dye transport appeared to be the result of flow along vertical macropores comprised predominantly of earthworm burrows.

It is acknowledged that the transport of Brilliant Blue dye solution used in these experiments is not the same as water or other dissolved species of concern. The dye undergoes nonlinear sorption which results in a sharp front that is retarded relative to the infiltrating water [*German-Heins and Flury*, 2000]. Flury and Fluhler [1995] showed in a field experiment that Brilliant Blue FCF was retarded by a factor of 1.2 relative to a conservative iodide tracer. The dye can be considered representative of a low to moderately retarded species that provides a reasonable and highly visual indication of solute transport through the soil. In other words, the dye is conservative in the sense that the actual movement of a non-sorbing tracer would be even greater.

Soil samples collected from the excavated sections were analyzed for the presence of microspheres. Sample locations were chosen based on the observed dye patterns with the goals of obtaining samples with a range of dye intensity (i.e., concentration) and comparing transport of microspheres relative to dye at and beyond the limits of the observable dye. The sample locations and results for vertical soil sections from the TI tests at Elora and Walkerton are shown in Figure 5.5

and Figure 5.6, respectively. The results of all microsphere analyses are provided in Appendix E. All microsphere concentrations referred to here represent the larger 3.7 μm microspheres, since they were the only ones that could be quantified. The occurrence of the smaller microspheres is indicated in the figures with a "+" or "-" sign as being present or absent, respectively. The highest microsphere counts occurred in heavily dye stained regions within 5 cm of ground surface. The larger microspheres were applied to the soil at a density 2.6 x 10^5 spheres cm^{-2}. This resulted in average microsphere counts of 1.78 x 10^5 spheres g^{-1} soil for samples collected from the infiltration surface of the three TI tests at Walkerton. Relative to this input concentration, microsphere concentrations decreased by more than two orders of magnitude in the near surface soils (Figure 5.5 and Figure 5.6). At depths greater than 5 cm, large microsphere concentrations were relatively steady and ranged between 20 and 260 spheres g^{-1} in the dye stained regions. Microspheres were generally detected to the maximum depth of the visible dye staining. Samples collected from immediately below the maximum depth of dye staining contained no large microspheres, but small microspheres were detected in more than half of the samples (see for example Figure 5.6b and c). There were no detectable microspheres of either size in any of the control samples collected from obviously non-dyed regions farther from the wetting front. These findings are consistent with other colloid transport studies. Field studies of bacterial transport in unsaturated soils by Natsch et al. [1996] and Tallon et al. [2007] have shown that bacteria are preferentially retained in the surface soil layer, but were transported in much the same manner as a conservative tracer at greater depths. Laboratory studies of colloid transport in saturated porous media report that colloid distributions follow a hyperexponential deposition profile that is attributed primarily to straining within the smallest pores near the input source [*Bradford et al.*, 2002]. With increasing travel distance, the colloids are less likely to be retained because they have already undergone straining and those that remain are primarily transported in larger, more conductive pore spaces [*Bradford et al.*, 2006].

There was a strong interrelationship between microsphere concentrations, depth, and the intensity of dye staining. Figure 5.7 presents the 3.7 μm diameter microsphere concentrations for all of the TI tests plotted against depth and the intensity of dye staining (i.e., dye category). The intensity of dye staining was determined by image analysis and separated into distinct dye categories, as described in Section 5.2.5. Dye category zero represents no dye staining and categories one, two, and three represent low, moderate, and heavily dye stained soils, respectively. The dye category referred to in Figure 5.7 is based on the predominant dye category or categories of the soil area from which each sample was collected. As indicated above, the highest microsphere concentrations were measured in shallow, heavily dyed soils. Microsphere concentrations declined with depth, but these declines appeared to be strongly linked with the intensity of dye staining. Within a given dye category, there was considerable variability in microsphere concentrations and often no readily apparent trends with

depth. In some instances, such as dye category 1.0 in Figure 5.7a, there was a steady decline in microsphere concentrations with depth, but this appeared to be the exception rather than the rule. Relative to the source concentrations, the detection limit for the microspheres is much lower than for the dye. As such, the concentrations of the two species are not directly comparable. Still, the similarity in solute and colloid distributions within the soil would indicate that solute and colloid species are likely to be transported to similar depths during infiltration in natural soils. Figure 5.7 also shows the influence of the different infiltration pressures. As an example, in the two tests at Elora (Figure 5.7a) the microsphere concentrations tended to be similar for a specific depth and dye category. Test EL-D2, however, had more samples with dye staining deeper in the soil profile because of preferential flow generated by the larger infiltration pressure.

Possible retention mechanisms for the microspheres include mechanical filtration, straining, attachment to soil grains, attachment to AW or AWS interfaces, or film straining. It is impossible to identify specific retention mechanisms with the existing data. Nevertheless, a comparison of dye versus microsphere distributions reveals some interesting features. In general, subsurface microsphere distributions were closely correlated with the observed dye patterns. A total of 225 soil samples were analyzed for microspheres in all TI tests and 157 of these had visible dye staining. Only 10 samples had no visible dye and yet still contained either large or small microspheres. Of these ten samples, eight contained only the smaller 0.53 μm spheres, suggesting that the smaller microspheres were transported to greater distances at the wetting front than the larger microspheres. It is possible that microspheres were transported in thin films or attached to the moving AW interface at the leading edge of the infiltrating water front. There is support for transport of colloids by AW interfaces at the leading edge of infiltration in a study by El-Farhan et al. [2000]. Lysimeters were used to monitor soil particle breakthrough during field infiltration experiments, and peak particle concentrations detected near the rising and falling limbs were attributed to colloids attached to the moving AW interfaces during imbibition and drainage.

A much larger percentage of the samples had visible dye, but did not contain microspheres. In soil samples with visible dye staining, fifteen (15) samples had neither small nor large microspheres. Five of these fifteen samples were from test WK-D1, which was conducted at the lowest (most negative) pressure head. Figure 5.6a also shows that there were four additional samples in test WK-D1 that were dye stained and contained the small microspheres, but had no detectable large microspheres. This data indicates that there was greater retention of microspheres, particularly the larger microspheres, relative to the dye in test WK-D1. The lower applied pressure head in test WK-D1 caused infiltration at a lower soil water content, resulting in a corresponding increase in air-water interfacial areas [*Or and Tuller*, 1999] and a decrease in water film thicknesses [*Tokunaga and Wan*,

1997; *Wan and Tokunaga*, 1997]. Microspheres were then more easily trapped very close to the surface along AW and AWS interfaces or in thin liquid films [*Wan and Wilson*, 1994b; *Wan and Tokunaga*, 1997; *Zevi et al.*, 2005]. The lower capillary pressure in test WK-D1 also causes the remaining flow to be restricted to the smaller pores, increasing the potential for physical straining between soil grains [*Bradford et al.*, 2006]. The fact that the concentration of large microspheres in surface samples (<2 mm depth) collected from the infiltration area of test WK-D1 (3.34×10^5 spheres g^{-1}) were more than three times higher than those from tests WK-D2 (1.10×10^5 spheres g^{-1}) and WK-D3 (8.91×10^4 spheres g^{-1}) further supports the contention that microsphere retention was enhanced very near the soil surface by lower (more negative) infiltration pressures. Increased retention of colloids at lower soil pressure potentials (or water contents) has been demonstrated in transport experiments using bacteria in intact soil columns [*Jiang et al.*, 2005] and microspheres of various sizes in packed sand columns [*Wan and Tokunaga*, 1997].

It can also be inferred from the data that large microspheres underwent a greater degree of retention than the small microspheres. Small microspheres were far more likely to be present in the dyed samples than the large microspheres. In soil samples where dye was detected, thirty-eight (38) had detectable levels of small microspheres with no large microspheres, compared to only two samples where large microspheres were detected and small microspheres were absent. In both cases, these samples tended to be from lightly dyed regions near the lateral or vertical limits of infiltration. Similar numbers of samples representing each case (small present-large absent or vice versa) would be expected if the difference in detections was due solely to sampling or analysis protocols. Acknowledging that there is a possibility that a small number of the microsphere sample results were either false positives or false negatives, the overall trends are still compelling. It is proposed that physical retention or retardation mechanisms have a greater influence on the larger microspheres. For example, larger colloids would be expected to undergo greater physical straining in small pores or in thin water films [*Zevi et al.*, 2005; *Bradford et al.*, 2006].

Shallow dye patterns extended laterally well beyond the edge of the TI disc as illustrated for example in test WK-D1 (Figure 5.8). The dye patterns are the result of capillary forces drawing the infiltration solution both vertically and horizontally away from the TI disc. Given the significant microsphere retention that was observed in the near surface soil, the detection of microspheres in shallow samples from outside the TI disc area was surprising and significant. Figure 5.8 shows microsphere samples taken on a horizontal soil section at 2 cm depth. Two of the samples were collected from dyed regions outside the TI disc area and both had detectable levels of the large and small microspheres. Neither sample was located near visible macropores. One of these samples, in particular, was situated approximately 9 cm away from the edge of the disc. It is also worth noting

that these samples came from test WK-D1 with the lowest infiltration pressure, and thus the largest microsphere retention capability. There were many other examples of shallow (2-5 cm depth) samples collected from dyed regions outside the disc area that contained microspheres. These observations hint at the importance of advection in transporting dye and microspheres through the soil matrix. Lateral advection has the potential to move microspheres away from the infiltration source and into the soil matrix. This effectively decreases the number of microspheres available for vertical transport along macropores. Following an infiltration event, the microspheres bound in the matrix have an increased chance to adhere to soil grains or AWS interfaces and are less likely to be preferentially transported downward in subsequent infiltration events.

Advective transfer between the macropores and matrix during infiltration was also noted deeper in the soil profile. Figure 5.3 shows several examples of dye stained halos that formed around macropores as a result of macropore-matrix interaction. The conceptual model used to describe these halos is dye solution migrating vertically downward along the macropore is imbibed into the soil matrix by capillary forces. Flow within the larger macropores is believed to occur as thin films, rivulets, or within irregular grooves under negative pressure conditions as discussed in Chapter 4. Microspheres are also subject to advective transfer from the macropores into the matrix. Figure 5.9 shows dye patterns and microsphere concentrations on a horizontal soil section from test EL-D2. Of particular note is the highlighted region showing an earthworm burrow and surrounding dye stained soil. Microsphere concentrations were highest in the soil sample taken from the lining of the earthworm burrow. Microspheres were also discovered in the dye stained soil adjacent to the worm burrow, but not in the non-dyed soil farther from the burrow. These results confirm the importance of macropore-matrix interactions under partially saturated conditions and again demonstrate the concomitant transport of dye and microspheres through the soil.

There are important differences in colloid transport between partially and fully saturated porous media. In the current study, there was little evidence for enhanced transport of microspheres relative to the dye tracer. At the same time, lateral migration of microspheres either into or through the soil matrix was important. Both of these observations differ from what is expected under saturated conditions. In saturated media, where all pores are water filled, colloids can be transported more quickly than nonreactive solutes, particularly in macroporous systems [*Harvey et al.*, 1989; *McKay et al.*, 1993a; *McKay et al.*, 1999]. The enhanced colloid transport has been attributed to pore size exclusion. That is, colloids are excluded from the smaller pores because of their larger size (and hence lower diffusion rate), and transported preferentially in the larger pores which have higher flow velocities. Because capillary forces are absent in the saturated zone, advection through the matrix is low and lateral migration of colloids into the matrix is primarily diffusion controlled. Studies on

saturated shale and sandstone saprolite cores showed colloid migration from fractures into the matrix was limited to a few millimeters due to low diffusion rates [*Cumbie and McKay*, 1999; *Driese and McKay*, 2004]. In the vadose zone, the addition of capillary forces creates a considerable advective component to macropore-matrix transfer and results in greater penetration of colloids into the matrix. As with soluble contaminant species, the increased macropore-matrix mass transfer happening in partially saturated soils is critical in that it effectively retards the vertical migration of colloids. Based on this, it is expected that the available soil moisture storage capacity (i.e., antecedent soil moisture) will play an important role in determining the likelihood of colloid breakthrough in field soils.

5.3.3.2 Simulated Rainfall Experiment

A vertical profile of the classified dye patterns and microsphere concentrations from test WK-RS1 is given in Figure 5.10. Based on the initial soil water content, the 36 mm of applied water would be sufficient to uniformly saturate the soil to a depth of 12 cm. Flow was not uniform, but rather showed significant spatial variability and was dominated by preferential flow along macropores. By 10 cm depth, there were already large portions of the soil that were not dye stained (Figure 5.10). A photograph of the horizontal soil section at 5 cm depth is shown in Figure 5.11. Image analysis of this photograph indicates that dye staining covered 97% of the soil at this shallow depth, yet there were clearly preferred areas for infiltration. In particular, dye coverage and intensity were increased along the existing crop rows (Figure 5.11). The primary reason for this was that infiltration was focused along plant roots at or near ground surface. Since surface vegetation was removed prior to infiltration, canopy interception and channeling along plant stems was not considered a major factor. Root-focused infiltration was not observed during the TI tests, likely because of the smaller infiltration footprint of the TI disc relative to the rainfall simulator plot. In test WK-RS1, increased dye staining at 5 cm depth was also observed surrounding fractures and earthworm burrows throughout the soil. The dye patterns suggest preferential flow was initiated within 5 cm of ground surface and corroborate the indirect evidence of preferential flow inferred from the shallow water content measurements.

Deeper in the soil profile, essentially all dye stained areas could be directly attributed to vertical transport along macropores. During excavation, half of the plot was examined by excavating vertical sections to the maximum depth of dye staining, while horizontal excavations were conducted beneath the other half to a maximum depth of 42 cm. On the 42 cm depth horizontal section (60 × 120 cm), there were 19 discrete locations of visible dye breakthrough. All of these dyed breakthrough areas occurred along well defined individual worm burrows or clusters of burrows, with the exception of the two smallest dyed areas (which were connected to vertical macropores that terminated slightly above 42 cm depth). Still, the number of dyed macropores was only a fraction of the 468 total

macropores identified on the horizontal section. Beneath the other half of the plot (60 × 120 cm), 13 dye stained pathways extended deeper than 40 cm and were tracked to their maximum depth. Dye staining in five (5) of the macropores went deeper than 80 cm, and three (3) of those extended to greater than 100 cm depth. The maximum depth of dye staining was 126 cm. Again, all stained pathways were earthworm burrows except for staining along one fracture and the surface of a large rock, both of which likely intersected worm holes further up in the soil profile.

The spatially irregular flow patterns and small size of the macropores made it difficult to measure preferential flow at depth using the TDR probes in the simulated rainfall experiment. The dye stain patterns confirmed that the water content observations were related to macropore flow due to the fact that the TDR probes showing the greatest water content response had the largest dye stained soil area in the vicinity of the probes. During test WK-RS1, only one of the five TDR probes at 25 cm or greater depth exhibited a clear water content increase in response to infiltration. Figure 5.4a shows a water content change of about 3% for TDR probe P5, while approximately 40% of the soil surrounding this probe was dye stained. In the remaining deep TDR probes (which showed little or no water content response), dye stained soil contacted at least some part of each TDR probe, but soil dye coverage along the probes was less than 20% in all cases. All dye staining in the vicinity of the probes was associated with flow along vertical macropores. Although the dye showed that flowing macropores intersected each TDR probe, the large volume of soil measured by the TDR relative to the macropore volume resulted in no distinctly measurable response. As such, caution should be used when utilizing TDR as the sole or primary means of detecting preferential flow in macroporous soils.

Figure 5.10 overlays the concentrations of large (3.7μm diameter) and small (1.5 μm diameter) microspheres on the classified dye image. Notice that the diameter of the small microspheres used in this test (1.5 μm) was larger than those used in the TI tests (0.53 μm) and could be readily quantified. Also, the number of soil samples collected for analysis of microspheres was much smaller in the rainfall simulation experiment. The smaller sample population makes it more difficult to evaluate microsphere retention behaviour, but the colloid distributions still provide useful insights. A random scraping from the infiltration surface revealed concentrations of large and small microspheres of 1.13 x 10^5 and 2.03 x 10^5 spheres g^{-1} soil, respectively. Microsphere concentrations detected in the soil were smaller than the surface concentrations by three orders of magnitude (Figure 5.10). The largest microsphere concentrations (360 and 280 spheres g^{-1} of the large and small sizes, respectively) were detected in heavily dyed soil less than 2 cm below surface. Microspheres were detected in all samples collected from dye stained regions, including two lightly dyed samples over 100 cm deep. All but one of the non-dyed samples had microsphere concentrations at or below the detection limit of 20 spheres g^{-1}. One non-dyed sample collected at 19 cm depth, about 3 cm below a region of

moderate dye staining, had an abnormally high concentration of 100 spheres g^{-1} of the large microspheres. As in the TI tests, there is close agreement between dye and microsphere distributions, and a strong indication that microspheres can be transported to the same depths as the dye during a rainfall event.

At several locations, the concentration of the large microspheres was greater than the small microspheres. Since the two sizes of microspheres were applied to the soil at identical rates and TI results showed a greater retention efficiency for larger sized microspheres, this observation is difficult to explain. Perhaps the 3.7 and 1.5 µm diameter microspheres are close enough in size that they possess very similar transport and retention characteristics. At the relatively low concentrations detected, the differences may be solely due to sampling and analytical variability. The data set is considered too small to draw any reliable conclusions on transport behaviour for the different microsphere sizes.

As stated earlier, the depths and rates of application in WK-RS1 were similar to those from TI tests WK-D3 and WK-D4 conducted at the highest pressure heads. Thus, it is useful to compare these tests to examine whether there were differences in transport resulting from differences in the surface boundary conditions. The general dye patterns in WK-RS1 (Figure 5.10) are much the same as those in test WK-D3 (Figure 5.6c), and suggest similar subsurface flow regimes for the different infiltration methods. The spatial distribution and concentrations of microspheres were also similar for these different tests. The most obvious difference in transport patterns was the depth of transport, which is shown most clearly in the dye patterns. The maximum depths of dye staining were 70 and 74 cm in TI tests WK-D3 and WK-D4, respectively, compared to 126 cm in the rainfall simulation WK-RS1 (Table 5.1). The most likely reason for the increased depth of dye penetration in the simulated rainfall experiment is localized ponding in microdepressions on the soil surface. The TI experiments showed that the depth of dye migration is sensitive to the infiltration pressure head at the soil surface (see Figure 5.6). During the simulated rainfall, ponding was observed in small, isolated topographic depressions across the soil surface. The depth of ponding appeared to be limited to a few millimeters (although not measured) and no significant lateral surface flow was observed between microdepressions. The ponding would generate slightly positive infiltration pressures locally and enhance infiltration into both the matrix and the macropores. The small increase in pressure head could potentially fill larger macopores and increase vertical flow rates, which in turn would result in greater depths of dye transport. This process has been shown in laboratory infiltration experiments by Trojan and Linden [1992], where worm burrows located at the base of microdepressions had deeper dye staining than burrows located at other topographic positions. A second possible explanation for deeper dye staining under test WK-RS1 is the influence of edge effects on the different plot sizes.

During infiltration, water flows laterally away from the infiltration area through the near surface soils, thereby reducing soil water content and the potential for vertical flow in either the matrix or macropores. These lateral surface flows have a smaller effect on the much larger simulated rainfall plot and allow a greater volume of the infiltration solution to flow vertically downward.

Based on the results presented here, microspheres are expected to be transported to at least the same depth as the visible dye, and possibly deeper for smaller microspheres. This leads to the question of whether contaminants could reach the water table and, more importantly for the Walkerton site, whether colloids from surface could reach the shallow bedrock aquifer? The water table at Walkerton ranged between 1.1 and 1.5 m below ground surface over the 2006 growing season in the vicinity of the infiltration tests and was even shallower (<80 cm) beneath topographic lows within the same field. Based on the observed depths of dye and microspheres in the soil, there is a strong possibility that surface applied contaminants (both dissolved and colloidal) could reach the water table during a large rainfall event such as the one simulated in this study. Although the mass of contaminants reaching the water table in any single macropore was likely very small, it still represents a significant concern for two main reasons. First, certain contaminants represent a health concern even at very small concentrations. This is particularly true for pathogens, such as *E. coli* O157:H7, where infective doses can be as low as 10 organisms [*Rosen*, 2000; *Cicmanec*, 2001]. Second, the collective contribution of breakthrough in many macropores over a large area may be significant. In test WK-RS1, approximately four macropores per m^2 showed dye staining to depths of more than one meter. This equates to 2.3×10^5 active macropores over the entire 5.8 ha field that could potentially transport contaminants to the water table for a rainfall event of similar duration and intensity. A more intense or longer duration rainfall event, such as the one that occurred prior to the Walkerton groundwater tragedy of 2000, would no doubt result in further increases in transport rates via the existing macropore network.

The possibility of contaminants, particularly colloids, reaching the bedrock aquifer by infiltration along vertical macropores is more difficult to assess. The bedrock aquifer was encountered at depths ranging from 2.7 to 4.8 m across the field at Walkerton. Water samples were not collected from the bedrock aquifer in this study and thus there was no direct evidence of microspheres reaching the aquifer. The rapid response of the bedrock aquifer to precipitation events (data not shown) suggests that there is a strong hydraulic connection with the surface, but hydraulic head fluctuations are transmitted through the subsurface much more quickly than the fluids themselves. In order for colloids to reach the aquifer they would have to be transported across the water table and through a minimum of 1.5 m of saturated overburden material. This would require that macropores extend all the way through the overburden or that colloids are transported through the matrix material. It is

highly unlikely that earthworm burrows, the most common transport pathway, extend much beyond the seasonal maximum depth of the water table. Fractures could extend to greater depths, but they were not identified as significant pathways for deep dye or colloid movement at the Walkerton site. If deeper fractures or other macropores were present and interconnected with the vadose zone macropore network, colloid transport to the bedrock aquifer would likely be rapid. This topic represents an opportunity for further study.

5.4 Summary and Conclusions

The results of TI and simulated rainfall experiments showed that macropores were an important transport pathway for solutes and colloids in field soils. The tension infiltration tests demonstrated that the degree of macropore flow and transport was dependent on the infiltration rate, which was determined by the pressure head applied to the TI disc. Transport of dye and microspheres via macropores occurred in the TI tests when maximum pressure heads were greater than -3.0 cm, and the corresponding infiltration rates exceeded 1.0-2.0 cm hr^{-1}. Dye and microspheres were detected at depths greater than 70 cm in the TI tests with the highest infiltration rates from both sites (i.e., EL-D2, WK-D3, and WK-D4). The rainfall simulation experiment, conducted with a similar infiltration rate similar (representing a 7 to 8 year return period event), also produced significant preferential flow with dye and microsphere transport to depths greater than 1.2 m. Earthworm burrows were the dominant macropore type at both the Elora and Walkerton sites as well as the main pathway for deep transport.

Microspheres appeared to be preferentially retained in the top few centimeters of soil, but at greater depths the microsphere distributions closely followed the dye patterns. This is consistent with colloid deposition profiles described in other field studies [*Natsch et al.*, 1996; *Tallon et al.*, 2007]. Microsphere concentrations at all depths were closely related to the intensity (or concentration) of dye. It is concluded that the dye tracer served as an excellent surrogate for colloid distributions in the vadose zone, and could potentially be used to evaluate the vulnerability of soils to colloid migration under the right conditions. This has a practical benefit in that dye tracers are generally much simpler and less expensive to work with than microspheres (or other colloid tracers) and provide a rapid visual indication of flow pathways. Certain microsphere transport characteristics were inferred from the presence or absence of microspheres (both large and small) and dye throughout the soil profile. The smaller diameter microspheres were detected more often than the larger microspheres near the leading edge of infiltration (as defined by dye staining). The greater extent of transport for the smaller microspheres is consistent with current theory and experimental evidence [*Wan and Tokunaga*, 1997; *Zevi et al.*, 2005; *Bradford et al.*, 2006]. In addition, there was increased retention

of microspheres in the soil matrix at lower water contents (i.e., infiltration potentials), likely due to pore straining, film straining, or increased attachment to AWS and AW interfaces.

Although it may seem obvious, it is worth stressing the importance of flow processes in governing contaminant transport. This is particularly true in the vadose zone where fluxes and pathways are dependent on soil moisture conditions, resulting in a complex, highly transient flow system. In this study, the strong correlation between dye and microsphere distributions in all tests was dictated by the flow pathways that developed. In other words, the overriding influence of the flow system affected transport to a much greater degree than differences between dissolved and colloidal species. Some of the flow processes are unique to the vadose zone. For example, the advective transport of the tracers from the macropores into the soil matrix was driven by capillary forces, which are absent in saturated porous media. The end result is much more extensive mass transfer of solutes and (especially) colloids between macropore and matrix in partially saturated soils. One can reiterate the statements of Denovio et al. [2004] that we must improve our understanding of macropore flow processes (*e.g.*, initiation conditions, flow paths, macropore connectivity) in the vadose zone because of their importance for colloid transport, among other things.

The infiltration experiments highlight the vulnerability of thin macroporous soils, particularly low permeability soils, to vertical contaminant migration. Although dye and colloid migration to depths greater than 40 cm was limited to a small fraction of the macropores, there is a potential for significant vertical mass flux at the field scale because of the relatively high density of macropores. Underlying groundwater resources would be particularly vulnerable to biocolloids (i.e., bacteria, viruses) because they can be a health concern at very low concentrations. The results show that colloids applied to the soil surface, in the form of manure or biosolids, could reach a shallow water table following a short (<1 hour), high intensity rainfall event. More extreme rainfall events would very likely exacerbate the situation. Furthermore, the very fast vertical dye migration shown along macropores in Chapter 4 would suggest rapid downward transport of colloids through soils.

The TI test results closely approximated those of the artificial rainfall test when using nearly equivalent infiltration depths and durations. The dye and colloid tracers tended to go deeper for the simulated rainfall event, which was attributed to edge effects and ponding within microdepressions. Despite this difference, there were enough similarities in terms of water content variations (spatial and temporal), dye patterns, transport along macropores and macropore-matrix interaction, that the TI tests are considered a reasonable surrogate for rainfall events. The TI tests have the added advantage that the infiltration pressures can be used to control the degree of macropore flow. This could be used in the future to provide more detailed evaluations of in situ macropore flow and transport, such as

determining the thresholds of rainfall intensity and duration required for the onset of macropore flow in different soils.

5.5 References

Bales, R.C., S.M. Li, T.C.J. Yeh, M.E. Lenczewski, and C.P. Gerba (1997), Bacteriophage and microsphere transport in saturated porous media: Forced-gradient experiment at Borden, Ontario, *Water Resour. Res.*, *33*(4), 639-648.

Becker, M.W., S.A. Collins, D.W. Metge, R.W. Harvey, and A.M. Shapiro (2004), Effect of cell physicochemical characteristics and motility on bacterial transport in groundwater, *J. Contam. Hydrol.*, *69*(3-4), 195-213.

Beven, K. and P. Germann (1982), Macropores and water flow in soils, *Water Resour. Res.*, *18*(5), 1311-1325.

Blake, G.R. and K.H. Hartge (1986), Bulk density, in *Methods of soil analysis. Part 1.*, Agronomy No. 9, edited by A. Klute, pp. 363-375, American Society of Agronomy, Madison, WI.

Bradford, S.A., J. Simunek, M. Bettahar, M.T. van Genuchten, and S.R. Yates (2006), Significance of straining in colloid deposition: Evidence and implications, *Water Resour. Res.*, *42*(12), W12S15, doi:10.1029/2005WR004791.

Bradford, S.A., S.R. Yates, M. Bettahar, and J. Simunek (2002), Physical factors affecting the transport and fate of colloids in saturated porous media, *Water Resour. Res.*, *38*(12), 1327, doi:10.1029/2002WR001340.

Carter, M.R. and B.C. Ball (1993), Soil porosity, in *Soil sampling and methods of analysis*, edited by M.R. Carter, pp. 581-588, Lewis Publishers, Boca Raton, FL.

Cicmanec, J. (2001), Emerging issues in quantitative microbial risk assessment, in *Presented at EPA 2001 Regional Risk Assessors Training and Conference*, United States Environmental Protection Agency, Bandera, Texas, 21-24 May 2001.

Coles, N. and S. Trudgill (1985), The movement of nitrate fertiliser from the soil surface to drainage waters by preferential flow in weakly structured soils, Slapton, S. Devon, *Agr. Ecosyst. Environ.*, *13*(3-4), 241-259.

Cumbie, D.H. and L.D. McKay (1999), Influence of diameter on particle transport in a fractured shale saprolite, *J. Contam. Hydrol.*, *37*(1-2), 139-157.

de Jonge, L.W., C. Kjaergaard, and P. Moldrup (2004), Colloids and colloid-facilitated transport of contaminants in soils: An introduction, *Vadose Zone J.*, *3*(2), 321-325.

DeNovio, N.M., J.E. Saiers, and J.N. Ryan (2004), Colloid movement in unsaturated porous media: Recent advances and future directions, *Vadose Zone J.*, *3*(2), 338-351.

Driese, S.G. and L.D. McKay (2004), Epi-fluorescence micromorphology of saprolite reveals evidence for colloid retention in microscale pore systems, *Geoderma*, *121*(1-2), 143-152.

El Farhan, Y.H., N.M. DeNovio, J.S. Herman, and G.M. Hornberger (2000), Mobilization and transport of soil particles during infiltration experiments in an agricultural field, Shenandoah Valley, Virginia, *Environ. Sci. Technol.*, *34*(17), 3555-3559.

Fidler, S.R. (1997), Spatial and temporal variability of hydraulic response in fractured low permeability sediments, PhD thesis, University of Waterloo, Waterloo, Ontario, Canada.

Flury, M. and H. Fluhler (1995), Tracer characteristics of Brilliant Blue FCF, *Soil Sci. Soc. Am. J.*, *59*(1), 22-27.

Flury, M., H. Fluhler, W.A. Jury, and J. Leuenberger (1994), Susceptibility of soils to preferential flow of water: a field study, *Water Resour. Res.*, *30*(7), 1945-1954.

Forrer, I., A. Papritz, R. Kasteel, H. Fluehler, and D. Luca (2000), Quantifying dye tracers in soil profiles by image processing, *Eur. J. Soil Sci.*, *51*(2), 313-322.

German-Heins, J. and M. Flury (2000), Sorption of Brilliant Blue FCF in soils as affected by pH and ionic strength, *Geoderma* , *97*(1-2), 87-101.

Ghodrati, M. and W.A. Jury (1990), A field-study using dyes to characterize preferential flow of water, *Soil Sci. Soc. Am. J.*, *54*(6), 1558-1563.

Ginn, T.R., B.D. Wood, K.E. Nelson, T.D. Scheibe, E.M. Murphy, and T.P. Clement (2002), Processes in microbial transport in the natural subsurface, *Adv. Water Resour.*, *25*(8-12), 1017-1042.

Goss, M.J., D.A.J. Barry, and D.L. Rudolph (1998), Contamination in Ontario farmstead domestic wells and its association with agriculture: 1. Results from drinking water wells, *J. Contam. Hydrol.*, *32*(3-4), 267-293.

Harvey, R.W., L.H. George, R.L. Smith, and D.R. LeBlanc (1989), Transport of microspheres and indigenous bacteria through a sandy aquifer: results of natural- and forced-gradient tracer experiments, *Environ. Sci. Technol.*, *23*(1), 51-56.

Hendrickx, J.M.H. and M. Flury (2001), Uniform and preferential flow mechanisms in the vadose zone, in *Conceptual Models of Flow and Transport in the Fractured Vadose Zone*, edited by National Research Council, pp. 149-187, National Academy Press, Washington, D.C., USA.

Hinsby, K., L.D. McKay, P. Jorgensen, M. Lenczewski, and C.P. Gerba (1996), Fracture aperture measurements and migration of solutes, viruses, and immiscible creosote in a column of clay-rich till, *Ground Water*, *34*(6), 1065-1075.

Hoffman, D.W., B.C. Matthews, and R.E. Wicklund (1963), Soil survey of Wellington County, Ontario, Report No. 35 of the Ontario Soil Survey, Canada Department of Agriculture and the Ontario Agricultural College, Guelph, Ontario.

Hoffman, D.W. and N.R. Richards (1954), Soil survey of Bruce County, Ontario, Report No. 16 of the Ontario Soil Survey, Canada Department of Agriculture and the Ontario Agricultural College, Guelph, Ontario.

Hrudey, S.E., P. Payment, P.M. Huck, R.W. Gillham, and E.J. Hrudey (2003), A fatal waterborne disease epidemic in Walkerton, Ontario: comparison with other waterborne outbreaks in the developed world, *Water Sci. Technol.*, *47*(3), 7-14.

Jacobsen, O.H., P. Moldrup, C. Larsen, L. Konnerup, and L.W. Petersen (1997), Particle transport in macropores of undisturbed soil columns, *J. Hydrol.*, *196*(1-4), 185-203.

Jensen, M.B., H.C.B. Hansen, and J. Magid (2002), Phosphate sorption to macropore wall materials and bulk soil, *Water Air Soil Pollut.*, *137*(1-4), 141-148.

Jiang, G.M., M.J. Noonan, G.D. Buchan, and N. Smith (2005), Transport and deposition of Bacillus subtilis through an intact soil column, *Austral. J. Soil Res.*, *43*(6), 695-703.

Karathanasis, A.D. and D.M.C. Johnson (2006), Stability and transportability of biosolid colloids through undisturbed soil monoliths, *Geoderma*, *130*(3-4), 334-345.

Kulli, B., C. Stamm, A. Papritz, and H. Fluehler (2003), Discrimination of flow regions on the basis of stained infiltration patterns in soil profiles, *Vadose Zone J.*, *2*(3), 338-348.

Kung, K.-J.S., E.J. Kladivko, T.J. Gish, T.S. Steenhuis, G. Bubenzer, and C.S. Helling (2000), Quantifying preferential flow by breakthrough of sequentially applied tracers: silt loam soil, *Soil Sci. Soc. Am. J.*, *64*(4), 1296-1304.

Kung, K.J.S. (1990), Preferential flow in a sandy vadose zone: 1. Field observation, *Geoderma*, *46*(1-3), 51-58.

Laegdsmand, M., K.G. Villholth, M. Ullum, and K.H. Jensen (1999), Processes of colloid mobilization and transport in macroporous soil monoliths, *Geoderma*, *93*(1-2), 33-59.

Macler, B.A. and J.C. Merkle (2000), Current knowledge on groundwater microbial pathogens and their control, *Hydrogeol. J.*, *8*(1), 29-40.

McCarthy, J.F. and L.D. McKay (2004), Colloid transport in the subsurface: Past, present, and future challenges, *Vadose Zone J.*, *3*(2), 326-337.

McCarthy, J.F., L.D. McKay, and D.D. Bruner (2002), Influence of ionic strength and cation charge on transport of colloidal particles in fractured shale saprolite, *Environ. Sci. Technol.*, *36*(17), 3735-3743.

McKay, L.D., D.J. Balfour, and J.A. Cherry (1998), Lateral chloride migration from a landfill in a fractured clay-rich glacial deposit, *Ground Water*, *36*(6), 988-999.

McKay, L.D., J.A. Cherry, R.C. Bales, M.T. Yahya, and C.P. Gerba (1993a), A field example of bacteriophage as tracers of fracture flow, *Environ. Sci. Technol.*, *27*(6), 1075-1079.

McKay, L.D., J.A. Cherry, and R.W. Gillham (1993b), Field experiments in a fractured clay till: 1. Hydraulic conductivity and fracture aperture, *Water Resour. Res.*, *29*(4), 1149-1162.

McKay, L.D., J. Fredericia, M. Lenczewski, J. Morthorst, and K.E.S. Klint (1999), Spatial variability of contaminant transport in a fractured till, Avedøre Denmark, *Nord. Hydrol.*, *30*(4-5), 333-360.

McMurry, S.W., M.S. Coyne, and E. Perfect (1998), Fecal coliform transport through intact soil blocks amended with poultry manure, *J. Environ. Qual.*, *27*(1), 86-92.

Natsch, A., C. Keel, J. Troxler, M. Zala, N. Von Albertini, and G. Défago (1996), Importance of preferential flow and soil management in vertical transport of a biocontrol strain of *Pseudomonas fluorescens* in structured field soil, *Appl. Environ. Microbiol.*, *62*(1), 33-40.

Or, D. and M. Tuller (1999), Liquid retention and interfacial area in variably saturated porous media: Upscaling from single-pore to sample-scale model, *Water Resour. Res.*, *35*(12), 3591-3605.

Passmore, J. (2005), An analysis of the transport of bacteria from biosolids through the unsaturated profiles of three different soils, MSc thesis, University of Guelph, Guelph, Ontario, Canada.

Perillo, C.A., S.C. Gupta, E.A. Nater, and J.F. Moncrief (1999), Prevalence and initiation of preferential flow paths in a sandy loam with argillic horizon, *Geoderma*, *89*(3-4), 307-331.

Perroux, K.M. and I. White (1988), Designs for disc permeameters, *Soil Sci. Soc. Am. J.*, *52*(5), 1205-1215.

Petersen, C.T., S. Hansen, and H.E. Jensen (1997), Depth distribution of preferential flow patterns in a sandy loam soil as affected by tillage, *Hydrol. Earth Syst. Sci.*, *1*(4), 769-776.

Poulsen, T.G., P. Moldrup, L.W. de Jonge, and T. Komatsu (2006), Colloid and bromide transport in undisturbed soil columns: Application of two-region model, *Vadose Zone J.*, *5*(2), 649-656.

Reynolds, W.D. (1993), Saturated hydraulic conductivity: laboratory measurement, in *Soil sampling and methods of analysis*, edited by M.R. Carter, pp. 589-597, Lewis Publishers, Boca Raton, FL.

Rosen, B.H. (2000), Waterborne pathogens in agricultural watersheds, United States Department of Agriculture, Natural Resources Conservation Service.

Rudolph, D.L., D.A.J. Barry, and M.J. Goss (1998), Contamination in Ontario farmstead domestic wells and its association with agriculture: 2. Results from multilevel monitoring well installations, *J. Contam. Hydrol.*, *32*(3-4), 295-311.

Rudolph, D.L., R.G. Kachanoski, M.A. Celia, D.R. LeBlanc, and J.H. Stevens (1996), Infiltration and solute transport experiments in unsaturated sand and gravel, Cape Cod, Massachusetts: Experimental design and overview of results, *Water Resour. Res.*, *32*(3), 519-532.

Ryan, J.N. and M. Elimelech (1996), Colloid mobilization and transport in groundwater, *Colloid. Surf. A*, *107*, 1-56.

Schrader, S., H. Rogasik, I. Onasch, and D. Jegou (2007), Assessment of soil structural differentiation around earthworm burrows by means of X-ray computed tomography and scanning electron microscopy, *Geoderma*, *137*(3-4), 378-387.

Sen, T.K. and K.C. Khilar (2006), Review on subsurface colloids and colloid-associated contaminant transport in saturated porous media, *Adv. Colloid Interface Sci.*, *119*(2-3), 71-96.

Sheldrick, B.H. and C. Wang (1993), Particle size distribution, in *Soil sampling and methods of analysis*, edited by M.R. Carter, pp. 499-511, Lewis Publishers, Boca Raton, FL.

Steenhuis, T.S., A. Dathe, Y. Zevi, J.L. Smith, B. Gao, S.B. Shaw, D. DeAlwis, S. Amaro-Garcia, R. Fehrman, M.E. Cakmak, I.C. Toevs, B.M. Liu, S.M. Beyer, J.T. Crist, A.G. Hay, B.K. Richards, D. DiCarlo, and J.F. McCarthy (2006), Biocolloid retention in partially saturated soils, *Biologia*, *61/Suppl. 19*, S229-S233.

Stehouwer, R.C., W.A. Dick, and S.J. Traina (1994), Sorption and retention of herbicides in vertically oriented earthworm and artificial burrows, *J. Environ. Qual.*, *23*(2), 286-292.

Tallon, L.K., B.C. Si, D. Korber, and X. Guo (2007), Soil wetting state and preferential transport of Escherichia coli in clay soils, *Can. J. Soil Sci.*, *87*(1), 61-72.

Tokunaga, T.K. and J. Wan (1997), Water film flow along fracture surfaces of porous rock, *Water Resour. Res.*, *33*(6), 1287-1295.

Topp, G.C., Y.T. Galganov, B.C. Ball, and M.R. Carter (1993), Soil water desorption curves, in *Soil sampling and methods of analysis*, edited by M.R. Carter, pp. 569-579, Lewis Publishers, Boca Raton, FL.

Trojan, M.D. and D.R. Linden (1992), Microrelief and rainfall effects on water and solute movement in earthworm burrows, *Soil Sci. Soc. Am. J.*, *56*(3), 727-733.

Unc, A. and M.J. Goss (2003), Movement of faecal bacteria through the vadose zone, *Water Air Soil Pollut.*, *149*(1-4), 327-337.

van Elsas, J.D., J.T. Trevors, and L.S. van Overbeek (1991), Influence of soil properties on the vertical movement of genetically-marked Pseudomonas-fluorescens through large soil microcosms, *Biol. Fertil. Soils*, *10*(4), 249-255.

Villholth, K.G., N.J. Jarvis, O.H. Jacobsen, and H. de Jonge (2000), Field investigations and modeling of particle-facilitated pesticide transport in macroporous soil, *J. Environ. Qual.*, *29*(4), 1298-1309.

Wan, J. and T.K. Tokunaga (1997), Film straining of colloids in unsaturated porous media: Conceptual model and experimental testing, *Environ. Sci. Technol.*, *31*(8), 2413-2420.

Wan, J. and J.L. Wilson (1994a), Colloid transport in unsaturated porous media, *Water Resour. Res.*, *30*(4), 857-864.

Wan, J. and J.L. Wilson (1994b), Visualization of the role of the gas-water interface on the fate and transport of colloids in porous media, *Water Resour. Res.*, *30*(1), 11-23.

Weiler, M. and H. Fluhler (2004), Inferring flow types from dye patterns in macroporous soils, *Geoderma*, *120*(1-2), 137-153.

Zevi, Y., A. Dathe, J.F. McCarthy, B.K. Richards, and T.S. Steenhuis (2005), Distribution of colloid particles onto interfaces in partially saturated sand, *Environ. Sci. Technol.*, *39*(18), 7055-7064.

5.6 Figures and Tables

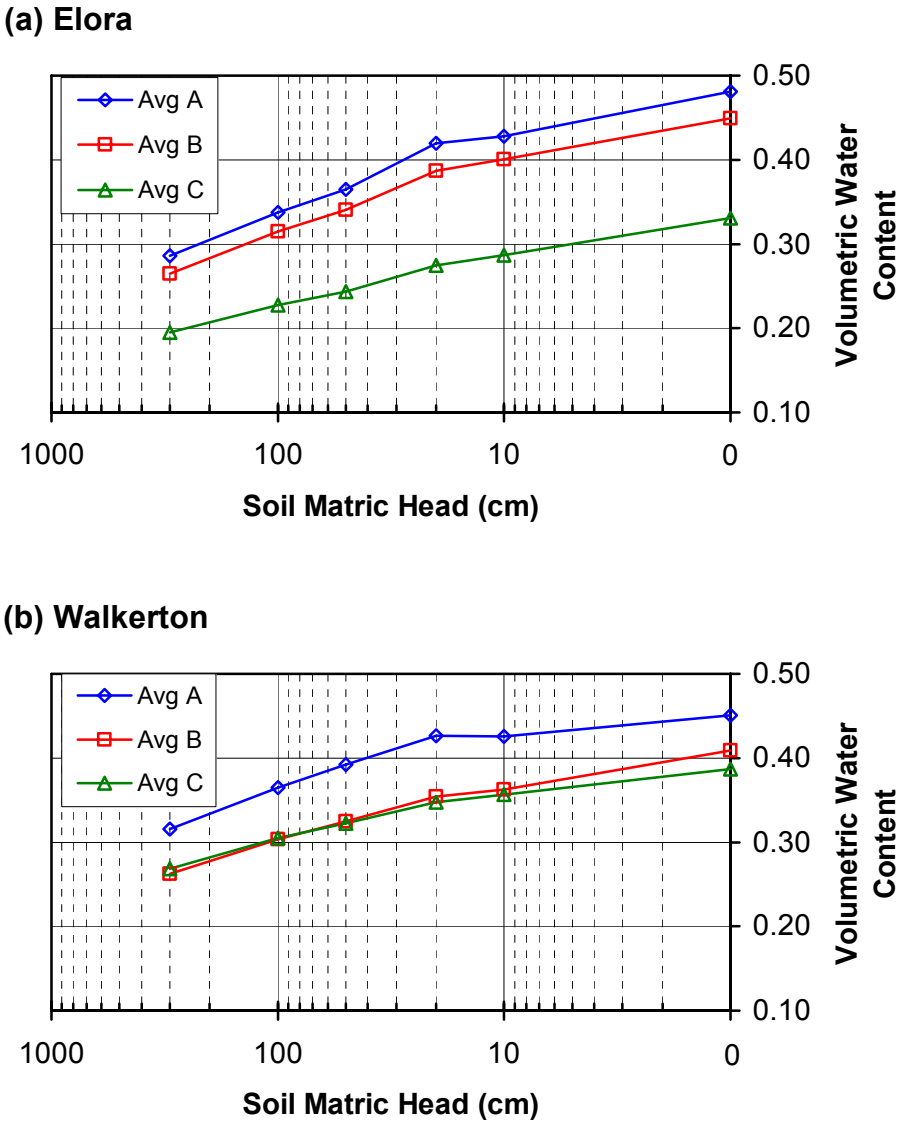

Figure 5.1. Soil water retention curves for the (a) Elora and (b) Walkerton sites. The plots represent average values for each soil horizon, with each curve consisting of measurements from two to five distinct soil samples.

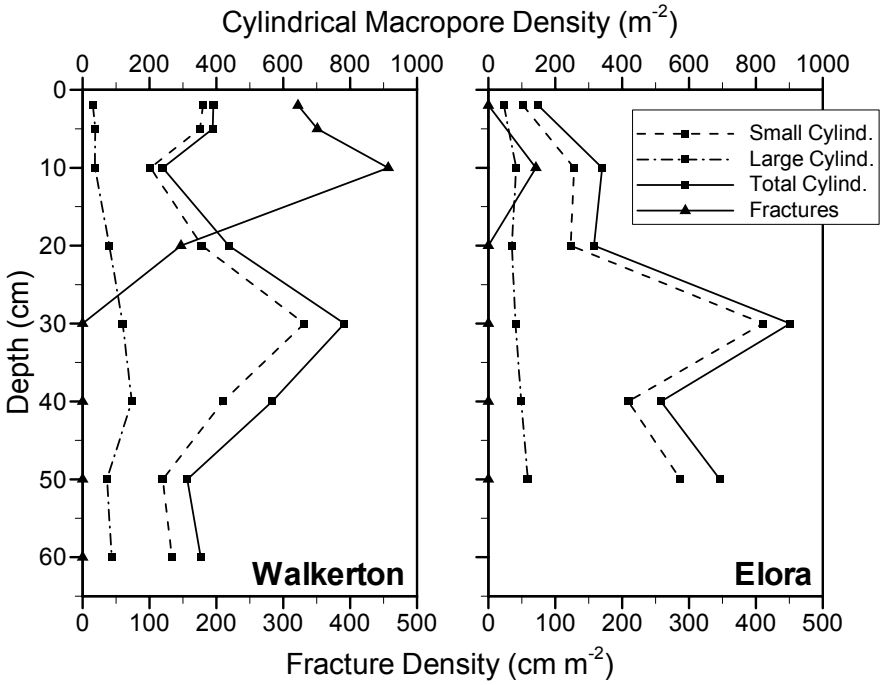

Figure 5.2. Plot of macropore density versus depth. The square (■) symbols represent linear cylindrical macropores and the triangle (▲) symbols represent planar fractures. The cylindrical macropores are subdivided further into small (dash-dot line), large (dashed line), and total (solid line) macropore numbers. Small macropores are assigned as those with diameters less than 5 mm, while large macropore diameters have diameters equal to or greater than 5 mm.

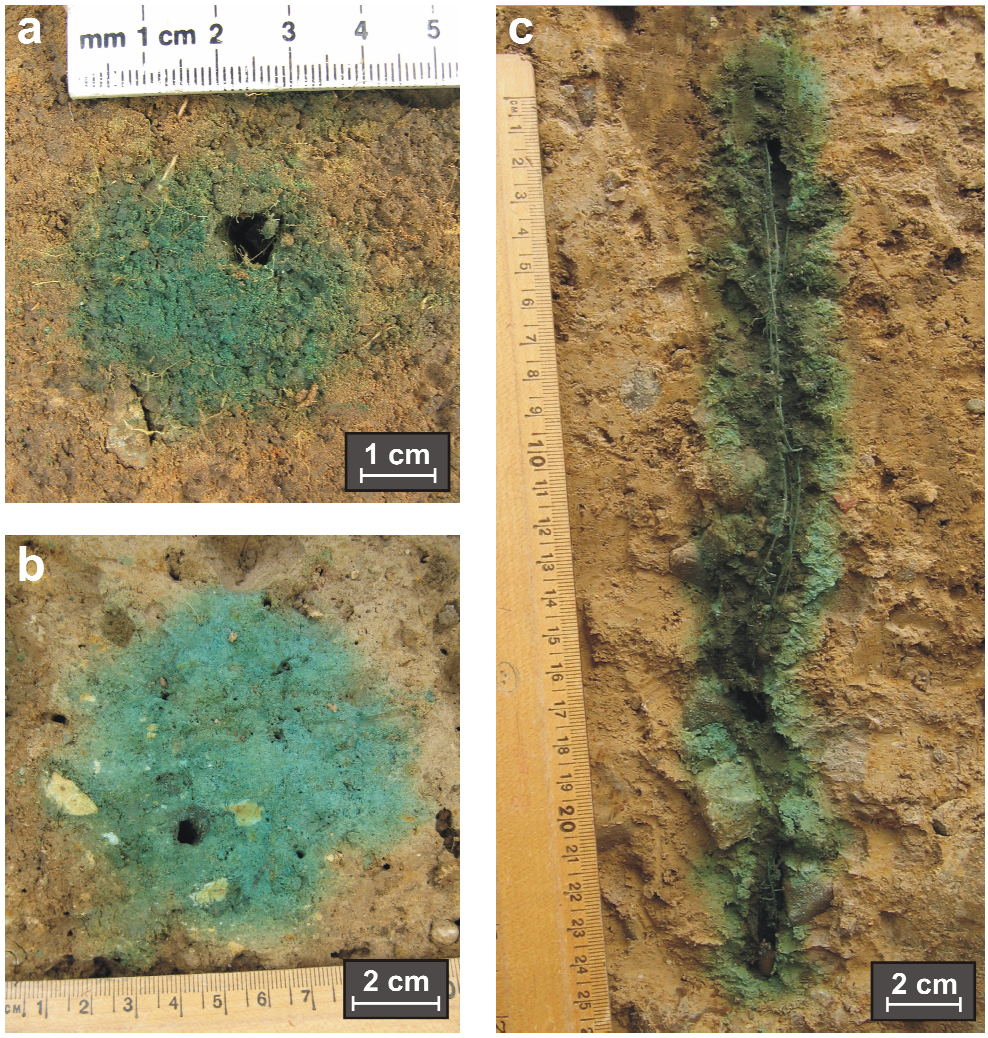

Figure 5.3. Photographs of typical earthworm burrows and associated dye stain patterns: (a) large earthworm burrow from a horizontal section at 20 cm depth from test EL-D2; (b) collection of large and small earthworm burrows on a horizontal section at 42 cm depth in test WK-RS1; and, (c) wormhole extending vertically from 25 to 50 cm depth in test WK-D4. Halos of dye stained soil surround the macropores in all photographs. Contrast the extensive coating along the burrow walls in (c) with the apparent lack of coating along the burrow shown in (a). Also, note the presence of roots growing inside the worm burrows in both (a) and (c).

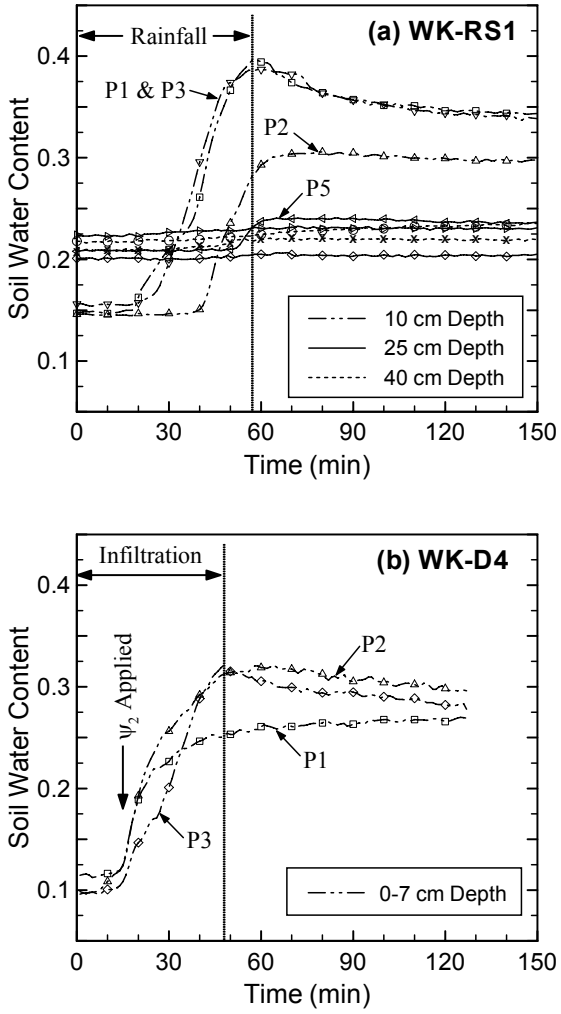

Figure 5.4. Soil water content measurements for tests (a) WK-RS1 and (b) WK-D4. Test WK-RS1 was measured using horizontally installed TDR probes at 10, 25, and 40 cm depth. Test WK-D4 was measured using inclined probes that integrated from 0 to 7 cm depth. Select TDR probe numbers are labelled and indicated with arrows (*e.g.*, P1, P2, P3 and P5 in WK-RS1).

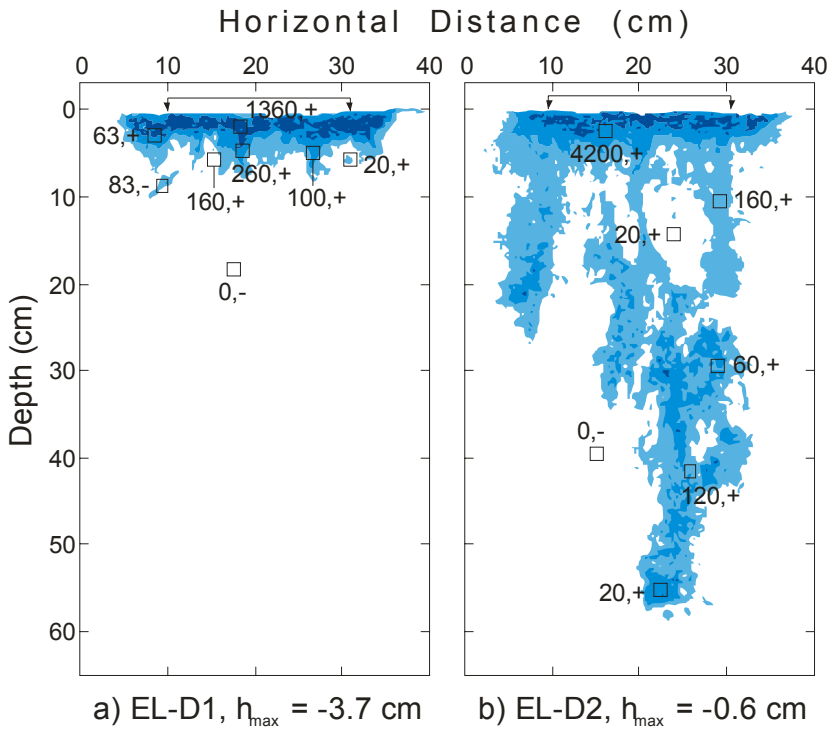

Figure 5.5. Classified dye patterns and colloid concentrations measured on vertical soil sections for the tension infiltration tests at Elora. Microsphere sample locations are indicated by squares. Next to each sample location, concentrations of the 3.7 µm microspheres are shown numerically (g^{-1} soil) and the presence (+) or absence (-) of the 0.53 µm microspheres is indicated. The dyed regions are separated into three dye intensity categories. All profiles are taken through the centre of the infiltration area with the disc location indicated on the surface.

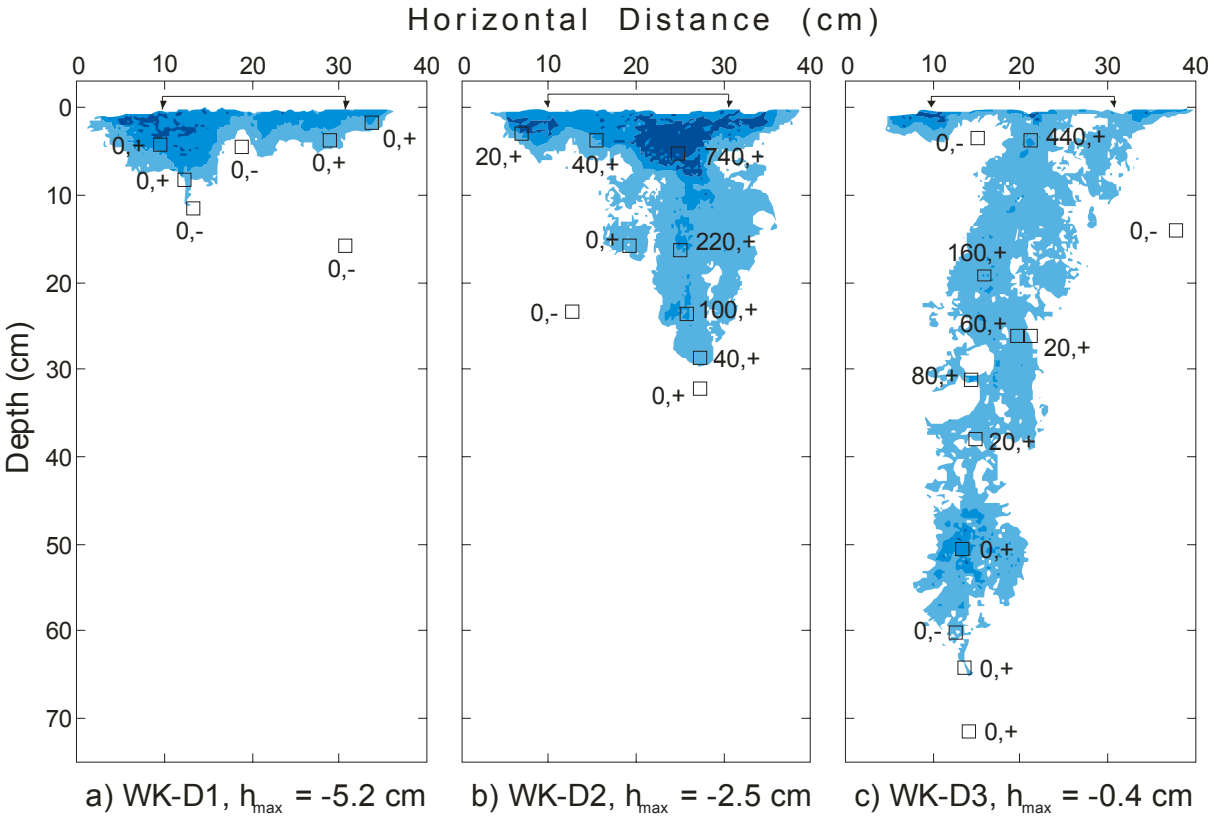

Figure 5.6. Classified dye patterns and colloid concentrations measured on vertical soil sections for the tension infiltration tests at Walkerton. Microsphere sample locations are indicated by squares. Next to each sample location, concentrations of the 3.7 µm microspheres are shown numerically (g^{-1} soil) and the presence (+) or absence (-) of the 0.53 µm microspheres is indicated. The dyed regions are separated into three concentration categories: 0.2-1.5 g/L, 1.5-3.0 g/L, and >3.0 g/L. All profiles are taken through the centre of the infiltration area with the disc location indicated on the surface.

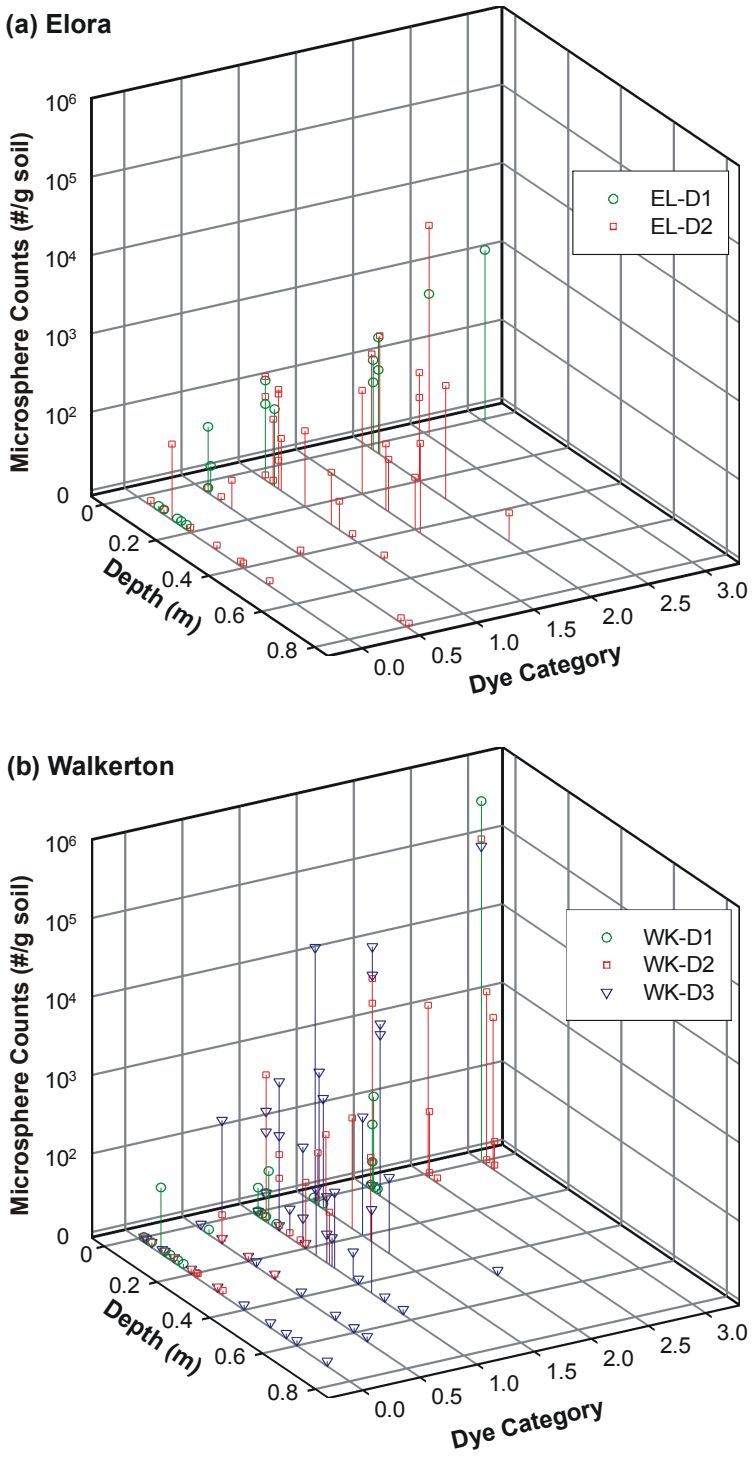

Figure 5.7. Plot of 3.7 µm diameter microsphere concentrations as a function of depth and dye stain intensity for (a) Elora and (b) Walkerton TI tests. Dye category is based on the predominant dye intensity (from image analysis) of the area from which sample was collected. Zero represents no dye staining and categories one, two, and three represent low, moderate, and heavily dye stained soils, respectively. If the sample location was nearly evenly split across two dye intensity categories, the average of the two categories was selected.

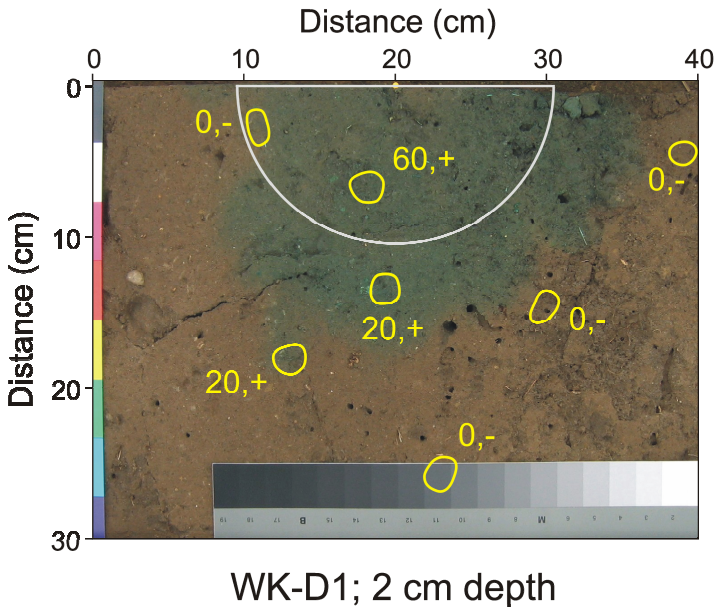

Figure 5.8. Photograph of the dye patterns on the horizontal soil section at 2 cm depth from test WK-D1. Microsphere sample locations and concentrations are overlain on the image. Concentrations of the 3.7 µm microspheres are shown numerically (g^{-1} soil) and the 0.53 µm microspheres are signified by either presence (+) or absence (-). The TI disc location is indicated by the semi-circle.

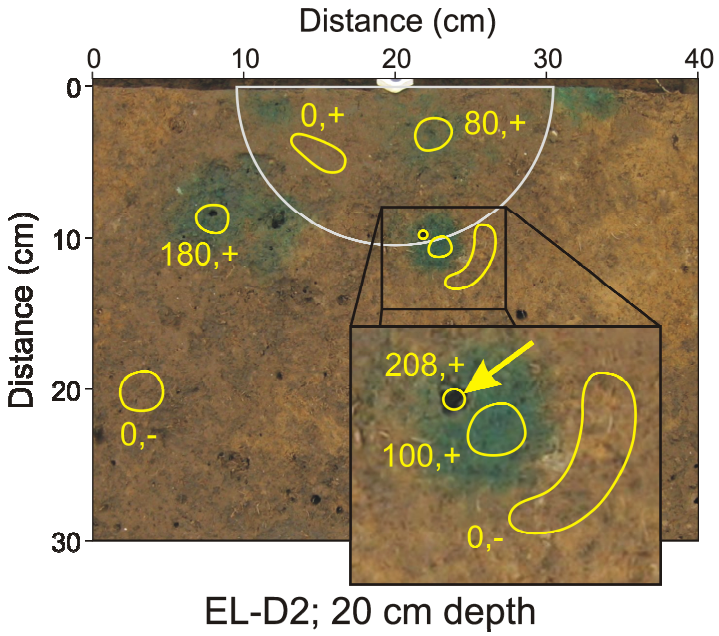

Figure 5.9. Photograph of the dye patterns on the horizontal soil section at 20 cm depth from test EL-D2. Microsphere sample locations and concentrations are overlain on the image. Concentrations of the 3.7 µm microspheres are shown numerically (g^{-1} soil) and the 0.53 µm microspheres are signified by either presence (+) or absence (-). The TI disc location is indicated by the semi-circle. The arrow points to the location of the sampled earthworm burrow.

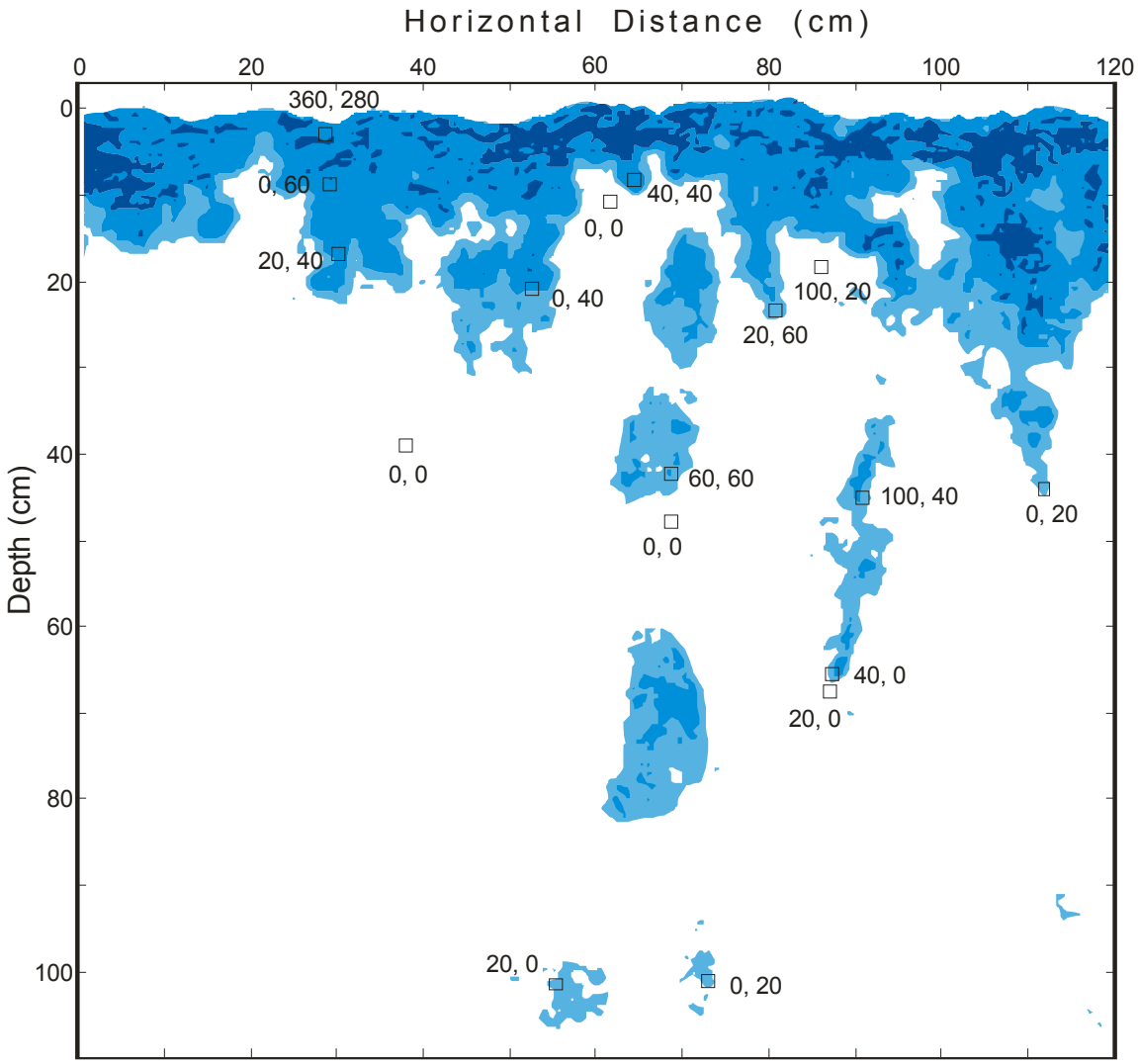

Figure 5.10. Classified dye patterns and colloid concentrations measured on a vertical soil section along the centreline of the simulated rainfall test WK-RS1. Microsphere sample locations are indicated by squares. Next to each sample location, concentrations of the 3.7 µm and 1.5 µm diameter microspheres are shown (g^{-1} soil). The dyed regions are separated into three concentration categories: 0.2-1.5 g/L, 1.5-3.0 g/L, and >3.0 g/L.

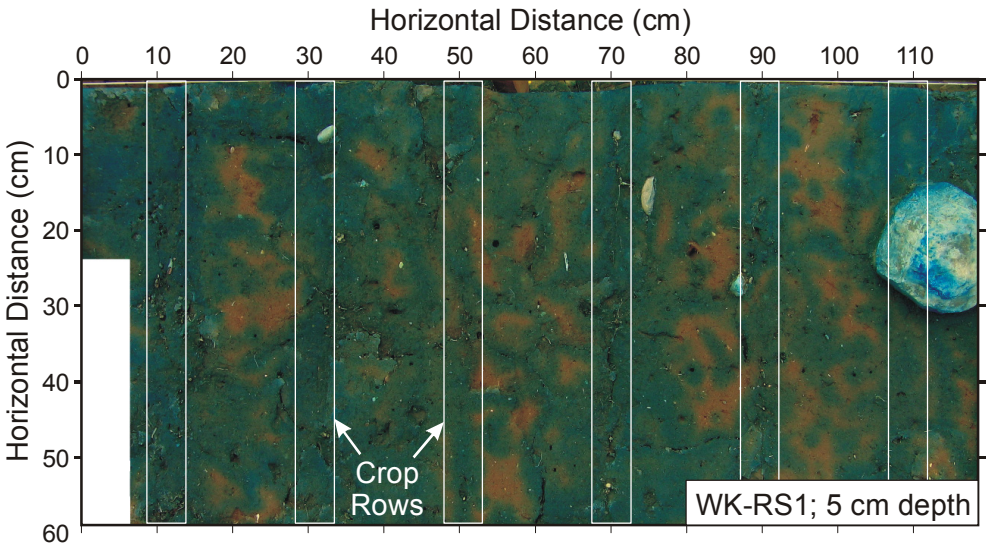

Figure 5.11. Photograph of dye patterns on the horizontal soil section at 5 cm depth from test WK-RS1. Note the increased dye intensity along the crop rows showing the influence of preferential flow along root channels.

Table 5.1. Characteristics of the infiltration tests at Elora and Walkerton.

Test	Pressure Head[a], ψ (cm H_20)	Time Period of Application (min)	Infiltration Rate[b] (cm hr^{-1})	Maximum Depth of Dye (cm)
EL-D1	-8.8	60	0.48	10
	-3.7	152	0.97	
EL-D2	-16.4	60	0.24	98
	-11.2	62	0.34	
	-4.8	65	1.15	
	-0.6	22	11.2	
WK-D1	-10.3	23	0.42	11
	-5.2	335	0.52	
WK-D2	-6.4	20	0.69	31
	-2.5	65	2.47 (4.04)[c]	
WK-D3	-11.5	15	0.45	70
	-0.4	41	4.14 (5.12)[c]	
WK-D4	-12.8	15	1.4	74
	-0.5	32.8	4.23	
WK-RS1	na	57	3.8	126

[a]The pressure head, ψ, is taken at base of the tension infiltrometer disc where it touches the glass bead contact material.
[b]Represents a quasi-steady infiltration rate for the TI tests.
[c]Value in brackets was the maximum infiltration rate observed near the end of the infiltration period.

Table 5.2. Average soil properties determined from core and bulk samples collected at the infiltration sites.

Site	Soil Horizon	Depth (cm)	Porosity ($cm^3\ cm^{-3}$)	Bulk Density ($g\ cm^{-3}$)	K_{sat} ($m\ s^{-1}$)	Clay/Silt/Sand/Gravel (%)
Elora	A	0-20	0.48	1.47	8×10^{-6}	13/64/22/1
	B	20-45	0.45	1.55	2×10^{-6}	22/46/31/1
	C	45-80	0.33	1.84	9×10^{-7}	21/44/29/6
Walkerton	A	0-25	0.45	1.48	9×10^{-5}	7/46/47/0
	B	25-45[a]	0.41	1.60	5×10^{-5}	16/36/48/0
	C	45[a]-80	0.39	1.67	6×10^{-5}	9/44/35/12

[a]The B-C soil horizon boundary at the Walkerton site varied with location from 25-55 cm below ground surface.

Table 5.3. Macropore type and density as a function of depth.

Site	Depth	Cylindrical Macropore Density			Fracture
		Small[a]	Large[b]	Total	Trace Length
	(cm)	(m^{-2})	(m^{-2})	(m^{-2})	(cm m^{-2})
Elora	2	103	46	149	0
	10	256	83	340	71
	20	246	70	316	0
	30	821	81	902	0
	40	418	98	516	0
	50	574	118	692	0
Walkerton	2	360	31	391	322
	5	351	38	389	351
	10	203	37	240	457
	20	357	80	437	147
	30	663	120	783	0
	40	420	147	567	0
	50	240	73	313	0
	60	267	87	353	0

[a]Macropores less than 5 mm in diameter, consisting of mainly wormholes and root holes.
[b]Macropores greater than 5 mm in diameter, consisting entirely of wormholes.

Chapter 6
Conclusions and Recommendations

6.1 Summary of Conclusions

An investigation of macropore flow and transport through partially saturated, low permeability soil was carried out using a combination of numerical simulations and field experiments. Overall, the results of this study indicated that macropores play an important role in controlling the rate and depth of contaminant migration.

Modelling of simple fractured systems showed that variations in matrix properties had a greater influence on flow system dynamics than fracture properties, even though the majority of vertical fluid flow occurred through the fractures. Small-scale fracture features, such as roughness and unsaturated fracture hydraulic conductivity, had relatively little influence on the bulk flow response. This is advantageous because detailed fracture geometry data, let alone fracture roughness data, is difficult to obtain in the field. It is theorized that the sensitivity to matrix properties (and insensitivity to fracture properties) is due to the significant influence of fracture-matrix interactions. Numerical simulations demonstrated that fracture-matrix interaction was a critical factor in controlling water and contaminant movement through these types of fractured flow systems. Unsaturated soils have a potentially large capacity to store infiltrating water, and as a result imbibition from the fracture into the soil matrix limited downward flow within the fractures. The coupling of macropore and matrix flow processes in the model was essential for quantifying the variability of vertical macropore and matrix fluxes, given the significant and highly transient nature of the fracture-matrix mass exchange.

In the end, numerical simulations showed that the vulnerability of overburden deposits was dependent on matrix hydraulic properties, antecedent moisture, and the density and continuity of the macropore network. Lower permeability materials were more susceptible to fast vertical transport of contaminants because the primary vertical flow mechanism switches from matrix-dominated flow in high permeability materials to fracture-dominated flow in low permeability materials. The results demonstrated that macropore flow initiation was controlled by soil pressure potentials (or saturations) and the extent of macropore-matrix interaction. As a consequence, soils with higher antecedent moisture contents were more susceptible to preferential flow and transport. This helps to explain why low intensity, long duration rainfall events, which have a greater volume of total rainfall, were more likely to result in significant macropore flow to depth. Because of the importance of macropores for water and contaminant fluxes, it is proposed that macropore continuity may be a more important

measure than soil thickness in evaluating aquifer vulnerability. This further suggests that methods for improving our ability to assess the connectivity and vertical continuity of macropores in the field are needed.

The model also showed some important features related to contaminant movement in the subsurface. Contaminants contained in the soil matrix, whether by initial infiltration into the soil or by imbibition from fractures, were not likely to be mobilized back into the fracture and thus were not subject to preferential transport. Additionally, shallow soils were particularly susceptible to rapid colloid transport (> 10 m/hr) in simulations with shallow water table conditions (i.e., wet soils). Under deeper water table conditions, the depths of colloid transport were limited by the depth of infiltrating water, which was consistent with the later field experiments.

The field infiltration experiments at Elora and Walkerton clearly demonstrated that preferential flow within partially saturated macropores can be an important process for water and contaminant migration. Earthworm burrows were the predominant macropore type and the main preferential flow pathways at both sites. The extent of preferential flow in the TI experiments was related to soil pore water pressure, with flow in macropores occurring when infiltration pressure heads were greater than -3 cm. The results demonstrated an important concept: macropores flow under negative pressure conditions and will increasingly contribute to flow as soil water potentials increase. Existing liquid-configuration models that describe saturation and flow in irregularly shaped pores could explain the observed flow behaviour. There was also clearly a soil water potential threshold at some small negative pressure head, above which macropore flow increased significantly. The implication is that surface ponding or saturation of subsurface soil layers are not prerequisites for significant preferential flow in macropores.

The infiltration tests revealed the potential for significant flow and transport to depth along macropores. Natural macroporous soils appear to have a large capacity to infiltrate water that is likely to be exceeded only during long duration or high intensity rainfall events. Flow along the earthworm burrows resulted in dye staining and microsphere transport to over 1.0 m depth. Transport was also very rapid along the macropores, with measured flow velocities in excess of 20 m/d. Although preferential flow to depths greater than 40 cm was limited to a small fraction of the visible macropores, the dye and microsphere transport observations nevertheless underscored the vulnerability of thin, macroporous soils.

Soil water content measurements and dye tracer patterns suggested a dynamic flow system that was characterized by a high degree of macropore-matrix interaction. As with the numerical experiments, imbibition from the macropores into the matrix served to limit the depth of water and

contaminant migration. This was evidenced by prominent dye stained halos surrounding individual worm burrows and increased lateral infiltration in the shallow soil matrix under drier soil conditions. The results confirm the importance of soil matrix properties in dictating preferential flow behaviour.

In all field experiments, microspheres were preferentially retained in the upper few centimeters of the soil profile, presumably by pore straining and attachment mechanisms. It was difficult to precisely determine microsphere retention mechanisms, but analysis of the data provided evidence that smaller microspheres were transported greater distances than larger microspheres. In addition, there was increased retention of microspheres at lower infiltration pressures because of increased pore straining, film straining, or air-water interface attachment at lower soil water contents. The influence of these colloid retention mechanisms was considered relatively minor, however, as nearly simultaneous transport of dye and microspheres was observed deeper in the soil profile. The strong correlation between dye and microsphere distributions at depth was attributed to the fact that the flow system in this case was governed by capillary forces. This represents a stark contrast to the solute and colloid transport behaviour observed in saturated flow systems. The results suggest that dye tracers could be used as a reasonable surrogate for short-term (i.e., event-based) colloid transport studies in the vadose zone.

The TI was an excellent tool for controlling the initiation of macropore flow and examining in situ flow processes. The infiltration of dye tracer via the TI provided a relatively simple and accurate means of evaluating the potential for macropore flow in shallow field soils. TI tests are faster and more cost-effective to conduct than artificial rainfall experiments and, although the volume of soil tested is smaller, the resulting flow and transport pathways are comparable (at least in the absence of substantial surface ponding). The TI data, however, should be used with caution when estimating unsaturated soil properties that may rely on highly simplistic assumptions which are not applicable to macroporous soils. For example, estimates of soil macroporosity using TI data are likely to underestimate the true effective macroporosity if the underlying conceptual flow model does not consider partially saturated flow within pores of all sizes (including macropores). Likewise, the TDR method was effective at measuring the water content response of the soil matrix and thus can be useful for monitoring the shallow flow system during infiltration. On the other hand, even a dense network of TDR probes is likely to be ineffective for detecting water flow along macropores deeper in the subsurface.

6.2 Recommendations for Future Research

The numerical simulations presented in this thesis were conducted by representing macropores as planar fracture features. This was based on earlier work in clay-rich deposits where fractures were

identified as the predominant macropore type. Following the field experiments, it became clear that there are situations where the majority of preferential flow occurs in cylindrical macropores. This changing conceptual model is bound to have an influence on flow and transport behaviour. For example, cylindrical macropores have a much smaller surface area to volume ratio, which may reduce the extent of macropore-matrix interaction. Future research could address the differences in flow and transport behaviour between cylindrical and planar macropore types. It is also recommended that the field infiltration experiments be simulated as the detailed data set that was collected can serve as a valuable reference for assessing the results of cylindrical macropore simulations.

It would be useful to assess the relationship between different physical parameters and their affect on macropore flow by examining several factors in combination. Numerical models are particularly well suited for this task and simulations to further quantify the relationship between rainfall intensity, rainfall duration, and antecedent soil moisture are recommended.

Colloid transport in this thesis was simulated in a highly simplistic fashion and a more realistic approach that includes relevant colloid attenuation mechanisms (i.e., filtration, film straining, a range of attachment mechanisms, etc.) is recommended for future simulations. There continue to be improvements in our understanding of colloid transport and attenuation mechanisms in partially saturated systems. Incorporating these new concepts into existing models, particularly models such as HydroGeoSphere that can properly capture the physics of macropore-matrix interactions, would undoubtedly provide new capabilities for investigating colloid transport phenomena.

Physically-based liquid configuration models for describing pressure-saturation-hydraulic conductivity relationships should be employed in numerical models. In this study, the empirical Brooks-Corey model was employed to describe partially saturated flow in macropores. Liquid-configuration models provide a more realistic description of macropore hydraulic properties. It is not clear if liquid-configuration models could improve flow predictions, but they would provide a valuable test of whether existing empirical approaches designed for porous media are appropriate for describing macropore hydraulic properties. They would also represent a valuable step toward the goal of developing a sound, physically-based model for flow and transport in macroporous soils. Liquid-configuration approaches may also provide a means of incorporating important colloid attenuation mechanisms, such as attachment to air-water interfaces, in a physically meaningful way.

There are also excellent opportunities for future field research to address several outstanding issues. First, TI experiments similar to those conducted here should be completed on a broader range of soils to examine the potential for preferential flow in different soil environments. It would be worthwhile to examine the influence of various soil features, such as soil texture, macropore type

(fracture vs. cylindrical), tillage method, or crop/root type, on flow and transport. For example, these types of tests could be conducted in sandy or layered soils to investigate other types of preferential flow (*e.g.*, fingering, funnel flow). Further to this point, future investigations into the influence of antecedent moisture on macropore flow and transport are recommended. The results presented in this study generally supported the idea that increasing soil water content resulted in increased preferential flow within macropores, but the field evidence was by no means conclusive. For example, in comparing tests at Walkerton with similar infiltration pressures, there appeared to be more shallow lateral flow in the drier soil, but the overall depth of dye staining in the macropores was not significantly different. Given that some other studies in the literature have identified increased macropore flow under drier soil conditions, further field-based studies are warranted.

The design of the TI also provides some unique opportunities for field investigations. In particular, the ability of the TI to conduct infiltration experiments on exposed soil sections represents a significant opportunity to examine the development of flow under transient conditions. Similarly, the non-destructive nature of the TI tests allows repeated infiltration measurements over time. Field investigations could be designed to evaluate the development of macroporosity over the course of the growing season, for example. Finally, the ability to control the degree of macropore flow using various infiltration pressures could be used to determine the thresholds of rainfall intensity and duration required for the onset of macropore flow in different soils.

This study has shown that macropores were significant pathways for water and contaminant movement in soils to depths of over one meter. However, it remains to be seen what affect the macropores will have on field-scale transport to underlying aquifers and several questions remain. How deep can macropores effectively transport contaminants? Are the cumulative mass fluxes through the macropores significant at a field scale? What happens to the contaminants once they reach the water table or an aquifer? Investigations designed to answer these questions, particularly at field sites with documented cases of aquifer contamination (i.e., Walkerton), would be highly beneficial.

Appendix A
HydroGeoSphere Modifications and Model Input Parameters

All numerical simulations were conducted using HydroGeoSphere with select modifications as described in Chapter 2. These modifications included the following:

- Using a modified form of the van Genuchten-Mualem to describe soil matrix constitutive relations (after Vogel et al., 2001);
- Incorporation of fracture roughness by assigning spatially variable apertures within the fracture plane;
- Application of the Brooks-Corey model to describe the constitutive relations for the fracture on an element-by-element basis; and,
- Adding the ability to numerically monitor vertical water and tracer fluxes crossing a plane and separating the fracture and matrix contributions.

The above noted modifications were implemented either by modifying the original model code or by varying model input data. The executable code for the modified version of the model was designated "Grok_cey.EXE" and "Hydro_cey.EXE" to distinguish it from the original version.

The model input parameters for all simulations presented in Chapter 2 are provided in tabulated form on the following page.

Table A.1. Model input parameters for simulations in Chapter 2.

No.	HS Filename	Sensitivity Tested	Sol'n Mode[a]	Model Grid Dimensions			Model Element Size			No. of Fractures	Initial Conditions		Boundary Conditions		
											Initial Total Head	Water Table Depth	Upper Bound Const. Flux	Flux Duration	Lower Bound Const. Head
				x (m)	y (m)	z (m)	Δx (m)	Δy (m)	Δz (m)		(m)	(m)	(m/day)	(d)	(m)
Base	Base01	Base Case	FD	0.5	0.5	2.0	0.02	0.002 to 0.02	0.02	1	-1.0	3.0	0.05	entire (5 d)	-1.0
1	C01_Ksat	Matrix Ksat (10x smaller)	FD	0.5	0.5	2.0	0.02	0.002 to 0.02	0.02	1	-1.0	3.0	0.05	entire (5 d)	-1.0
2	C02_Ksat	Matrix Ksat (10x larger)	FD	0.5	0.5	2.0	0.02	0.002 to 0.02	0.02	1	-1.0	3.0	0.05	entire (5 d)	-1.0
3	C03_VG	VG α (2x), n (+0.5)	FD	0.5	0.5	2.0	0.02	0.002 to 0.02	0.02	1	-1.0	3.0	0.05	entire (5 d)	-1.0
4	C04_VG	VG α (0.5x), n (-0.2)	FD	0.5	0.5	2.0	0.02	0.002 to 0.02	0.02	1	-1.0	3.0	0.05	entire (5 d)	-1.0
5	C05_bmean	Mean aperture (0.5x)	FD	0.5	0.5	2.0	0.02	0.002 to 0.02	0.02	1	-1.0	3.0	0.05	entire (5 d)	-1.0
6	C06_bmean	Mean aperture (2x)	FD	0.5	0.5	2.0	0.02	0.002 to 0.02	0.02	1	-1.0	3.0	0.05	entire (5 d)	-1.0
6b	C06b_200pp	Mean aperture (2x), parallel plate	FD	0.5	0.5	2.0	0.02	0.002 to 0.02	0.02	1	-1.0	3.0	0.05	entire (5 d)	-1.0
7	C07_bvar	Aperture variance (2.25x)	FD	0.5	0.5	2.0	0.02	0.002 to 0.02	0.02	1	-1.0	3.0	0.05	entire (5 d)	-1.0
8	C08_pp	Aperture variance (none), parallel plates	FD	0.5	0.5	2.0	0.02	0.002 to 0.02	0.02	1	-1.0	3.0	0.05	entire (5 d)	-1.0
9	C09_WT	Water table (depth = 1 m)	FD	0.5	0.5	2.0	0.02	0.002 to 0.02	0.02	1	1.0	1.0	0.05	entire (5 d)	1.0
10	C10_WT	Water table (depth = 5 m)	FD	0.5	0.5	2.0	0.02	0.002 to 0.02	0.02	1	-3.0	5.0	0.05	entire (5 d)	-3.0
11	C11_Prec	Precip: int (2.5x), dur (0.2x)	FD	0.5	0.5	2.0	0.02	0.002 to 0.02	0.02	1	-1.0	3.0	0.125	1.0 d	-1.0
12	C12_Prec	Precip: int (24x), dur (0.0083x)	FD	0.5	0.5	2.0	0.02	0.002 to 0.02	0.02	1	-1.0	3.0	1.20	0.041667 d (1 hr)	-1.0
13	C13_bmean	Mean aperture (4x)	FD	0.5	0.5	2.0	0.02	0.002 to 0.02	0.02	1	-1.0	3.0	0.05	entire (5 d)	-1.0

No.	HS Filename	Matrix Properties							Fracture Properties						Model Run Time
		Ksat	Specific Storage, Ss	Porosity, θsat	Mprops Matrix Filename	Residual Water Content, θres	VGM[b] alpha, α	VGM[b] n	Geometric Mean Aperture, b	Variance of ln (b)	Spatial Corr. Length	Aperture Field Filename	Residual Saturation	BC[c] λ	
		(m/day)	(1/m)	(-)		(-)	(1/m)	(-)	(mm)	(-)	(m)		(-)	(-)	(hr)
Base	Base01	0.02	1.00E-04	0.4	MatrixMod01	0.08	1	1.5	0.100	0.64	0.1	Base.real.2.hfld	0.05	4.0	6.54
1	C01_Ksat	0.002	1.00E-04	0.4	MatrixMod01	0.08	1	1.5	0.100	0.64	0.1	Base.real.2.hfld	0.05	4.0	43.22
2	C02_Ksat	0.2	1.00E-04	0.4	MatrixMod01	0.08	1	1.5	0.100	0.64	0.1	Base.real.2.hfld	0.05	4.0	0.78
3	C03_VG	0.02	1.00E-04	0.4	MatrixMod02	0.08	2	2.0	0.100	0.64	0.1	Base.real.2.hfld	0.05	4.0	10.90
4	C04_VG	0.02	1.00E-04	0.4	MatrixMod03	0.08	0.5	1.3	0.100	0.64	0.1	Base.real.2.hfld	0.05	4.0	4.63
5	C05_bmean	0.02	1.00E-04	0.4	MatrixMod01	0.08	1	1.5	0.050	0.64	0.1	aper50.real.2.hfld	0.05	4.0	7.26
6	C06_bmean	0.02	1.00E-04	0.4	MatrixMod01	0.08	1	1.5	0.200	0.64	0.1	aper200.real.2.hfld	0.05	4.0	6.17
6b	C06b_200pp	0.02	1.00E-04	0.4	MatrixMod01	0.08	1	1.5	0.200	na	na	na	0.05	4.0	3.49
7	C07_bvar	0.02	1.00E-04	0.4	MatrixMod01	0.08	1	1.5	0.100	1.44	0.1	var144.real.2.hfld	0.05	4.0	7.36
8	C08_pp	0.02	1.00E-04	0.4	MatrixMod01	0.08	1	1.5	0.100	na	na	na	0.05	4.0	3.61
9	C09_WT	0.02	1.00E-04	0.4	MatrixMod01	0.08	1	1.5	0.100	0.64	0.1	Base.real.2.hfld	0.05	4.0	11.75
10	C10_WT	0.02	1.00E-04	0.4	MatrixMod01	0.08	1	1.5	0.100	0.64	0.1	Base.real.2.hfld	0.05	4.0	11.93
11	C11_Prec	0.02	1.00E-04	0.4	MatrixMod01	0.08	1	1.5	0.100	0.64	0.1	Base.real.2.hfld	0.05	4.0	9.62
12	C12_Prec	0.02	1.00E-04	0.4	MatrixMod01	0.08	1	1.5	0.100	0.64	0.1	Base.real.2.hfld	0.05	4.0	68.30
13	C13_bmean	0.02	1.00E-04	0.4	MatrixMod01	0.08	1	1.5	0.400	0.64	0.1	aper400.real.2.hfld	0.05	4.0	5.63

[a]All final simulations were conducted using finite difference solution mode.

[b]Parameters of the van Genuchten-Mualem model that define the constitutive relations between capillary pressure, saturation, and relative hydraulic conductivity for the matrix.

[c]Brooks-Corey model parameter defining the constitutive relations between capillary pressure, saturation, and relative hydraulic conductivity for the fracture.

Shaded regions indicate the model input parameters that were modified from the Base Case.

Appendix B
Image Analysis Methods

The image analysis procedures used closely followed those outlined by Weiler and Fluhler [2004] and, to a lesser extent, Forrer et al. [2000], with selected modifications to improve discrimination of dye patterns and ensure consistency between images. All images underwent the following procedures: geometric correction, background subtraction, color adjustment, histogram stretching, dye classification, and a final visual check. Image processing was completed using IDL software (ITT Visual Information Solutions version 6.2) along with standard photo-editing software packages.

The images were corrected for geometric distortion by picking "tie points" at known locations along the graduated grey frame. The selected tie points are fitted with a first degree polynomial using least squares regression, resulting in a linear geometric transformation to the true coordinates. The colors in the corrected image are assigned using nearest neighbour sampling, which preserves the color information from the original image. The spatial resolution of the images is reduced during geometric correction with each pixel in the corrected images representing 0.5 x 0.5 mm on the soil sections.

A technique known as background subtraction was used to correct for uneven lighting of the images. First, the image was converted from RGB (red-green-blue) to HSV (hue-saturation-value) color space. The gray frame that surrounded the soil profile is considered to have a constant brightness or value (V). A total of 24 (horizontal sections) to 30 (vertical sections) points were selected along the gray frame, fitted with a smooth quintic surface, and normalized by dividing through by the mean V of the selected points. Corrected V-space values were then calculated for each pixel by dividing the V-space values from the original image by the normalized V-space values. The corrected V-space values were then recombined with the original H and S terms, and the image was converted back into RGB color space.

Color adjustment and histogram stretching were then applied to ensure consistency of color and contrast between images. Color adjustment (also referred to as white balance) corrects for color tints that may appear in the images as a result of the changing spectral composition of daylight. The first step in proper color adjustment was applied in the field, by setting a custom white balance on the camera immediately prior to photographing each soil profile. During image processing, minor color adjustments were made using the Kodak gray scale, which consists of 20 gray level patches from white to black. By definition, each grey patch should have equal R, G, and B values. To apply a

correction the mean RGB value was calculated for 10 of the 20 reference gray patches (i.e., every second patch beginning with the darkest). Correction factors were calculated for all color channels by dividing the mean RGB value for each patch by the actual values from the R, G, and B channels, respectively. For each color channel, a third-degree polynomial was fitted to the calculated correction factors in order to estimate a correction factor over the full color scale (0 to 255). The final RGB values for each pixel were calculated as the original R, G, or B pixel value multiplied by the interpolated correction factor for the same color channel.

Each of the R, G, and B color channels can be represented as a histogram of values ranging from 0 to 255. The histograms were stretched to consistent values for all images. For all color channels, the histograms were adjusted so that the value of the darkest gray patch (no. 19) was set to 35 and the second lightest patch (no. 1) was set to 255. All remaining values were linearly scaled relative to these two set points. This approach differs from the methods of Weiler and Fluhler [2004] and Forrer et al. [2000], where all values were scaled between 0 and 255. The lower limit of 35 for the dark region of the images was selected as it was close to the mean RGB value of the darkest patch for all images. It was found that stretching the RGB values for the darkest color patch to zero tended to result in undesirable shifts of hue in the HSV color space, where classification of the dye stained regions is conducted. Many images had dark regions, especially in heavily dye stained A horizon soils, where the RGB values for pixels were less than the mean RGB value of the darkest gray patch. Setting the darkest gray scale patch to zero would result in the R, G, and B values for these pixels being clipped to zero, since they cannot have negative values. Depending on the color of the pixels, the R, G, and B values would be clipped to varying degrees, resulting in unwanted shifts in hue and poorer discrimination of dye stain patterns. As a final step, the fully corrected images were cropped to the inside of the gray frame and all non-soil regions (*e.g.*, Kodak scales, nameplates, vegetation and objects above the soil surface) were blanked from the images by designating them as white (R=G=B=255).

A variety of methods are available for classification and quantification of dye patterns in soil [*Aeby et al.*, 1997; *Ewing and Horton*, 1999; *Forrer et al.*, 2000; *Weiler and Fluhler*, 2004; *Persson*, 2005]. A slightly modified version of the method of Weiler and Fluhler [2004] was adopted for this study because it provides a relatively simple, objective means of discriminating dyed versus non-dyed soil, while also providing additional information on dye concentrations and patterns within stained regions. Weiler and Fluhler [2004] define a threshold variable T related to the intensity of visible dye staining. After examining several combinations of variables, in both RGB and HSV color space, T was calculated as

$$T = \sin\left(\frac{H \cdot \pi}{360}\right)(1 - V) \cdot 100 \quad (1)$$

where H and V are the hue and value, respectively of each pixel in HSV color space. A threshold range was specified based on the calculated T values and a conditional dilation algorithm was applied to separate dyed from non-dyed soil. At the Walkerton site, dye calibration patch images were used to further classify the dye stained soil regions into three concentration categories: 0.2-1.5 g/L, 1.5-3.0 g/L, and >3.0 g/L. A 5 x 5 median filter was applied to remove spurious pixels while preserving edge detail. Finally, the classified images were compared to the original unclassified images and underwent visual inspection to remove obviously misclassified pixel regions. The area of misclassified pixels was small in all images and generally limited to very dark soil regions (*e.g.*, shadows) or stained areas around cobbles and rocks.

References

Aeby, P., J. Forrer, C. Steinmeier, and H. Fluhler (1997), Image analysis for determination of dye tracer concentrations in sand columns, *Soil Sci. Soc. Am. J.*, *61*(1-2), 33-35.

Ewing, R.P. and R. Horton (1999), Discriminating dyes in soil with color image analysis, *Soil Sci. Soc. Am. J.*, *63*(1), 17-24.

Forrer, I., A. Papritz, R. Kasteel, H. Fluehler, and D. Luca (2000), Quantifying dye tracers in soil profiles by image processing, *Eur. J. Soil Sci.*, *51*(2), 313-322.

Persson, M. (2005), Accurate dye tracer concentration estimations using image analysis, *Soil Sci. Soc. Am. J.*, *69*(4), 967-975.

Weiler, M. and H. Fluhler (2004), Inferring flow types from dye patterns in macroporous soils, *Geoderma*, *120*(1-2), 137-153.

Appendix C
Soil Sampling Data

Soil physical property data measured on samples collected from the Elora and Walkerton sites is provided on the following pages. This includes:

- Grain size distribution curves measured on bulk soil;
- Soil water retention curves measured on soil core samples;
- Best-fit van Genuchten-Mualem parameters to the average soil water retention curves for each soil horizon; and,
- Hydraulic conductivity measurements.

Grain Size Distribution Curves

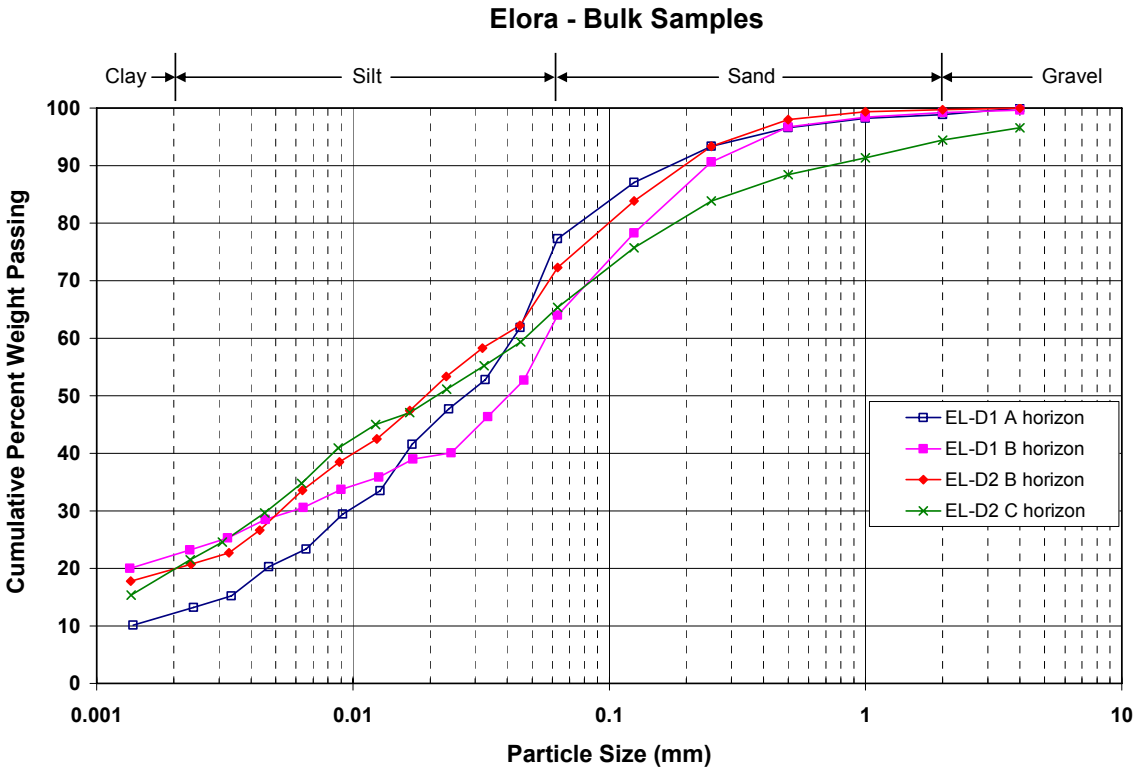

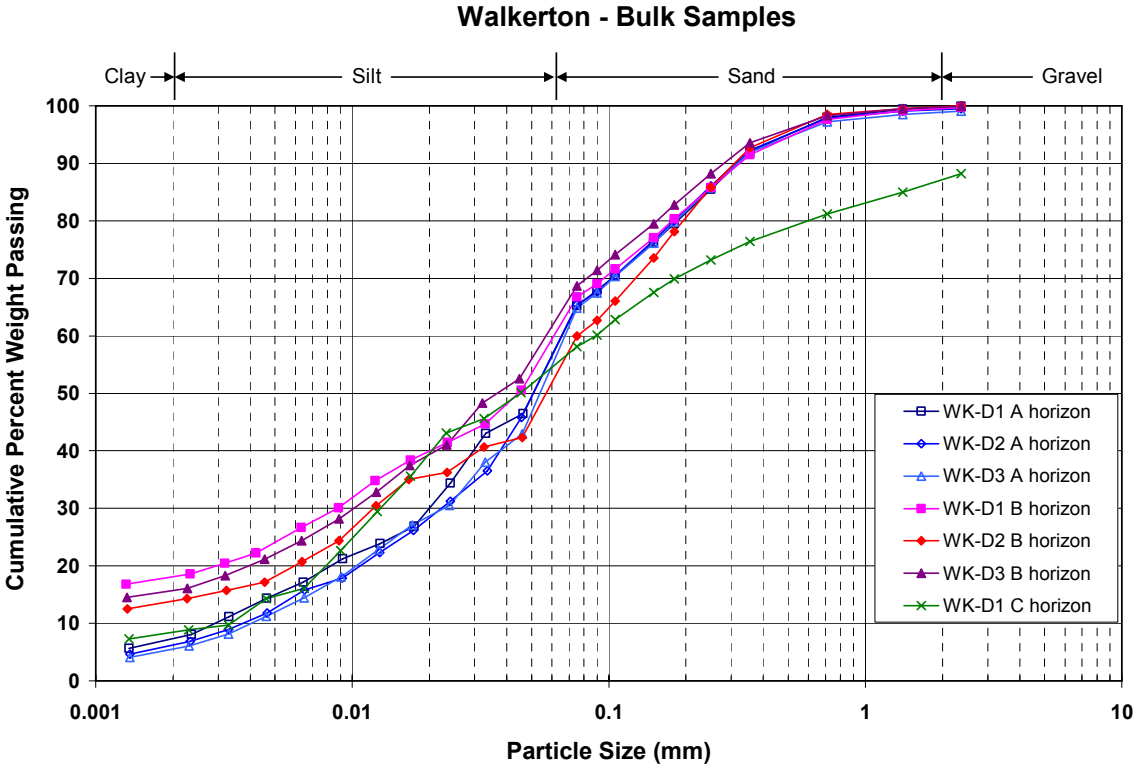

Soil Water Retention Curves

Elora

Core No.	Core Name	Volumetric Water Content (cm^3 cm^{-3}) at Different Potentials					
		0 m (0 kPa) (0 bar)	0.1 m (1 kPa) (0.01 bar)	0.2 m (2 kPa) (0.02 bar)	0.5 m (5 kPa) (0.05 bar)	1 m (10 kPa) (0.1 bar)	3 m (30 kPa) (0.3 bar)
1	ELD1-A1	0.467	0.428	0.428	0.373	0.342	0.281
2	ELD1-A2	0.537	0.434	0.405	0.346	0.316	0.258
3	ELD2-A1	0.480	0.456	0.454	0.395	0.366	0.313
4	ELD2-A2	0.439	0.392	0.390	0.347	0.326	0.294
5	ELD1-B1	0.459	0.423	0.417	0.371	0.343	0.287
6	ELD1-B2	0.428	0.375	0.357	0.309	0.284	0.240
7	ELD2-B1	0.461	0.422	0.409	0.367	0.344	0.299
8	ELD2-B2	0.449	0.381	0.365	0.315	0.288	0.233
9	ELD1-C1	0.321	0.286	0.278	0.253	0.239	0.209
10	ELD2-C1	0.342	0.288	0.271	0.234	0.217	0.181
Avg A Horizon		**0.481**	**0.428**	**0.419**	**0.365**	**0.338**	**0.286**
Avg B Horizon		**0.449**	**0.400**	**0.387**	**0.340**	**0.315**	**0.265**
Avg C Horizon		**0.331**	**0.287**	**0.275**	**0.243**	**0.228**	**0.195**

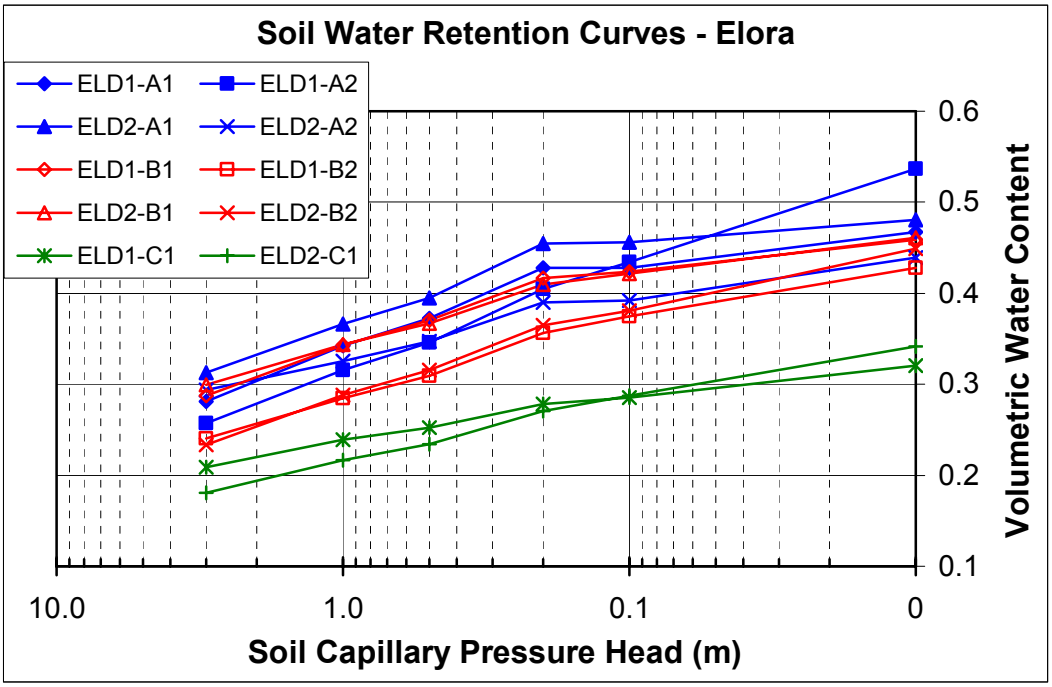

Walkerton

Core No.	Core Name	Volumetric Water Content (cm^3 cm^{-3}) at Different Potentials					
		0 m (0 kPa) (0 bar)	0.1 m (1 kPa) (0.01 bar)	0.2 m (2 kPa) (0.02 bar)	0.5 m (5 kPa) (0.05 bar)	1 m (10 kPa) (0.1 bar)	3 m (30 kPa) (0.3 bar)
1	WKD1-A1	0.467	0.421	0.416	0.377	0.349	0.299
3	WKD2-A1	0.492	0.472	0.467	0.417	0.381	0.325
5	WKD3-A1	0.444	0.406	0.410	0.385	0.362	0.314
8	WKD4-A1	0.438	0.423	0.423	0.395	0.372	0.329
9	WKD4-A2	0.414	0.409	0.415	0.385	0.359	0.311
2	WKD1-B1	0.403	0.354	0.345	0.317	0.296	0.247
4	WKD2-B1	0.402	0.355	0.346	0.314	0.291	0.252
6	WKD3-B1	0.421	0.378	0.370	0.342	0.324	0.288
7	WKD3-C1	0.425	0.396	0.391	0.371	0.355	0.321
10	WKD4-C1	0.348	0.316	0.304	0.275	0.255	0.217
	Avg A Horizo	**0.451**	**0.426**	**0.426**	**0.392**	**0.365**	**0.316**
	Avg B Horizo	**0.409**	**0.362**	**0.354**	**0.325**	**0.304**	**0.263**
	Avg C Horizo	**0.387**	**0.356**	**0.347**	**0.323**	**0.305**	**0.269**

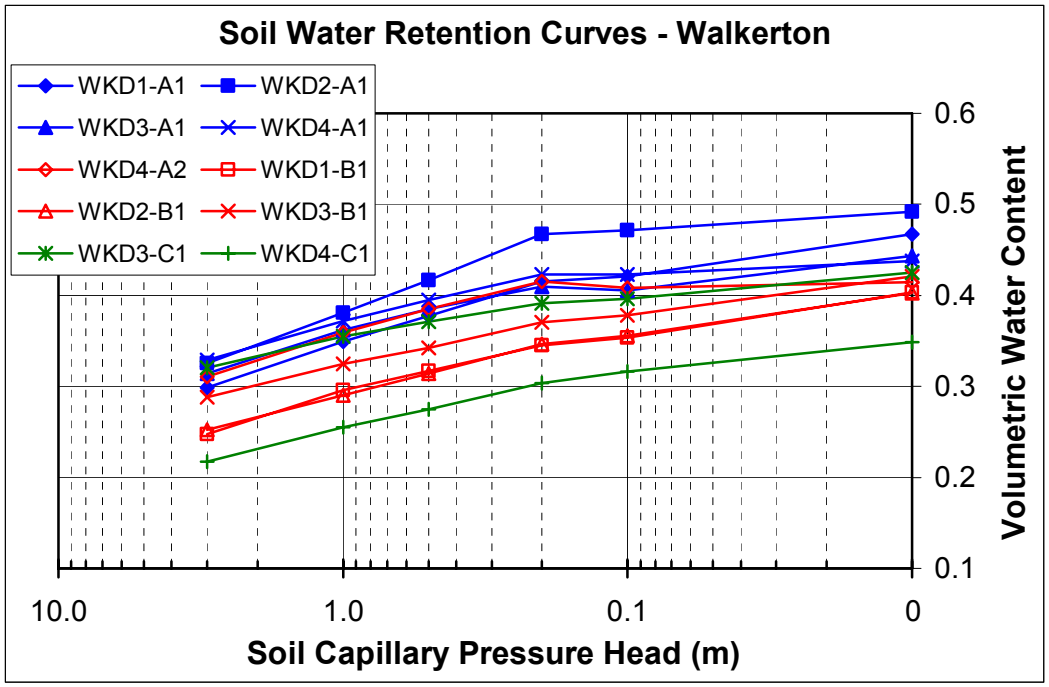

Best Fit van Genuchten-Mualem Parameters

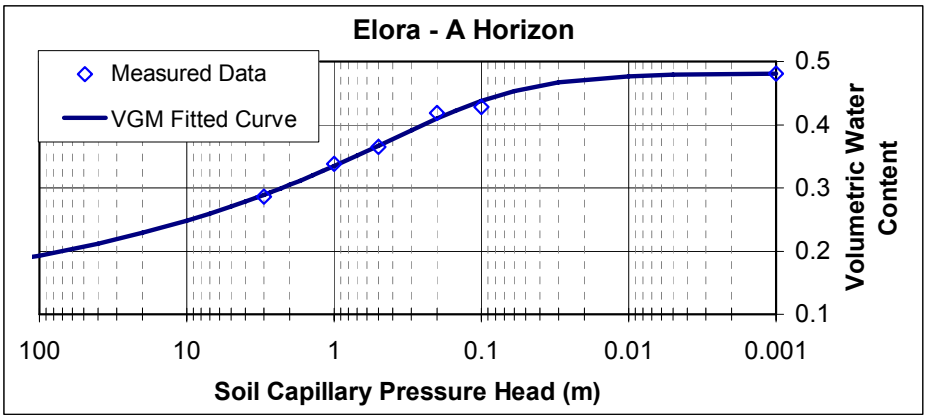

VGM Model Parameters

Fitted
α = 10.3 m^{-1}
n = 1.20

Measured/Fixed
θ_{res} = 0.10
θ_{sat} = 0.48

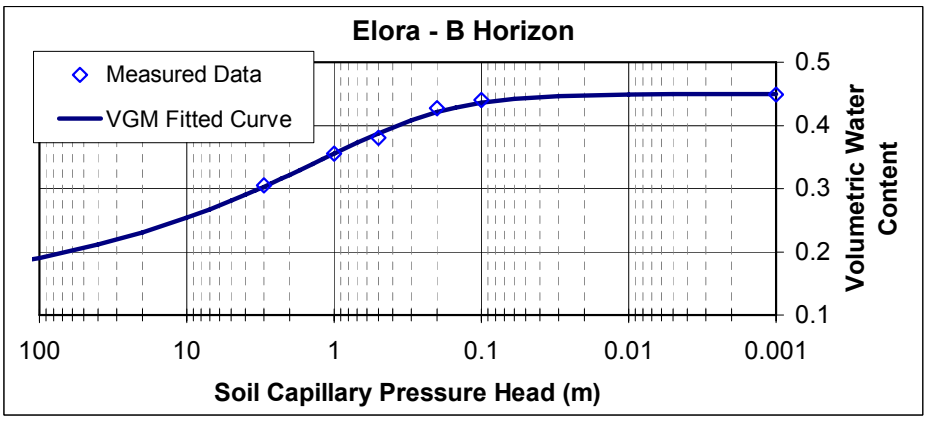

VGM Model Parameters

Fitted
α = 3.20 m^{-1}
n = 1.24

Measured/Fixed
θ_{res} = 0.10
θ_{sat} = 0.45

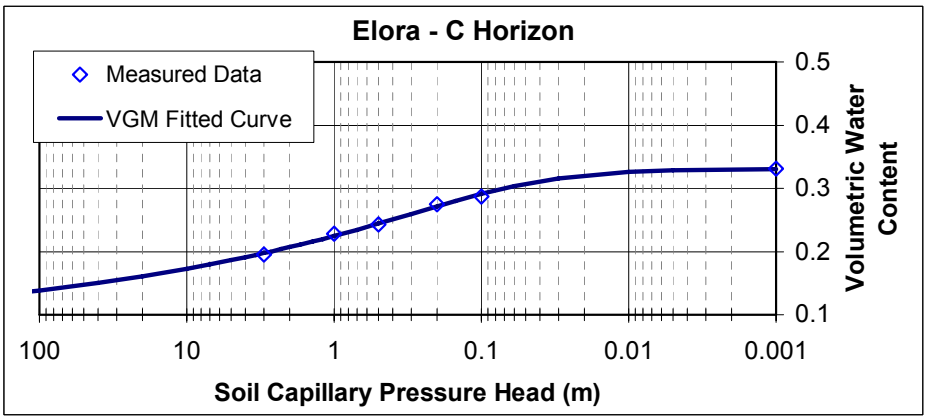

VGM Model Parameters

Fitted
α = 17.9 m^{-1}
n = 1.18

Measured/Fixed
θ_{res} = 0.07
θ_{sat} = 0.33

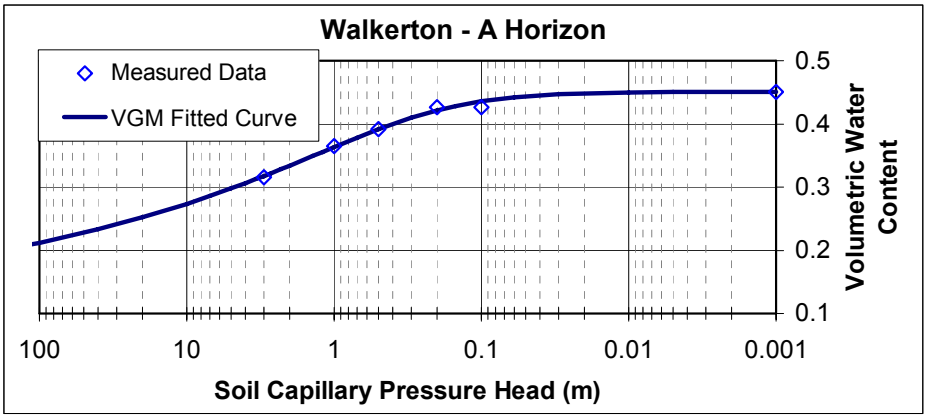

VGM Model Parameters

Fitted
α = 3.81 m^{-1}
n = 1.19

Measured/Fixed
θ_{res} = 0.10
θ_{sat} = 0.45

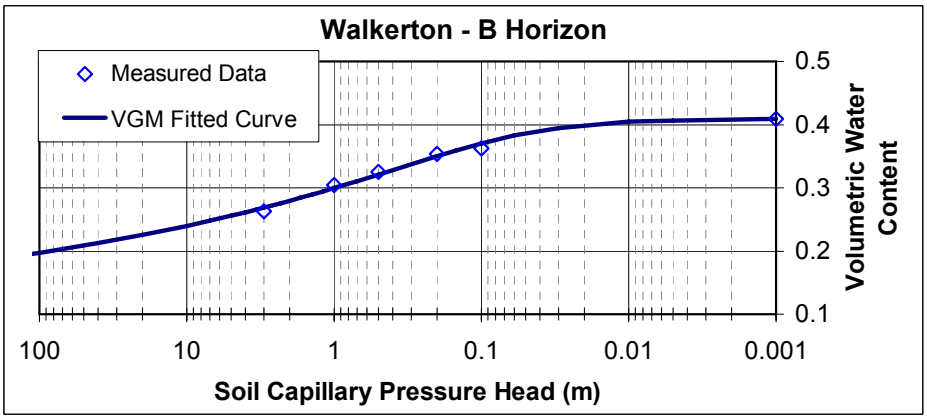

VGM Model Parameters

Fitted
α = 15.6 m^{-1}
n = 1.16

Measured/Fixed
θ_{res} = 0.10
θ_{sat} = 0.41

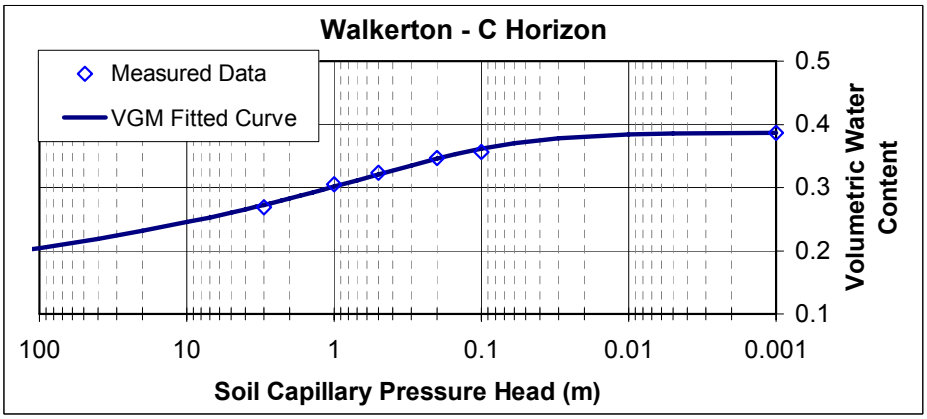

VGM Model Parameters

Fitted
α = 10.7 m^{-1}
n = 1.15

Measured/Fixed
θ_{res} = 0.10
θ_{sat} = 0.39

Hydraulic Conductivity Measurements

Table C.1. Hydraulic conductivity measurements from laboratory permeameter tests on intact soil cores from the Elora and Walkerton sites.

Site	Core Name	Soil Horizon	Hydraulic Conductivity, K_{sat} (m/s)
Elora	ELD1-A1	A	7.3×10^{-7}
	ELD1-A2	A	3.6×10^{-6}
	ELD2-A1	A	3.1×10^{-4}
	ELD2-A2	A	3.8×10^{-6}
	ELD1-B1	B	2.4×10^{-6}
	ELD1-B2	B	8.2×10^{-7}
	ELD2-B1	B	2.6×10^{-6}
	ELD2-B2	B	1.1×10^{-6}
	ELD1-C1	C	8.6×10^{-7}
	ELD2-C1	C	9.6×10^{-7}
Walkerton	WKD1-A1	A	6.9×10^{-5}
	WKD2-A1	A	8.0×10^{-5}
	WKD3-A1	A	1.8×10^{-4}
	WKD4-A1	A	1.0×10^{-4}
	WKD4-A2	A	7.5×10^{-5}
	WKD1-B1	B	2.7×10^{-5}
	WKD2-B1	B	4.0×10^{-5}
	WKD3-B1	B	1.1×10^{-4}
	WKD3-C1	C	9.2×10^{-5}
	WKD4-C1	C	4.3×10^{-5}

Elora results were obtained from constant head tests and are given as the geometric mean of 12 repetitions (2 applied heads x 6 repetitions per head).

Walkerton results were obtained from falling head tests and are given as the geometric mean of 3 repetitions.

Appendix D

Dye Classified Soil Sections

The following tables list the soil sections on which image analysis was completed at the Elora and Walkerton sites. Figures showing the classified dye patterns are provided on the pages that follow.

Site	Test Number	Section Name	Horizontal or Vertical?	Distance or Depth[a] (cm)
Elora	D1	EL-D1V00	V	0
		EL-D1V10	V	10
		EL-D1H02	H	0
		EL-D1H04	H	2
		EL-D1H07	H	5
	D2	EL-D2V00	V	0
		EL-D2V10	V	10
		EL-D2H02	H	0
		EL-D2H04	H	2
		EL-D2H07	H	5
		EL-D2H12	H	10
		EL-D2H22	H	20
		EL-D2H32	H	30
		EL-D2H42	H	40
		EL-D2H52	H	50

[a]Refers to the distance from the centre of the infiltration area (TI disc) for vertical sections or the depth below ground surface for horizontal sections.

Site	Test Number	Section Name	Horizontal or Vertical?	Distance or Depth[a] (cm)
Walkerton	D1	WK-D1V00	V	0
		WK-D1V10	V	10
		WK-D1H00	H	0
		WK-D1H02	H	2
		WK-D1H05	H	5
	D2	WK-D2V00	V	0
		WK-D2V10	V	10
		WK-D2H00	H	0
		WK-D2H02	H	2
		WK-D2H05	H	5
		WK-D2H10	H	10
		WK-D2H20	H	20
		WK-D2H30	H	30
	D3	WK-D3V00	V	0
		WK-D3V10	V	10
		WK-D3V20	V	20
		WK-D3H00	H	0
		WK-D3H02	H	2
		WK-D3H05	H	5
		WK-D3H10	H	10
		WK-D3H20	H	20
		WK-D3H30	H	30
		WK-D3H40	H	40
		WK-D3H50	H	50
		WK-D3H60	H	60
	D4	WK-D4V00	V	0
		WK-D4H00	H	0
		WK-D4H10	H	10
	RS1	WK-RS1V00	V	0[b]
		WK-RS1H05	H	5
		WK-RS1H20	H	20
		WK-RS1H42	H	42

[a]Refers to the distance from the centre of the infiltration area (TI disc) for vertical sections or the depth below ground surface for horizontal sections.
bVertical soil section taken through the centre of the simulated rainfall infiltration plot.

Dye Test EL-D1

Vertical Soil Sections

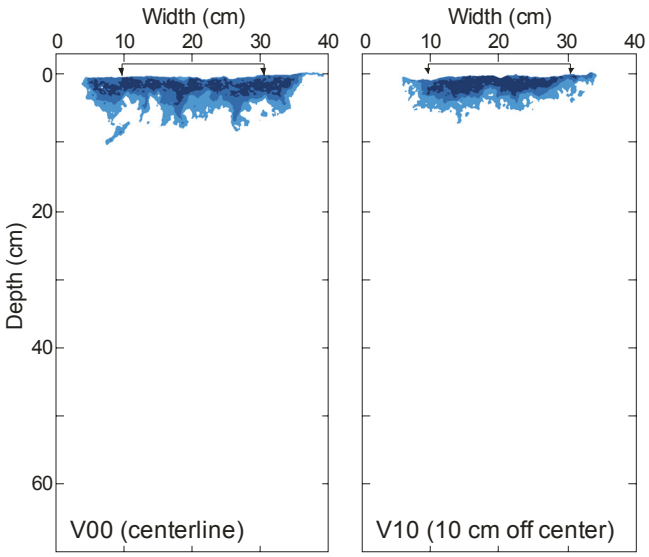

Horizontal Soil Sections

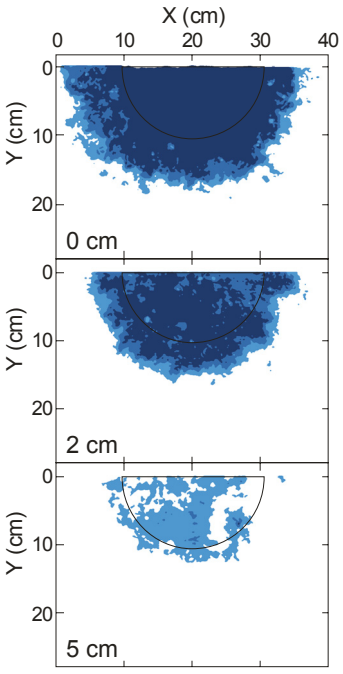

Dye Test EL-D2

Vertical Soil Sections

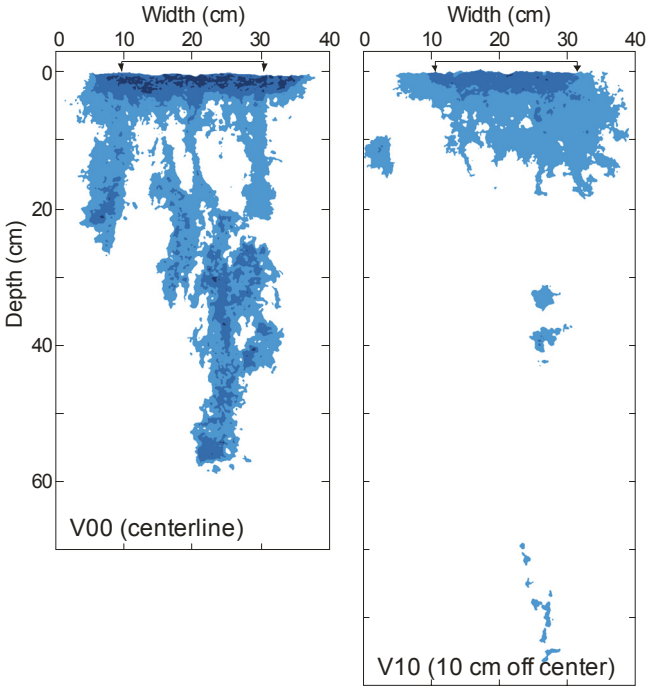

Horizontal Soil Sections

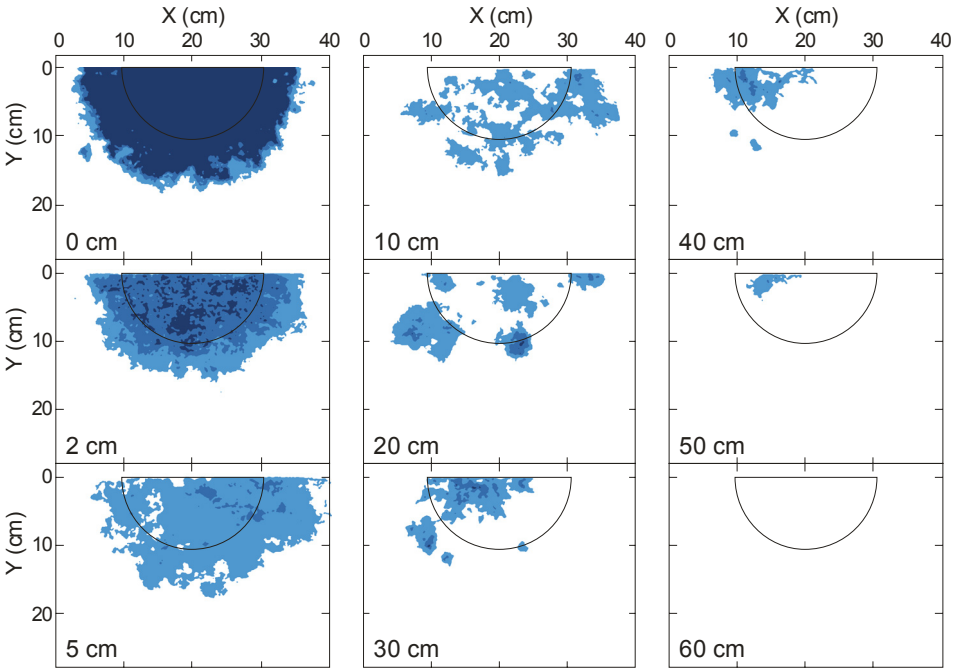

Dye Test WK-D1

Vertical Soil Sections

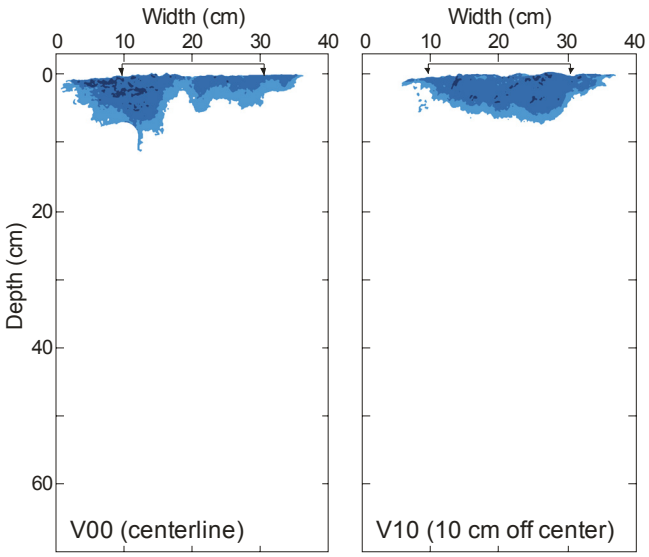

Horizontal Soil Sections

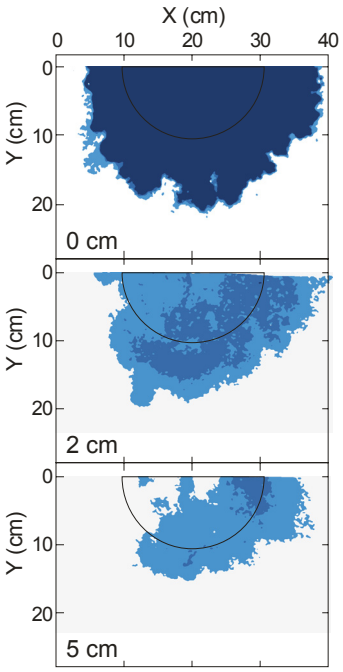

Dye Test WK-D2

Vertical Soil Sections

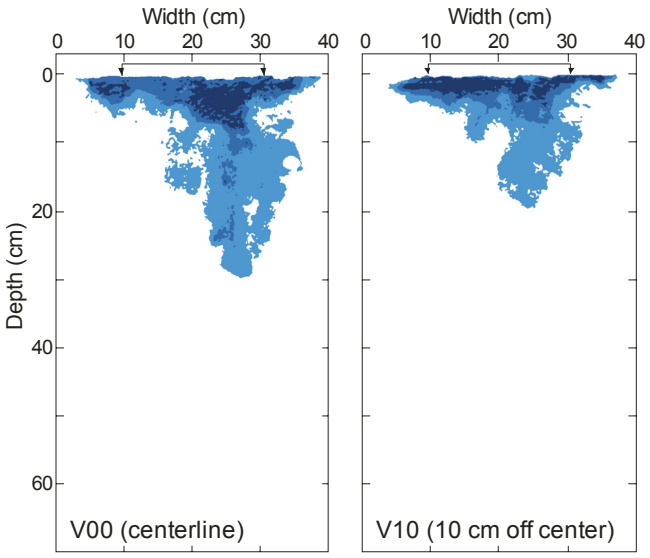

Horizontal Soil Sections

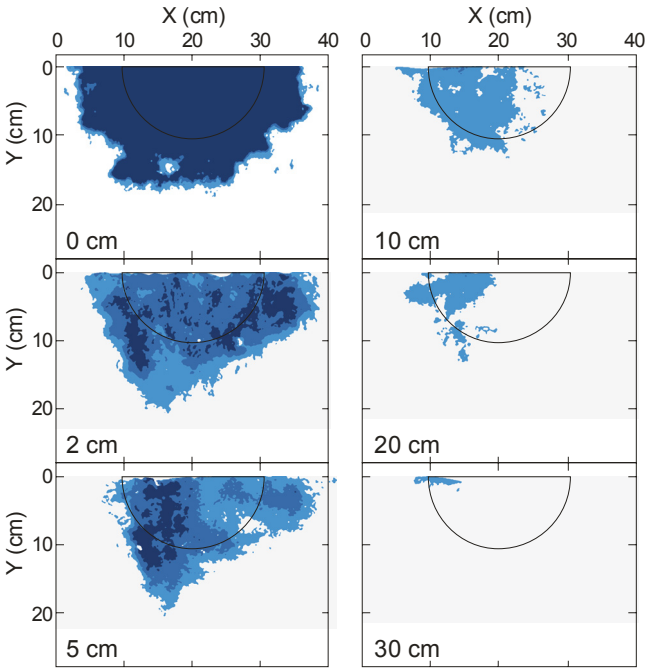

Dye Test WK-D3

Vertical Soil Sections

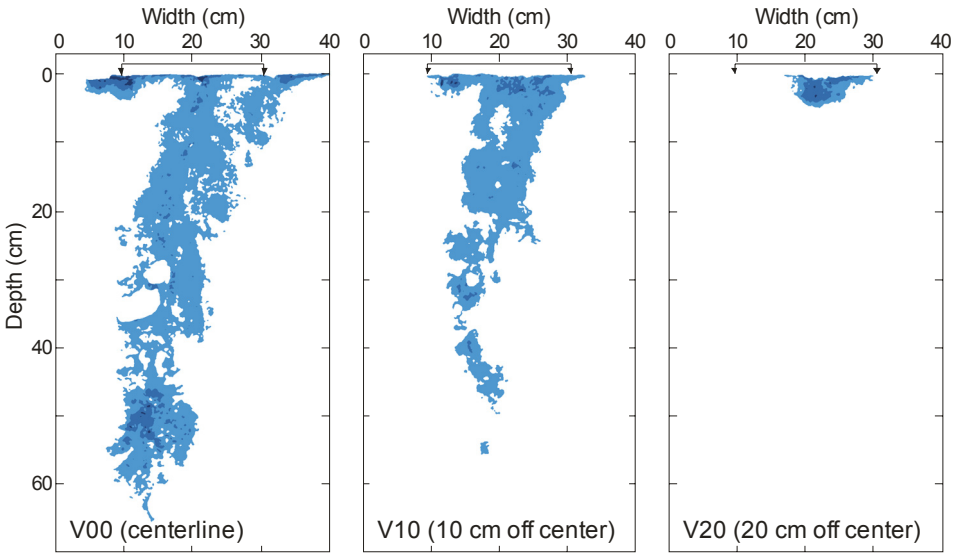

Horizontal Soil Sections

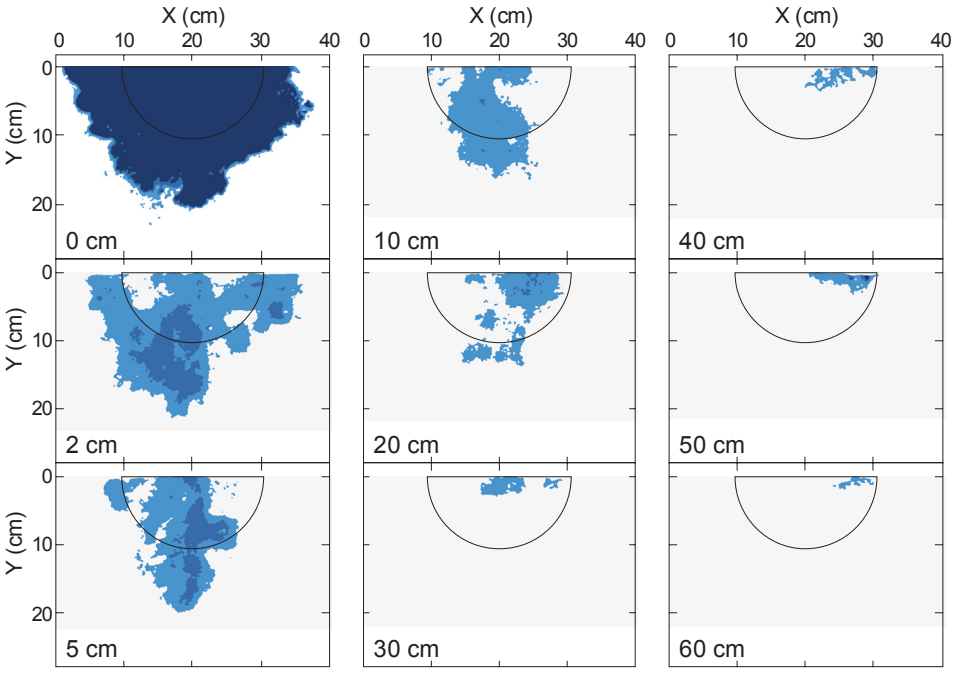

Dye Test WK-D4

Vertical Soil Sections

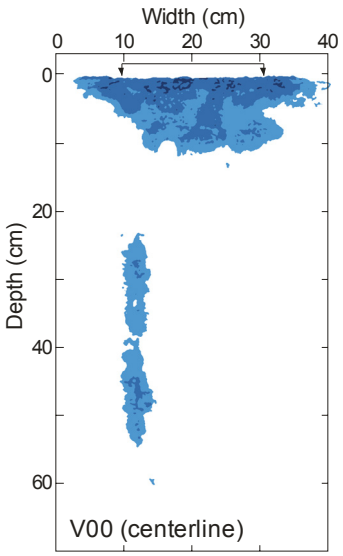

Horizontal Soil Sections

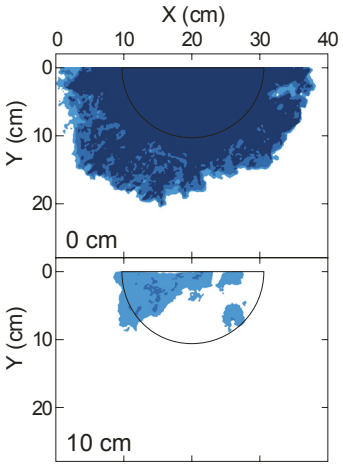

Simulated Rainfall Test WK-RS1

Vertical Soil Sections

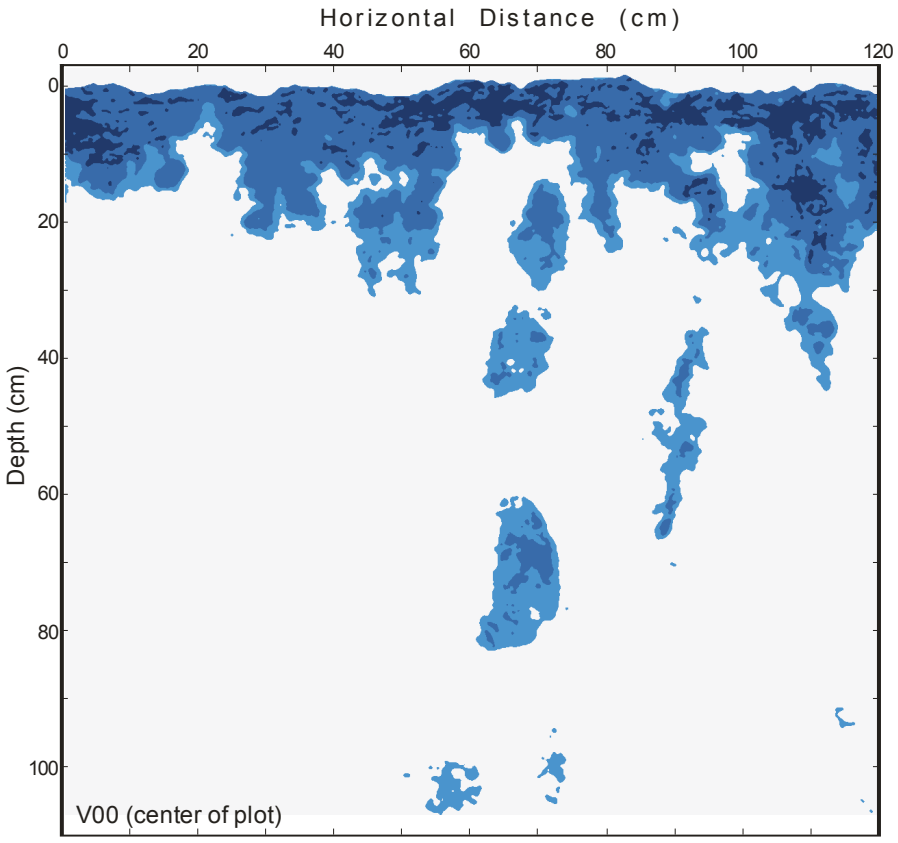

Simulated Rainfall Test WK-RS1

Horizontal Soil Sections

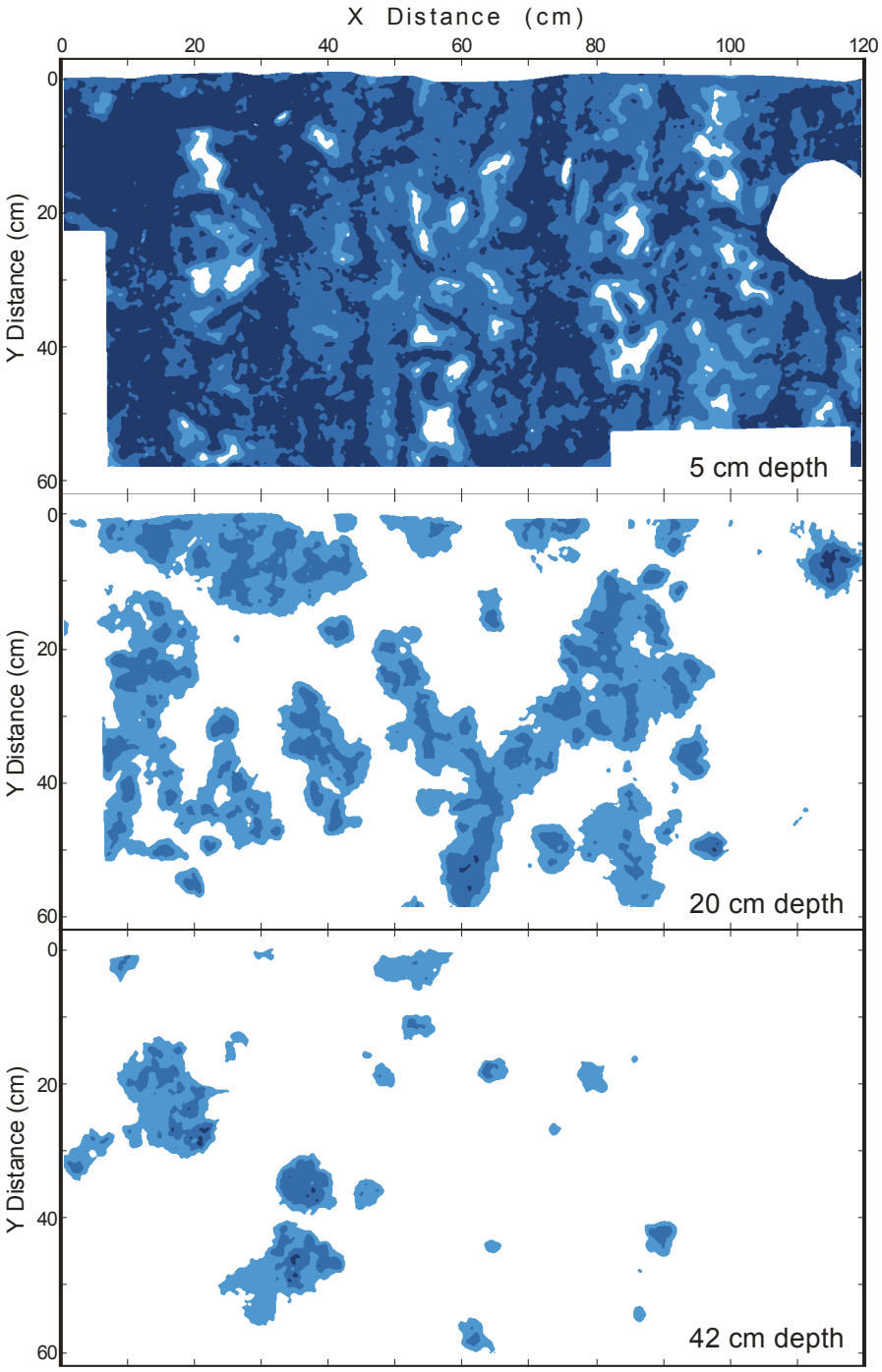

Appendix E
Microsphere Results

The microspheres were purchased from Bangs Laboratories of Fishers, Indiana and the physical characteristics listed by the manufacturer are provided in Table E.1 below. The results of microsphere analyses for the soil samples from Elora TI tests are provided in Table E.2 while the results from the Walkerton TI and simulated rainfall tests are provided in Table E.3 and Table E.4, respectively. The microsphere results are also displayed on photographs of the soil sections following the tabulated data.

Table E.1. Microsphere characteristics.

Color Designation	Material	Diameter		Fluorescence		Solid Density	Tests Used[b]
		Mean (μm)	SD[a] (μm)	Excitation Wavelength (nm)	Emission Wavelength (nm)	(g/cm^3)	
Dragon Green	polystyrene 11% DVB	3.69	0.34	480	520	1.068	Elora TI Walkerton TI Walkerton RS
Plum Purple	polystyrene	0.53	na	360	420	1.05	Elora TI Walkerton TI
Twilight Blue	polystyrene	1.51	0.10	425	480	1.05	Walkerton RS

[a]Standard deviation
[b]TI and RS refer to tension infiltration and rainfall simulation experiments, respectively.

Table E.2. Microsphere results for the Elora TI tests.

Test	Section	Sample ID	Dye Category[a]	Depth	Microsphere Concentration		Field description
				(m)	3.7 µm (spheres/g)	0.53 µm (presence/ absence)[b]	
D1	**V10**	D1-V10-1	2	0.025	120	+	heavy dye zone
		D1-V10-2	0	0.15	0	-	light dye-stained root
		D1-V10-3	0	0.08	0	-	earthworm hole
		D1-V10-4	2.5	0.02	560	+	heavy dye zone
		D1-V10-5	0	0.165	0	-	background (no dye)
	V00	D1-V0-1	2	0.025	63	+	earthworm burrow in dye
		D1-V0-2	1	0.085	83	-	dye-stained root hole (~7 cm)
		D1-V0-3	3	0.015	1360	+	heavy dye stain
		D1-V0-4	2	0.045	260	+	lighter dye stain
		D1-V0-5	2	0.045	100	+	lighter dye stain
		D1-V0-6	0.5	0.06	20	+	v. light dye stain (near earthworm burrow) (~5 cm)
		D1-V0-7	1	0.05	160	+	adjacent to dye stain
		D1-V0-8	0	0.185	0	-	background (no dye)
	H07	D1-H7-1	1	0.05	80	+	heavy dye-stain (possible microfracture)
		D1-H7-2	0.5	0.05	0	+	lighter dye stain
		D1-H7-3	0.5	0.05	60	+	no dye stain, but within disc area
	H12	D1-H12-1	0	0.1	0	-	no dye, shaved off area in center of disc

[a]Dye category refers to the dye stain intensity category of soil in which the sample was collected (0=no dye up to 3=heavily dyed).

[b]The presence or absence of the small microspheres is indicated by a + or - sign, respectively.

E.B. indicates sample collected from an earthworm burrow between soil sections.

B.E.B. indicates a sample collected from beside an earthworm burrow between soil sections.

Table E.2. Microsphere results for the Elora TI tests (continued).

Test	Section	Sample ID	Dye Category[a]	Depth	Microsphere Concentration		Field description
				(m)	3.7 µm (spheres/g)	0.53 µm (presence/ absence)[b]	
D2	V10	D2-V10 E.B.	0.5	0.81	0	-	sampled at 81 cm depth - earthworm burrow
		D2-V10-1	0.5	0.78	0	+	dyed earthworm burrow in C-horizon (~78 cm depth)
		D2-V10-2	1	0.38	0	+	dye stain in B-horizon
		D2-V10-3	1	0.33	20	+	2nd dye stain in B-horizon, 5-7 cm above #2
		D2-V10-4	1	0.11	40	+	dyed root and isolated from main
		D2-V10-5	0	0.13	80	+	non-dyed sample
		D2-V10-6	1	0.08	0	+	lightly dyed soil directly below TI
		D2-V10-7	1	0.08	60	+	lightly dyed below edge of TI
		D2-V10-8	2	0.02	140	+	heavy dye stain near soil surface
	V00	D2-V0 E.B.	na	0.4	80	+	sampled at 40 cm depth - earthworm burrow
		D2-V0 B.E.B.	na	0.4	0	-	sampled at 40 cm depth - beside earthworm burrow
		D2-V0-1	2	0.54	20	+	bottom-most dye stained soil (B-C horizon)
		D2-V0-2	1.5	0.42	120	+	dye stained finger
		D2-V0-3	0.5	0.14	20	+	non-dyed soil b/w dyed soil fingers
		D2-V0-4	1	0.1	160	+	lightly stained finger (shallow depth)
		D2-V0-5	2.5	0.02	4200	+	heavy dye stain near soil surface
		D2-V0-6	0	0.39	0	-	background (no dye)
		D2-V0-7	1.5	0.29	60	+	moderatly dye-stained B-horizon
	H07	D2-H7-1	2	0.05	280	+	heavy dye stain near center of TI
		D2-H7-2	1	0.05	100	+	moderate dye stain
		D2-H7-3	1	0.05	180	+	moderate dye stain
		D2-H7-4	0.5	0.05	0	+	light dye stain
		D2-H7-5	1	0.05	0	+	light dye stain
		D2-H7-6	0	0.05	0	-	background (no dye)
	H12	D2-H12-1	1	0.1	20	+	heavy dye stain with earthworm burrows
		D2-H12-2	1	0.1	140	+	dyed wormhole
		D2-H12-3	0.5	0.1	0	-	light dye stained matrix with roots
		D2-H12-4	1	0.1	20	+	lightly dye stained soil matrix
		D2-H12-5	0	0.1	0	-	background (no dye)
	H22	D2-H22-1	1.5	0.2	180	+	dyed wormhole (possible extention of D2-H12-2)
		D2-H22-2	2	0.2	208	+	inside portion of dyed wormhole
		D2-H22-3	2	0.2	100	+	halo of dye around wormhole from #2
		D2-H22-4	0	0.2	0	-	non-dyed soil near wormhole from #2
		D2-H22-5	1	0.2	80	+	moderately stained matrix
		D2-H22-6	0	0.2	0	+	very lightly stained soil below TI
		D2-H22-7	0	0.2	0	-	background (no dye)
	H32	D2-H32-1	1	0.3	40	+	dyed wormhole
		D2-H32-2	2	0.3	240	+	heavy dyed soil matrix
		D2-H32-3	1.5	0.3	40	+	dyed medium size holes (ants?)
		D2-H32-4	0	0.3	0	-	background (no dye)
	H42	D2-H42-1	1.5	0.4	40	+	heavy dye stained matrix
		D2-H42-2	0.5	0.4	0	+	dyed wormhole
		D2-H42-3	0	0.4	0	-	unstained soil beneath TI
		D2-H42-4	0	0.4	0	-	background (no dye)
	H52	D2-H52-1	1	0.5	0	+	dyed wormhole
		D2-H52-2	0	0.5	0	-	non-dyed soil below TI
		D2-H52-3	0	0.5	0	-	background (no dye)

[a]Dye category refers to the dye stain intensity category of soil in which the sample was collected (0=no dye up to 3=heavily dyed).

[b]The presence or absence of the small microspheres is indicated by a + or - sign, respectively.

E.B. indicates sample collected from an earthworm burrow between soil sections.

B.E.B. indicates a sample collected from beside an earthworm burrow between soil sections.

Table E.3. Microsphere results for Walkerton TI tests.

Test	Section	Sample ID	Dye Category[a]	Depth	Microsphere Concentration		Field description
				(m)	3.7 µm (spheres/g)	0.53 µm (presence/ absence)[b]	
D1	V10	D1 V10-1	0	0.085	60	+	non-dyed soil below max depth of staining
		D1 V10-2	1	0.06	40	-	dyed soil at max depth (~7cm) of staining
		D1 V10-3	2	0.03	0	+	heavily dyed soil matrix
		D1 V10-4	2	0.025	140	+	heavily dyed soil matrix
		D1 V10-5	2	0.015	0	-	dyed soil outside of disc area
		D1 V10-6	0	0.17	0	-	non-dyed control
	V00	D1-V00-1	0	0.12	0	-	non-dyed soil below max depth of staining
		D1-V00-2	1	0.09	0	+	v. lightly dyed soil (w/ roots) around a rock
		D1-V00-3	2	0.04	0	+	heavily dyed soil matrix
		D1-V00-4	0	0.05	0	-	non-dyed pocket of soil directly under disc
		D1-V00-5	1	0.035	0	+	mod dyed soil under disc
		D1-V00-6	1.5	0.015	0	+	dyed soil outside of disc area
		D1-V00-7	0	0.15	0	-	non-dyed control
	H00	D1 H00	3	0	333824	+	surface (approx. 1 mm) sample from within disk area only
	H02	D1 H02-LUD	na	0.02	260	+	scraped bulk sample from disc area
		D1 H02-1	1	0.02	20	+	dye stained soil along fracture, located furthest from disc
		D1 H02-2	2	0.02	20	+	dyed soil matrix outside disc
		D1 H02-3	2	0.02	60	+	heavly dyed soil under disc area
		D1 H02-4	0	0.02	0	-	non-dyed macropores
		D1 H02-5	0	0.02	0	-	non-dyed soil matrix
		D1 H02-6	1	0.02	0	-	lightly dyed soil matrix
		D1 H02-7	0	0.02	0	-	non-dyed control
	H05	D1 H05-LUD	na	0.05	0	+	scraped bulk sample from disc area
		D1 H05-1	0.5	0.05	0	-	v. lightly dyed soil within disc area
		D1 H05-2	0	0.05	0	-	no visible dye near center of disc
		D1 H05-3	1.5	0.05	0	-	heavly dyed soil under disc area
		D1 H05-4	1	0.05	0	-	mod-heavy dyed soil on fracture near edge of dye staining
		D1 H05-5	0	0.05	0	-	non-dyed macropore (large)
		D1 H05-6	0	0.05	0	-	non-dyed soil matrix
		D1 H05-7	1	0.05	20	+	heavily dyed soil matrix outisde disc area
		D1 H05-8	0	0.05	0	-	non-dyed control
	H10	D1 H10-LUD	0	0.1	0	-	scraped bulk sample from disc area - no visible dye

[a]Dye category refers to the dye stain intensity category of soil in which the sample was collected (0=no dye up to 3=heavily dyed).

[b]The presence or absence of the small microspheres is indicated by a + or - sign, respectively.

LUD indicates layer under disc sample collected by scraping a thin (1-2 mm) layer from the TI disc area.

Table E.3. Microsphere results for Walkerton TI tests (continued).

Test	Section	Sample ID	Dye Category[a]	Depth	Microsphere Concentration		Field description
				(m)	3.7 µm (spheres/g)	0.53 µm (presence/ absence)[b]	
D2	V10	D2 V10-1	1	0.18	0	+	lightly dye stained
		D2 V10-2	1	0.14	0	+	lightly dye stained
		D2 V10-3	1.5	0.06	80	+	lightly dye stained (soy root observed)
		D2 V10-4	3	0.02	1380	+	heavy dye staining adjacent to large soy root
		D2 V10-5	2.5	0.015	1320	+	heavy dye staining among small roots
		D2 V10-6	2.5	0.02	0	+	dye stained soil beyond edge of disk
		D2 V10-7	0	0.135	0	-	non-dyed control
		D2 V10-8	0	0.225	0	-	non-dyed soil below deepest observed dye
	V00	D2 V00-1	0	0.32	0	+	non-dyed soil below deepest observed dye
		D2 V00-2	1	0.29	40	+	deepest observed dye 'finger'
		D2 V00-3	1.5	0.23	100	+	dyed soil at edge of wormhole; some roots
		D2 V00-4	1.5	0.16	220	+	dyed soil around same wormhole as sample 3
		D2 V00-5	3	0.045	740	+	heavy dye stained soil matrix
		D2 V00-6	1.5	0.03	40	+	moderately-heavy dyed soil with medium sized root
		D2 V00-7	2	0.02	20	+	dyed soil outside permiameter of TI disc
		D2 V00-8	0	0.22	0	-	non-dyed control
		D2 V00-9	1	0.016	0	+	lightly dyed soil adjacent to approx. 1mm diam. soy root
	H00	D2 H00	3	0	110080	+	surface (approx. 1 mm) sample from within disk area only
	H02	D2 H02-LUD	na	0.02	2260	+	thin bulk sample from Layer Under Disk
		D2 H02-1	2	0.02	2100	+	dye stained wormhole
		D2 H02-2	3	0.02	0	+	moderate dye stained soil outside disc area
		D2 H02-3	2.5	0.02	60	+	moderate dye stained soil outside disc area
		D2 H02-4	2	0.02	4320	+	heavy dyed soil near center of disc
		D2 H02-5	0	0.02	0	-	non-dyed soil east of
		D2 H02-6	0	0.02	0	-	non-dyed control
	H05	D2 H05-LUD	na	0.05	160	+	scraped bulk sample from disc area
		D2 H05-1	3	0.05	0	+	dyed wormhole outside disc area
		D2 H05-2	2.5	0.05	0	+	moderate dye stained soil outside disc area
		D2 H05-3	1	0.05	0	-	lightly dyed soil near edge of staining
		D2 H05-4	1	0.05	0	+	v. lightly dyed soil matrix
		D2 H05-5	1	0.05	640	+	v. lightly dyed wormhole at edge of dye
		D2 H05-6	0	0.05	0	-	non-dyed control
		D2 H05-7	3	0.05	20	+	mod. dyed soil matrix inside disc area
	H10	D2 H10-LUD	na	0.1	20	+	scraped bulk sample from disc area
		D2 H10-1	0	0.1	0	+	non-dyed soil inside disc area
		D2 H10-2	1	0.1	80	+	dye stained soil (w/ roothole??)
		D2 H10-3	1	0.1	40	+	dye stained soil in fracture (root along crack just below)
		D2 H10-4	1	0.1	0	+	moderate dye staining under disc
		D2 H10-5	0.5	0.1	20	+	v. light dye stained soil
		D2 H10-6	0.5	0.1	0	+	non-dyed wormhole (below sample D2 H05-5)
		D2 H10-7	0	0.1	0	-	non-dyed control
	H20	D2 H20-LUD	na	0.2	0	-	scraped bulk sample from disc area
		D2 H20-1	0	0.2	0	-	non-dyed soil inside disc area
		D2 H20-2	1	0.2	60	+	moderately heavy dyed soil
		D2 H20-3	1	0.2	0	+	dyed wormhole and soil
		D2 H20-4	0.5	0.2	0	+	lightly dyed soil outside footprint of disc
		D2 H20-5	0	0.2	0	+	non-dyed wormhole (below sample D2 H05-5)
		D2 H20-6	0	0.2	0	-	non-dyed control
	H30	D2 H30-LUD	na	0.3	0	-	scraped bulk sample from disc area
		D2 H30-1	0.5	0.3	0	-	lightly dye stained soil
		D2 H30-2	0	0.3	0	-	non-dyed soil within disc area
		D2 H30-3	0	0.3	0	-	non-dyed control

[a]Dye category refers to the dye stain intensity category of soil in which the sample was collected (0=no dye up to 3=heavily dyed).

[b]The presence or absence of the small microspheres is indicated by a + or - sign, respectively.

LUD indicates layer under disc sample collected by scraping a thin (1-2 mm) layer from the TI disc area.

Table E.3. Microsphere results for Walkerton TI tests (continued).

Test	Section	Sample ID	Dye Category[a]	Depth	Microsphere Concentration		Field description
				(m)	3.7 µm (spheres/g)	0.53 µm (presence/ absence)[b]	
D3	V20	D3 V20-1	2	0.02	0	+	moderately dyed soil with soybean roots (large)
		D3 V20-2	0	0.06	0	-	non-dyed soil below dyed area
		D3 V20-3	0	0.08	0	-	non-dyed control
	V10	D3 V10-1	0	0.56	0	+	non-dyed soil below max depth of staining
		D3 V10-2	0.5	0.53	0	-	dyed wormhole and halo
		D3 V10-3	1	0.45	100	+	side of dyed wormhole and halo
		D3 V10-4	1	0.4	0	+	dyed wormhole and halo
		D3 V10-5	1	0.31	80	+	dyed wormhole and halo
		D3 V10-6	1	0.24	60	+	dyed soil, broke through into wormhole
		D3 V10-7	0.5	0.23	0	+	dyed soil around roothole
		D3 V10-8	1	0.19	20	+	dyed soil, broke through into wormhole
		D3 V10-9	1	0.14	20	+	dyed soil matrix
		D3 V10-10	1	0.14	20	+	dyed soil matrix
		D3 V10-11	1	0.05	120	+	dyed soil matrix
		D3 V10-12	1.5	0.02	15759	+	heavily dyed soil
		D3 V10-13	0	0.09	0	-	non-dyed control
	V00	D3 V00-1	0	0.715	0	+	non-dyed soil below/behind max. depth of dyed soil
		D3 V00-2	0.5	0.65	0	+	lightly dyed soil around edge of rock (soft calcite)
		D3 V00-3	1	0.57	0	-	mod-heavy dyed soil matrix
		D3 V00-4	2	0.495	0	+	heavily dyed soil matrix in C-horizon
		D3 V00-5	1	0.38	20	+	lightly-mod dyed soil in B-horizon
		D3 V00-6	1.5	0.3	80	+	dyed soil b/w 2 rocks
		D3 V00-7	1	0.28	60	+	dyed inside of wormhole (23-30 cm deep)
		D3 V00-8	1	0.28	20	+	dyed halo beside wormhole (23-30 cm deep)
		D3 V00-9	1	0.19	160	+	dyed soil near bottom of A-horizon
		D3 V00-10	0	0.03	0	-	non-dyed soil under disc
		D3 V00-11	1.5	0.035	440	+	heavily dyed soil under center of disc
		D3 V00-12	0	0.135	0	-	non-dyed control
	H00	D3 H00	3	0	89088	+	surface (approx. 1 mm) sample from within disk area only
	H02	D3 H02-LUD	na	0.02	480	+	scraped bulk sample from under disc
		D3 H02-1	2	0.02	11060	+	dyed wormhole within disc area
		D3 H02-2	2	0.02	4800	+	dyed fracture beneath disk
		D3 H02-3	2	0.02	0	+	dyed fracture outside of disk area
		D3 H02-4	1	0.02	0	-	mod-heavy dyed soil at edge of stained area
		D3 H02-5	0	0.02	0	-	non-dyed soil just beyond stained area
		D3 H02-6	0.5	0.02	0	+	dyed soil fracture located furthest from disk
		D3 H02-7	0	0.02	0	-	non-dyed control

[a]Dye category refers to the dye stain intensity category of soil in which the sample was collected (0=no dye up to 3=heavily dyed).

[b]The presence or absence of the small microspheres is indicated by a + or - sign, respectively.

LUD indicates layer under disc sample collected by scraping a thin (1-2 mm) layer from the TI disc area.

Table E.3. Microsphere results for Walkerton TI tests (continued).

Test	Section	Sample ID	Dye Category[a]	Depth	Microsphere Concentration		Field description
				(m)	3.7 µm (spheres/g)	0.53 µm (presence/ absence)[b]	
D3	H05	D3 H05-LUD	na	0.05	200	+	scraped bulk sample from under disc
		D3 H05-1	2	0.05	1340	+	dyed wormhole within disc area
		D3 H05-2	2	0.05	980	+	heavily dyed fracture within disc area
		D3 H05-3	1.5	0.05	220	+	heavliy dyed fracture ouside disc area
		D3 H05-4	1	0.05	20	+	lightly dyed soil at end of fracture
		D3 H05-5	1	0.05	220	+	lightly dyed soil matrix in disc area
		D3 H05-6	0	0.05	0	-	v. lightly dyed soil (isolated)
		D3 H05-7	0	0.05	0	+	non-dyed soil within disc area
		D3 H05-8	0	0.05	0	-	non-dyed control
	H10	D3 H10-LUD	na	0.1	140	+	scraped bulk sample from under disc
		D3 H10-1	0.5	0.1	320	+	dyed wormhole within disc area
		D3 H10-2	1	0.1	680	+	heavily dyed soil matrix
		D3 H10-3	1	0.1	0	-	lightly dyed soil matrix in disc area
		D3 H10-4	1	0.1	140	+	heavily dyed soil along fracture with roots
		D3 H10-5	0.5	0.1	0	+	lightly dyed soil (furthest dye from center)
		D3 H10-6	0	0.1	0	-	non-dyed soil within disc area
		D3 H10-7	0	0.1	0	-	non-dyed control
	H20	D3 H20-LUD	na	0.2	20	+	scraped bulk sample from under disc
		D3 H20-1	1.5	0.2	280	+	moderatly dyed soil matrix near disc center
		D3 H20-2	0.5	0.2	0	-	non-dyed soil; thin coarse-grained layer may be dyed
		D3 H20-3	1	0.2	0	-	dyed isolated blob inside disc area
		D3 H20-4	1	0.2	0	-	dyed isolated blob outside disc area
		D3 H20-5	0	0.2	0	-	apparently non-dyed wormhole near center of disc
		D3 H20-6	0	0.2	0	-	non-dyed control
	H30	D3 H30-LUD	na	0.3	0	+	scraped bulk sample from under disc
		D3 H30-1	1	0.3	20	+	dye stained soil near disc center
		D3 H30-2	0.5	0.3	0	+	isolated blob of stained soil
		D3 H30-3	0	0.3	0	+	non-dyed soil under disc area
		D3 H30-4	0	0.3	0	-	non-dyed control
	H40	D3 H40-1	1	0.4	0	+	dyed soil matrix
		D3 H40-2	0.5	0.4	0	+	dyed soil matrix halo around rock
		D3 H40-3	0	0.4	0	+	non-dyed within disc area
		D3 H40-4	0	0.4	0	-	non-dyed control
	H50	D3 H50-1	1	0.5	0	+	dyed soil near center of disc
		D3 H50-2	1	0.5	0	+	dyed soil matrix around rock
		D3 H50-3	0	0.5	0	+	non-dyed soil under disc area
		D3 H50-4	0	0.5	0	-	non-dyed control
	H60	D3-H60-1	0.5	0.6	0	+	dye-stained soil; only visible spot
		D3-H60-2	0	0.6	0	-	non-dyed soil within disc area
		D3-H60-3	0	0.6	0	-	non-dyed control

[a]Dye category refers to the dye stain intensity category of soil in which the sample was collected (0=no dye up to 3=heavily dyed).

[b]The presence or absence of the small microspheres is indicated by a + or - sign, respectively.

LUD indicates layer under disc sample collected by scraping a thin (1-2 mm) layer from the TI disc area.

Table E.4. Microsphere results for Walkerton rainfall simulation test.

Test	Section	Sample ID	Dye Category[a]	Depth	Microsphere Concentration		Field description
					3.7 µm	1.51 µm	
				(m)	(spheres/g)	(spheres/g)	
RS1	H00	RS1 H00	3	0	113323	203093	random surface scraping; exposed soil only
RS1	V00	RS1 V00-1	0.5	1.02	20	0	mod. dye stained soil around rocks
		RS1 V00-2	1	1.02	0	20	mod dye stained wormhole
		RS1 V00-3	0	0.68	20	0	non-dyed soil beneath end of dyed wormhole
		RS1 V00-4	1.5	0.66	40	0	dyed soil near end of wormhole noted in #3
		RS1 V00-5	1.5	0.45	100	40	higher up in same wormhole
		RS1 V00-6	1	0.24	20	60	soil at bottom of dye-stained root
		RS1 V00-7	0	0.19	100	20	non-dyed A horizon
		RS1 V00-8	2	0.16	20	40	mod dyed A horizon
		RS1 V00-9	2	0.08	0	60	mod dyed A horizon w/ small roots
		RS1 V00-10	2.5	0.015	360	280	heavily dyed A horizon near surface
		RS1 V00-11	0	0.48	0	0	non-dyed C horizon soil below blob of dye
		RS1 V00-12	1.5	0.43	60	60	mod dyed C horizon soil just above sample 11
		RS1 V00-13	0	0.115	0	0	non-dyed A horizon below centerline
		RS1 V00-14	2	0.09	40	40	heavily dyed tounge of soil
		RS1 V00-15	0	0.39	0	0	control
		RS1 V00-16	0.5	0.44	0	20	dyed C horizon soil at bottom of dyed soil tongue
		RS1 V00-17	2	0.2	0	40	mod dyed soil tongue at A-C horizon boundary

[a]Dye category refers to the dye stain intensity category of soil in which the sample was collected (0=no dye up to 3=heavily dyed).

Plots of Microsphere Results

The microsphere results are displayed on the original, uncorrected soil section photographs in the following figures. The soil sample locations are indicated by yellow irregular shapes. The microsphere concentrations are shown in brackets next to each sample location. For all TI tests, the number before the comma indicates the concentration of large (3.7 µm diameter) spheres per gram of soil, while the presence or absence of the small (0.53 µm diameter) microspheres is indicated after the comma by a + or - sign, respectively. For the simulated rainfall experiment at Walkerton, the first number represents the concentration of large (3.7 µm diameter) microspheres per gram of soil and the second number the concentration of small (1.51 µm diameter) microspheres per gram of soil. For scale reference, the black graduations on the grey frame surrounding each soil section are 10 cm increments. The approximate position of the TI disc is indicated by white dashed lines on both the horizontal (H) and vertical (V) sections.

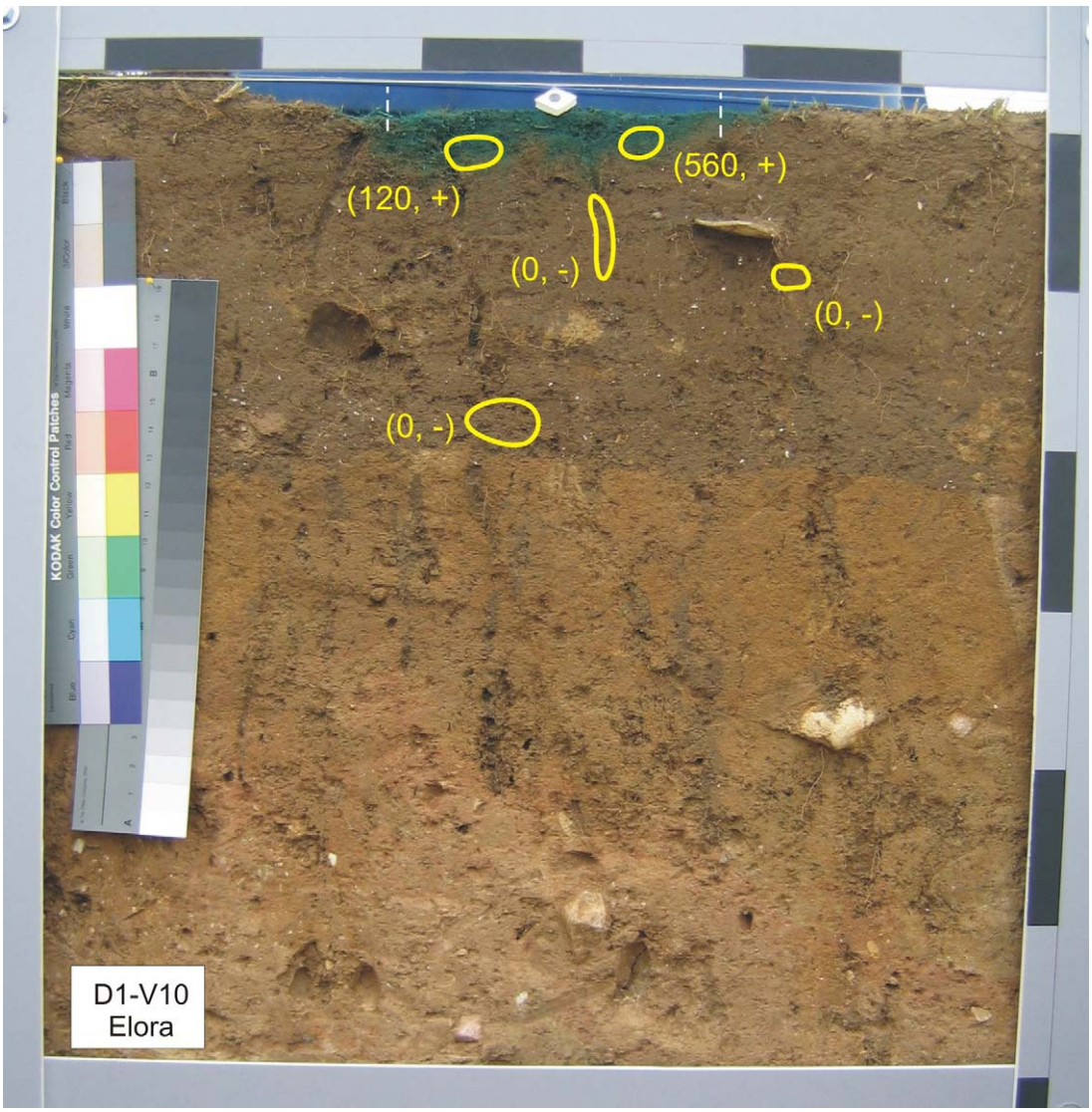

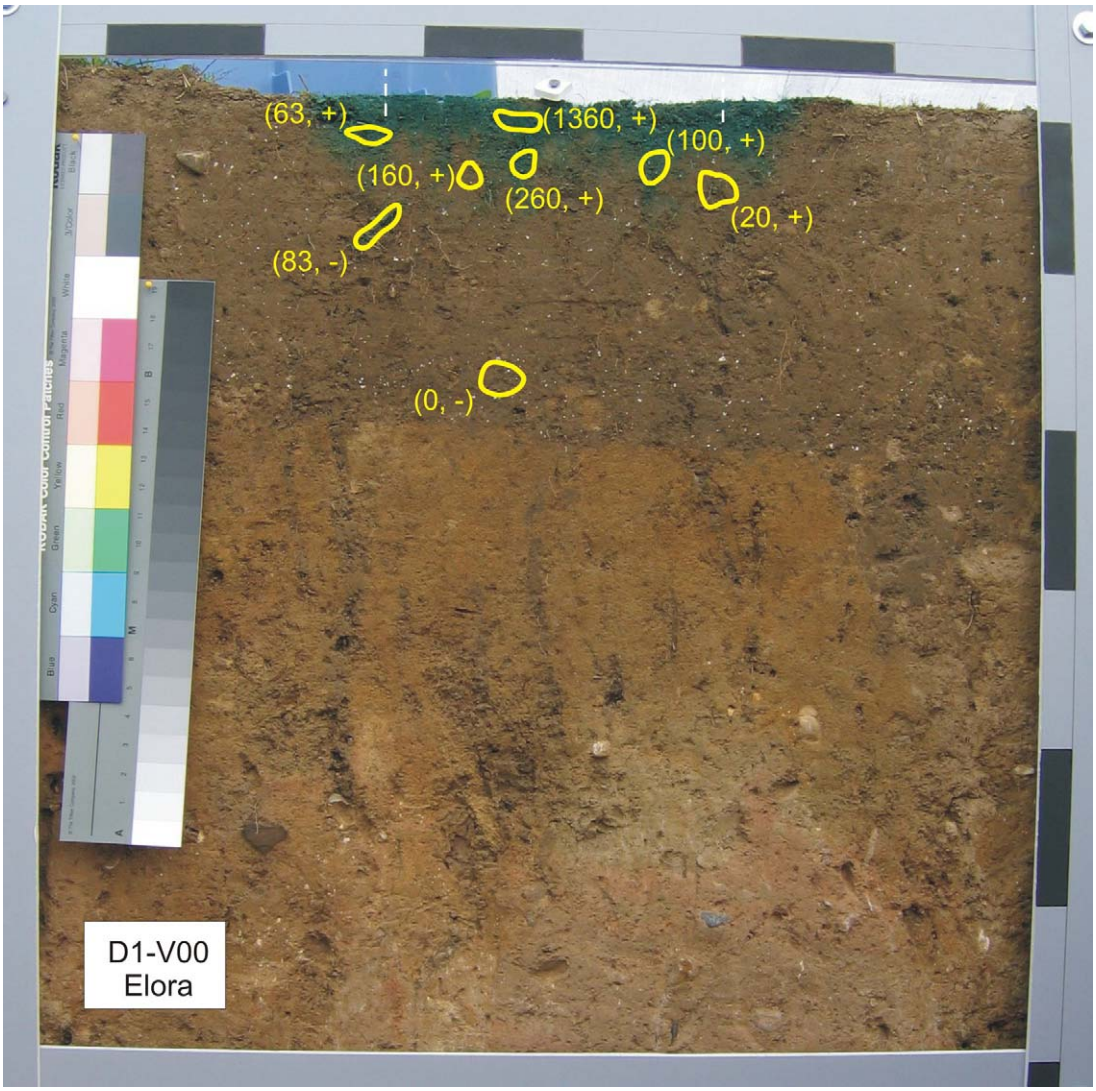
(63, +)
(1360, +)
(100, +)
(160, +)
(260, +)
(20, +)
(83, -)
(0, -)
D1-V00
Elora

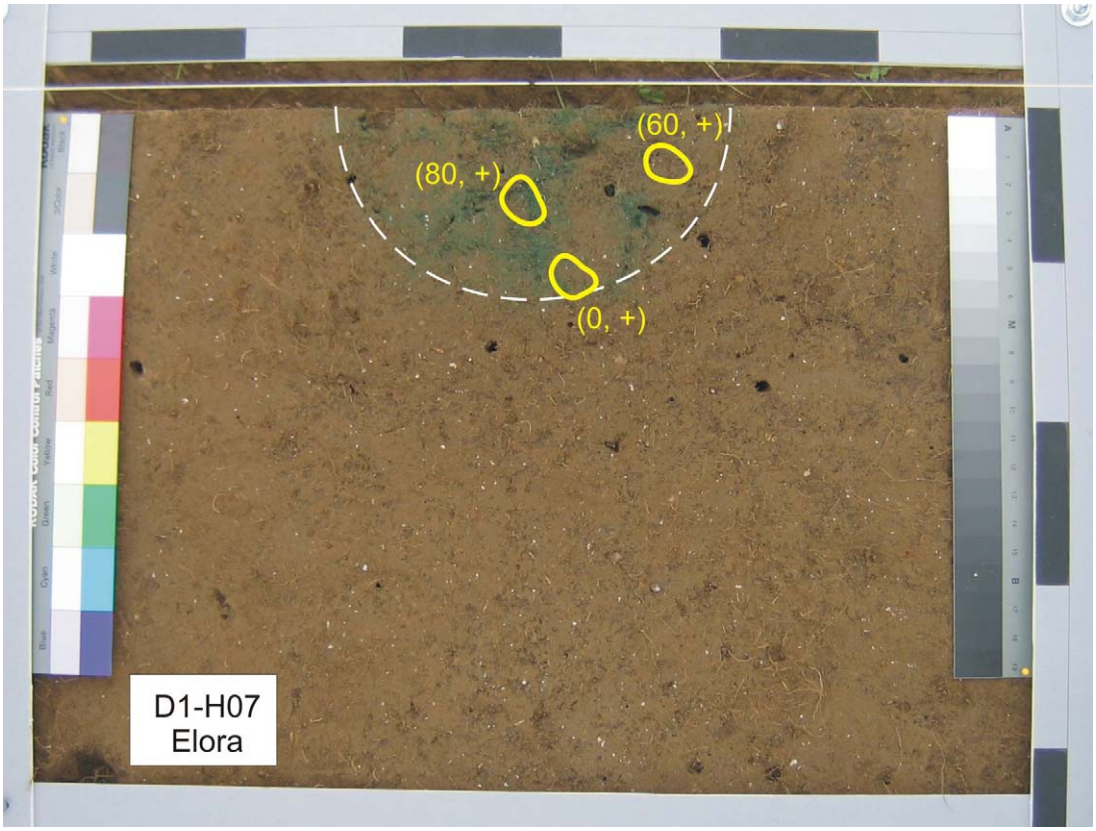
(60, +)
(80, +)
(0, +)
D1-H07
Elora

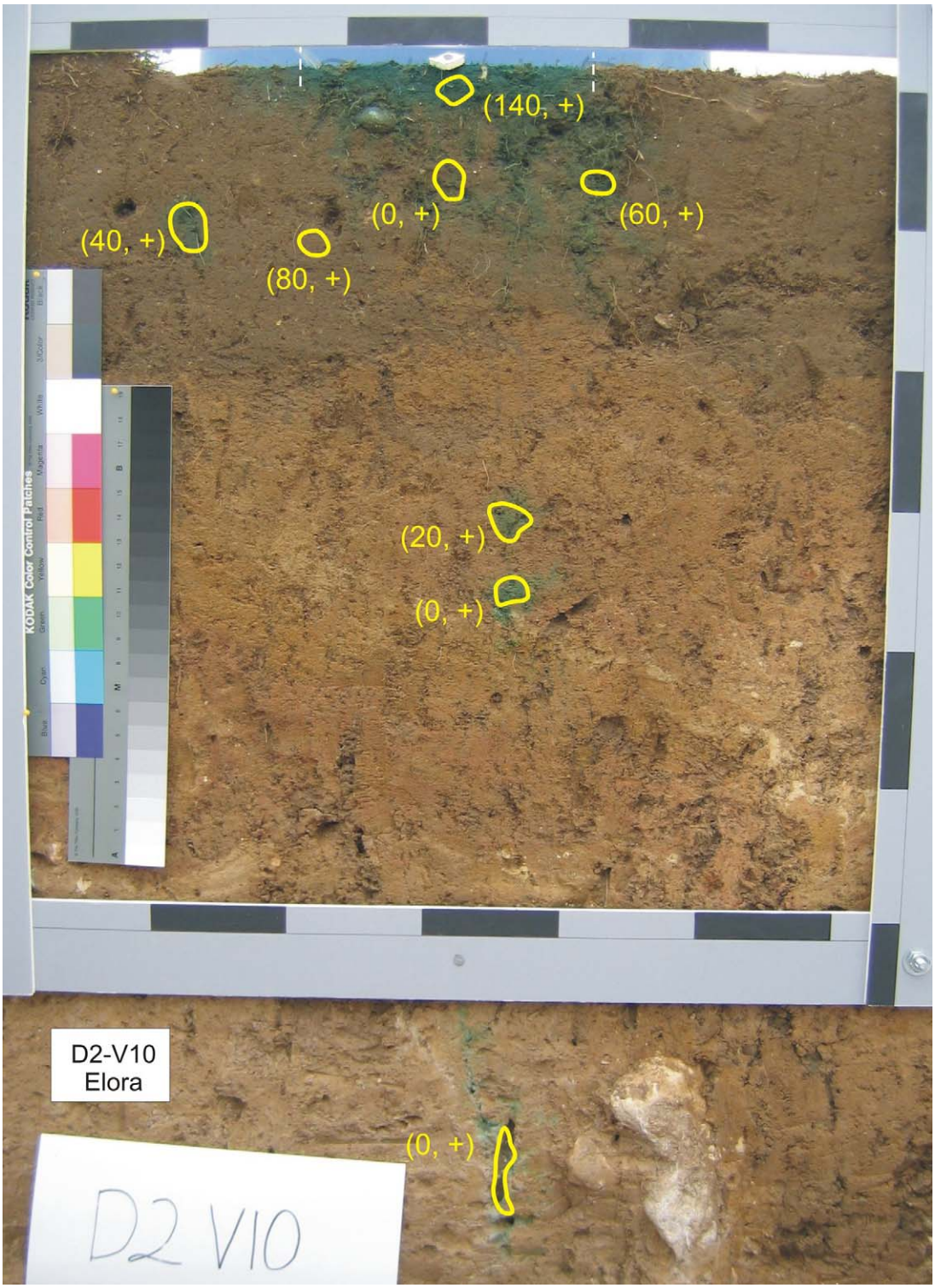
(140, +)
(0, +)
(60, +)
(40, +)
(80, +)
(20, +)
(0, +)
D2-V10
Elora
(0, +)
D2 V10

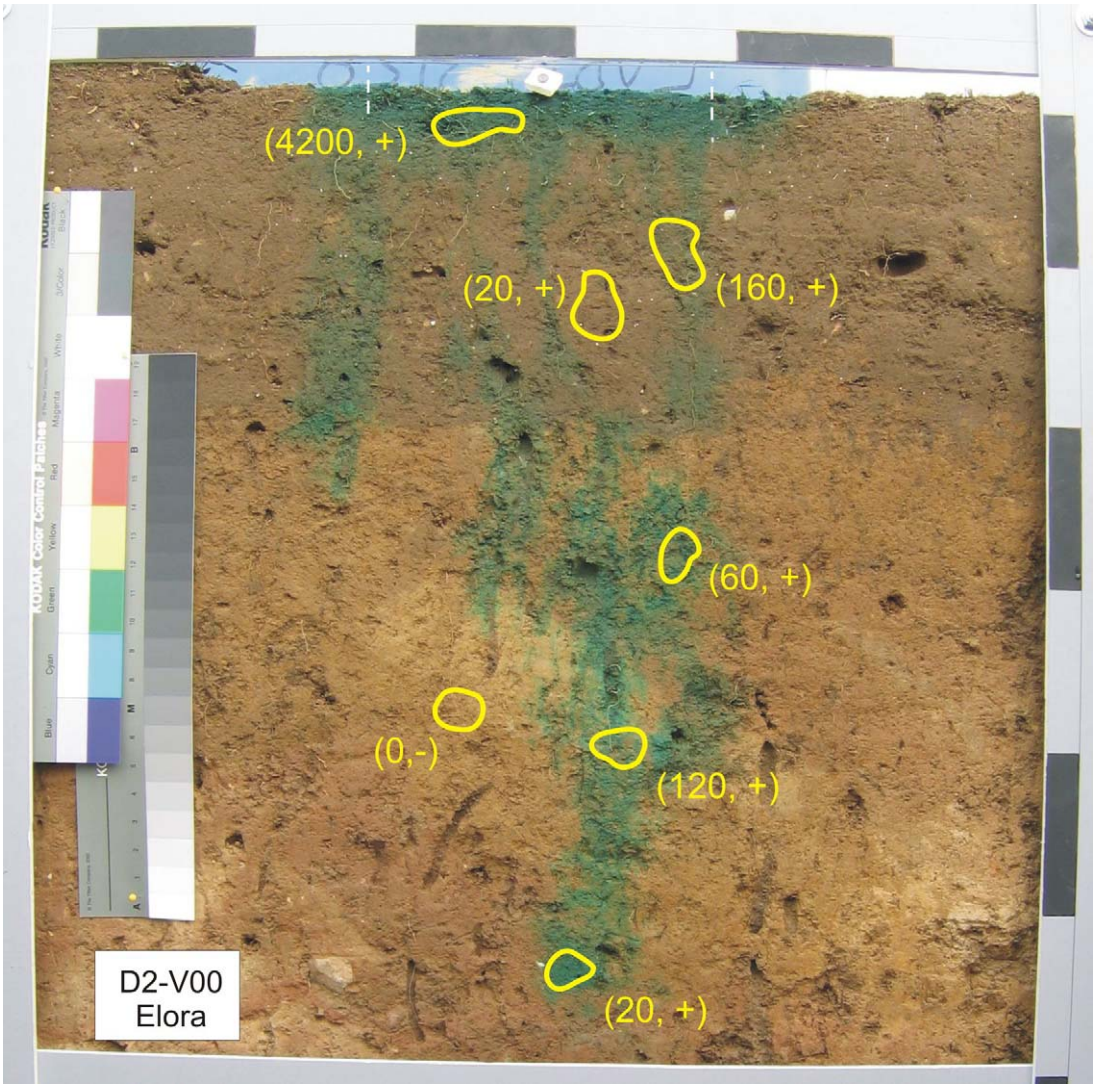
(4200, +)
(20, +)
(160, +)
(60, +)
(0,-)
(120, +)
(20, +)
D2-V00
Elora

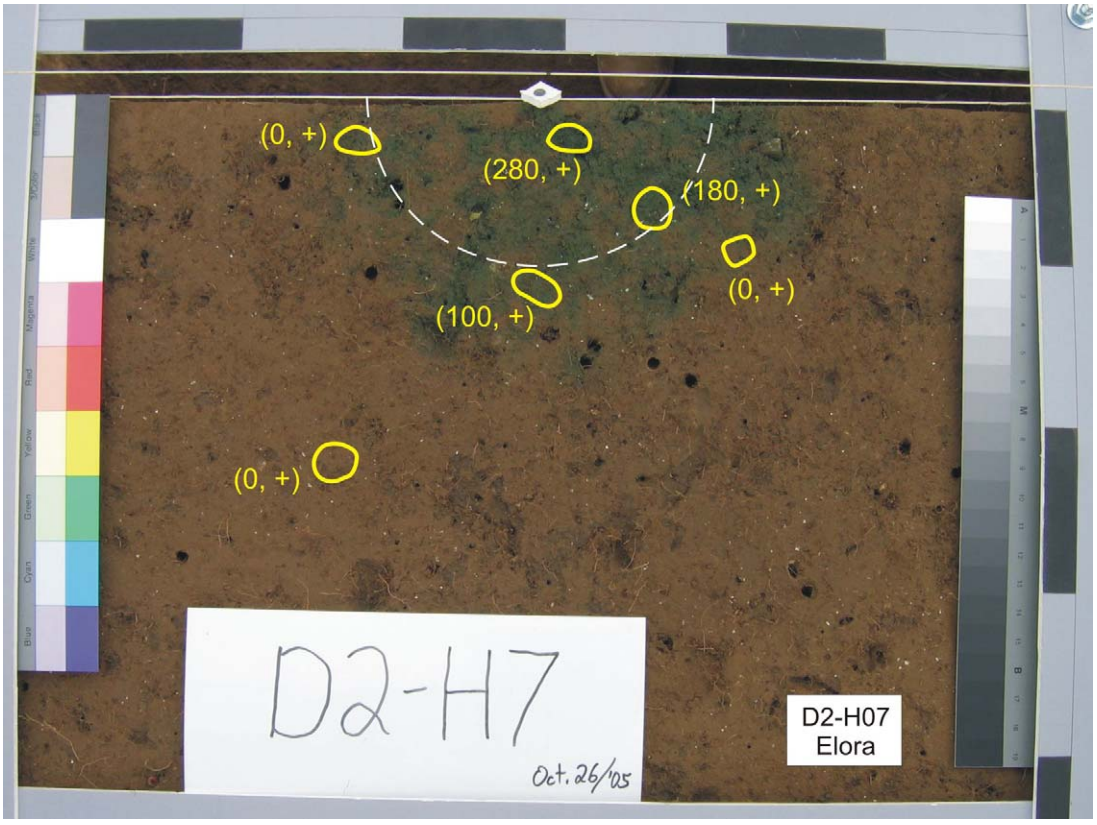
(0, +)
(280, +)
(180, +)
(0, +)
(100, +)
(0, +)
D2-H7
Oct. 26/05
D2-H07
Elora


(20, +)
(140, +)
(20, +)
(0, -)
(0, -)
D2-H12
Elora
D2 H12

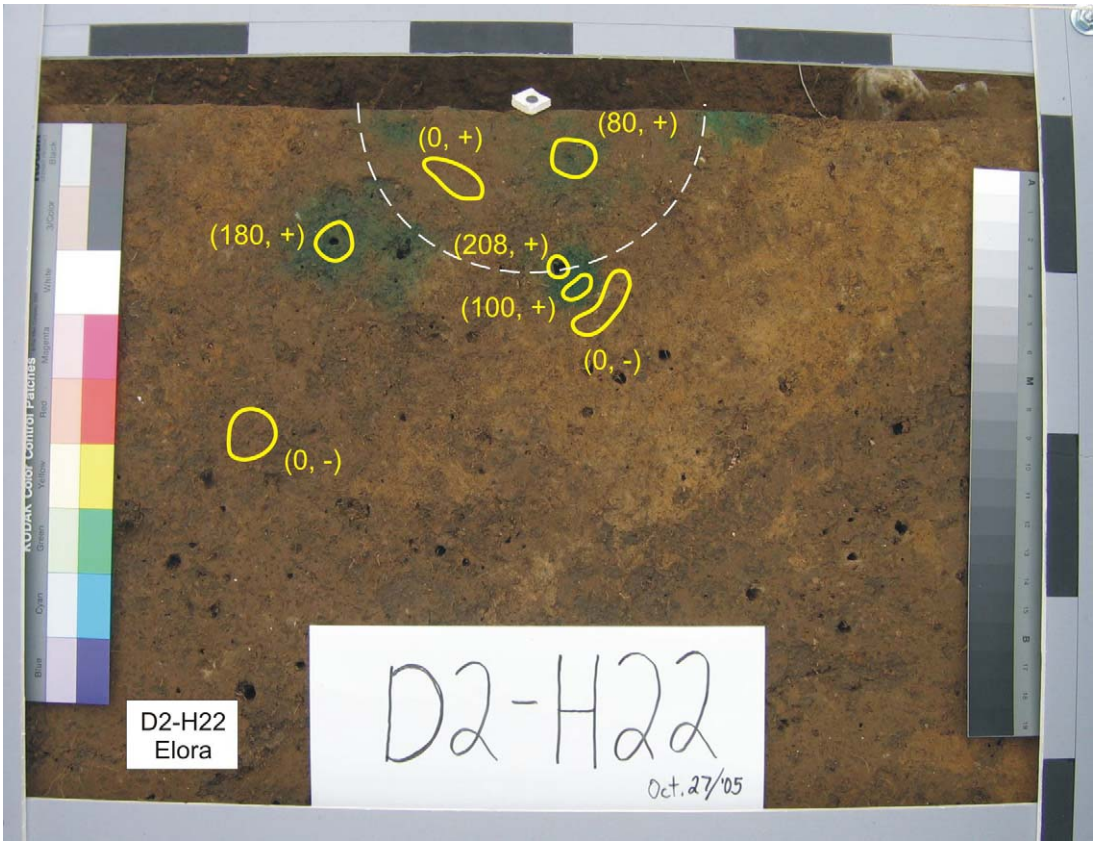
(0, +)
(80, +)
(180, +)
(208, +)
(100, +)
(0, -)
(0, -)
D2-H22
Elora
D2-H22
Oct. 27/05

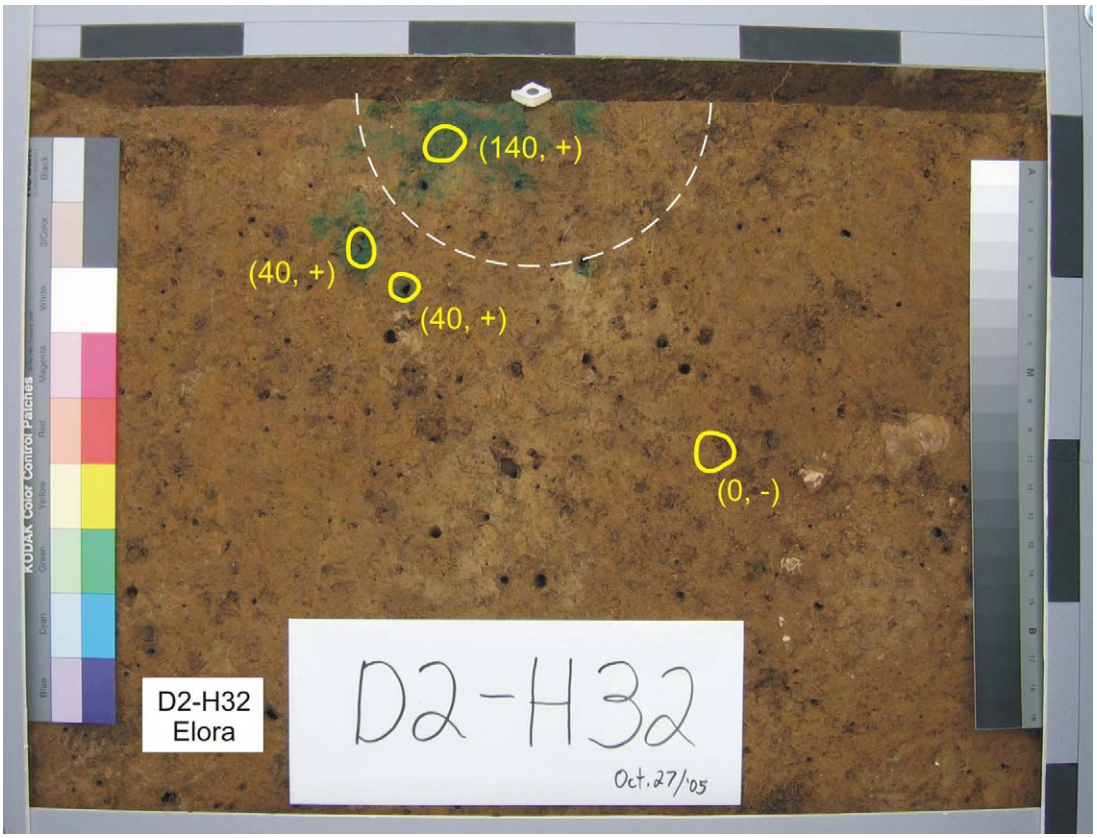
(140, +)
(40, +)
(40, +)
(0, -)
D2-H32
Elora
D2-H32
Oct. 27/05

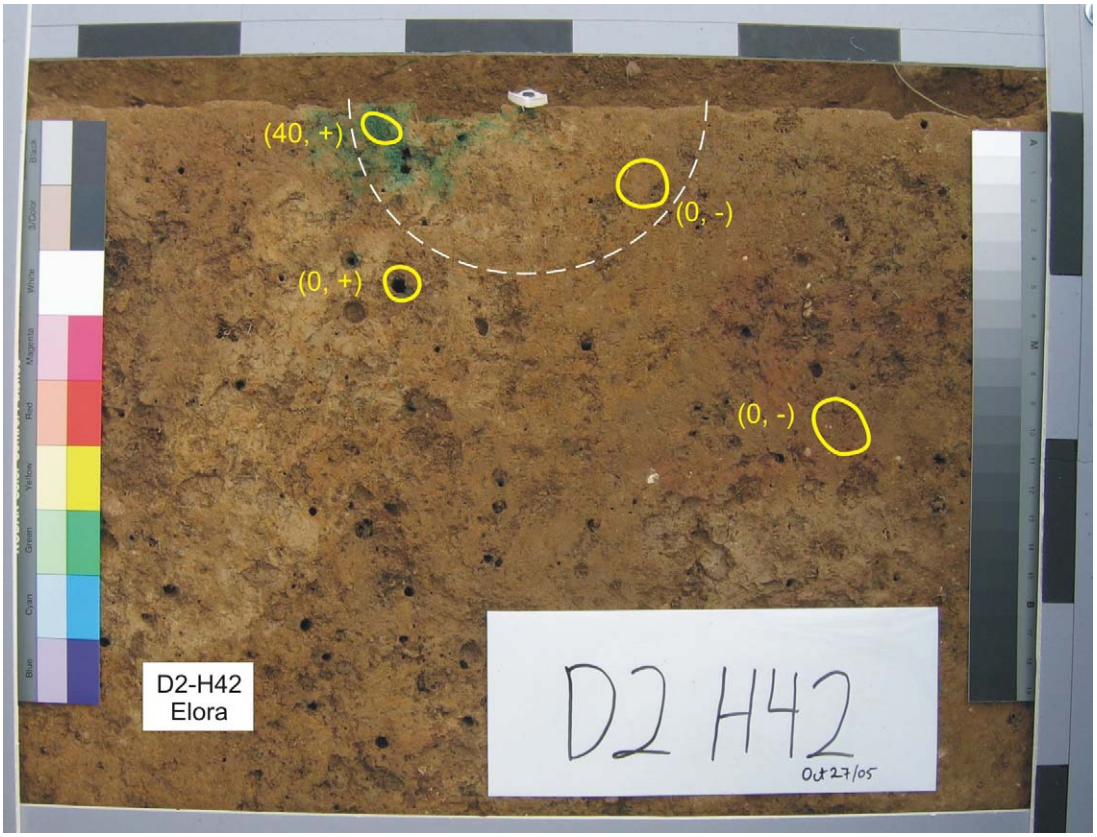
(40, +)
(0, -)
(0, +)
(0, -)
D2-H42
Elora
D2 H42
Oct 27/05

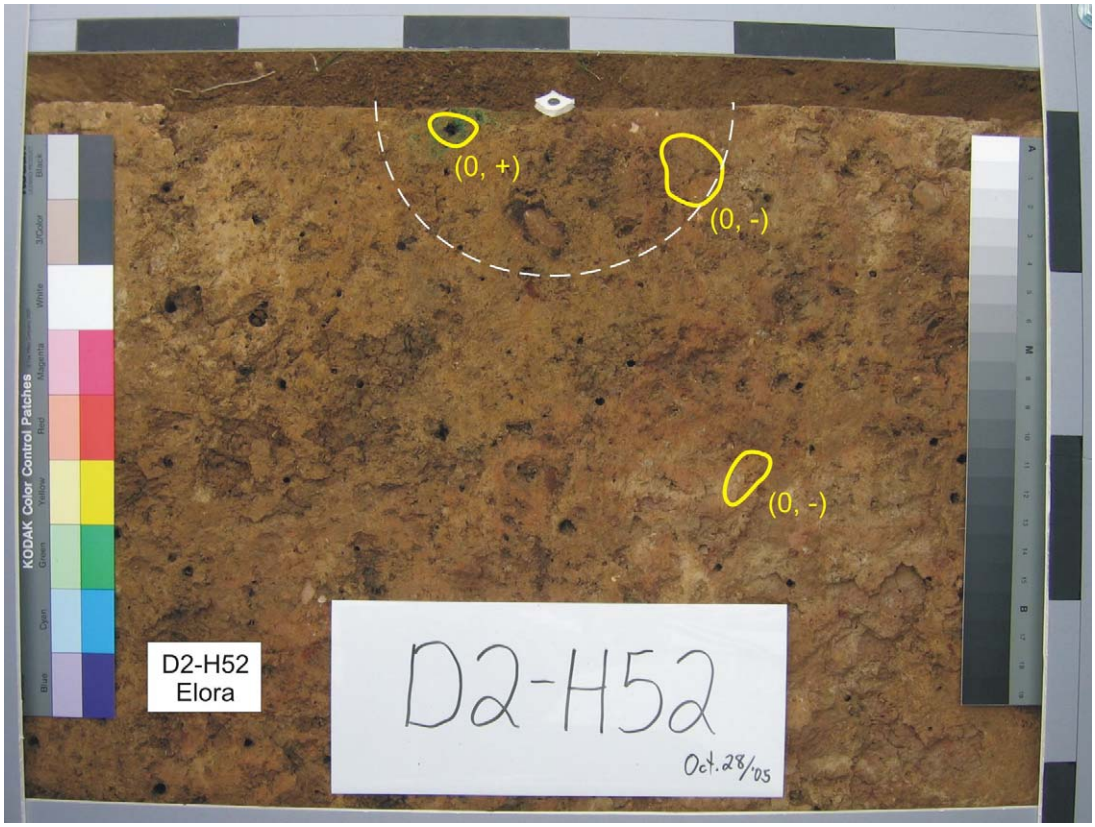
(0, +)
(0, -)
(0, -)
KODAK Color Control Patches
D2-H52
Elora
D2-H52
Oct. 28/05

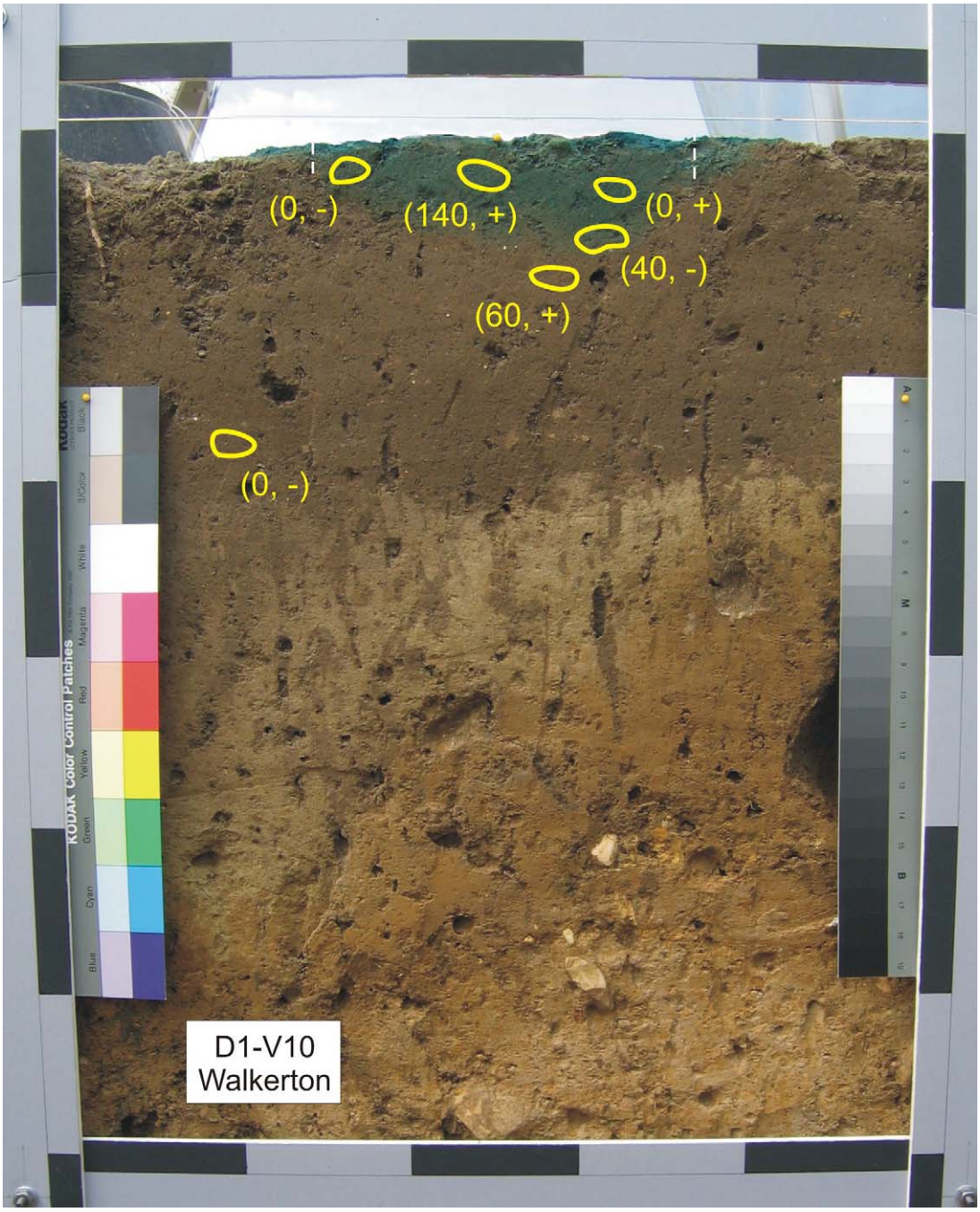
(0, -)
(140, +)
(0, +)
(40, -)
(60, +)
(0, -)
KODAK Color Control Patches
D1-V10
Walkerton

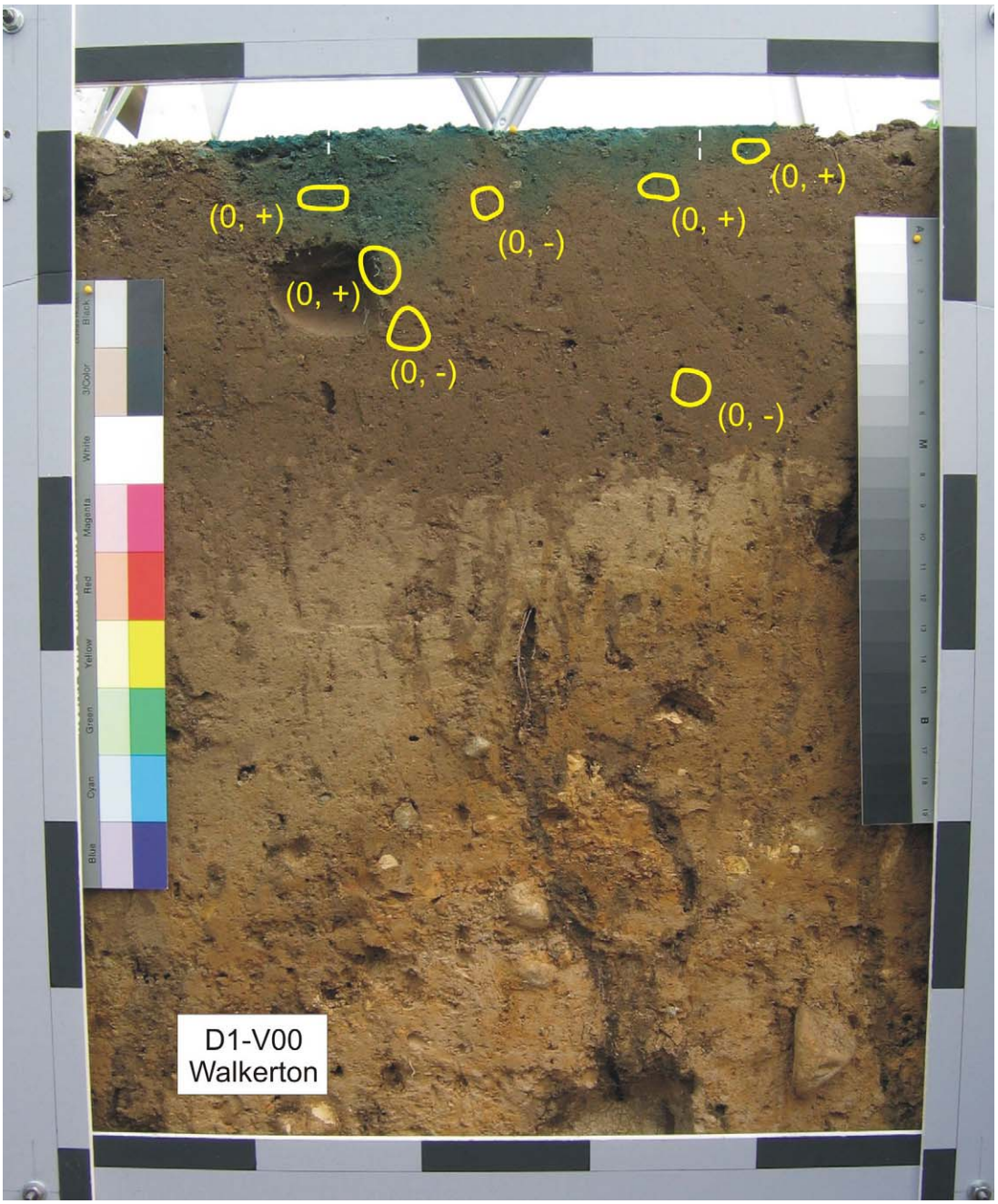
(0, +)
(0, -)
(0, +)
(0, +)
(0, +)
(0, -)
(0, -)
D1-V00
Walkerton

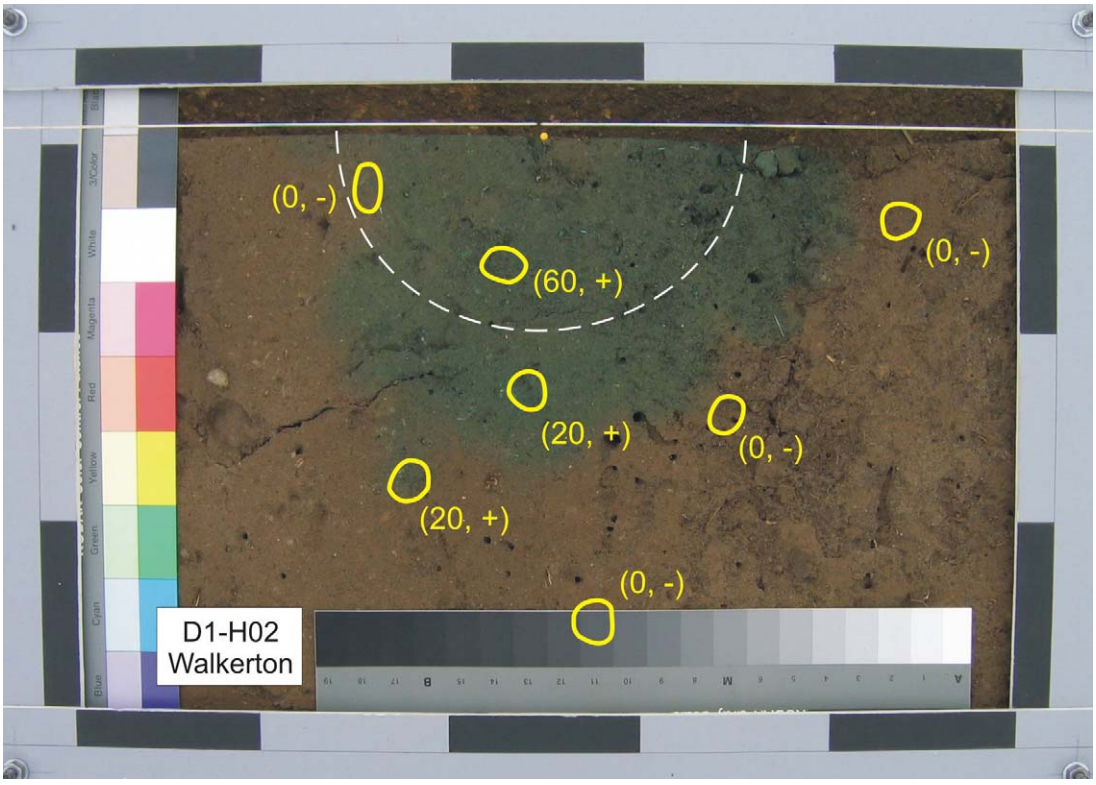
(0, -)
(60, +)
(0, -)
(20, +)
(0, -)
(20, +)
(0, -)
D1-H02
Walkerton

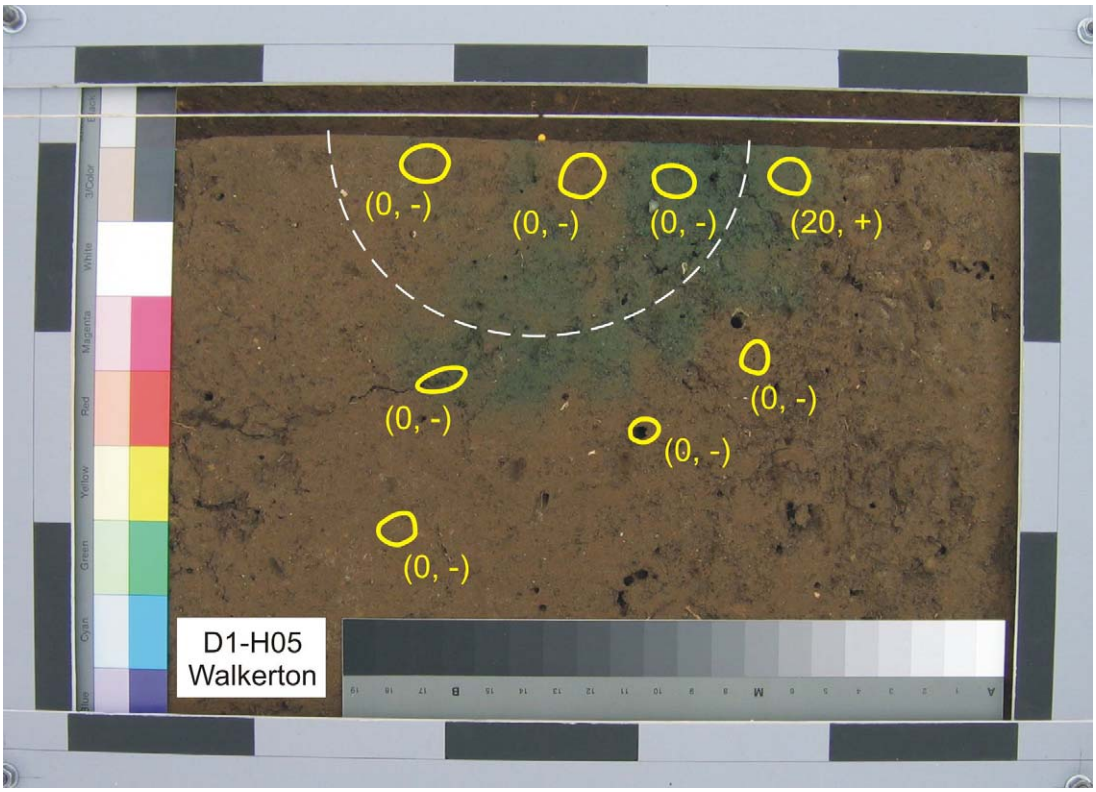
(0, -)
(0, -)
(0, -)
(20, +)
(0, -)
(0, -)
(0, -)
(0, -)
D1-H05
Walkerton

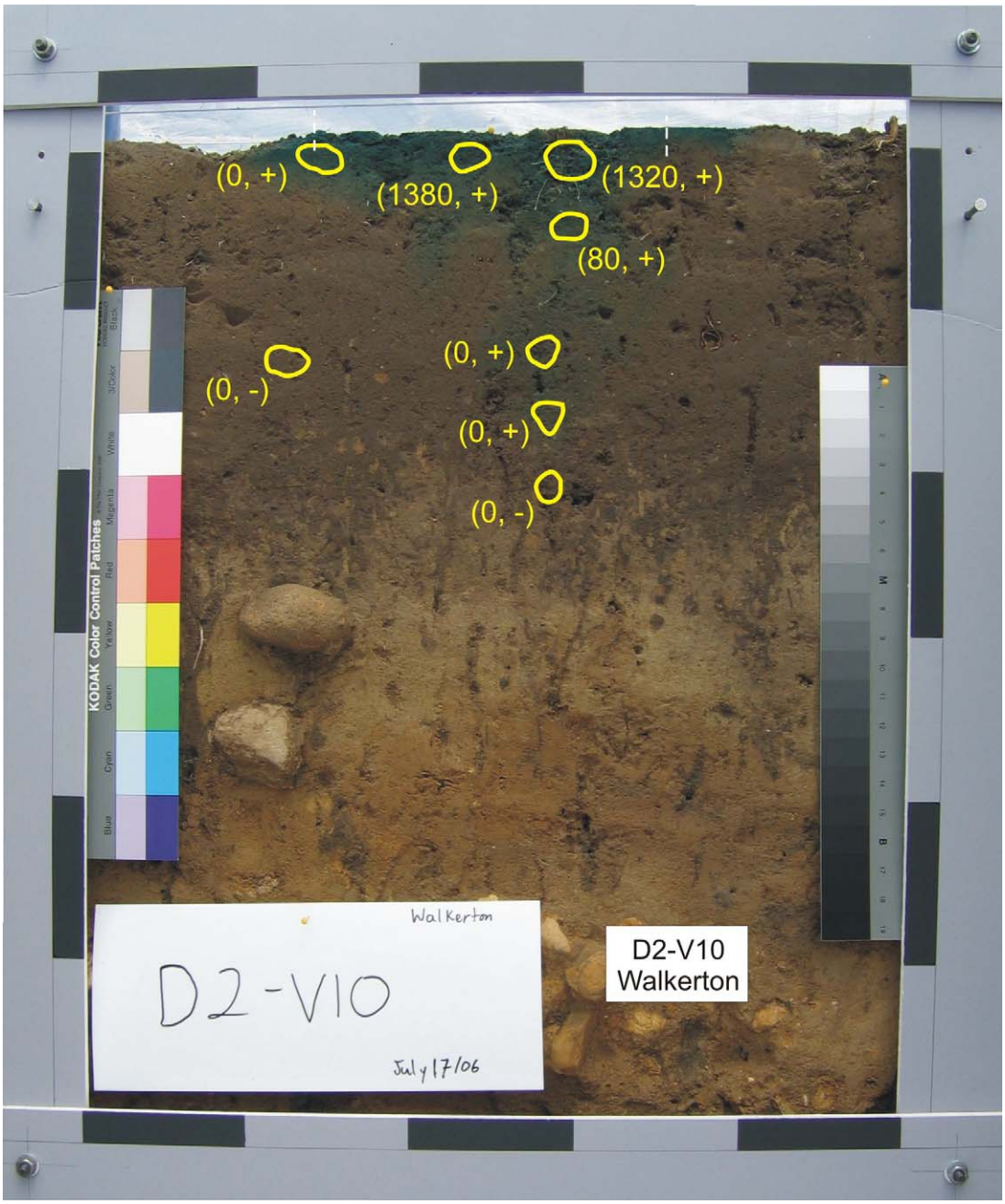
(0, +)
(1380, +)
(1320, +)
(80, +)
(0, -)
(0, +)
(0, +)
(0, -)
KODAK Color Control Patches
Walkerton
D2-V10
July 17/06
D2-V10
Walkerton

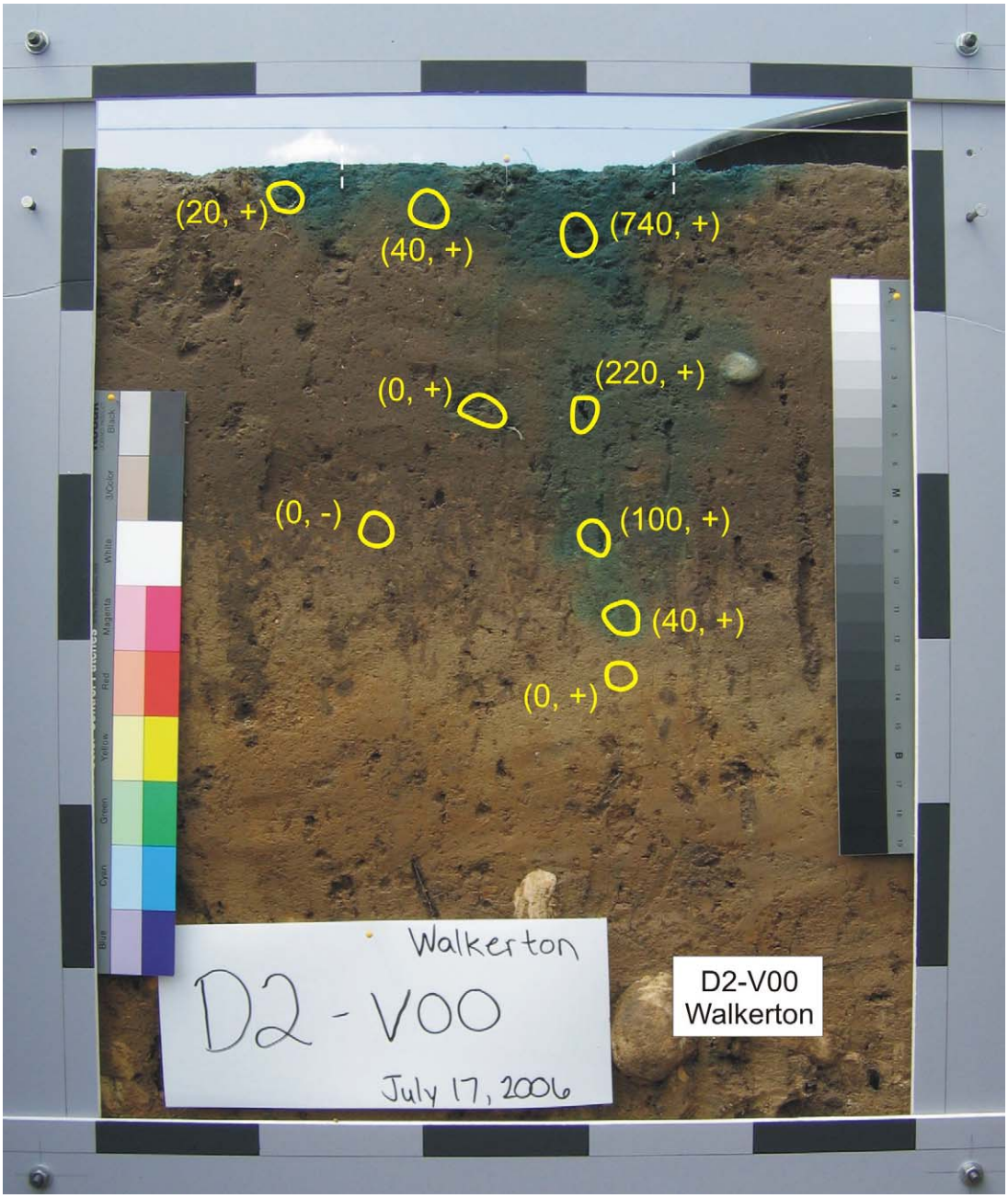
(20, +)
(40, +)
(740, +)
(0, +)
(220, +)
(0, -)
(100, +)
(40, +)
(0, +)
Walkerton
D2 - V00
July 17, 2006
D2-V00
Walkerton

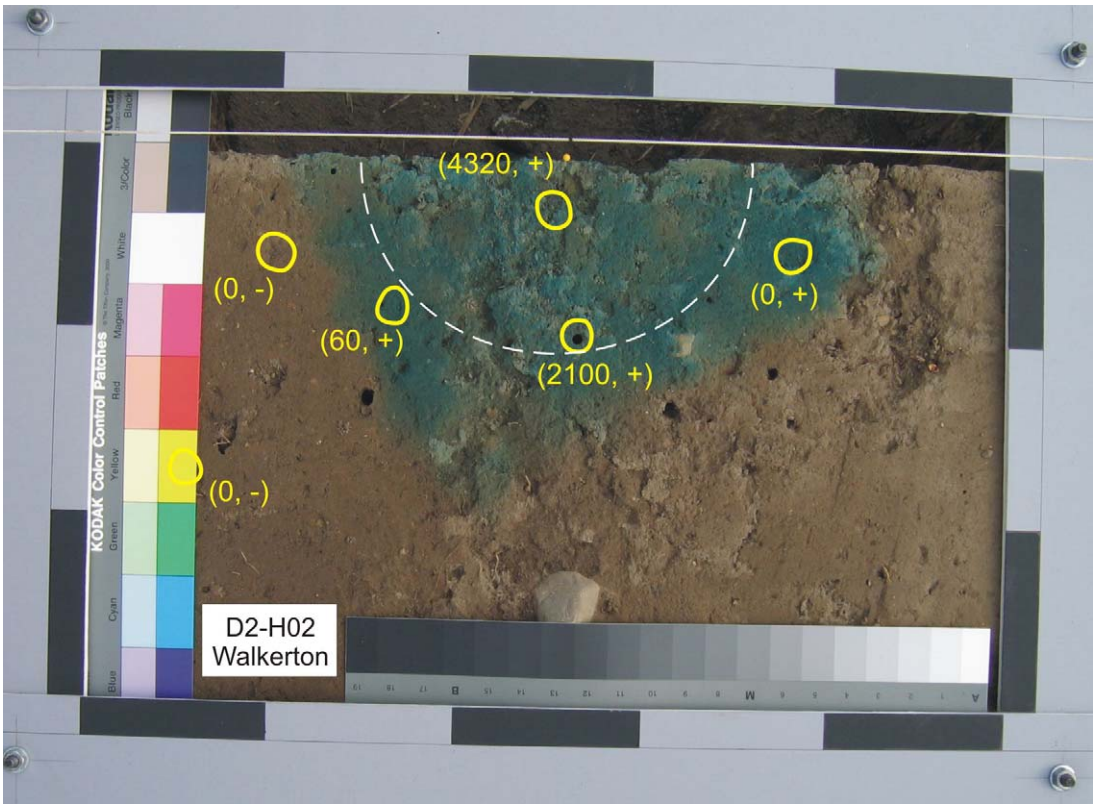
(4320, +)
(0, -)
(0, +)
(60, +)
(2100, +)
(0, -)
KODAK Color Control Patches
D2-H02
Walkerton

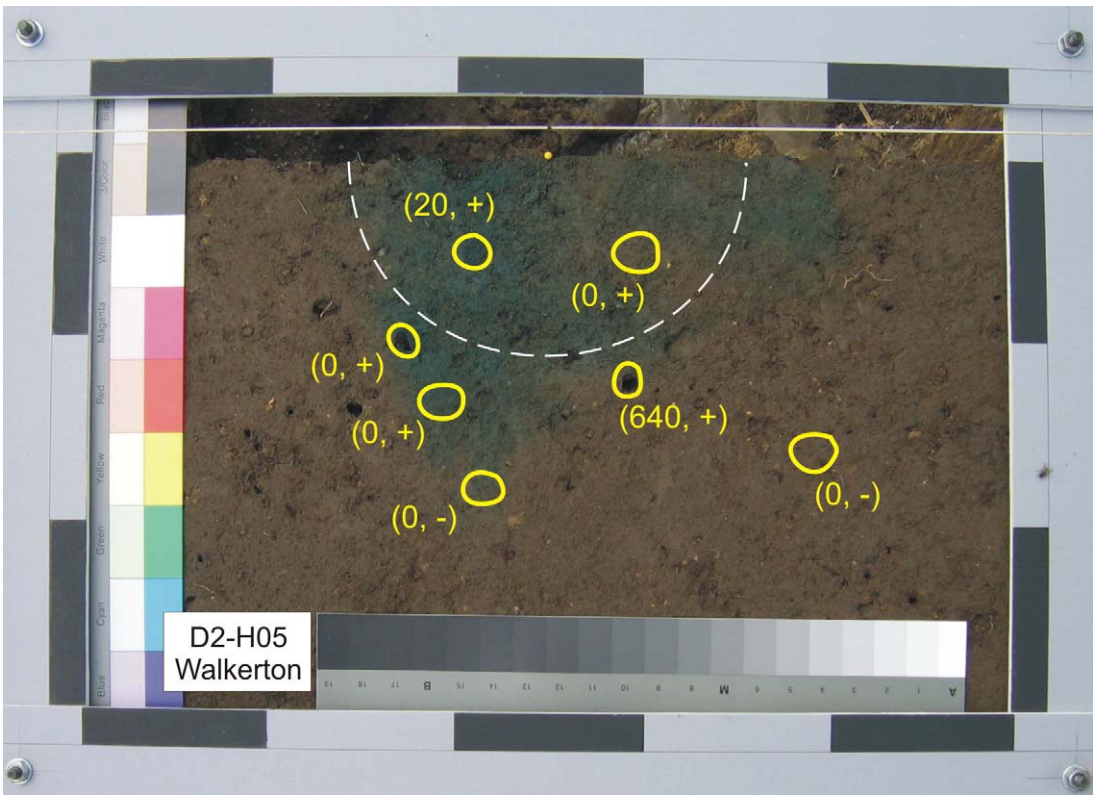
(20, +)
(0, +)
(0, +)
(640, +)
(0, +)
(0, -)
(0, -)
D2-H05
Walkerton

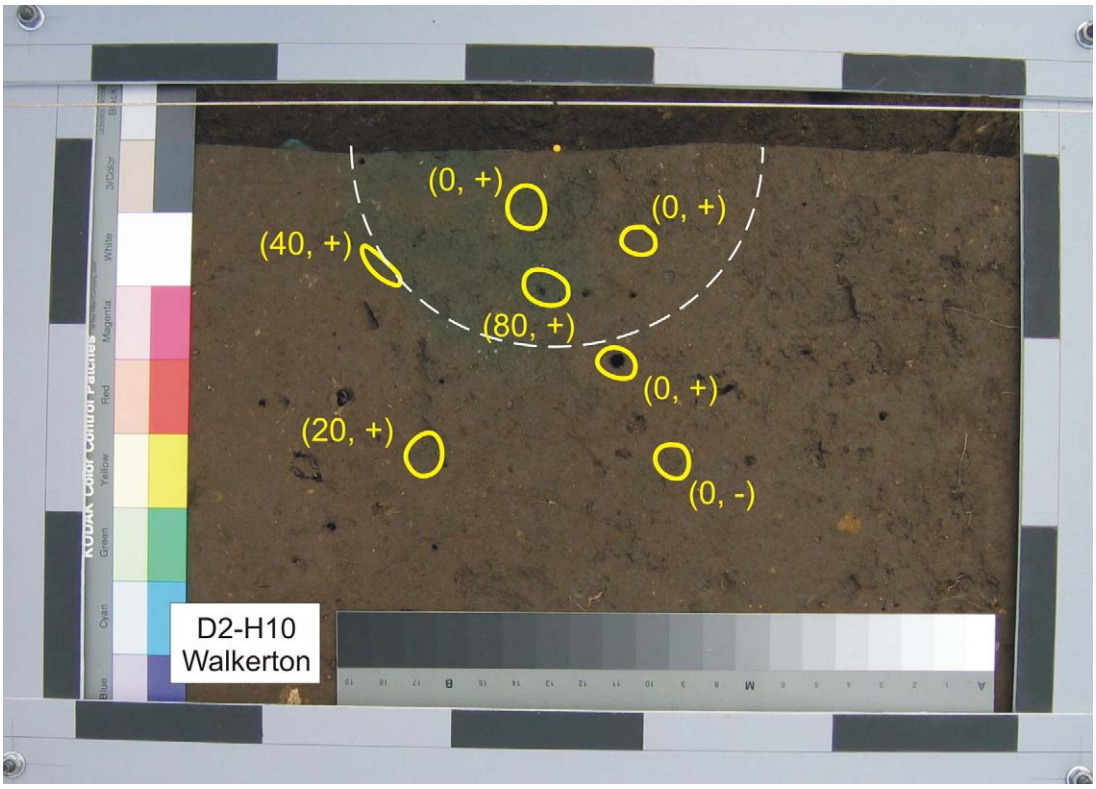
(0, +)
(0, +)
(40, +)
(80, +)
(0, +)
(20, +)
(0, -)
D2-H10
Walkerton

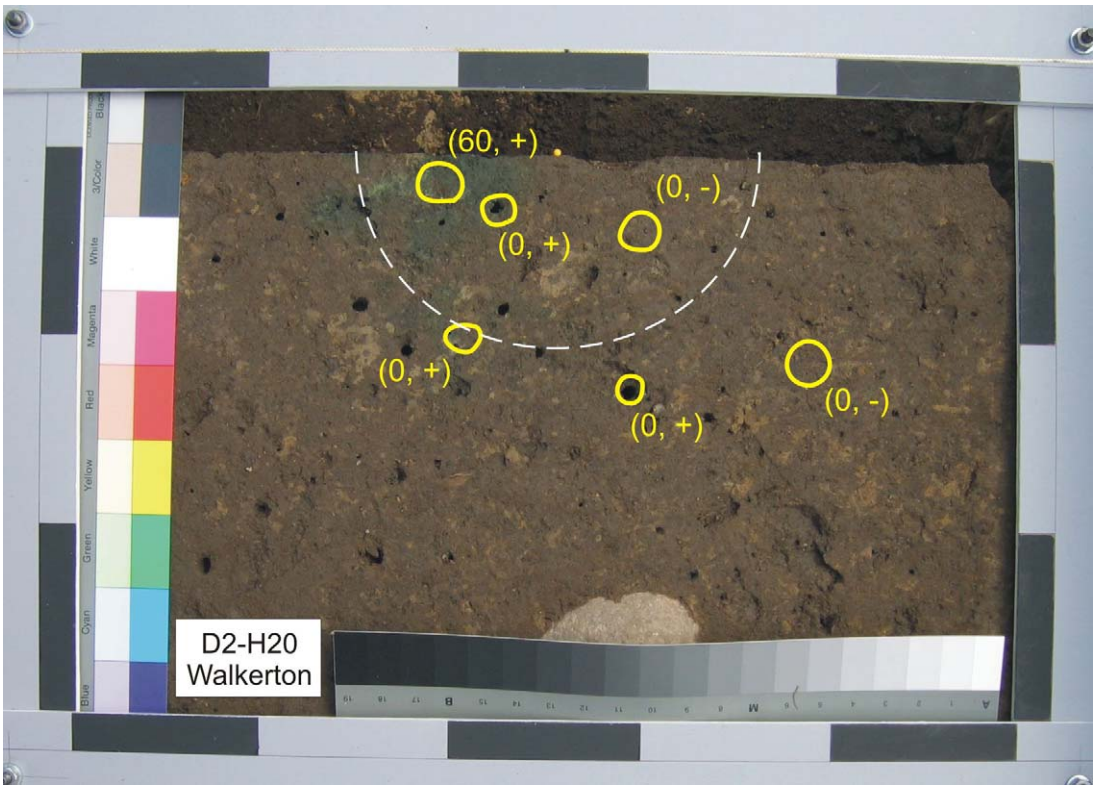
(60, +)
(0, -)
(0, +)
(0, +)
(0, +)
(0, -)
D2-H20
Walkerton

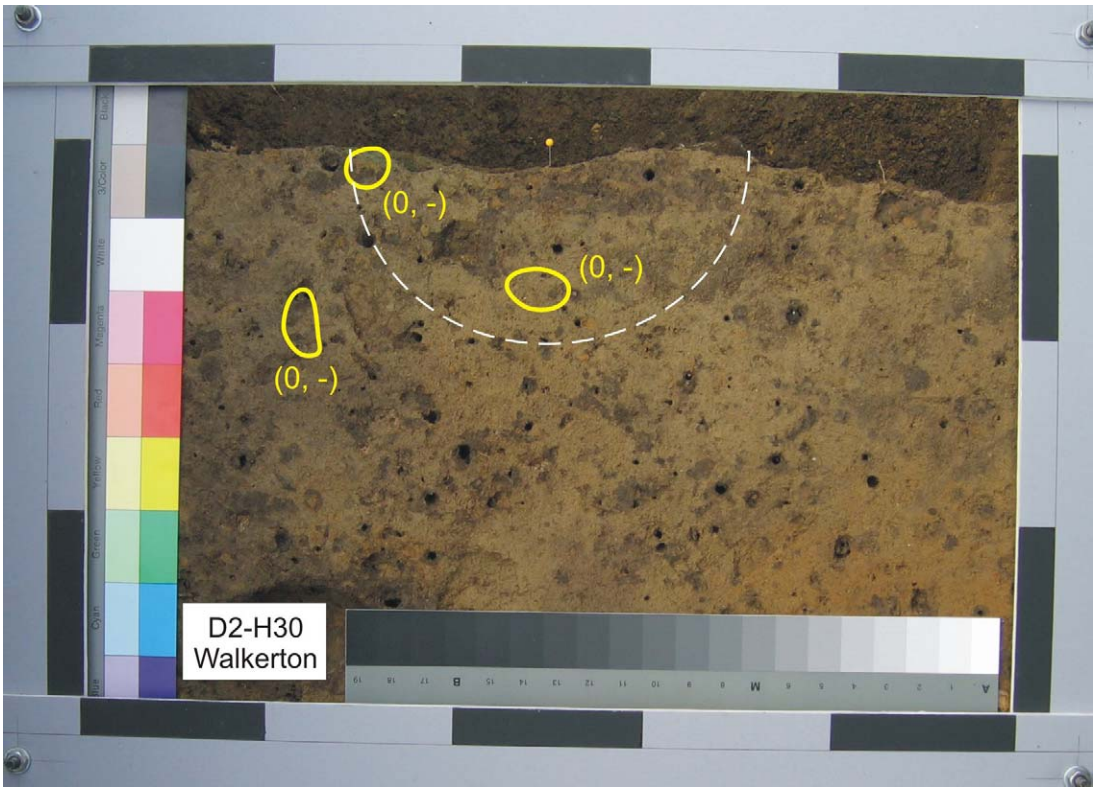
(0, -)
(0, -)
(0, -)
D2-H30
Walkerton

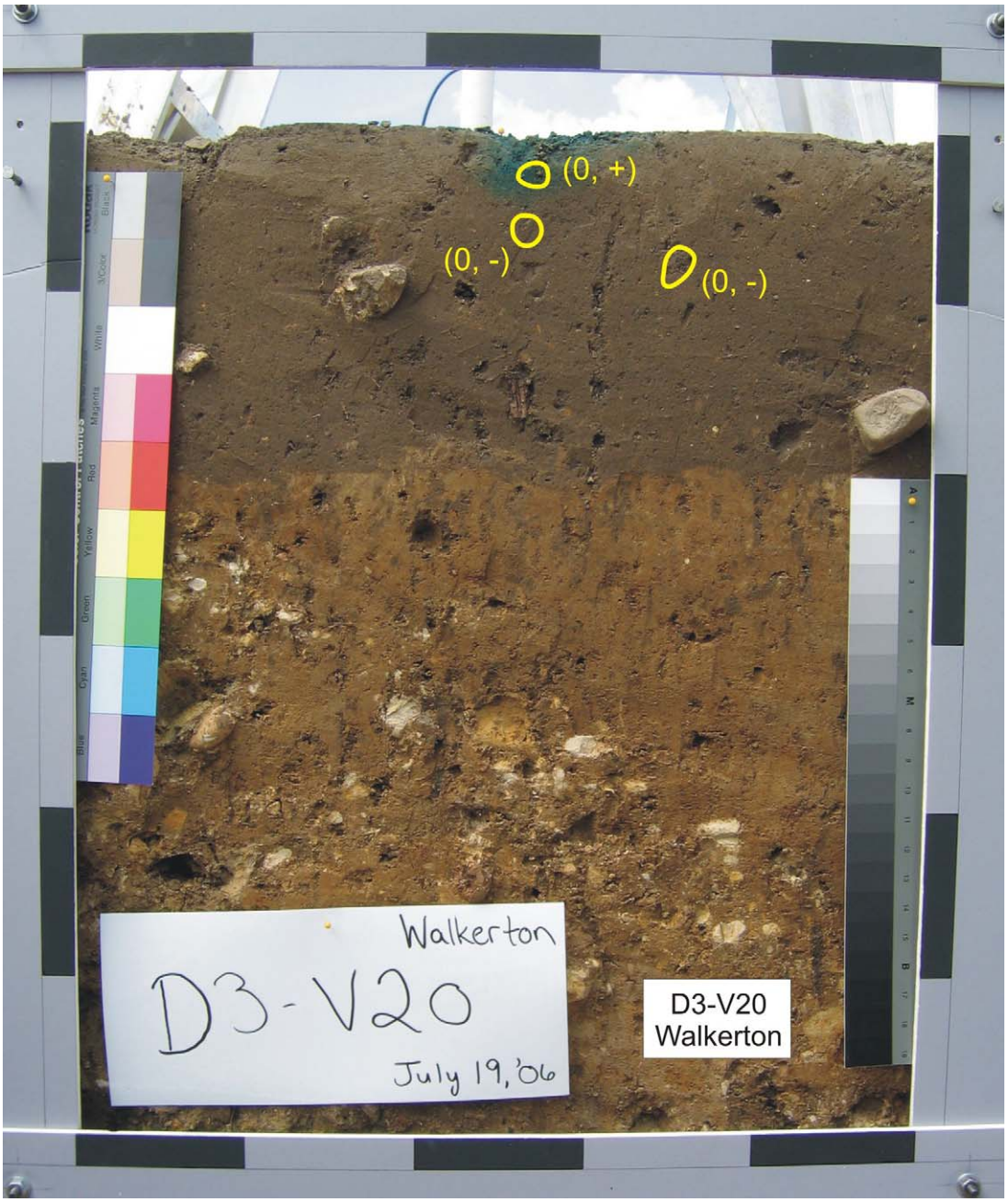
(0, +)
(0, -)
(0, -)
Walkerton
D3-V20
July 19, '06
D3-V20
Walkerton

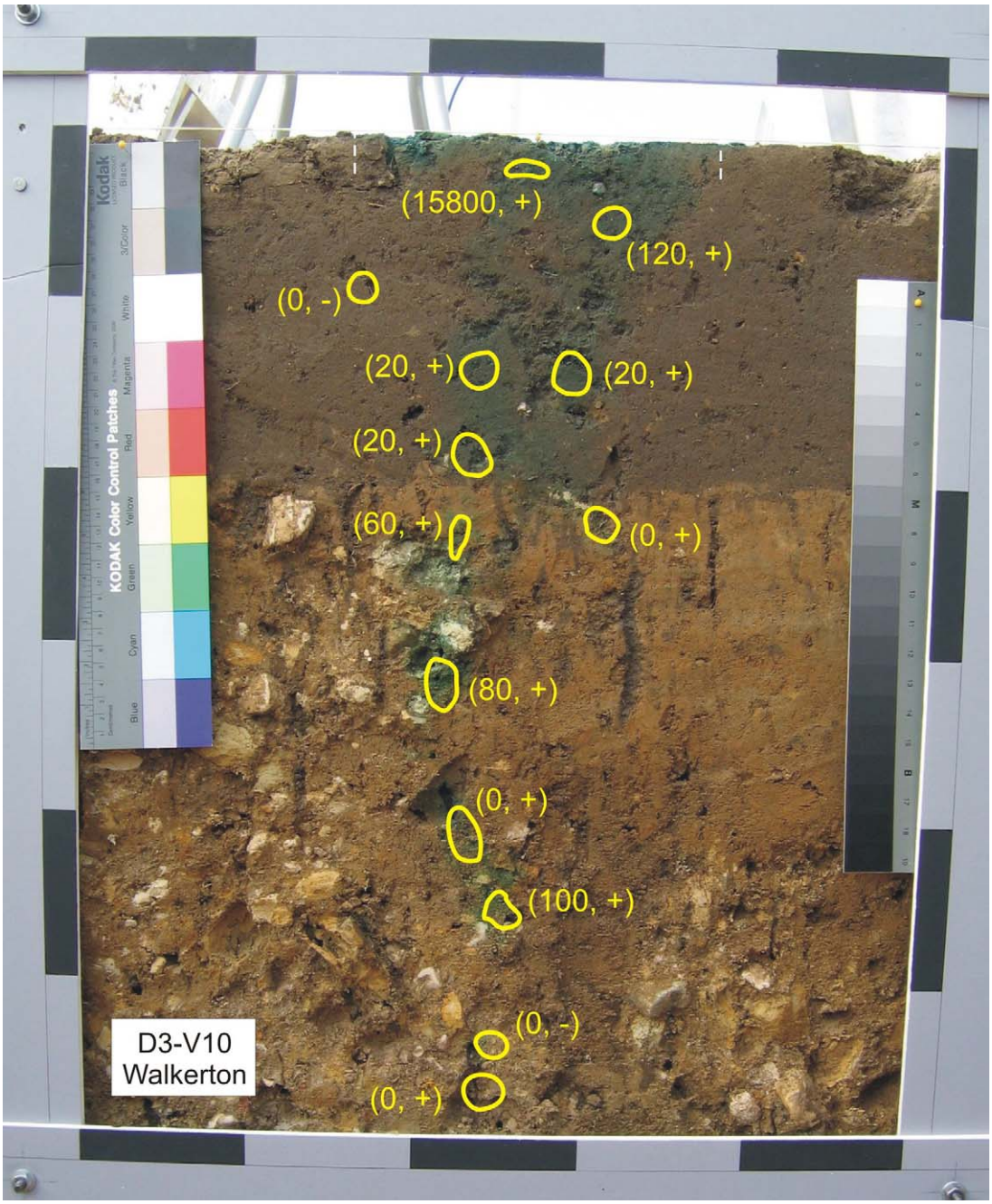
(15800, +)
(120, +)
(0, -)
(20, +)
(20, +)
(20, +)
(60, +)
(0, +)
(80, +)
(0, +)
(100, +)
(0, -)
(0, +)
D3-V10
Walkerton

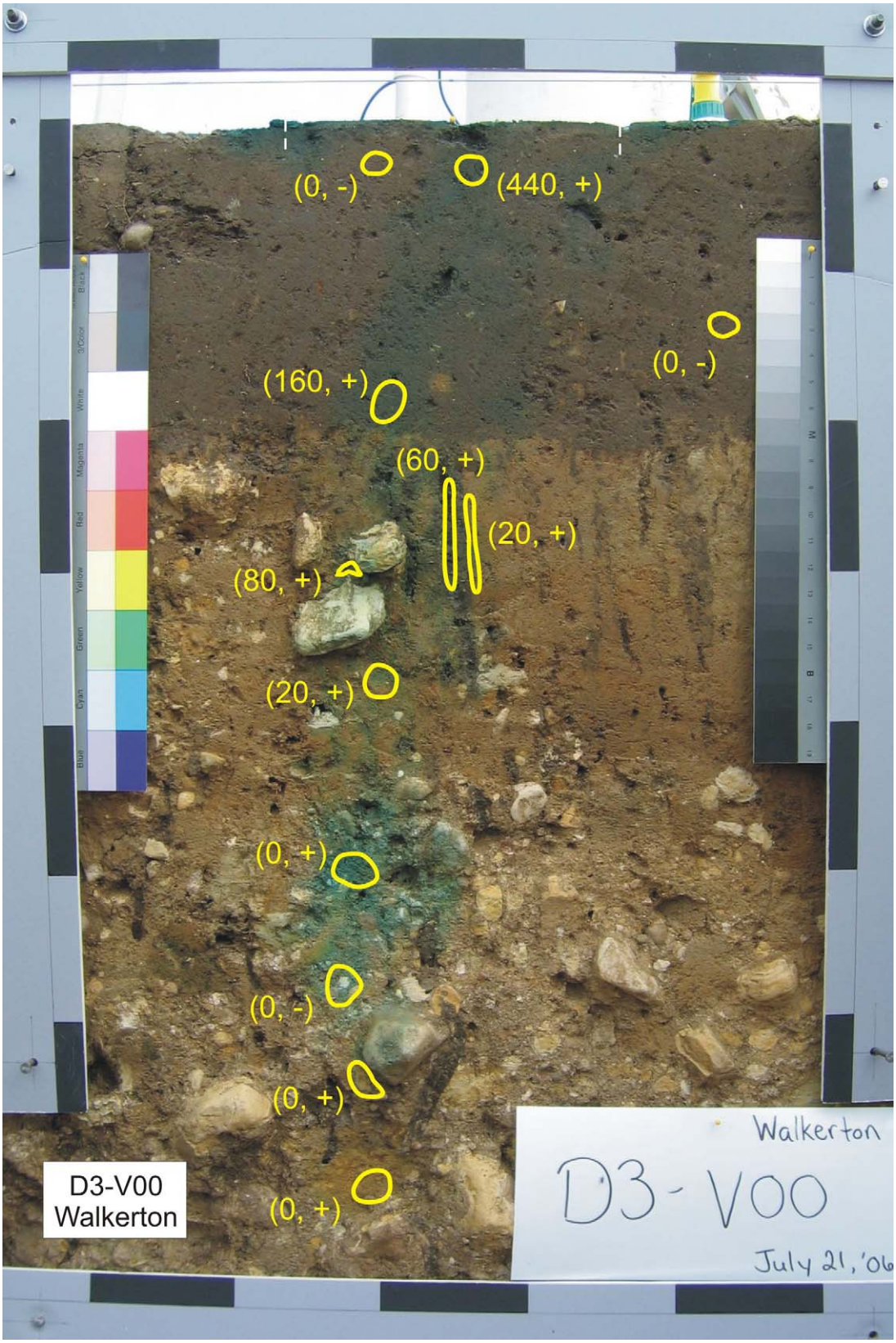
(0, -)
(440, +)
(0, -)
(160, +)
(60, +)
(20, +)
(80, +)
(20, +)
(0, +)
(0, -)
(0, +)
(0, +)
D3-V00
Walkerton
Walkerton
D3 - V00
July 21, '06

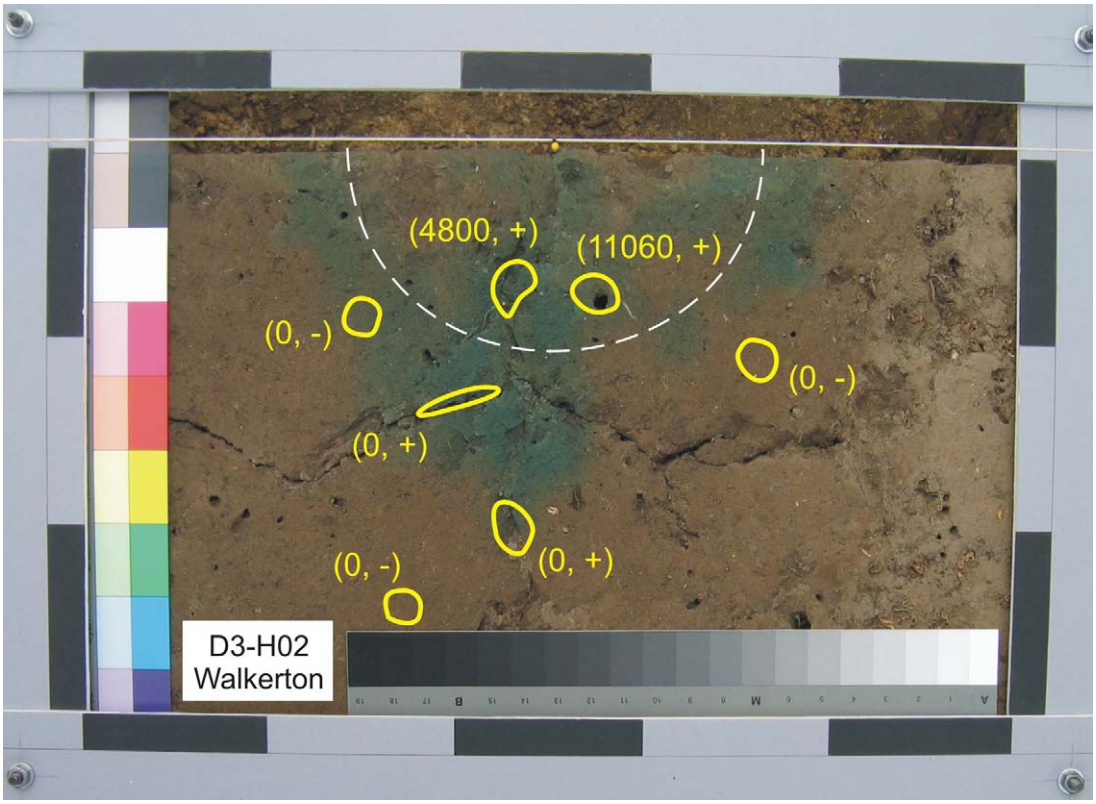
(4800, +)
(11060, +)
(0, -)
(0, -)
(0, +)
(0, +)
(0, -)
D3-H02
Walkerton

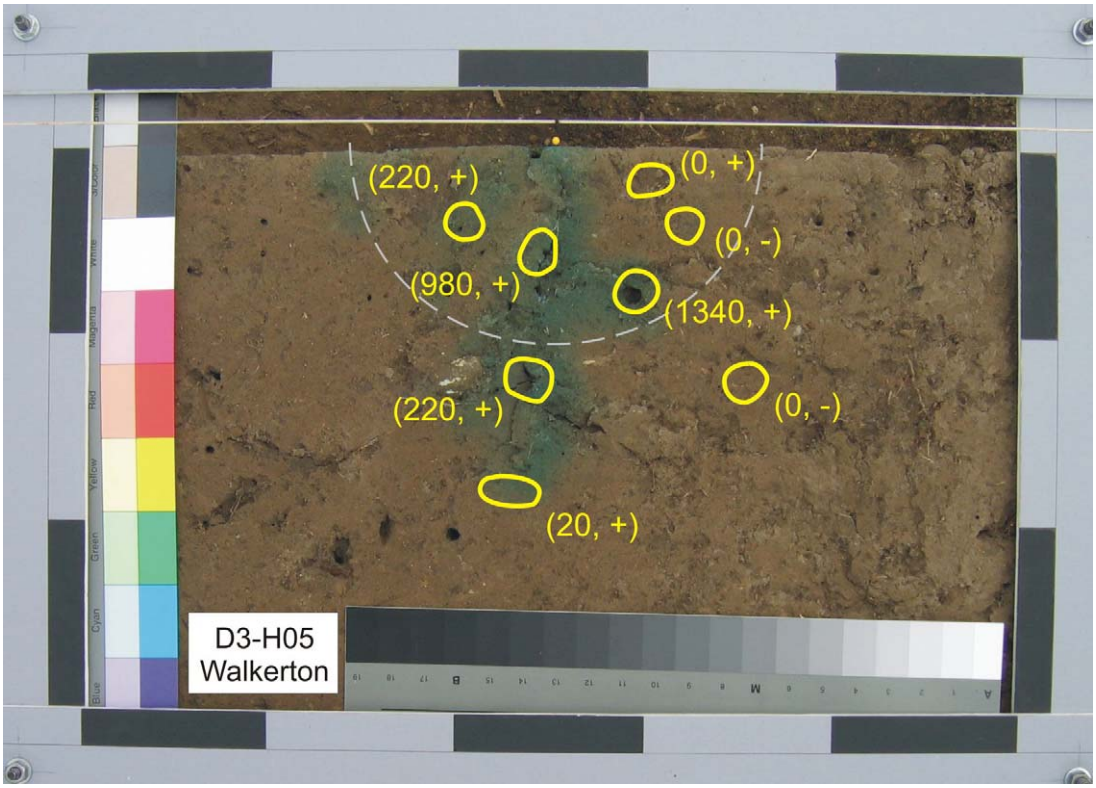
(220, +)
(0, +)
(0, -)
(980, +)
(1340, +)
(220, +)
(0, -)
(20, +)
D3-H05
Walkerton

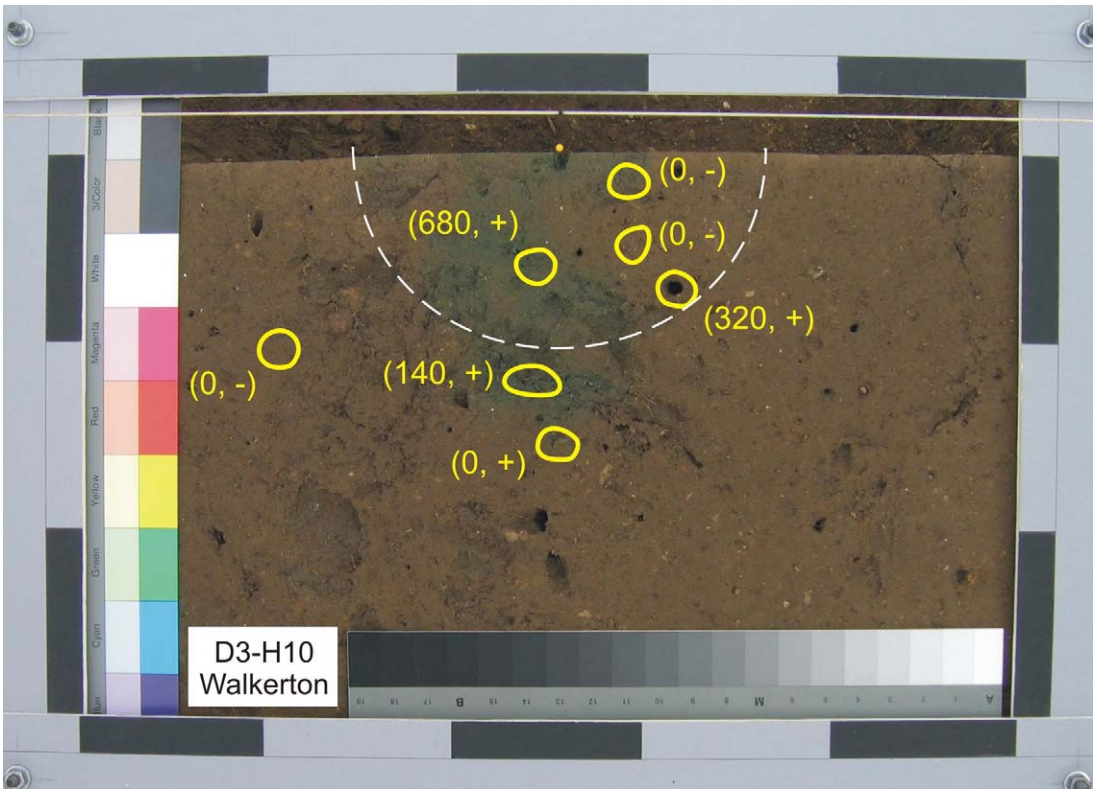
(0, -)
(680, +)
(0, -)
(320, +)
(0, -)
(140, +)
(0, +)
D3-H10
Walkerton

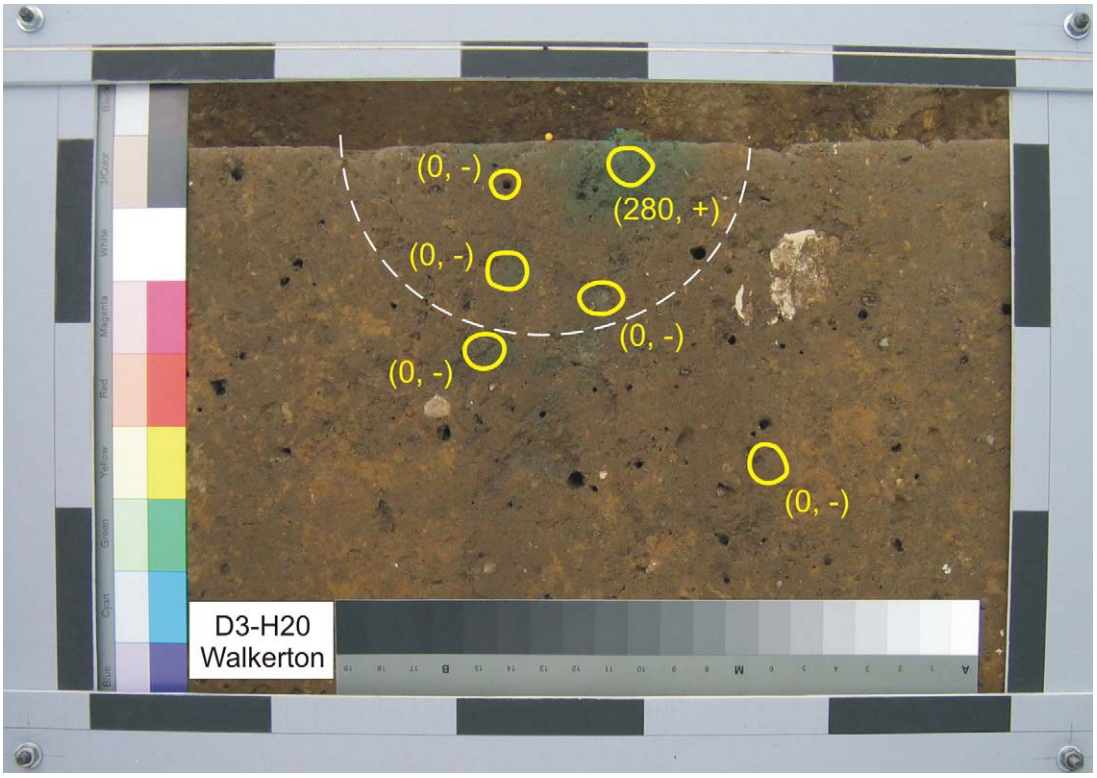
(0, -)
(280, +)
(0, -)
(0, -)
(0, -)
(0, -)
D3-H20
Walkerton

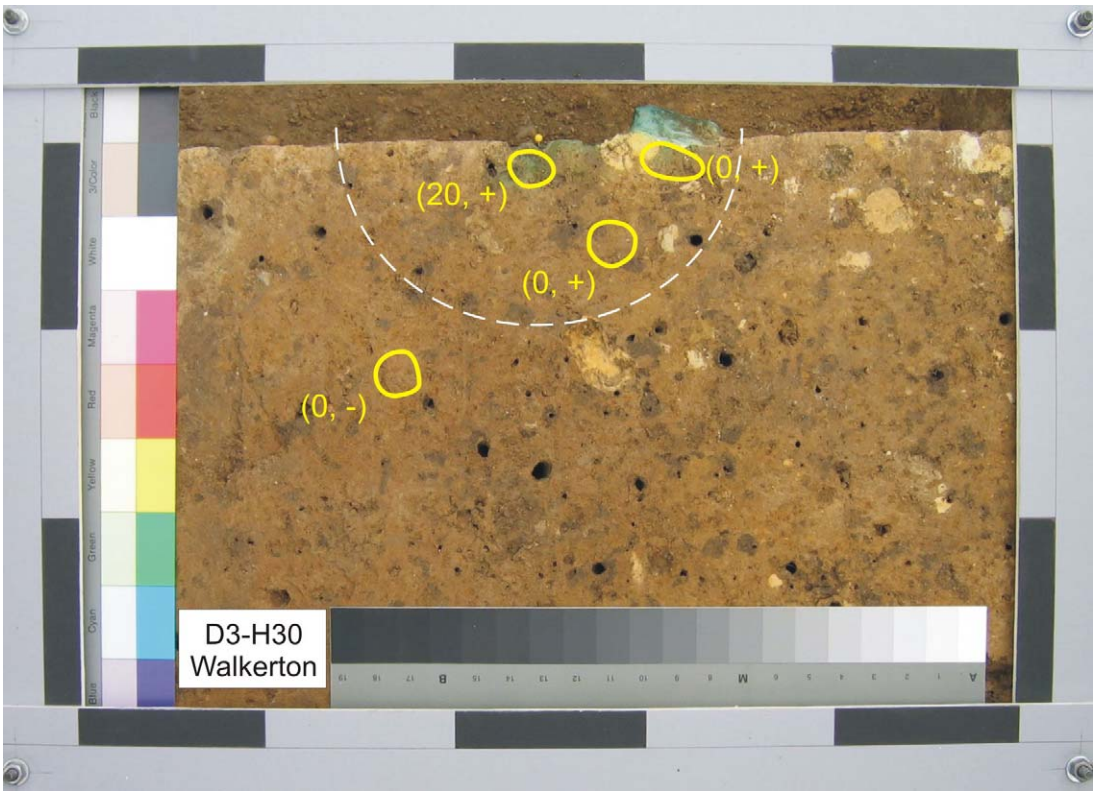
(20, +)
(0, +)
(0, +)
(0, -)
D3-H30
Walkerton

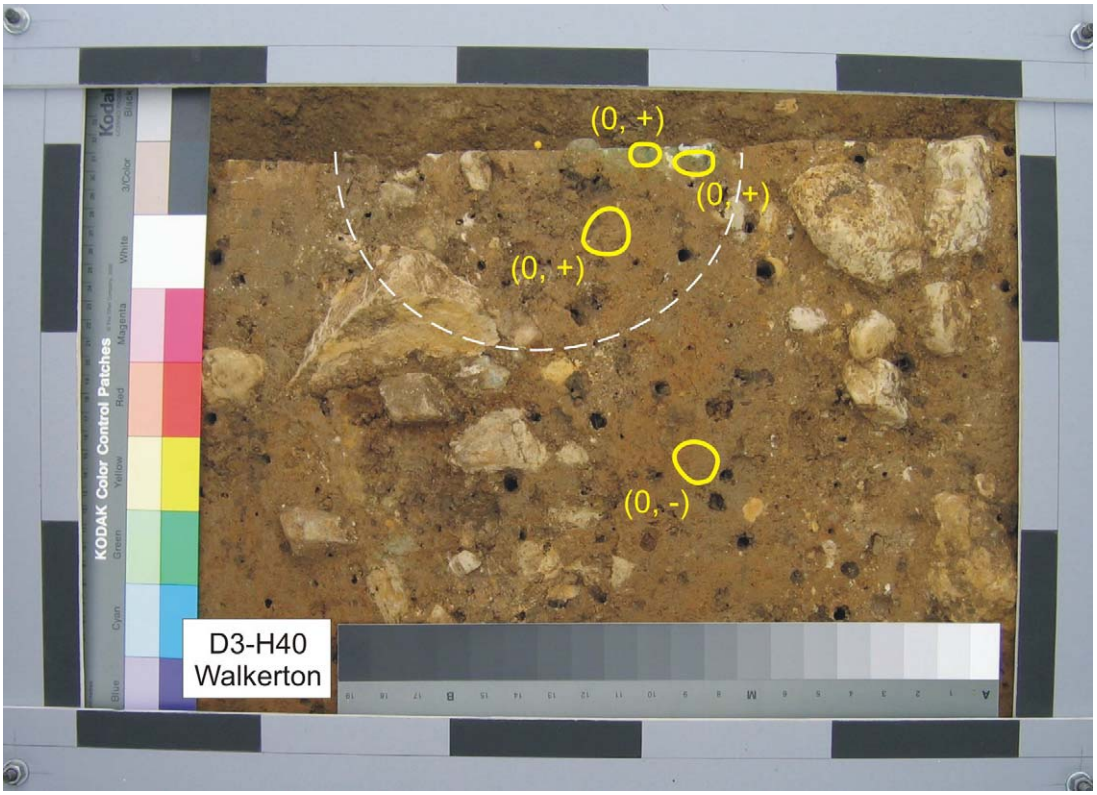
(0, +)
(0, +)
(0, +)
(0, -)
KODAK Color Control Patches
D3-H40
Walkerton

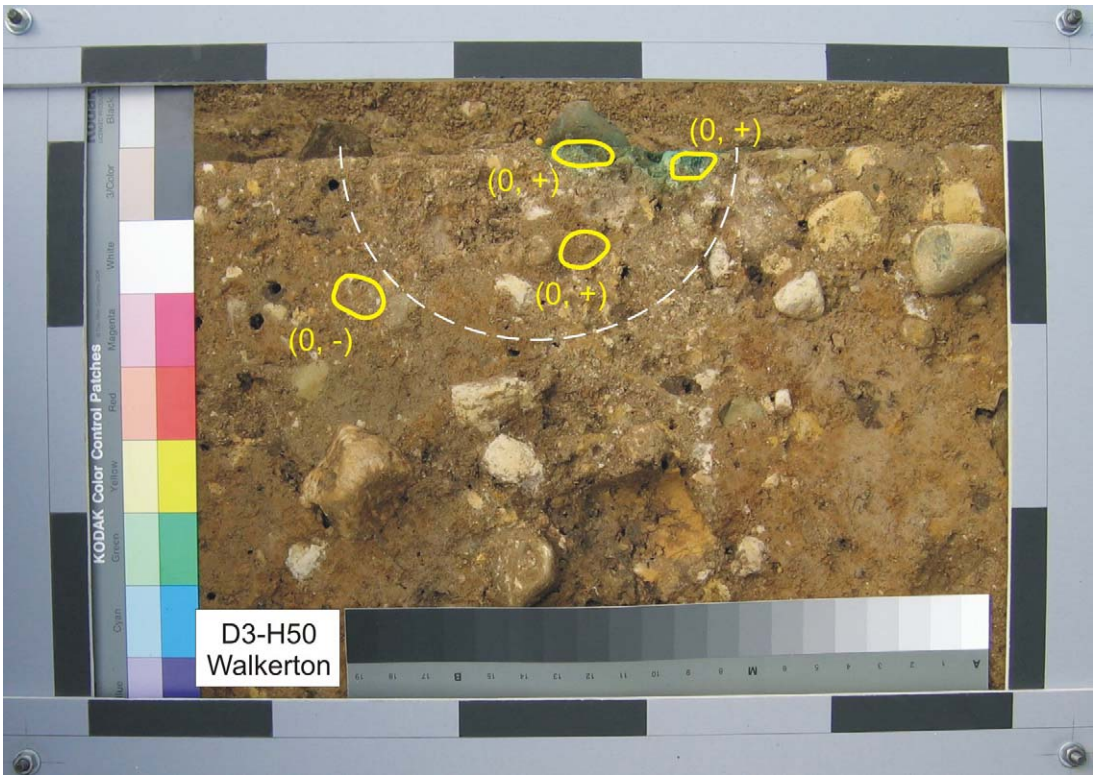
(0, +)
(0, +)
(0, +)
(0, -)
KODAK Color Control Patches
D3-H50
Walkerton

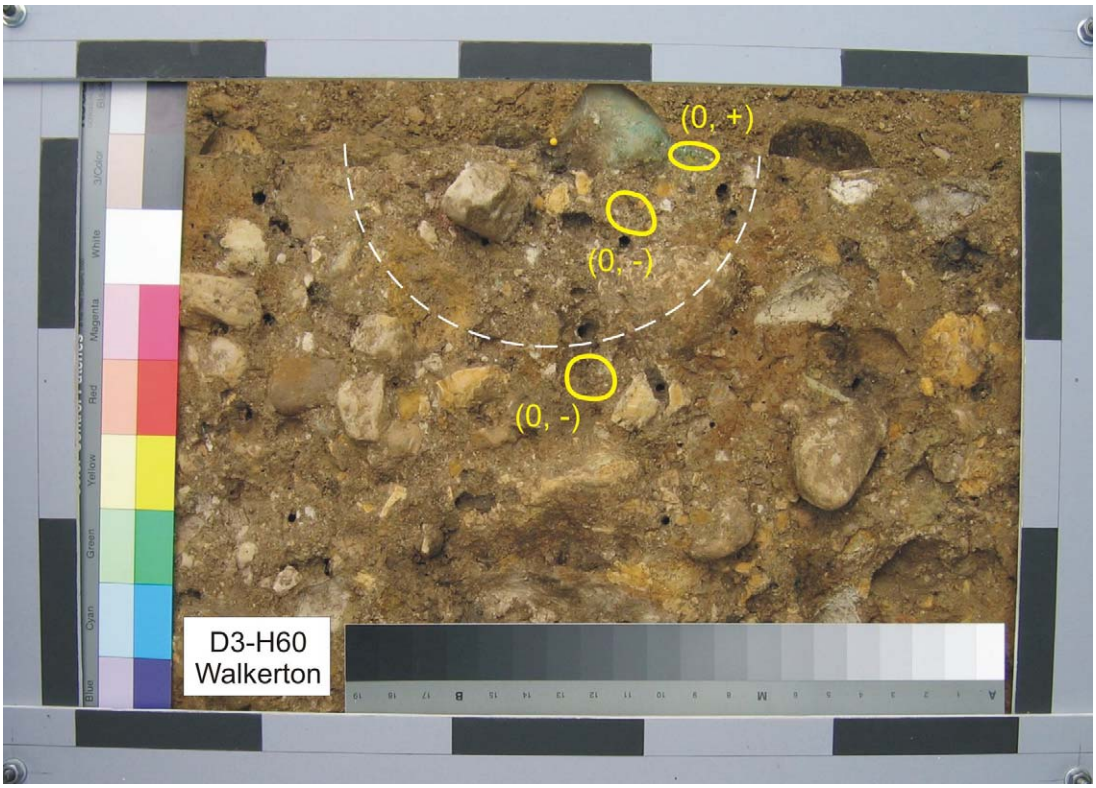
(0, +)
(0, -)
(0, -)
D3-H60
Walkerton

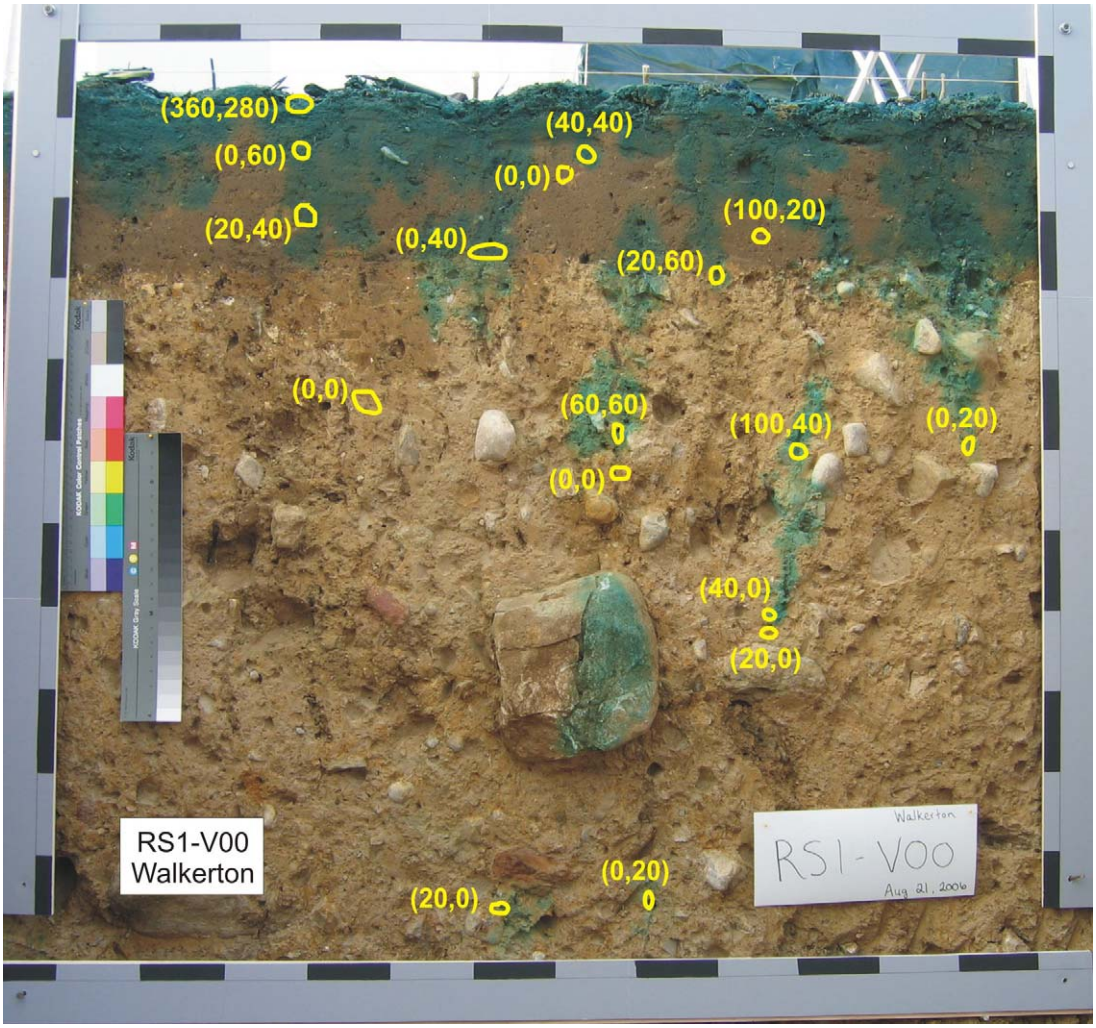
(360,280)
(0,60)
(20,40)
(40,40)
(0,0)
(0,40)
(100,20)
(20,60)
(0,0)
(60,60)
(0,0)
(100,40)
(0,20)
(40,0)
(20,0)
(20,0)
(0,20)
RS1-V00
Walkerton
Walkerton
RS1-V00
Aug 21, 2006